Synthetic and Computational Investigation of Phosphorus containing Lewis acids bound by 2,6-Bis(benzimidazol-2-yl)pyridine.

by

Ksenia Varga

A thesis submitted to the Faculty of Graduate and Postdoctoral Affairs in partial fulfillment of the requirements for the degree of

Master of Science
In
Chemistry

Carleton University
Ottawa, Ontario

Abstract

Main group chemistry has seen a resurgence in recent years, which has led to alternatives to the traditionally used transition metals – species which are often costly and pose toxicity concerns. Phosphorus is of particular interest due to its versatility of chemistry displayed by compounds containing phosphorus. New synthetic approaches towards Lewis acidic phosphorus containing compounds have been developed; they apply coordination chemistry and take advantage of well-established ligand libraries for transition metal catalyst systems which stabilize multiple cationic charges on the Lewis acidic phosphorus center. In this work, a series of dicationic and Lewis acids were synthesized and characterized using spectral and computational methods. The general composition of the Lewis acids involves Phosphorus as the electron deficient center bound by 2,6-Bis(benzimidazol-2'-yl)pyridine ligand which is highly rigid and tunable. The phosphorus centre is also bonded to a substituent (R'), either phenyl or dimethylamine to influence the electron-deficiency of the Phosphorus center. The resulting cation is supported by triflate [OTf] or barfate [$BArF_{24}$] counter anion. This design leads to systems in which the Lewis acidic phosphorus lies within the plane of the ligand and the R group on the phosphorus is almost perpendicular to the ligand plane, which leaves the Lewis acidic site exposed. The Lewis acids were then characterized using various analytical techniques (multinuclear NMR, HRMS, EA, UV-vis, FT-IR, single crystal XRD, etc.) and computational approaches. The Lewis acidity was probed experimentally using Gutmann-Beckett tests which suggest high Lewis acidity for all compounds; this conclusion was corroborated using the Fluoride Ion Affinity calculations. The catalytic reactivity of the Lewis acids was probed.

Acknowledgements

I would like to acknowledge the following people for their continuous support and investment in me as a scientist and individual.

Family; All of my dearest family members for their encouragement and support throughout my studies and life in general. Special thank you to my special husband who keeps me motivated.

Committee Members; I would like to thank the committee members for their time and dedication.

The Macdonald and Barry lab groups; I would like to express my deepest appreciation for Dr. Charles L.B. Macdonald for allowing me to develop into the scientist I am today and Dr. Sean Barry for his continuous support in research and life. The Macdonald and Barry lab group members for the help in research and the fun times spent together.

The Department of Chemistry; The department of chemistry has really become my second home over the past 7 years and I am very grateful to each and everyone I have been lucky to meet along the way. Namely, Dr. Bob Burk for sparking my interest in chemistry and seeing the potential in me before I ever did, Dr. Peter Buist for the fun conversations and lessons, Dr. Maria DeRosa for being an inspiration to me as a woman in science, Dr. Tyler Avis for this kindness and great teaching approach. I would also like to thank Dr. Manthorpe, Dr. J. Smith, Elena Munteanu, Daniel Sun, Gosho Marinov, Natalie Mesnic, Monica Gill, Chantelle Gravelle and the amazing science store staff for their contributions to me as a student. Last, but certainly not least, I would like to thank my students I have had throughout the years for their feedback and kindness to me throughout the years.

Table of Contents

List of Figures

List of Tables

List of Equations

List of Schemes

Introduction

Main group chemistry

Continuous advancements in the scientific research have led to an establishment of a distinctive branch in inorganic chemistry – main group chemistry. Main group chemistry explores the reactivity of compounds based on the s and p-block elements of the periodic table. In recent years, one prominent direction in main group chemistry research is the search for effective alternatives to transition metals for important catalytic processes. Compounds containing transition metals (TM), the elements of the d-block of the periodic table, have proven to be particularly effective for many of the catalytic processes that underpin well-known industrial processes. This utility of transition metals in these processes is typically a consequence of the energetically accessible chemistries and oxidation states permitted by d-orbitals.[1] The typically partially occupied valence d-orbitals allow for predictable reactivity and use of the transition metal compounds. Specific examples of d-block compounds employed as catalysts in industrial chemical processes include: the Haber-Bosch catalysis which produces ammonia with the assistance of the Iron-based catalyst, and the hydrogenation process in manufacturing of margarine in the presence of the Nickel-based catalyst. With increasing population, the demand for transition metals has also risen, which consequently led to scarcity (also described as “endangerment”) of some transition metals.[2] The American Chemical Society Green Chemistry Institute has reported that 44 elements are currently on the spectrum of limited availability to serious threat of depletion.[3]

In addition to their scarcity, these precious metals are typically extracted directly from the Earth’s crust which ultimately raises a concern about eco-viability of this methodology.[4] Lastly, due to the limited availability and the extraction process, the cost of transition metals continues to rise.

Faced with these adverse challenges, multiple research groups began to deliberately conduct research into recycling of transition metals, while others have shifted their efforts into finding alternatives to transition metals.

Main group elements (MGE) come as an inspiring alternative to traditional transition metals. Many main group elements are highly abundant in nature – making up 80% of the Earth's crust and present in all biological systems.[5] In addition to their abundance, main group elements are exceptionally chemically diverse which makes them useful for multiple applications of economic, environmental and industrial importance. Other key advantages include generally lower cost, which makes them more attractive to industry, and many have significantly lower toxicity compared with heavy metals.[6]

The chemical capabilities of the main group elements come from the s and p valence orbitals, the energies and directional properties of which can be "engineered" by coordinated moieties and ligands. Main group elements have been implemented in several notable processes, which traditionally would have relied on the incorporation of transitional metals. For example, Zhuang, *et al* have reported a boron-based electrolyte additive which enhanced the lithium-selenium battery performance by one hundred and thirty percent (Scheme 1).[7] The electrolyte additive consists of tris(trimethylsilyl) moieties on the central boron atom coordinated in a trigonal planar manner. This coordination enhances the fluoride-acceptor behaviour of the unoccupied valence orbitals of the boron atom. Hence, the impressive efficacy of this boron-based electrolyte additive lies upon the ability of the boron atom to absorb the undesired fluoride and polyanionoic (PF_x^-) groups, which prevents the formation of LiF layer and consequently allows for more lithium ions to be released. As a result, the electrochemical performance of the battery is significantly improved. Similarly, Reiter *et al* reported silylated silicon-carbonyl complexes as mimics of the traditional transition-metal carbonyls.[8] The mimicry of their compound is based on the Dewar-Chatt-Duncanson model of CO bonding.[9] Since silicon is a p-block element, it is unusual to see pi-back bonding to the carbonyl moiety, however Reiter *et al* demonstrate a bent donor-acceptor bonding motif, where the sigma donation is from the CO -> Si and pi-backdonation is from the silylene moiety to the carbonyl group. (Scheme 1). The mimicry of transition-metals extends further in Legare *et al* publication reporting dinitrogen conversion to ammonium chloride using a boron-based main group complex.[10] Dinitrogen is an inert, stable molecule, previously known to be cleaved using various transition-metal containing complexes, typically requiring extreme conditions. However, Legare

et al, reported a boron-based main group complex which was able to achieve nitrogen cleavage and conversion to ammonium chloride in a one-pot, room temperature reaction. The original intension was to convert dinitrogen to ammonia, which could serve as an alternative method to ammonia production, the primary ingredient in fertilizers. However, the authors were only able to produce ammonium, de-acification of which did not lead to ammonia production. The one-pot reaction involving the boron-based main group compound relies on the reduction and protonation steps, which are frequently observed in transition-metal based catalytic cycles.

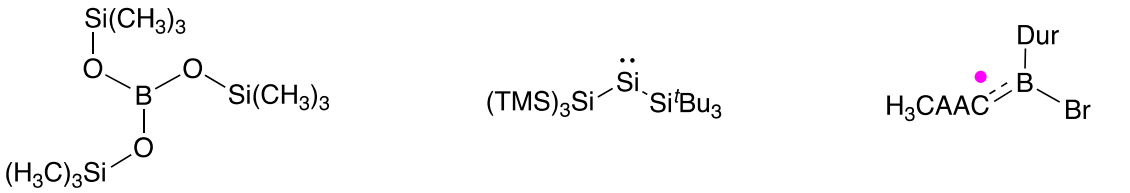

Zhuang *et al*, 2021 **Reiter *et al*, 2020** **Legare *et al*, 2020**

Scheme 1: Literature reported examples of main group element-based compounds with useful applications.

The potential of main-group based chemistry continues to grow and provide ecologically sustainable solutions to existing transition-metal relied upon processes. Although, main group elements may not be able to completely replace transition metals for all purposes, they have proved to be chemically capable of providing reliable and sometimes superior alternatives in many applications.

Main Group Element Catalysis

Chemical catalysis is a tremendously important and valuable field due to its ability to simplify the process conditions by lowering the activation energy for the desired chemical transformations. Most industrial processes such as oil refining, ammonia production, pollution control, and various others highly depend on catalysis to achieve the desired outcome.[11] Traditionally, homogeneous and heterogeneous catalysts are based on the d-block transition metal centers, which offer energetically accessible valence orbitals available for occupation by d electrons. As a result, transition metals provide predictable oxidation state changes and potentially advantageous substrate activation and transition state stabilization. Additionally, d-

block based catalysts can be further modified with steric and electronic effects of the ancillary ligand framework. The continuously growing field of catalyst development has led to a remarkable spectrum of catalyst systems capable of providing numerous chemical transformations more efficiently.[12] Nevertheless, main group species have demonstrated competitive and sometimes improved catalytic capabilities, especially towards activation of small molecules.

The principle behind reactivity of the main group species is based upon their increasing atomic radii and ns-np orbital energy gap, going down the periodic table. Second row elements exhibit especially interesting chemistry due to their atomic radii – the s and p orbitals are still relatively close in size to permit for s and p hydridization with substituents. Going down the row of the p-block, the larger atomic radii and increased energy gap between the s and p orbitals leads to a decreased propensity for the s-p hybridization and increases ns2 non-bonding ("lone pair") character.[13] As a result of this, heavier main group elements (E) tend to adopt trans-bent configurations, which contain substantially weaker π bonds (E=E), compared to traditionally seen multiple bonds between first-row p-block elements (B,C,N,O,F).[1] Additionally, these effects are seen in weakened σ-bond in E-H, E-E and E-E' type bonds. Therefore, in considerations of p-block element-based catalyst, the catalyst must be sufficiently reactive towards activation of the E-H bonds, but simultaneously remain considerably mild to sustain the resulting E-E and E-E' bonds. Furthermore, the energies of transition states and intermediates can be influenced by controlled substrate reactivity, which depends to relative polarity of the E-H bond. Importantly, the polarity of the E-H bond can reverse on the descending group in the p-block. Hence, the design of the prospective catalyst relies on careful considerations of the properties of the p-block element involved and the tuning of the MG element by the ligand framework or moieties.

Catalysts are generally classified into three main categories; homogeneous, heterogenous and biocatalysts. Biocatalysts are the naturally existing biological entities which speed up or enable certain chemical reactivity. Some examples include enzymes and nucleic acids, which are known to vector specific chemical reactions even outside living cells. Heterogenous catalysts

are generally synthetic chemical systems and they are often found in major industrial processes, due to their general ability for easy recovery and generation of the desired product. Heterogenous catalysts are catalysts which exist in a different phase than the reaction mixture, which tends to facilitate separation and purification to the target compounds. Such catalysts are used in, for example, the Fischer-Tropsch process, which is a process used for production of different hydrocarbons and the Haber-Bosch process for generation of ammonia. Homogenous catalysts are in the same phase as the reaction mixture. The homogeneity of the mixture allows for more direct interactions between all reaction species, and therefore high reactivity and selectivity of the reaction under mild reaction conditions. Furthermore, the homogeneity of the systems also facilitates characterization and renders them excellent for mechanistic studies. Examples of homogeneous types of catalysts include discrete olefin metathesis catalysts, and numerous catalysts employed in cross-coupling reactions.[14,15]

Lewis acid type catalysts are commonly seen in synthetic chemistry due to their well-established catalytic mechanism. They possess an electron-deficient site, which reacts by accepting electron-density from an electron-rich, Lewis basic species. Lewis acid catalysts have been employed in oxidation reactions,[16] hydrogenation,[17] cyanation,[18] ring-opening,[19] and various other chemical transformations. Increased development of Lewis acid catalysts, has led to development of Lewis acidity metric systems, which assesses the relative Lewis acidity of a given compound. Two of the most common Lewis acidity assessments methods are the Gutmann-Beckett test and the Fluoride Ion Affinity test.

Gutmann-Beckett Method

The Gutmann-Beckett (GB) test is based on the changes in chemical shifts observed in the Nuclear Magnetic Resonance (NMR) spectra. Specifically, the Lewis acidity of a given compound is assigned by examining the chemical shift of the Gutmann-Beckett reagent in the presence of the Lewis acid. The GB reagent is typically triethylphosphine oxide (Et_3PO) due to its solubility in most solvents and simplified tracking of the ^{31}P spectrum. Analogues of Et_3PO, such as Ph_3PO

have also been used but are less ideal because of the steric and electronic complications of the aryl groups.

Scheme 2: Gutmann-Beckett method for Lewis acidity strength determination.

The underlying principle for the test is that the lone pairs on the oxygen of Et_3PO will act as a Lewis base towards the Lewis acidic site of the compound and that stronger Lewis acids will coordinate the oxygen more strongly which will cause a greater downfield shift in ^{31}P. The difference in the chemical shift is then applied to equation 1 and an empirical acceptor number (AN) is determined.

$$AN = \frac{(\delta_{sample} - 41.0)}{86.14 - 41.0}\ x\ 100$$

Equation 1: Determination of the acceptor number (AN) used in the Gutmann-Beckett method.

In the equation 1 above, the δ_{sample} represents the ^{31}P chemical shift of the Lewis acid/Et_3PO adduct, 41.0 is the ^{31}P shift of Et_3PO in hexanes, a known weak acceptor and 86.14 is the ^{31}P shift of Et_3PO and $SbCl_5$, a known strong acceptor. These values are used as references to define the AN scale. The higher the acceptor number, the stronger the Lewis acid.

Fluoride Ion Affinity Method

Fluoride Ion Affinity (FIA) is a computational method of Lewis acidity assessment. The method is based on the enthalpic differences of the reactions in Scheme 3, from which the enthalpy of the adduct formation between the Lewis acid and the fluoride anion is calculated.

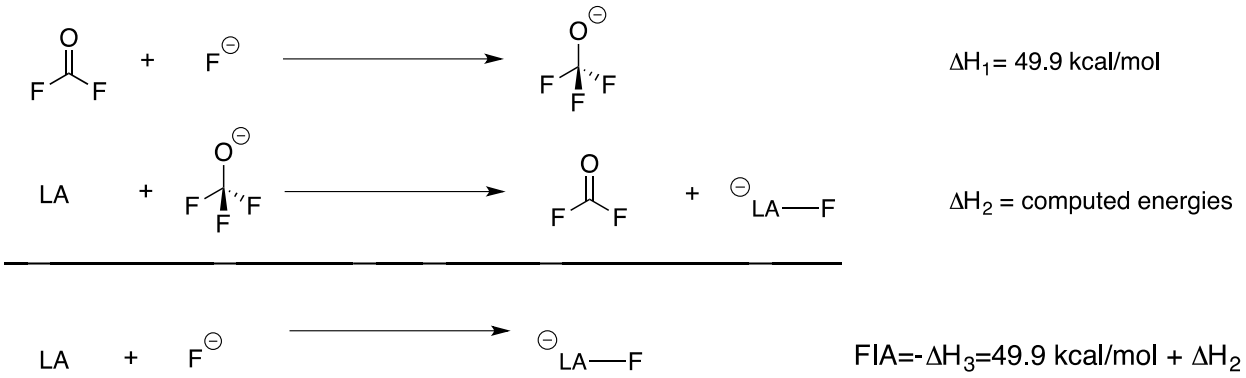

Scheme 3: Calculation of fluoride ion affinity for Lewis acid strength determination.

Similar to the GB method, the greater the negative value for FIA is (i.e. the more exothermic the process), the stronger the Lewis acid.

Since the initial reports of MGE-based Lewis acid catalysts, various other systems have been reported with their Lewis acidities assessed as shown in Figure 1. Special attention has been devoted to the design and synthesis of phosphorus-based Lewis acid catalysts, some of which are displayed in Figure 1.

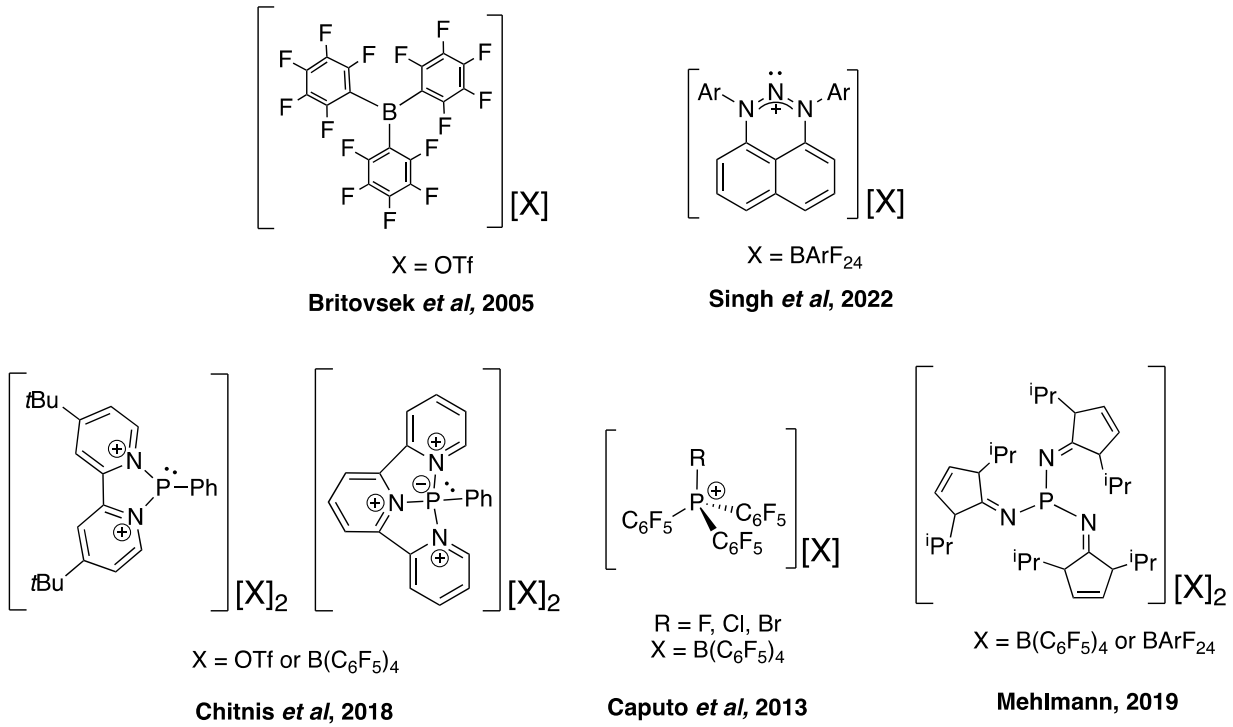

Figure 1: Literature reported examples of main group element-based catalysts.

Such concentrated efforts attributed to the development of phosphorus-based Lewis acids can be linked to the ability to influence the phosphorus' oxidation state by subsequent coordination. As mentioned previously, the second-row p-block elements, exhibit different behaviour from the first row, due to their low lying **σ*** orbital, which allows for hybridization with sigma orbitals of the substituents of interest, which can lead to influenced coordination and oxidation state of the phosphorus atom.

Phosphorus as alternative to Transition Metals

The discovery of phosphorus dates back to the late 17th century when the alchemist Hennig Brand was on the quest for the Philosopher's stone.[20] In his experiment of distillation of human urine, a white glowing solid now known as the elemental white phosphorus P_4 was produced and given the name "phosphoros" after the ancient Greek word for the planet Venus, meaning the "light bearer" or the morning star.[21]

Centuries later, phosphorus is classified as a non-metallic p-block element belonging to the group 15 pnictogens. It is an essential component of many biological systems with presence in nucleic acids, lipids, and plays a vital role in the formation of teeth and bones.[22] It is estimated that the earth's crust contains about 0.1% of phosphorus, making it 11th most abundant element. Industrially, phosphorus is highly demanded in fertilizer production, match-making, water-softening and organophosphorus compound generation.[23]

The accessibility of phosphorus and its rich chemical versatility has allowed research chemists to devote sufficient time and efforts into further investigation of phosphorus' nature and reactivity. The variety of possible oxidation states for phosphorus ranges from +5 to -3 with a maximum coordination number of six. This allowed for a prosperous library of phosphorus-based chemistries to be established, including materials and polymers,[24] and special dedication was allotted to trivalent organophosphorus compounds which were discovered to make excellent Lewis basic ligands, permitting for tunable reactivity and selectivity of organometallic compounds. Trivalent organophosphorus Lewis bases can be modified electronically and sterically by electron-donating or withdrawing substituents on the phosphine, which

subsequently influences the □-donating and □-accepting abilities of a given phosphine. The applicability of organophosphorus compound can be further extended to their use as Lewis acidic compounds, which has not been as exploited traditionally. One of the earliest introductions of Lewis acidic phosphorus reactivity was the Wittig reaction, which uses pentavalent phosphonium ylide (the Wittig reagent, P(V)) to convert aldehydes and ketones into alkenes.[25] More recently, research in phosphorus-based Lewis acids has been primarily focused on four-coordinate P(V) phosphonium salts with a positive charge. These often involve Lewis acidic cations with an accessible σ* orbital on the electron-deficient phosphorus center. The phosphorus cation is available for hypervalent interactions that would occur when an electron-donating substituent occupies the axial position on the phosphorus center, stabilizing the molecule.

Some of the earlier examples of phosphenium cations include the work of Cowley and Kemp,[26] which highlighted electrophilic reactions of phosphenium ions such as insertions into the C-H bonds in Cp_2Sn and reactions with 1,3- and 1,4-dienes to give cyclopentene-phosphonium derivatives. Gudat *et a*l.,[27] developed a N-heterocyclic phosphenium cation $[(C_2H_2NR)_2P]^+$ analogous of the well-known Arduengo's carbenes. They discovered that the cation exhibits a strong Lewis acidic character, rather than donating properties which are seen in N-heterocyclic carbenes (NHCs). Burford and Regogna reported examples of Lewis acidic phosphines involved in coordination chemistry.[28] In 2012, Slattery and Hussein investigated the Lewis acidity of phosphonium cations using the FIA method.[29] Their study concluded that phosphonium cations are significantly more Lewis acidic compared to other main group Lewis acids such as BF_3, BCl_3, ACl_3 and SbF_5.

An interesting case of both Lewis acidity and basicity present at a phosphorus center was reported by Dunn *et al*.[30] Starting with a three-coordinate P(III) compound, ammonia borane is activated by undergoing an oxidation to aminoborane with transferred hydrogens generating dihydridophosphorane, a pentavalent species P(V). An addition of azobenzene leads to the reduction of the P(V) back to P(III) as shown in Figure 2.

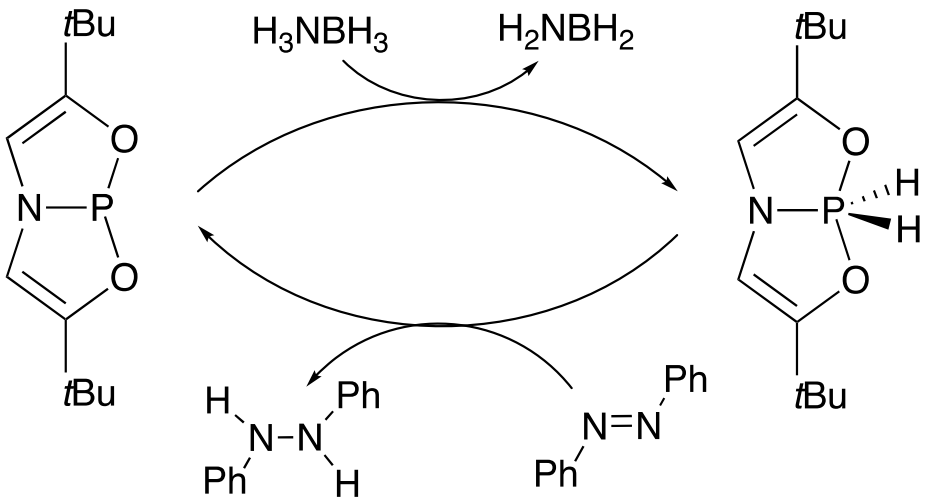

Figure 2: Catalytic two-electron redox reaction of a P(III)/P(V) redox species

The cycling between the two oxidation states of the phosphorus center is possible due to the distortion of the T-shaped geometry, where both the lone pair and the LUMO are easily accessible to the incoming substrates to distorted square pyramidal geometry seen in dihydridophosphorane. The influences on the reactivity of phosphorus induced by different substituents and ligands is related to another heavily researched subject in synthetic chemistry – the coordination chemistry.

Ligand design and Coordination Chemistry

The ligands or local environment around the acidic fragment is an important component in the design of a strong Lewis acid. Ideally, a ligand provides sufficient electronic stability to the center element, but does not interfere with the electrophilic center, whilst also being easily tunable upon desire to further enhance the compound's solubility characteristics. Such complex criteria have led to the development of various intricate ligand frameworks many of which include both symmetric and asymmetric multidentate systems.

In the design of a strong phosphorus-based Lewis acid, datively coordinating ligands, such as pyridine and its derivatives would make an ideal candidate, due to their σ-donating lone pair component. Chitnis *et al* have reported 2,2'-Bipyridine (bipy) and Terpyridine (terpy) – bound

strong Phosphorus-based Lewis acids,[31] while Gilhula and Radosevich employed a corrole-based ligand for a phosphorus-containing Lewis acid.[32] (Figure 3)

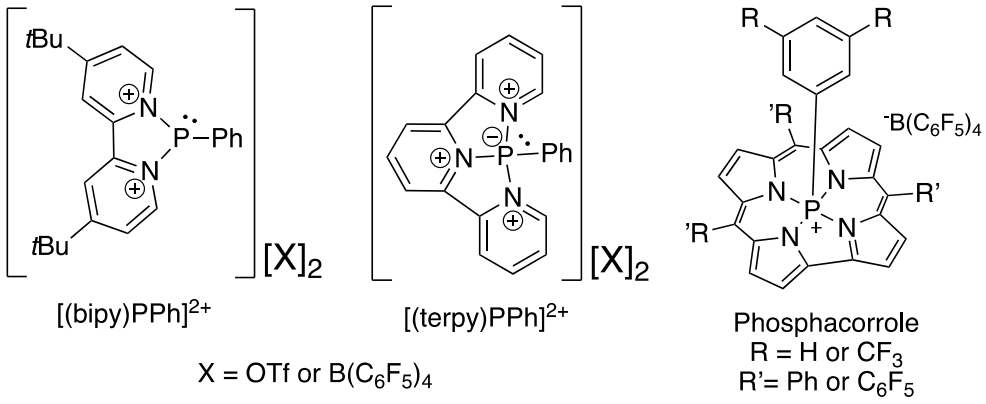

Figure 3: Literature reported examples of phosphorus-based Lewis acids.

A notable ligand framework which has been reported in synthesis with various transition metals and main group elements is the 2,6-Bis(benzimidazole-2-yl) pyridine (BZIMPY). Strauss *et al* investigated complexes bound by BZIMPY with Fe^{2+}, Mn^{2+}, Co^{2+}, Ni^{2+} and Zn^{2+},[33] while Wang *et al* reported BZIMPY synthesis with a lanthanide Lutetium (III).[34] Zhang *et al* showcased a unique self-assembly of platinum (II)-based BZIMPY compounds,[35] while Gunnaz reported an evaluation of catalytic reactivity of a copper (II) BZIMPY species.[36] Main group elements bound by the BZIMPY ligand have been reported by Swidan *et al*,[37] where germanium and tin of the group 14 were studied and Kocherga *et al* reported the synthesis of $Si(BZIMPY)_2$ complex as a potential electron transport layer and electroluminescent layer in organic electronic devices.[38]

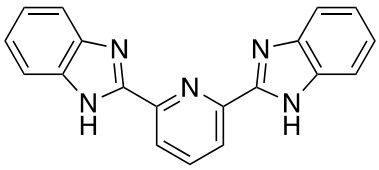

Figure 4: The general structure of 2,6-Bis(benzimidazole-2-yl) pyridine (NH-BZIMPY) ligand

The appeal of the BZIMPY ligand is based on its high rigidity and enforcement of tridentate coordination to the metal/MGE center, which provides electronic stabilization.[29] Furthermore,

the amine backbone of the ligand provides an easily accessible and highly modular substitution site, which can impart different steric, and electronic characteristics of the molecule. The selected substitutions can also contribute to the solubility of the complex and permit the use of less toxic and more environmentally conscious solvents.

The coordination of the BZIMPY ligand with phosphorus as the central element, permits for further optimizations of the given Lewis acid. Another coordination can occur directly at the phosphorus central atom and further influence the steric and electronic properties of the Lewis acidic phosphorus. Furthermore, the oxidation state of the phosphorus atom can be induced from P(III) to P(V) with the addition of a chalcogen element, further increasing the electron-deficiency of the phosphorus and therefore enhance the complex's Lewis acidity. The resulting phosphorus-based BZIMPY-bound cation, can be balanced with a selectively chosen counter anion which can also influence the solubility of the complex and permit for full expression of the complex' Lewis acidity.

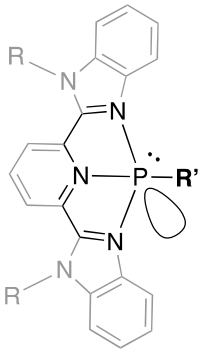

Figure 5: BZIMPY ligand induced electronics of the phosphorus atom

Scope of Thesis

The following work reports the synthesis of dicationic phosphorus-based BZIMPY bound Lewis acid variants, their spectral and computational characteristics and catalytic reactivity.

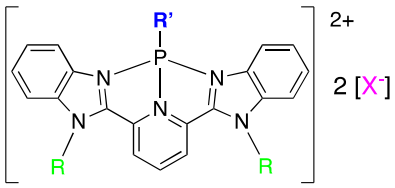

R = Allyl, Benzyl
R' = Ph, NMe_2
[X^-] = TMSOTf, $NaBArF_{24}$

Figure 6: The General Structure of [R-BZIMPY-R'][X]$_2$

The R substituents on the BZIMPY backbone were chosen to be allyl and benzyl groups to investigate steric, electronic and solubility influences on the compound. The R' moieties on the phosphorus central atom were selected to be a phenyl and dimethylamine groups to evaluate the impact of those groups on the electrophilic site. The X^- counter anion was chosen to be the triflate (OTf) and the barfate ($BArF_{24}$) to permit different expression of the Lewis acidity of the complex. The resulting Lewis acid variants were analyzed spectrally to confirm the structure using NMR, IR, UV-Vis, EA and XRD. The structures were further confirmed by computational calculations using the M06-2X/def2-TZVP level of theory. The Lewis acidity of the compounds was investigated by the experimental Gutmann-Beckett method and computational Fluoride Ion Affinity test. To further gain insight into the electronics of the synthesized Lewis acids, molecular orbitals HOMO and LUMO were computed using the M06-2X/def2-TZVP level of theory with GD3 empirical dispersion. Lastly, the prospective Lewis acid variants were tested as catalysts in the known/previously reported catalytic conversions.

Results and Discussion

A series of dicationic phosphorus-based Lewis acidic compounds were synthesized, characterized and tested in catalytic reactions (Figure 7). In general, all compounds were found to be prone to decomposition upon unintended introduction of moisture, oxygen, or other highly reactive species. Compounds **1a-d** and **2a-b** are yellow powders, whereas compounds **2c** and **2d** appear as red powders.

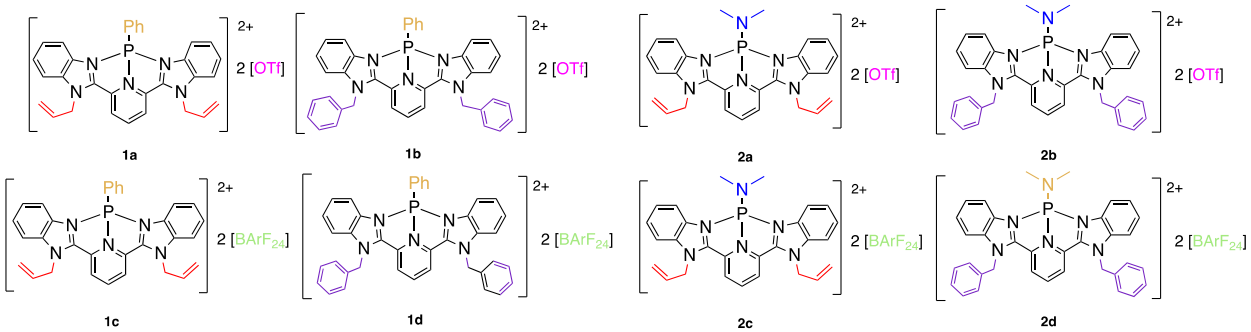

Figure 7: All variants of the dicationic Lewis acids displaying the allyl and benzyl BZIMPY backdones in red and purple, the phosphorus moieties phenyl and dimethylamino in orange and blue, and counter anions triflate and barfate in pink and green.

Synthesis and Characterization

Salts containing dicationic Lewis acids were synthesized under inert conditions and spectrally characterized using multinuclear nuclear magnetic resonance spectroscopy (NMR), infrared spectroscopy (IR), elemental analysis (EA), Ultraviolet-visible spectroscopy (UV-Vis) and X-Ray crystallography (XRD). Benzyl and Allyl variants of the 2,6-Bis(benzimidazole-2-yl) pyridine were synthesized and characterized as reported in the literature.[39,40] In each synthesis, a Benzyl or Allyl-substituted BZIMPY ligand was reacted in dichloromethane (DCM) at room temperature with a phosphorus source; either dichlorophenylphosphine ($PhPCl_2$) or dimethylaminophosphorus dichloride (Me_2NPCl_2) in the presence of two or four equivalents of the counter anion; either trimethylsilyl trifluoromethanesulfonate (TMSOTf) or sodium tetrakis[3,5-bis(trifluoromethyl)phenyl]borate (NaBArF) to afford the salts of the dicationic Lewis acids (Scheme 4) with impressively high yields of 86%, 83%, 89%, 87% for compounds **1a**, **1b**, **1c**, and **1d**, respectively and 94%, 94%,87%,99% for compounds **2a**, **2b** and **2c**, **2d** respectively.

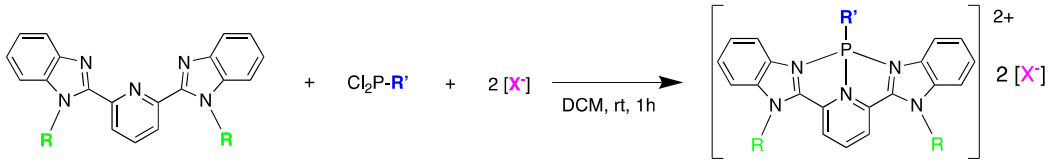

R = Allyl, Benzyl
R' = Ph, NMe_2
[X⁻] = TMSOTf, $NaBArF_{24}$

1a = $[Allyl\text{-}BZIMPY\text{-}PPh]^{2+}[OTf]_2$, 86%
1b = $[Benzyl\text{-}BZIMPY\text{-}PPh]^{2+}[OTf]_2$, 83%
1c = $[Allyl\text{-}BZIMPY\text{-}PPh]^{2+}[BArF_{24}]_2$, 89%
1d = $[Benzyl\text{-}BZIMPY\text{-}PPh]^{2+}[BArF_{24}]_2$, 87%
2a = $[Allyl\text{-}BZIMPY\text{-}PNMe_2]^{2+}[OTf]_2$, 94%
2b = $[Benzyl\text{-}BZIMPY\text{-}PNMe_2]^{2+}[OTf]_2$, 94%
2c = $[Allyl\text{-}BZIMPY\text{-}PNMe_2]^{2+}[BArF_{24}]_2$, 87%
2d = $[Benzyl\text{-}BZIMPY\text{-}PNMe_2]^{2+}[BArF_{24}]_2$, 99%

Scheme 4: Synthesis of the dicationic Lewis acids 1a-d and 2a-d.

The structure of compounds **1a-d** & **2a-d** was confirmed by ^{1}H NMR, with notable peaks at 4.92, 5.12, 5.41 and 5.91 ppm and 5.54, 6.81 and 7.15-7.25 ppm corresponding to allyl and benzyl backbone moieties of the BZIMPY-ligand, and 7.77 and 2.49 ppm peaks corresponding to phenyl and dimethylamine moieties on the central phosphorus atom. Heteronuclear single quantum coherence (HSQC) spectra were collected to confirm the connectivity between all proton and carbons atoms in the structure, notably, protons of the phenyl ring on the phosphorus atom correspond to carbons of the phenyl ring which signify a successful addition of the Ph-P moiety onto the BZIMPY ligand frame. Additionally, the protons of the dimethylamine correspond to peaks in ^{13}C, again, confirming successful addition of the Me_2NP onto the ligand framework.

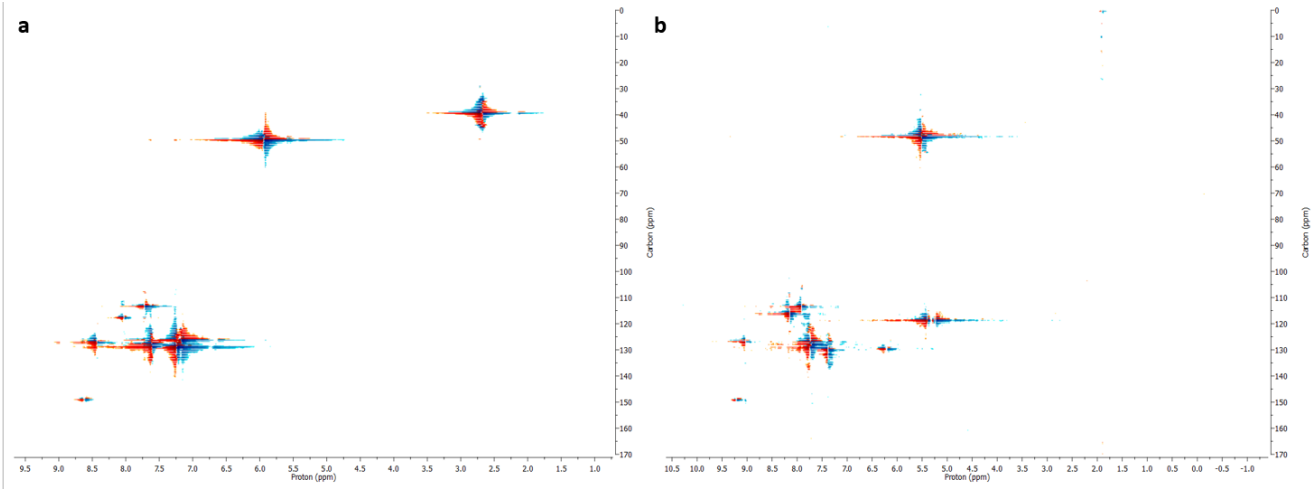

Figure 8: HSQC-NMR spectra demonstrating the connectivity between ^{1}H and ^{13}C of proton and carbon atoms in compound 1a (a) and 2b (b)

As indicated in Table 1, the ^{31}P chemical shifts of phenyl bound phosphorus were 10.7, 10.8, 14.9 and 15.4 ppm for compounds **1a**, **1b**, **1c** and **1d**, respectively. The resonances for the phosphorus atom bound to the dimethylamino fragments were located at 96.3, 96.3, 89.2 and 88.7 ppm for compounds **2a**, **2b**, **2c** and **2d**, respectively.

Table 1: $^{31}P[H]$ NMR signals of compounds 1a-d and 2a-d

Compound	31P[H] NMR chemical shift (ppm)
1a [Allyl-BZIMPY-PPh][OTf]$_2$	10.7
1b [Benzyl-BZIMPY-PPh][OTf]$_2$	10.8
1c [Allyl-BZIMPY-PPh][BArF]$_2$	14.9
1d [Benzyl-BZIMPY-PPh][BArF]$_2$	15.4
2a [Allyl-BZIMPY-PNMe$_2$][OTf]$_2$	96.3
2b [Benzyl-BZIMPY- PNMe$_2$][OTf]$_2$	96.3
2c [Allyl-BZIMPY- PNMe$_2$][OTf]$_2$	89.2
2d [Benzyl-BZIMPY- PNMe$_2$][OTf]$_2$	88.7

For compounds **1a,b** and **2a,b**, the ^{19}F spectra show a singlet peak at -79.3 ppm which is consistent with ^{19}F signal of the triflate [OTf] anion. For compounds **1c,d** and **2c,d**, ^{19}F spectra display a peak at -62.7 ppm corresponding to the signal of the -CF_3 in the barfate [$BArF_{24}$] anion. Finally, the ^{11}B spectra display a peak at -7.65 ppm, which is indicative of the 4-coordinate boron atom found in the anion of salts **1c,d** and **2c,d**. The integrations of phosphenium cation and borate anion match the 1:2 ratio of the salt. Elemental analysis (EA) further confirmed the composition of salts **1a-d** and **2a-d**, the experimental results were consistent with calculated The growth of high-quality crystals was attempted for all compounds, but only crystals of compound **1a** proved to be suitable for XRD (Figure 9). The crystal was obtained by slow-diffusion of the compound in acetonitrile with diethyl ether.

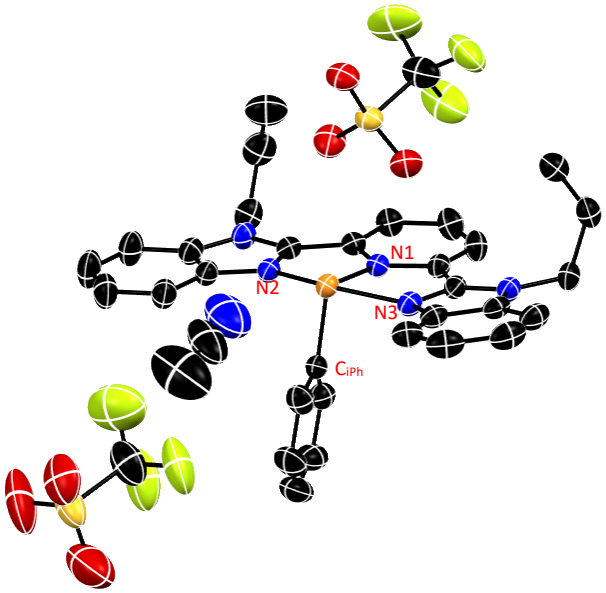

Figure 9: ORTEP (30% probability surface) depiction of compound 1a. Hydrogen atoms omitted for clarity. Acetonitrile solvent is included to show proximity to cation. Carbon: black,Phosphorus: orange,Nitrogen: blue,Fluorine: Neon-green,Sulfur: yellow,Oxygen: red.

The crystallographic data obtained confirms the formation of the target salt and reveals the structural arrangements of the atoms. The central phosphorus atom is coordinated in a tridentate manner to the 2,6-Bis(benzimidazol-2-yl) pyridine (BZIMPY) ligand, with a sum of angles adding up to 319.96^{O}, and the P atom is located in nearly the same plane as the ligand. The phenyl ring bound to the phosphorus by the ipso carbon atom (C_{ipso}Ph) is located perpendicularly to the rest of the structure with an angle of 90.14^{o} between the N1-P-C_{i}Ph atoms. This arrangement is consistent with the target arrangement that should allow the unoccupied orbitals of the phosphorus to be exposed to an incoming donor. Additionally, the dihedral angle measured between C_{o}Ph - C_{i}Ph -P-N1 is 179^{o}, indicating that the phenyl ring is not twisted to either side of the ligand. The structure also reveals that one of the triflate counter anions sits above the plane of the dication opposite the phenyl group and features distances of 3.312(3) Å & 3.352(3) Å between O1 & O3 of the anions to P of the dication. Interestingly, one acetonitrile solvent of crystallization is located in relatively proximity to the electron-deficient phosphorus, specifically, the bond length measured between the nitrogen atom of the acetonitrile to the phosphorus center is 4.017(7) Å, indicating a probability of the solvent

coordination to the Lewis acidic site, which would consequently decrease the reactivity of the dication. The bond length of the pyridyl nitrogen and phosphorus atom is 1.842(2) Å, which is consistent with a dative interaction.[41] The bond distances between the phosphorus centre and the nitrogen atoms of the bzimpy wings are notably different, with bond lengths of 1.899(2) Å and 2.064(2) Å for P-N2 and P-N3, respectively. For context, the standard P-N bond lengths reported in the literature[31] are displayed in Table 2. Similar literature compounds were found to have a P-N bond length of 1.82 Å for $[(terpy)PPh]^{2+}$,[31] and 1.76 Å, 1.81 Å and 1.80 Å for compounds $[(dmap)_2PPh]^{2+}$, $[(bipy)PPh]^{2+}$ and $[(Bbipy)PPh]^{2+}$.[42]

Table 2: Comparison of P-N bond lengths in 1a and literature reported compounds.

Compounds and P-N bonds	Bond Length (Å)
P-N	1.77
P=N	1.57
P≡N	1.49
1a	1.85
$[(terpy)PPh]^{2+}$	1.82
$[(dmap)2PPh]^{2+}$	1.76
$[(bipy)PPh]^{2+}$	1.81
$[(Bbipy)PPh]^{2+}$	1.80

Moisture/Oxygen Tolerance

Initial moisture instability of the dicationic Lewis acids was observed upon unintended exposure of them to air – from bright yellow powder salts, the compounds turned white. The decomposition product was characterized by ^{1}H NMR, which revealed an additional singlet at 13.9 ppm signifying protonation at the chelate/pincer site, as well as ^{31}P NMR which was silent, indicating the absence of the phosphorus atom in the compound. To further investigate the target of the protonation site, the allyl-BZIMPY ligand was reacted with 2 equivalents of the trifluoromethanesulfonic acid (HOTf) to observe the primary target for protonation of the ligand. Indeed, ^{1}H NMR confirmed the protonation at the pincer site of the ligand (Figure 68). The protonation site of the ligand was further confirmed by the obtained crystal structure

shown in Figure 10. The figure displays two hydrogen atoms at the nitrogen atoms of the Allyl-BZIMPY ligand.

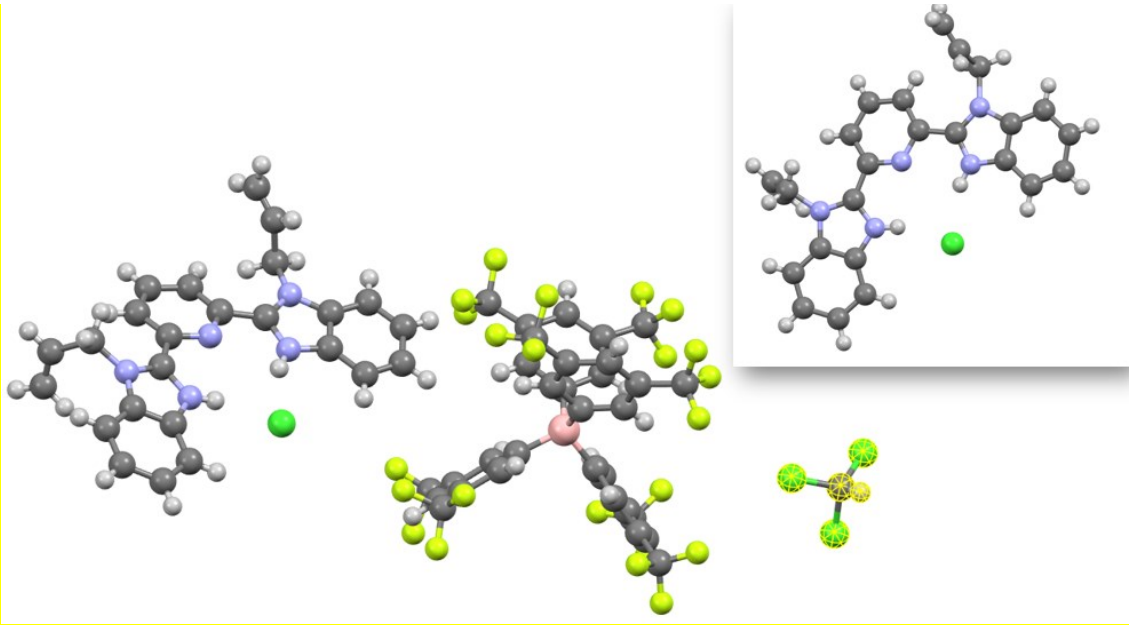

Figure 10: ORTEP of a protonated Allyl-BZIMPY ligand obtained by exposure to oxygen and moisture. The counter anion is $BArF_{24}$, the atom in green is Cl^- and the solvent in $CHCl_3$.

Compounds were further tested by direct exposure to H_2O and D_2O. Interestingly, all results varied from each other; the ^1H NMR shows a singlet at 4.80 ppm for water, however ^{31}P NMR spectra show different results for each compound. For compounds **1a** and **1b**, ^{31}P NMR spectra exhibited a singlet peak at 19.8 ppm, which has previously been reported for a H-P=O bond in compound HASPO[43] shown in Figure 11.

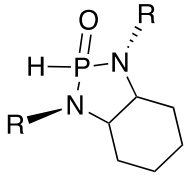

R = Mes, ^{t}Bu, Me,
Bn, Ph, ^{i}Pr
HASPO
Chang *et al*, 2016

Figure 11: Literature reported HASPO compound with H-P=O bond.

Compound **2a** showed peaks at 3.52, -4.92, and -156.73 ppm, compounds **1c** and **1d** were silent in ^{31}P NMR spectra, however, both compounds visually turned into a purple solution,

potentially signifying a formation of a radical. Finally, for compound **2c** a triplet was observed at 2.67 ppm, which has also been reported for P-D coupling in the byproduct of HOPD(=O)-O-PD(=O)OH and OPD(=O)-O-PD(=O)O^{2-},[43] and compound **2d** displayed a single peak at 36.59 ppm.

The Gutmann Beckett assessment of Lewis acidity

The Lewis acidity of compounds **1a-d** & **2a-d** was assessed experimentally using the Gutmann-Beckett (GB) test. Compounds **1a-d** & **2a-d** were reacted with Lewis basic GB reagents, such as triethylphosphine oxide (Et_3PO) in a 1:1 ratio and the difference in the chemical shift ($\Delta\delta$) of the ^{31}P NMR resonance was measured to calculate the acceptor number (AN) (Equation 1) as per reaction in Scheme 2. Based on the difference of the chemical shift in ^{31}P NMR, the acceptor number for each compound was calculated and are displayed in Table 3.

Table 3: The calculated Gutmann-Beckett acceptor numbers for Lewis acids 1a-d & 2a-d based off the changes in chemical shifts in ^{31}P NMR.

Lewis Acid	Acceptor Number
1a [Allyl-BZIMPY-PPh][OTf]$_2$	68
1b [Benzyl-BZIMPY-PPh][OTf]$_2$	116
1c [Allyl-BZIMPY-PPh][BArF]$_2$	116
1d [Benzyl-BZIMPY-PPh][BArF]$_2$	116
2a [Allyl-BZIMPY-PNMe$_2$][OTf]$_2$	120
2b [Benzyl-BZIMPY- PNMe$_2$][OTf]$_2$	120
2c [Allyl-BZIMPY- PNMe$_2$][OTf]$_2$	120
2d [Benzyl-BZIMPY- PNMe$_2$][OTf]$_2$	112

In the reaction of compound **1a** & **1b** with Et_3PO, a broad peak at 88 ppm is visible in each ^{31}P NMR spectrum. This peak is attributed to the adduct formed between the phosphorus of **1a** and **1b**, and the oxygen of the Et_3PO. The ^{31}P NMR spectra of compounds **2a-d**, & **1c** & **1d**, also display the adduct peaks at around 103 ppm, as well as a peak at approximately 135 ppm, which is postulated to be an oxygenated phosphorus compound such as [R-BZIMPY-PO][X], formed upon abstraction of the oxygen from triethylphosphine oxide. The calculated acceptor numbers for all Lewis acid suggest a highly Lewis acidic character.

In comparison, for other phosphorus-based Lewis acids reported in the literature (Scheme 12), the Gutmann-Beckett acceptor numbers were found to be lower, which suggests that BZIMPY-bound phosphorus-based Lewis acids exhibit superior Lewis acidity and potentially reactivity.

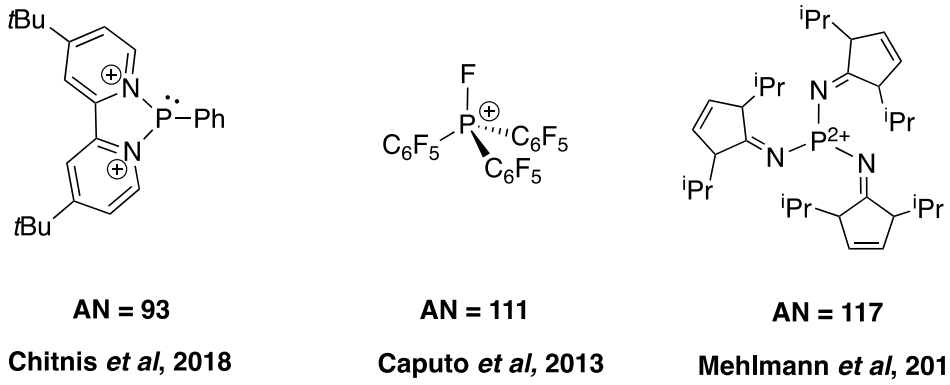

AN = 93 **AN = 111** **AN = 117**

Chitnis *et al*, 2018 **Caputo *et al,* 2013** **Mehlmann *et al*, 2019**

Figure 12: Literature reported phosphorus-based Lewis acids with calculated Gutmann-Beckett acceptor numbers.

Computational Assessment of Lewis acids

Structural Analysis of [(Me-BZIMPY-PR')$^{2+}$

Structural optimization of [(Me-BZIMPY)-R'] was completed using *Gaussian 16* package[44] using M06-2X[45] functional theory and the def2-TZVP[46] basis set with the inclusion of Grimme's GD3 empirical dispersion[47] method. For computational simplification, the allyl and benzyl substituents on N located at the back of the BZIMPY ligand were modeled as methyl substituents. The inductive donation of electron density from allyl and benzyl groups is similar to that of the methyl groups and the steric bulk imparted by the either the allyl or benzyl groups are directed away from the Lewis acidic phosphorus site, therefore the simplification is not anticipated to alter the results of the electronic structure substantially.

The optimized geometries of [(Me-BZIMPY)PR']$^{2+}$ where R' is PPh and $PNMe_2$ are displayed in Figure 13 and Figure 14.

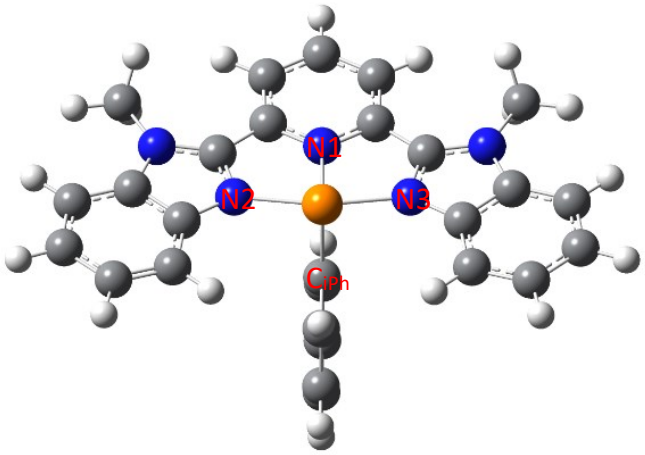

Figure 13: Computationally calculated optimized structure of [(Me-BZIMPY)PR'][2+]

The computed bond angles and distances for [Me-BZIMPY-PR']$^{2+}$ correspond to those collected by the XRD analysis. The comparison between the computed structure and experimentally obtained structure are depicted in Table 4.

Table 4: The comparison between the experimentally obtained crystal structure of compound 1a and computationally calculated bond angles and lengths of [Me-BZIMPY-PPh][2+.

	Experimental		Computed	
Bond (angle/distance)	**Angle (°)**	**Distance (Å)**	**Angle (°)**	**Distance (Å)**
iPh-P-N1/ P-N1	103.08(10)	1.842(2)	105.39	1.8496
iPh-P-N2/ P-N2	90.15(10)	1.899(2)	89.88	1.9687
iPh-P-N3/ P-N3	88.73(10)	2.064(2)	89.97	1.9641
N2-P-N1/ iPh-P	81.14(9)	1.839(2)	79.96	1.8198
N1-P-N3	79.29(9)		80	
N2-P-N3	159.60(9)		159.16	
SUM PNNN	320.03		319.12	
***o*Ph-*i*Ph-P-N1 (dihedral)**	156.5(2)		181.01	

An optimized structure was also computed for [Me-BZIMPY-PNMe$_2$]$^{2+}$ variant of the Lewis acid and is depicted below in Figure 14.

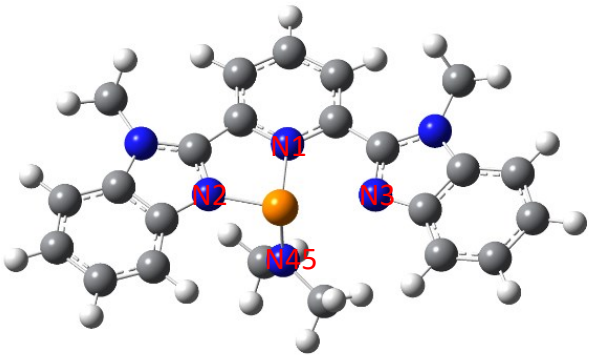

Figure 14: Computationally calculated optimized structure of [Me-BZIMPY-PNMe$_2$]$^{2+}$

Bond distances and angles were also computed to further gain insight into the structural arrangement of atoms in the Lewis acid depicted in Table 5.

Table 5: Computed bond angles and distances of [Me-BZIMPY-PNMe$_2$]$^{2+}$

Bond	Angle (°)	Bond	Distance (Å)
N45-P-N1	106.86	**P-N1**	1.9306
N45-P-N2	94.53	**P-N2**	1.823
N45-P-N3	89.78	**P-N3**	2.3878
N2-P-N1	81.17	**P-N45**	1.6397
N1-P-N3	74.99		
N2-P-N3	156		
SUM PNNN	312.16		
C46-N45-P-N1 (dihedral)	124.64		

The sum of angles measured between N1, N2 and N3 of the ligand and P was calculated to be 312.16°, which indicates that the phosphorus atom does not align within the plane of the pincer site of the ligand, but rather is slightly above the pincer plane. The calculated dihedral angle between C46-N45, the dimethyl moiety on the phosphorus, and P-N1, the pyridyl nitrogen of the ligand was 124.65°, while not as perpendicular to the ligand frame as in the case of the PPh variant, the dimethylamine moiety is oriented roughly perpendicular to the BZIMPY-Me ligand, which again is consistent with the target molecular geometry. In comparison, Marre *et al*[48] report a bond distance of 1.620(7) Å between the phosphorus and the nitrogen of

dimethylamino moiety and Brunel *et al*[49] report a distance of 1.633(2) Å for the same type of bond in their compound as shown in Figure 15.

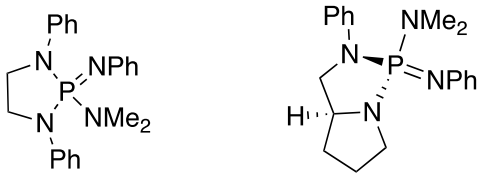

Marre *et al*, 1984 **Brunel *et al*, 1999**

Figure 15: Literature reported compounds containing P-NMe_2 bond for comparison with [Me-BZIMPY-PNMe2]$^{2+}$

Electronic distributions of [Me-BZIMPY-PR']

Natural Bond Orbitals (NBO) and Wiberg Bond Indices (WBIs)

Natural bond orbitals[50] were computed for the [Me-BZIMPY-PR']$^{2+}$ models to further understand the Lewis-like molecular bonding pattern of electrons and electron pairs in the optimized structures. The resultant NPA charge distributions are shown in Figure 16.

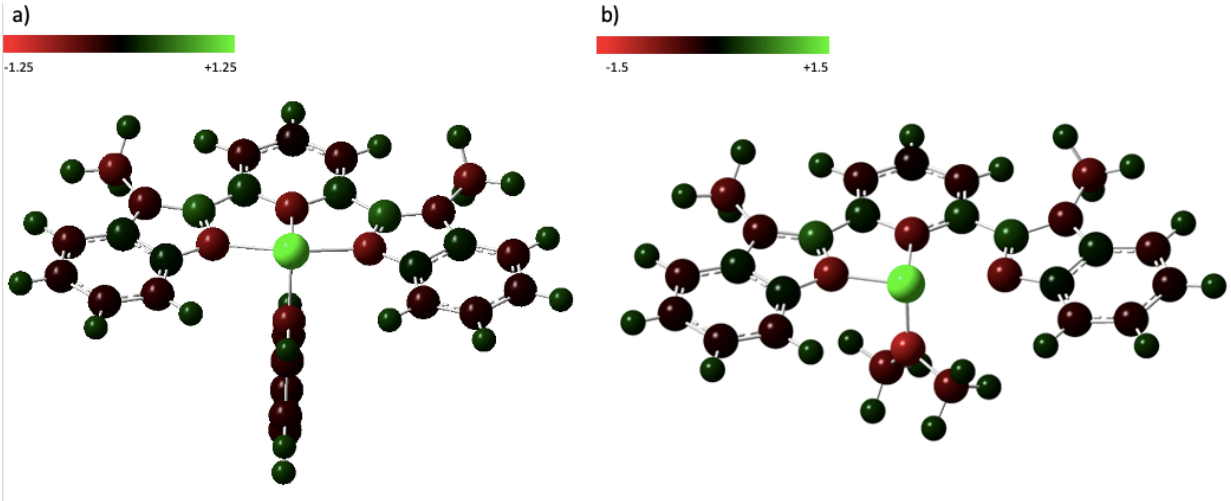

Figure 16: Computed NBOs charge distributions of [Me-BZIMPY-PPh]$^{2+}$ in a) and [Me-BZIMPY-PNMe2]$^{2+}$ using NBO 6.0[50] at the M06-2X/def2-TZVP level of theory.

Computations were performed at the M06-2X/def2-TZVP level of theory to assess the charge distributions among the Lewis acids. As assessed by natural atomic charges, the phosphorus atom was found to have the most cationic charge of 1.25 e and 1.50 e for structure in Figure

16a and 16b, respectively, whereas the pincer nitrogen atoms of the ligand (N1,N2 and N3) exhibit a negative charge of -1.25 e and -1.50 e, respectively. Wiberg bond indices were calculated to assess the magnitude of covalent electron population overlap between the atoms and the results are displayed in Table 6.

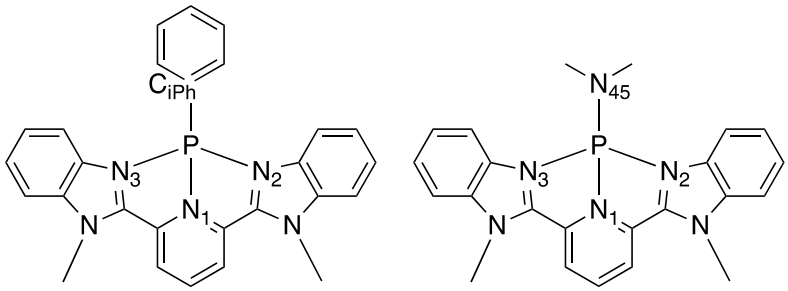

Figure 17: Representation of assigned atoms in [Me-BZIMPY-PPh]$^{2+}$ and [Me-BZIMPY-PNMe$_2$]$^{2+}$ for WBI

Table 6: Wiberg bond indices calculated for [Me-BZIMPY-PPh]$^{2+}$ and [Me-BZIMPY-PNMe2]$^{2+}$

Bond	WBI for [Me-BZIMPY-PPh]$^{2+}$	WBI for [Me-BZIMPY-PNMe2]$^{2+}$
P-N1	0.6443	0.5391
P-N2	0.4549	0.571
P-N3	0.4581	0.1922
P-iPh	0.9005	N/A
P-N45	N/A	0.979

The calculated WBIs suggest a single bond character of the phosphorus-phenyl bond (P-iPh of 0.90), a low single-bond character for the pyridyl nitrogen and phosphorus bond (P-N1), which is typical for single bonds with substantial ionic character and a partial bond character for the P-N2 and P-N3 bond of 0.45 and 0.46, respectively. These values are consistent with the relatively long bonds observed in the structure and are best understood as being typical donor-acceptor (dative, coordination) bonds. The similarity of the WBI values for the two benzimidazole contacts illustrates the relatively symmetrical binding of the P atom by the ligand. In contrast, the WBIs calculated for [Me-BZIMPY-PNMe$_2$]$^{2+}$ variant show a bond character of 0.54 and 0.57 for P-N1 and P-N2, respectively but the WBI for P-N3 is calculated to be 0.19, suggesting a much more asymmetric binding arrangement of the ligand, and perhaps suggests a greater measure of lability for one arm of the BZIMPY chelate. Finally, the WBI for P-N45 was calculated to be

0.98 consistent with the single bond character, as also seen in the optimized structure in Figure 14. It is possible that the presence of the additional non-bonding pair of electrons on the NMe_2 fragment may decrease the electron-deficiency of the P atom and favor the asymmetrical ligand binding.

Molecular Orbital Theory calculations for [Me-BZIMPY-PR']$^{2+}$

To assess the electron distribution among the orbitals of each atom in the Lewis acid, HOMO and LUMO structures were obtained and are displayed in Figure 18 and Figure 19.

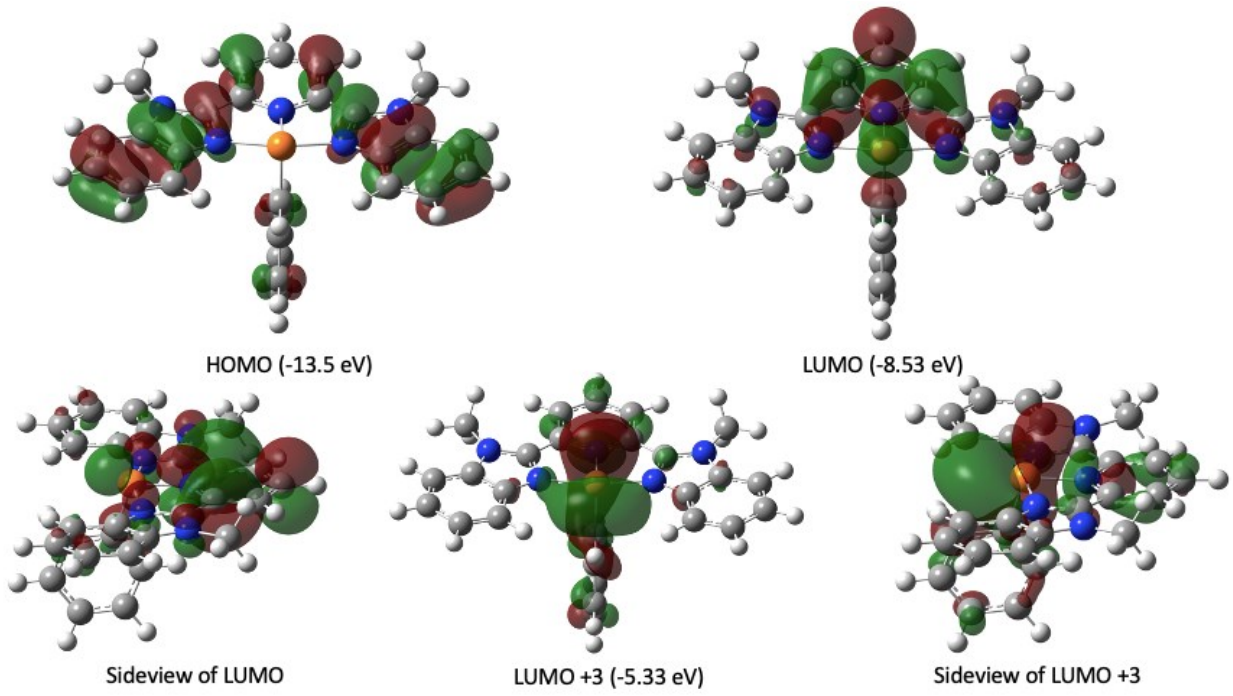

Figure 18: HOMO, LUMO and LUMO+3 of [Me-BZIMPY-PPh]$^{2+}$ calculated using M06-2X/def2-TZVP level of theory.

As depicted in Figure 18, the HOMO of [Me-BZIMPY-PPh]$^{2+}$ are distributed along the π systems of the BZIMPY ligand and the phenyl ring moiety of the phosphorus. The low-lying unoccupied orbitals of the [Me-BZIMPY-PPh]$^{2+}$ were calculated to reveal where the acceptor orbitals of the Lewis acids will be. As shown in Figure 18, the LUMO of the [Me-BZIMPY-PPh]$^{2+}$ was calculated to be -8.53 eV and with orbitals located primarily on the phosphorus atom and the pyridine ring of the BZIMPY ligand. LUMO +3 was calculated to be -5.33 eV and shows a large unoccupied orbital on the phosphorus atom, consistent with a 3p-type orbital with a vacant lobe extending

into the cavity of the complex. When comparing to other known phosphorus-based Lewis acids, the energy of LUMO is lower than that of Mehlmann's Lewis acid (-6.34 eV),[51] which has a tricoordinate arrangement, but is considerably larger than that of the phosphorus(III) dication $[Me_3P]^{2+}$ with the energy of -15.67 eV.[51] This is reasonable due to the electron-donating nature of the pincer nitrogens of the BZIMPY ligand. The antibonding P-N1 orbital corresponds to 49.7% of LUMO+3 and the antibonding orbital of P-iPh corresponds to 7.2% of LUMO+3. Similarly to $[Me\text{-}BZIMPY\text{-}PPh]^{2+}$ variant, the molecular orbitals were calculated and depicted for $[Me\text{-}BZIMPY\text{-}PNMe_2]^{2+}$ shown in Figure 19.

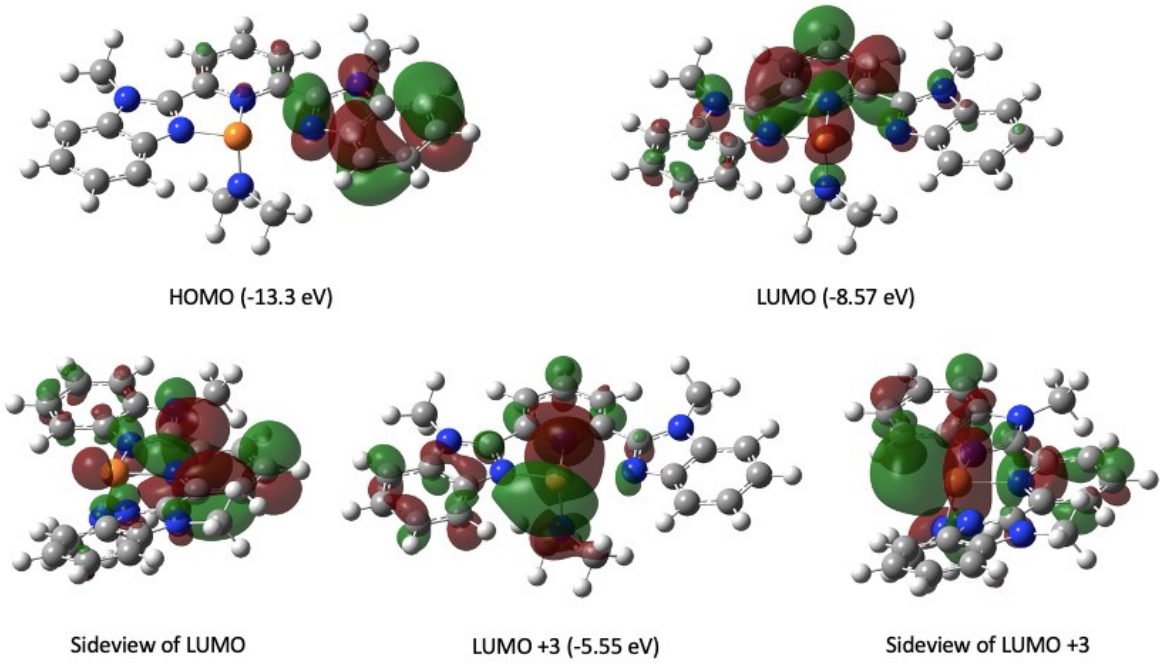

Figure 19: HOMO, LUMO and LUMO+3 of $[Me\text{-}BZIMPY\text{-}PNMe_2]^{2+}$ calculated using M06-2X/def2-TZVP level of theory.

As in the previous example, the HOMO of $[Me\text{-}BZIMPY\text{-}PNMe_2]^{2+}$ is distributed among the π orbitals of the aromatic BZIMPY ligand. Additionally, similarly to the previous variant depicted above in Figure 18, the LUMO of the Lewis acid located across the pyridyl ring of the BZIMPY ligand and the phosphorus atom. Again, the LUMO +3 shows a large lobe on the phosphorus atom, consistent with the possibility of the P atom to interact with donors. Interestingly, when comparing the LUMO +3 orbitals and their relative energies of the two $[Me\text{-}BZIMPY\text{-}PR']^{2+}$ Lewis acids, the $[Me\text{-}BZIMPY\text{-}NMe_2]^{2+}$ LUMO +3 energy is slightly lower than that of $[Me\text{-}BZIMPY\text{-}PPh]^{2+}$ variant. This result is consistent with the difference in electron-withdrawing abilities

between the carbon of the phenyl fragment to the phosphorus versus the nitrogen of the dimethylamine moiety to the phosphorus. With this in mind, the Lewis acidic phosphorus site can be influenced based on the moieties attached to it and different reactivity can be expected from the two variants.

Computational Assessment of Lewis acidity

Fluoride Ion Affinity (FIA) test was conducted to further investigate the Lewis acidity of [Me-BZIMPY-PR']. The test is based on the ability of the Lewis acid to abstract the fluoride anion, after which the FIA value is determined based on the enthalpies exerted by individual step reactions. The higher the FIA value, the higher the predicted Lewis acidity. The full reaction is exhibited in Scheme 5.

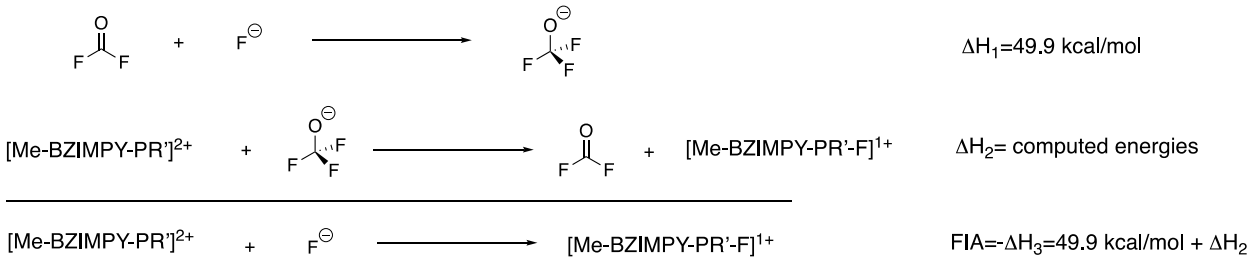

Scheme 5: FIA reaction for computational Lewis acid assessment of [Me-BZIMPY-PR']$^{2+}$

The computed FIA values for [Me-BZIMPY-PPh]$^{2+}$ and [Me-BZIMPY-PNMe$_2$]$^{2+}$ were 896 kJ/mol and 905 kJ/mol, respectively. The computational FIA results are consistent with the experimental Gutmann-Beckett test findings, indicating high Lewis-acidity for both variants of the compounds. For context, these FIA values can be compared to other reported Lewis acids and the results are shown in Table 7.

Table 7: Comparison of FIA values of the literature reported compounds and [Me-BZIMPY-PPh]$^{2+}$ and [Me-BZIMPY-PNMe$_2$]$^{2+}$

Lewis acid	FIA value (kJ/mol)
[Me-BZIMPY-PNMe$_2$]$^{2+}$	905
[Me-BZIMPY-PPh]$^{2+}$	896
[(bipy)PPh]$^{2+}$ [52]	803
[PPh$_2$]$^{+}$ [51]	795
[Si(Mes)$_3$]$^{+}$ [51]	793
[(terpy)PPh]$^{2+}$	783
[(C$_6$F$_5$)$_3$PF]$^{+}$ [53]	779
[Ph$_3$C]$^{+}$ [53]	657
B(C$_6$F$_5$)$_3$ [54]	445

It is evident that [Me-BZIMPY-PR']$^{2+}$ compounds presented in this work are superior to most of the acids reported in the literature and could therefore exhibit greater reactivity and catalytic performance.

Reactivity Studies

Stoichiometric and catalytic reactivity studies were performed to assess the performance of compounds **1a-d** and **2a-d**. For stoichiometric assessment, the Lewis acids were reacted in varying ratios with triphenylphosphine (PPh$_3$). This reagent was chosen as a good source of a Lewis base, which can be assessed by ^{31}P NMR. Compounds **1a**, **1b** and **2a** and **2b** show similar reactivity towards PPh$_3$ as shown in Figure 20.

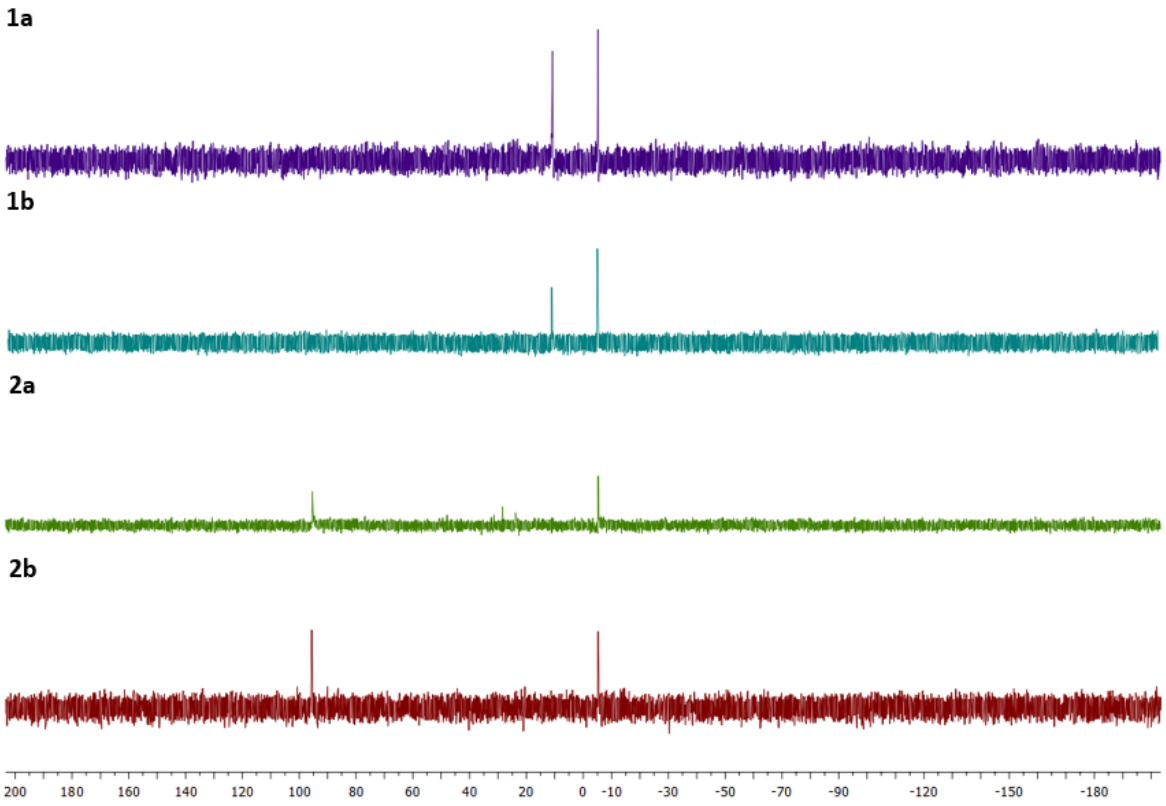

Figure 20: ^{31}P NMR spectra of the reaction between compounds 1a,b and 2a,b with 1 equivalent of PPh_3.

The stacked set of spectra above demonstrates the results of the reaction between **1a**, **1b**, **2a** and **2b** with PPh_3. For compounds **1a** and **1b**, the two peaks seen in ^{31}P NMR correspond to the phosphorus peaks of the Lewis acids at approximately 10 ppm and the phosphorus peak of triphenylphosphine at approximately -5.5 ppm. Spectra of compounds **2a** and **2b** also exhibit two peaks which correspond to the Lewis acid phosphorus nuclei at approximately 95 ppm and the triphenylphosphine phosphorus peak at about -5.5 ppm. The pyramidal shape of the PPh_3 allows for the lone pair on the phosphorus to serve as a donor to numerous acceptors, thus we wished to determine if it would act as the Lewis base towards the Lewis acidic site of compounds **1a,b** and **2a,b**. This type of bonding has the potential to result in a formation of an adduct of the two compounds or formation of a frustrated Lewis pair. However, as seen in Figure 20, no adducts were generated. This could be explained by considering the nature of the compounds in the mixture – both the triphenylphosphine and the Lewis acid variants are considered to be bulky molecules due to the possession of large aromatic groups. When reacting two or more bulky species, steric hindrance often takes place, and the formation of the

product becomes unfavourable. Perhaps more importantly, compounds **1a,b** and **2a,b** all contain triflate as their counter-anion, which is small enough to coordinate to the Lewis acidic site, and therefore decrease its reactivity. Lastly, having the triflate as the counter anion, makes these salts (**1a**, **1b** and **2a**, **2b**) only soluble in acetonitrile, which is a coordinating solvent that could also interact with the Lewis acid. Therefore, there are at least two competing species for the Lewis acidic site outside of any other reagents.

For this reason, the barfate salts were prepared in an attempt to access the targeted acidic behaviour. Gratifyingly, the results for the compounds **1c**, **1d**, **2c** and **2d** are drastically different than those of the triflate salts. Compound **1c**, when reacted in a 1:1 mole ratio with PPh_3 exhibits six peaks in ^{31}P NMR spectrum shown in Figure 21.

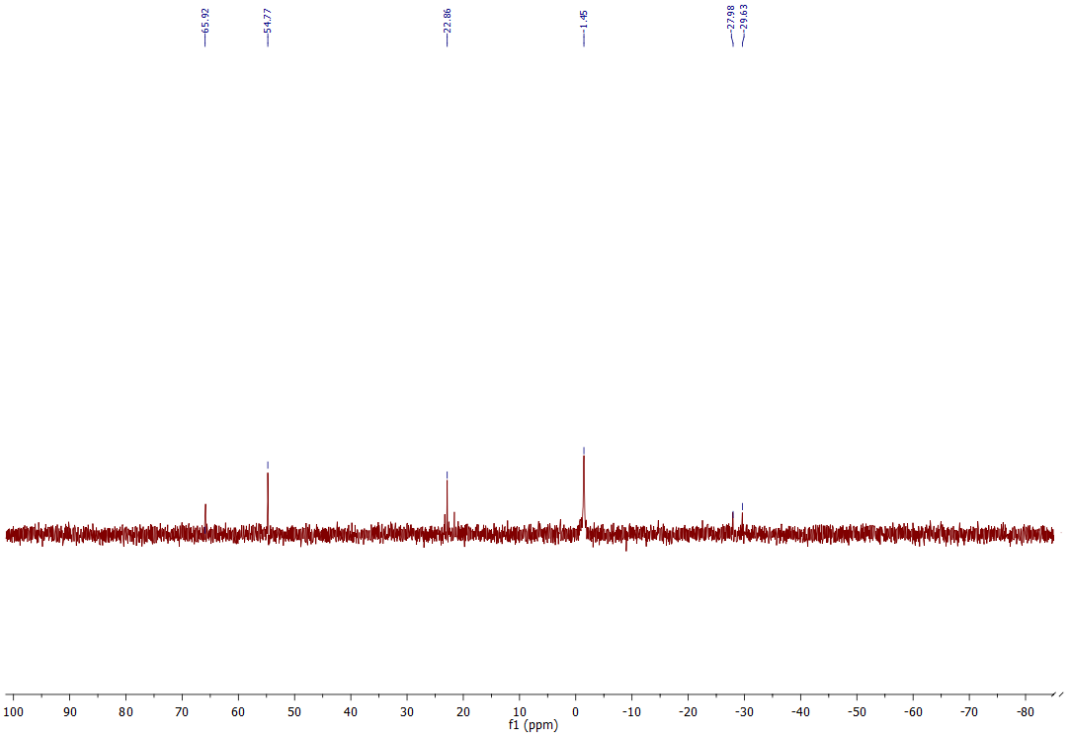

Figure 21: ^{31}P spectrum of the reaction between compound 1d and PPh_3 in a 1:1 ratio conducted in CD_2Cl_2 solvent at 400 MHz.

Each peak corresponds to the formation of various phosphorus containing species, as the outcome of the reaction between **1c** and PPh_3. Interestingly, the original peak ^{31}P NMR peak of **1c** at 14.9 ppm is not seen in the spectrum, indicating full conversion to other products. It is postulated that the peak at 22.8 ppm corresponds to either tetraphenylphosphonium (PPh_4^+),

the chemical shift of which is typically around 22 ppm with consideration to the solvent used or [pPh$_3$-Allyl-BZIMPY-PPh][BArF$_{24}$]$_2$ which has been previously observed in the Macdonald lab for [Allyl-BZIMPY-PCl][OTf]$_2$.[55] The doublets seen in the spectrum could correspond to the adduct of the two reagents, which could further be corroborated using VT-NMR or ^{31}P COZY.

The results for the reaction between **1d** and PPh$_3$ are displayed in ^{31}P NMR spectrum in Figure 22.

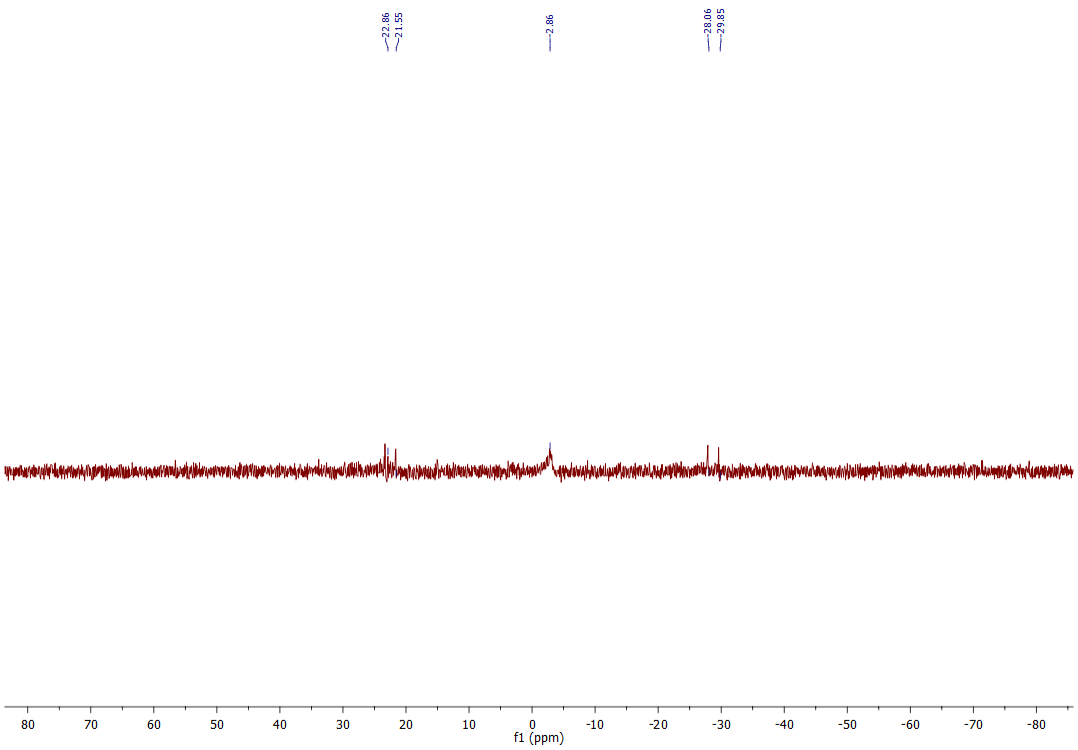

Figure 22: ^{31}P spectrum of the reaction between compound 1d and PPh$_3$ in a 1:1 ratio conducted in CD_2Cl_2 solvent at 400 MHz

The ^{31}P spectrum of the reaction between compound **1d** and PPh$_3$ displays fewer peaks for the products generated than the allyl variant of the Lewis acid shown in Figure 21. Again, the exhibited doublets are postulated to correspond to the formed adduct of **1d** and PPh$_3$ and the peak at -2.96 ppm corresponds to the shifted peak of the PPh$_3$.

Compound **2c** in the reaction with PPh$_3$ produces products shown in Scheme 6.

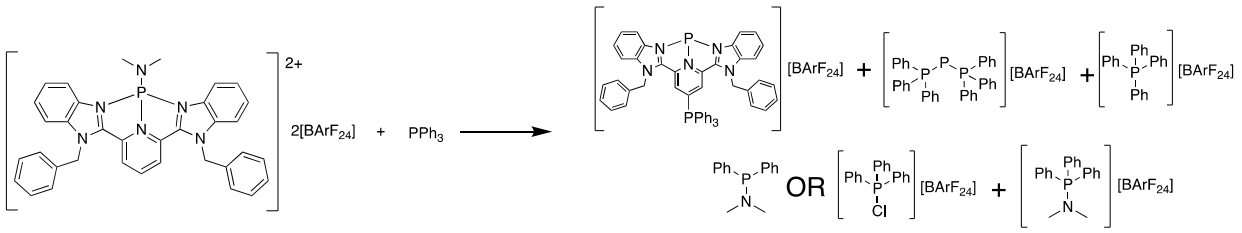

Scheme 6: Reaction results of compound 2c and PPh_3 in a 1:1 ratio.

The formation of such products is supported by the ^{31}P NMR spectrum of the reaction (Figure 23).

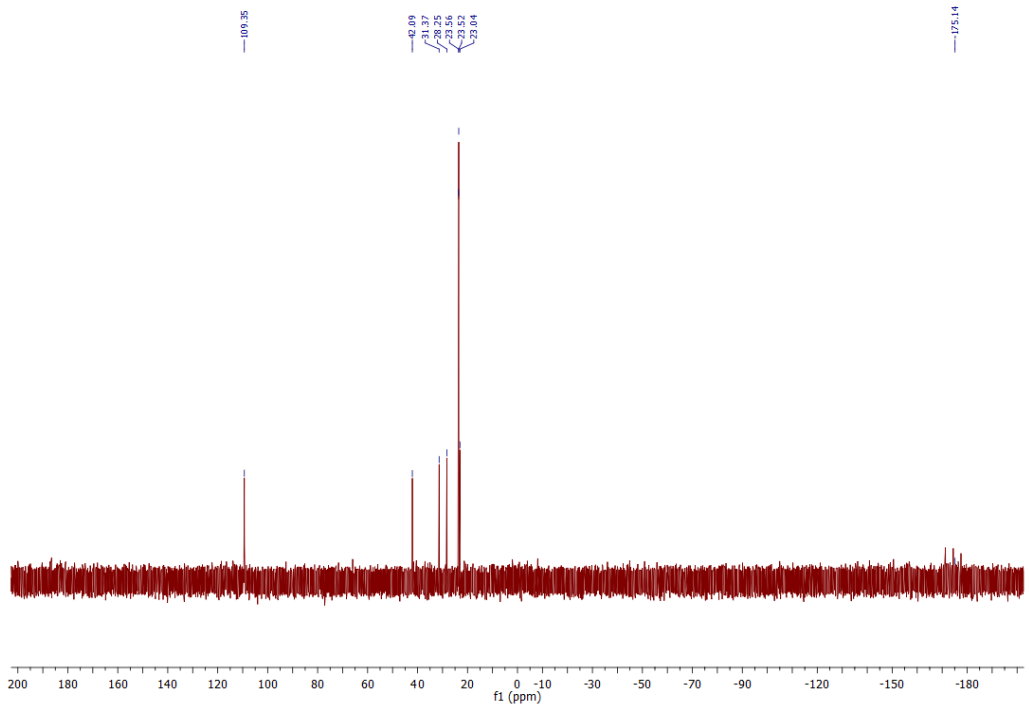

Figure 23: ^{31}P spectrum of the reaction between compound 2c and PPh_3 in a 1:1 ratio conducted in CD_2Cl_2 solvent at 400 MHz

The formed products have been identified by reference to the literature. The peak at 109.6 ppm correspond to the formation of P(I) in [*p*PPh_3-Allyl-BZIMPY-P][BArF] and the singlet at 23.5 ppm corresponds to the PPh_3 at the back of the BZIMPY ligand. These peaks have previously been observed in Macdonald *et al* conference presentation.[55] The product at 42.1 ppm has not been identified. Peaks at 31.4, 28.4 and -175 ppm correspond to $[(Ph_3P)_2P]$[BArF] salt previously reported in Ellis and Macdonald.[56]

The reaction of the benzyl-variant (compound **2d**) of the Lewis acid with PPh_3 produced similar results, with an additional peak at 66.1 ppm which corresponds to $[Ph_3PCl][BArF]$ with reported ^{31}P NMR peak at 66.2 ppm.[57] (Figure 24)

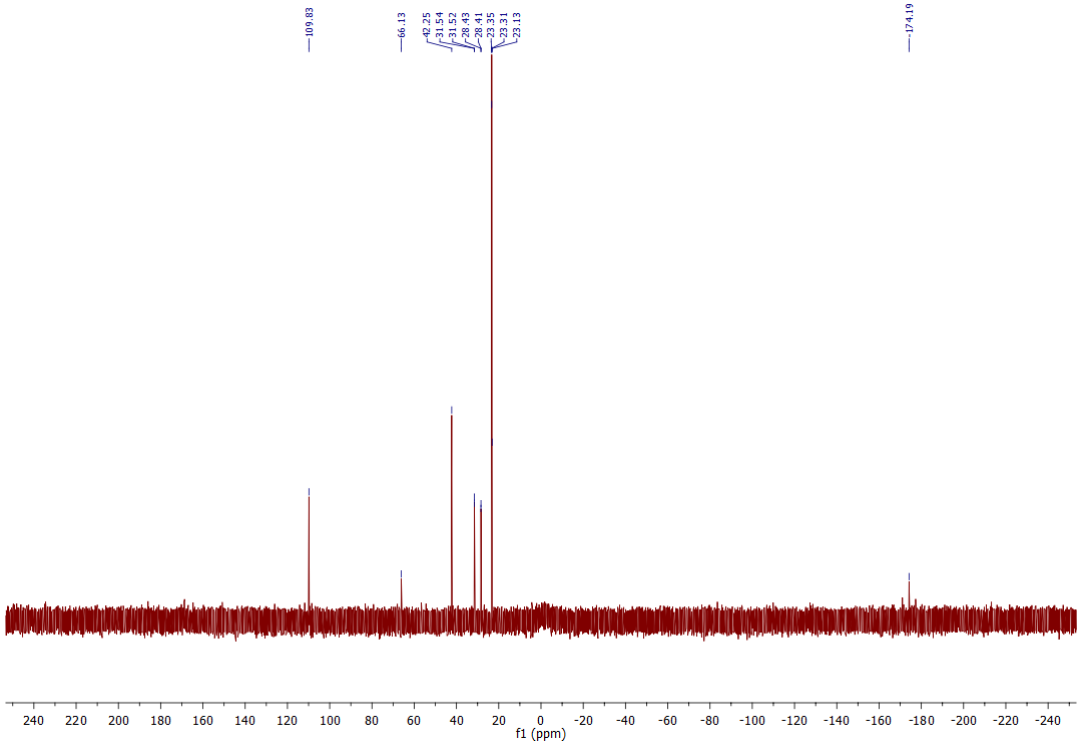

Figure 24: ^{31}P spectrum of the reaction between compound 2d and PPh_3 in a 1:1 ratio conducted in CD_2Cl_2 solvent at 400 MHz

The coordination of PPh_3 benzyl-BZIMPY pyridyl ring is achieved through the nucleophilic aromatic substitution, but the atypical transfer of the NMe_2^+ from the phosphorus atom to a different PPh_3 is rather unusual. To further investigate this reactivity, compound **2d** was reacted with trimethylphosphine (PMe_3) in a 1:1 mole ratio. The results are displayed in Figure 25.

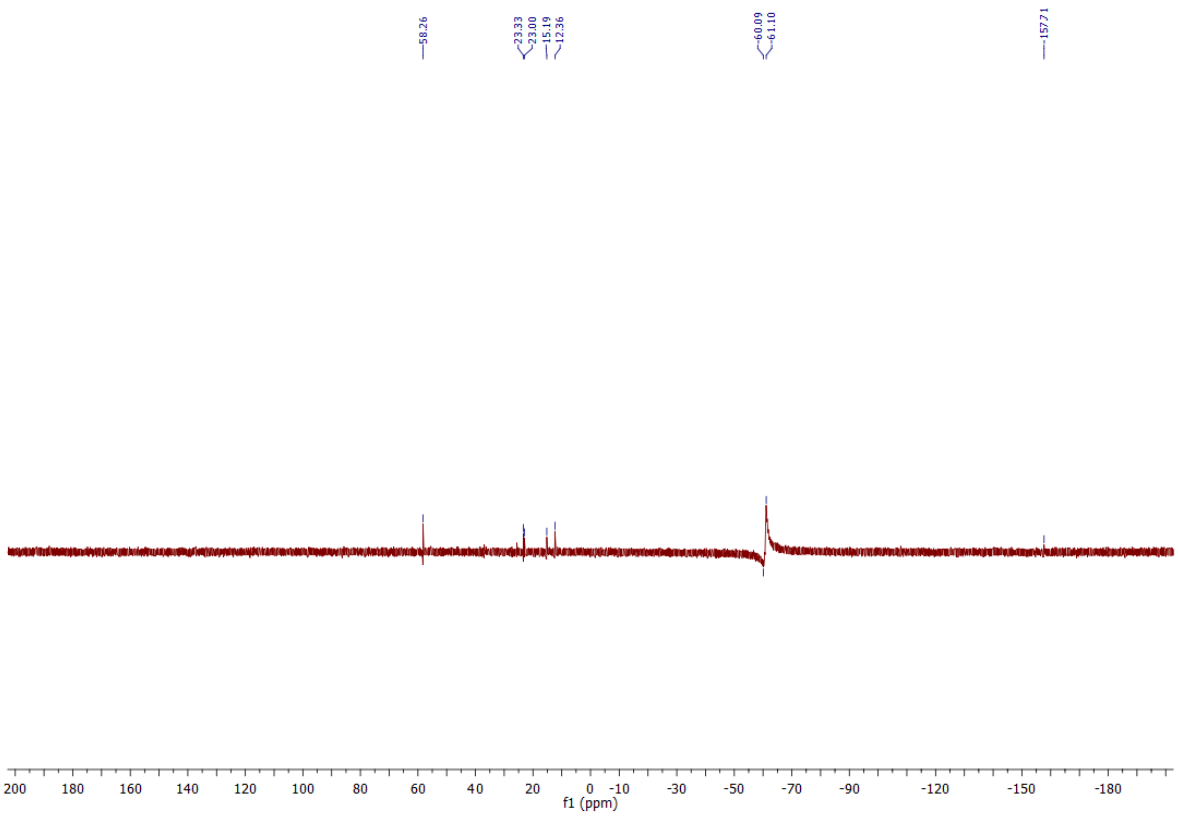

Figure 25: ^{31}P spectrum of the reaction between compound 2d and PPh_3 in a 1:1 ratio conducted in CD_2Cl_2 solvent at 400 MHz.

The ^{31}P NMR spectrum displays similar results as with the PPh_3 variant, but with -Me_3 moieties. The doublet at 23.3 ppm corresponds to the coordination complex formed between phosphorus of compound **2d** and PMe_3. The doublet at 15 and 12 ppm and the triplet at -157 ppm correspond to triphosphenium product seen in the previous reaction with PPh_3. Lastly, the peak at -60.9 ppm corresponds to the phosphorus peak of PMe_3.

Catalytic Reactivity of Lewis acid catalysts

The assessment of Lewis acidity of compounds **1a-d** and **2a-d** suggested high Lewis acidic character and promising reactivity. The catalytic reactivity of Lewis acids was probed using a series of benchmark reactions that are catalyzed by main group Lewis acids. The results are discussed below.

Hydroarylation of Diphenylamine with 1,1-diphenylethylene

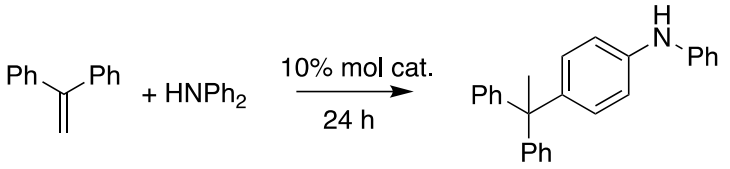

1a: 0% **2a**: 0%
1b: 0% **2b**: 0%
1c: 58% **2c**: 0%
1d: 81% **2d**: 0%

Scheme 7: Hydroarylation of Diphenylamine with 1,1-diphenylethylene using 10%mol catalyst with percent conversions.

The result yielded in this reaction showed 0% conversion to product when using catalysts **1a,b** and **2a-d**. Using 10% mole compound **1c** and **1d** yielded 58% and 81% conversion to product after 1 hour at room temperature. In comparison, Perez *et al*[58] observed full conversion to the product when using their phosphorus-based based catalyst.

Hydroarylation of Pyrrole with 1,1-diphenylethylene

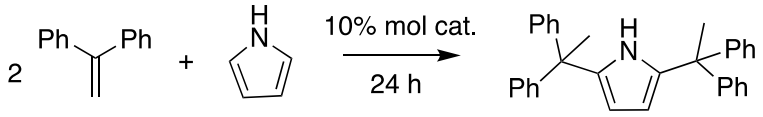

1a: 0% **2a**: 0%
1b: 0% **2b**: 0%
1c: 35% **2c**: 0%
1d: >99% **2d**: 0%

Scheme 8: Hydroarylation of Pyrrole with 1,1-diphenylethylene using 10% mol catalyst with percent conversions displayed.

The results of this reaction with different Lewis acids yielded similar results to the reaction above. Compounds **1a**, **1b** and **2a-d** demonstrated 0% conversion to the final product, whereas catalysts **1c** and **1d** showed 35% and >99% conversion, respectively. Similar to the comparison above, *Perez et al*[58] achieved 100% conversion to the product when using their phosphorus-based catalyst.

Hydrothiolation of 1,1-diphenylethylene with Thiophenol

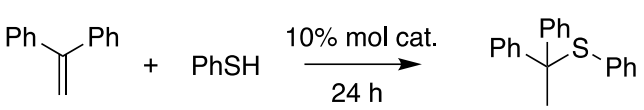

1a: 0% **2a**: 0%
1b: 0% **2b**: 0%
1c: 99% **2c**: 17%
1d: 66% **2d**: 64%

Scheme 9: Hydrothiolation of 1,1-diphenylethylene with Thiophenol using 10% mol catalyst with percent conversions displayed.

The results of this reaction vary among the triflate anion based catalysts (compounds **1a,b** and **2a,b**) versus barfate anion based compounds (compounds **1c,d** and **2c,d**). All triflate-based compounds yielded 0% conversion to the final product. In comparison, barfate-based compounds **1c,d** and **2c,d** show a conversion of 99%, 66%, 17% and 64%, respectively.

Dimerization of 1,1-Diphenylethylene

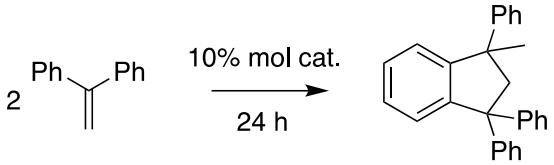

1a: 0% **2a**: 0%
1b: 0% **2b**: 0%
1c: 0% **2c**: 0%
1d: 0% **2d**: 0%

Scheme 10: Dimerization of 1,1-Diphenylethylene using 10% mol catalyst with percent conversions displayed.

The dimerization of 1,1-diphenylethylene using 10%mol catalysts **1a-d**, and **2a-d** was unsuccessful with reported 0% conversions. In comparison, Bayne and Stephan[59] report conversion of 0% for 2%mol catalysts **10.a**, **10.b**, **11.a** and **12.a** in Figure 26 and >99% and 35% for 2%mol catalysts **11.b** & **12.b**. Similarly, Mallov and Stephan[60] report conversions of 10%, 99% and 0% for 2%mol catalysts **13a**, **13b** and **13.c**, shown in Figure 26. The conditions of the reactions also vary from 24h at room temperature to up to 96h at 50°C.

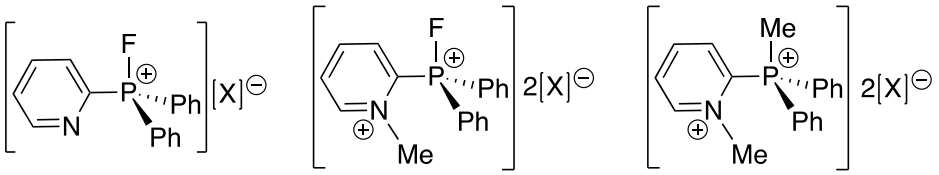

10.a: X = OTf
10.b: X = $B(C_6F_5)_4$

11.a: X = OTf
11.b: X = $B(C_6F_5)_4$

12.a: X = OTf
12.b: X = $B(C_6F_5)_4$

Bayne and Stephan

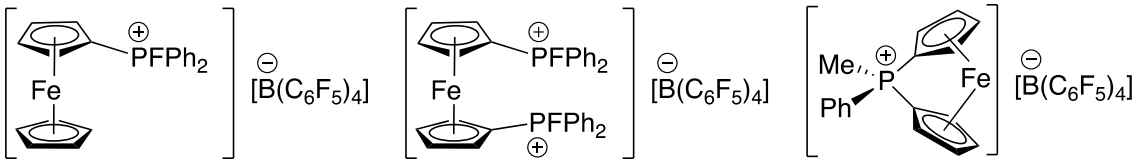

13a **13b** **13c**

Mallov and Stephan

Figure 26: Literature reported phosphorus-based compounds investigated using the same catalytic reactivity tests.

Hydrodefluorination of 1-fluoropentane

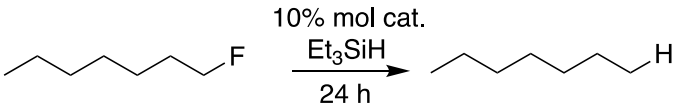

1a: <1% **2a**: 17% at 70°C
1b: <1% **2b**: 25% at 70°C
1c: 10% **2c**: 30%
1d: 66% at 70°C **2d**: 56%

Scheme 11: Hydrodefluorination of 1-fluoropentane using 10% mol catalyst with percent conversions displayed.

The results of the reaction reveal conversions for all catalysts with but with substantial variation in performance. Using standard conditions of 25°C and 24 hours, catalysts **1a** and **1b** yielded a negligible conversion of <1%. Catalysts **1c**, **2c** and **2d** showed conversions of 10%, 30% and 56% at the same conditions. In more forcing conditions of 70°C for 24h, catalysts **1d**, **2a** and **2b** demonstrated conversions of 66%, 17% and 25%, respectively. In comparison, Bayne and Stephan reported conversions of 0% for 5%mol catalysts **11.a** and **12.a** and 92% and 13% for catalysts **11.b** and **12.b** in Figure 26. Similarly, Mallov and Stephan reported conversion of <1% at 50°C for 96h for 2% mol catalyst **13.a**, 0% at 50°C and 72 hours for catalyst **13.b** and 55% at 25°C and 24 hours for catalyst **13.c**.[59,60]

Hydrosilylation of α-methylstyrene

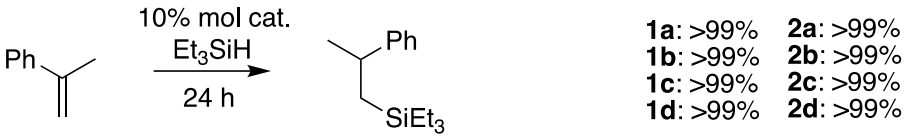

Scheme 12: Hydrosilylation of α-methylstyrene using 10%mol catalyst with percent conversions displayed.

The hydrosilylation of α-methylstyrene yielded astounding results when using 10%mol catalysts **1a-d** and **2a-d** with >99% conversion at room temperature after 1 hour. In comparison, Bayne and Stephan reported 0% conversion for 2% mol catalyst **11.a**, 99% conversion for catalyst **11.b**, 0% conversion for catalyst **12.a** and 78% conversion for catalyst **12.b** all displayed in Figure 26. These reactions were conducted at 45°C for 4 hours. Mallov and Stephan reported 27% conversion using 2% mol catalyst **13.a** at 50°C for 96h, >99% conversion for catalyst **13.b** at 25°C for 24h and 0% for catalyst **13.c** at 50°C for 72 hours.[59,60]

Dehydrocoupling of Phenol with Et_3SiH

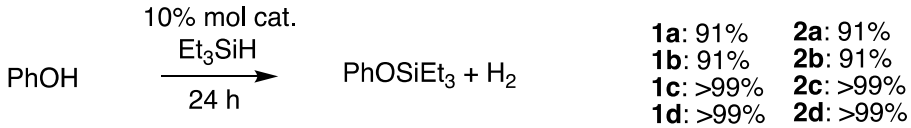

Scheme 13: Dehydrocoupling of Phenol with Et_3SiH using 10%mol catalyst with percent conversions displayed.

Dehydrocoupling of phenol using 10%mol catalyst yielded high percent conversions for all compounds; triflate-containing Lewis acids (compounds **1a,b** and **2a,b**) all yielded conversions of 91% after 1 hour at 25°C and barfate-containing Lewis acids (compounds **1c,d** and **2c,d**) yielded conversions of >99% after 1 hour at 25°C. Bayne and Stephan reported conversions of 0% for catalysts **11.a** and **12.a**, 99% for catalyst **11.b** and 95% for catalyst **12.b**. Mallov and Stephan reported conversions of 97% for 2%mol catalyst **13.a** after 7 days at 50°C, >99% conversion for catalyst **13.b** after 24 hours at 50°C and 0% for catalyst **13.c** after 72 hours at 50°C.[59,60]

Hydrodeoxygenation of Benzophenone

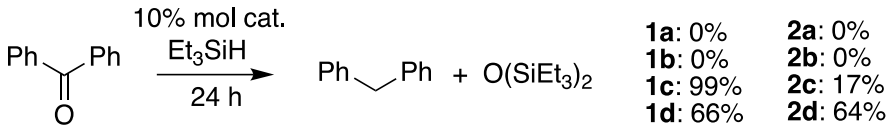

Scheme 14: Hydrodeoxygenation of Benzophenone using 10% mol catalyst with percent conversions displayed.

The results of this reaction are similar to that reported for hydrothiolation reaction above; the triflate anion catalysts (compounds **1a,b** and **2a,b**) yielded 0% conversions, whereas barfate anion catalysts (compounds **1c,d** and **2c,d**) varied with yields of 99% conversion using catalyst **1c**, 66% conversion using catalyst **1d**, 17% conversion using catalyst **2c** and 64% conversion using catalyst **2d**. In comparison, Bayne and Stephan reported conversions of 0% for 1% mol catalysts **11.a** and **12.a**, and >99% for catalysts **11.b** and **12.b**. Mallov and Stephan reported conversions of >99% for 2% mol catalysts **13.a** and **13.b** at 50°C for 7 days and 25°C for 5 days, respectively.[59,60]

Conclusions and Future Work

A series of novel dicationic Lewis acids were successfully synthesized, characterized and studied for reactivity. The yields of synthesized compounds were 86%, 83%, 89%, 87% for compounds **1a**, **1b**, **1c**, and **1d**, respectively and 94%, 94%, 87%, 99% for compounds **2a**, **2b** and **2c**, **2d.** Spectral characterizations methods include ^{31}P, ^{1}H, ^{13}C, ^{19}F, ^{11}B and HSQC nuclear magnetic resonance, as well as infrared spectroscopy by KBr pellet, ultraviolet-visible spectroscopy, and elemental analysis. All experimental structural analyses were consistent with expected results.

The compounds were found to be moderately air-and moisture- sensitive, which was further studied by direct reaction with H_2O and D_2O and observed by ^{1}H and ^{31}P NMR. The results were similar in ^{1}H NMR showing a peak at about 4.80 ppm for water, but ^{31}P NMR results varied for each compound. For compounds **1a** and **1b**, ^{31}P NMR spectra exhibited a singlet peak at 19.8 ppm, which corresponds to a ^{31}P NMR signal of 19.4 ppm reported for compound HASPO which contains a H-P=O bond[43], compound **2a** showed peaks at 3.52, -4.92, and -156.73 ppm, compounds **1c** and **1d** were silent in ^{31}P spectra, however, both compounds visually turned into a purple solution, potentially signifying a formation of a radical. Finally, for compound **2c** a triplet was observed at 2.67 ppm which corresponds to triplet of triplets peak reported for P-D coupling in the byproduct of HOPD(=O)-O-PD(=O)OH and OPD(=O)-O-PD(=O)O^{2-} in Chang *et al*.[43] Compound **2d** displayed a single peak at 36.59 ppm.

Experimental Lewis acidity assessment results demonstrate high Lewis acidic character with acceptor numbers of 68, 116, 116, 116 for compounds **1a**, **1b**, **1c** and **1d**, respectively and 120, 120, 120 and 112 for compounds **2a**, **2b**, **2c** and **2d**. Computational Lewis acidity assessment results calculated FIA values of 896 kJ/mol for [Me-BZIMPY-PPh]$^{2+}$ and 905 kJ/mol for [Me-BZIMPY-PNMe_2]$^{2+}$, further corroborating the experimental Gutmann-Beckett results and confirming high Lewis acidic character.

Structural assessment was completed by single crystal X-Ray crystallography and computationally optimized structures using the M06-2X/def2-TZVP level of theory. The XRD

crystal obtained for compound **1a** demonstrated the phosphorus atom lying within the BZIMPY ligand plane with the sum of angles adding to 320.03° between the pincer nitrogen atoms and the phosphorus atom. Additionally, the phenyl moiety on the phosphorus was located perpendicular to the P-BZIMPY plane with an angle of 81.14(9)° between the phosphorus atom and the *ipso* carbon of the phenyl moiety and a dihedral angle of 156.5(2)° between the pyridyl nitrogen of BZIMPY and *ortho* carbon of the phenyl. The position of the phenyl moiety with respect to the rest of the structure opens the Lewis acidic site of the phosphorus atom, permitting for better reactivity. Computationally obtained optimized structure of [Me-BZIMPY-PPh]$^{2+}$ where the BZIMPY backbone groups (allyl and benzyl) were simplified to methyl groups fully corroborated the experimentally obtained structure with bond distances and angles between individual atoms being close to the experimental values. The difference between the XRD structure and computed structure is seen in the dihedral angle between the pyridyl nitrogen of the BZIMPY ligand and the *ortho* carbon of the phenyl moiety with an angle of 181.01°, indicating that in the computationally optimized structure the phenyl ring is not twisted to either side of the ligand, whereas in the experimental structure a slight bend of the phenyl ring may be expected. The computed structure of [Me-BZIMPY-PNMe$_2$] was found to be slightly different from the phenyl variant, with the phosphorus atom lying a little out of the plane from the pincer nitrogen atoms of the bzimpy ligand with a sum angle of 312.16°. The dimethylamino moiety points down with respect to the P-BZIMPY plane with an angle of 106.86° between the pyridyl nitrogen of BZIMPY, the phosphorus atom and the nitrogen atom of dimethylamino moiety.

Electronic distributions calculated using the M06-2X/def2-TZVP level of theory for [Me-BZIMPY-PPh]$^{2+}$ and [Me-BZIMPY-PNMe$_2$]$^{2+}$ showed the most cationic charge of 1.25 *e* for the phosphorus atom and negative charge of -1.25 *e* on the pincer nitrogen atoms of the BZIMPY ligand for [Me-BZIMPY-PPh]$^{2+}$. Similarly, for [Me-BZIMPY-PNMe$_2$]$^{2+}$, the phosphorus atom exhibited a positive charge of 1.50 *e* and the BZIMPY pincer nitrogen atoms exhibited a negative charge of -1.50 *e*. The calculated Wiberg bond indices suggest a single bond character for the phosphorus-phenyl bond (P-iPh) of 0.90, a low single-bond character for the pyridyl nitrogen and phosphorus bond (P-N1), which is typical for single bonds with substantial ionic character

and a partial bond character for the P-N2 and P-N3 bond of 0.45 and 0.46, respectively. For the [Me-BZIMPY-PNMe$_2$]$^{2+}$ variant, the Wiberg bond indices show a bond character of 0.54 and 0.57 for P-N1 and P-N2, respectively but the WBI for P-N3 is calculated to be 0.19, suggesting a much more asymmetric binding arrangement of the ligand, and perhaps suggests a greater measure of lability for one arm of the BZIMPY chelate. Finally, the WBI for P-N45 was calculated to be 0.98 consistent with the single bond character, as also seen in the optimized structure.

Molecular orbitals were computed for [Me-BZIMPY-PPh]$^{2+}$ and [Me-BZIMPY-PNMe$_2$]$^{2+}$ using the M06-2X/def2-TZVP level of theory with GD3 empirical dispersion. The HOMO of both variants are distributed along the π systems of the BZIMPY ligand and for [Me-BZIMPY-PPh]$^{2+}$, the phenyl ring moiety of the phosphorus. The low-lying unoccupied orbitals of the [Me-BZIMPY-PPh]$^{2+}$ were located on the phosphorus atom with energy of -8.53 eV, whereas LUMO+3 was calculated to be -5.33 eV and shows a large unoccupied orbital on the phosphorus atom, consistent with a 3p-type orbital with a vacant lobe extending into the cavity of the complex. The LUMO of [Me-BZIMPY-PNMe$_2$]$^{2+}$ variant is consistent with the phenyl-variant and the LUMO+3 shows a large lobe on the phosphorus atom, consistent with the possibility of the P atom to interact with donors. Interestingly, when comparing the LUMO +3 orbitals and their relative energies of the two [Me-BZIMPY-PR']$^{2+}$ Lewis acids, the [Me-BZIMPY-NMe$_2$]$^{2+}$ LUMO +3 energy is slightly lower than that of [Me-BZIMPY-PPh]$^{2+}$ variant. This result is consistent with the difference in electron-withdrawing abilities between the carbon of the phenyl fragment to the phosphorus versus the nitrogen of the dimethylamine moiety to the phosphorus.

Lastly, stoichiometric, and catalytic reactivities of compounds **1a-d** and **2a-d** were investigated and yielded some interesting results. In the reaction of compounds **1a**, **1b**, **2a**, **2b** which can also be identified as the "triflate" variants, with triphenylphosphine (PPh_3) in a 1:1 mol ratio, two peaks are seen in the ^{31}P NMR which correspond to the ^{31}P peak of the phosphorus atom in the Lewis acids and the phosphorus atom of PPh_3 in the region of about -5 ppm. Barfate variants exhibit formations of new products in the reaction with PPh_3; compound **1c** in a 1:1 ratio with PPh_3 yields six peaks in the ^{31}P NMR spectrum – the peak at 22.8 ppm is thought to

be either tetraphenylphosphonium (PPh_4^+), the chemical shift of which is typically around 22 ppm with consideration to the solvent used or [*p*Ph_3-Allyl-BZIMPY-PPh][$BArF_{24}$]$_2$ which has been previously observed in the Macdonald lab for [Allyl-BZIMPY-PCl][OTf]$_2$.[55] For the benzyl-variant, compound **1d,** two sets of doublets are seen in ^{31}P NMR spectrum at 22.7 ppm and 29.3 ppm, which could correspond to the adduct of the two reagents, but this proposition could be further studied by variable-temperature (VT) NMR. The products for the reaction of **2c** and **2d** with PPh_3 have been identified and are presented in Scheme 6. The results of this reaction suggest further considerations for ligand design, such as including a ^{t}Bu group at the para position of the pyridine to prevent the SnAr substitution seen in the reaction of PPh_3 and PMe_3 with barfate salts. The dicationic Lewis acids were also probed for catalytic reactivity in various catalytic reactions. It was noted that compounds **1c** and **1d** were highly efficient in conversions of most reactions, while **2c** and **2d** performed moderately well as well, compared to compounds **1a** and **1b** which were inefficient for most reactions.

The work presented in this thesis is only the roots that could branch further to other applications, such as activation of small molecules or involvement in other transformation processes. The activation of small molecules such as H_2, CO_2, NH_3 has been observed in similar systems such as the ones reported by Arduengo *et al*,[61] McCarthy *et al*,[62] Zhao *et al*[63] and Cui *et al*[64] shown in Scheme 15 below.

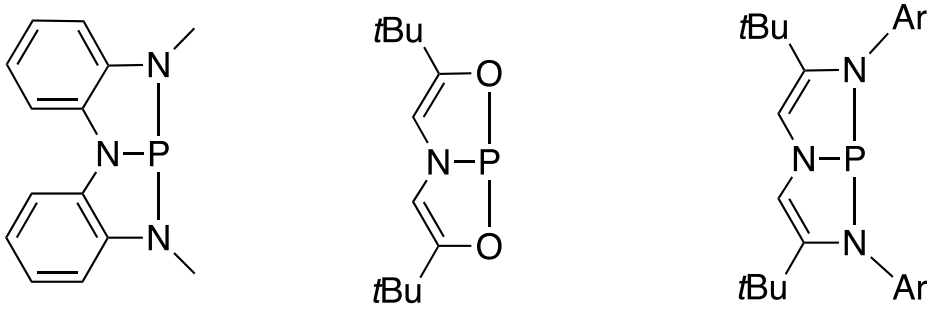

Zhao *et al*, 2014 **Arduengo *et al*, 1987** **McCarthy *et al*, 2014** **Cui *et al*, 2014**

Scheme 15: Literature reported Phosphorus (III) compounds that achieved small molecule activations.

Since it has been observed that compounds **2c** and **2d** convert to P(I) variants effortlessly, the chemistry of P(I) could be directed to activation of small molecules. However, isolation of these variants from their P(III) variants (**2c** and **2d**) must first be established and characterized. Similarly P(III) variants can be probed for small molecule activation. Additional work must be done in the studies of reactivity with H_2O and D_2O. More precise measurements of the reactants, as well as 2D NMR methods could aid in the identification of the formed products as seen in ^{31}P NMR. Similarly, in the studies of the reaction with PPh_3, employment of other techniques such as 2D NMR, mass spectrometry and single-crystal crystallography could further help in identification of the formed products. Upon complete identification of the reaction products, as well as isolation of the P(I) variants, further studies can be conducted leading to useful applications.

Experimental

Ligand Synthetic Methods

All ligands were synthesized in a fumehood using standard bench-top conditions and glassware. All reagents were purchased from Sigma Aldrich and used as received. All solvents were dried by distillation technique and stored over 3 Å molecular sieves before usage.

2,6-Bis(2-benzimidazyl) pyridine (NH-BZIMPY)

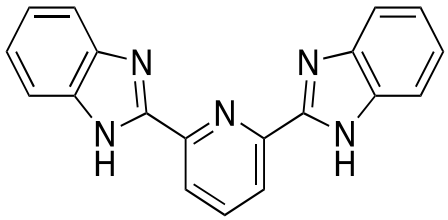

The NH-BZIMPY ligand was synthesized according to procedure reported in the literature.[65] The synthesis was scaled up by a factor of 5x. **Yield:** 58.3% mp: >400 ^{o}C **^{1}H NMR** (DMSO-d_6): δ 7.33-8.36 (m, aromatic), 13.02 (s, imino).

2,2'-(2,6-pyridinediyl)bis[1-(2-propenyl) (Allyl-BZIMPY)

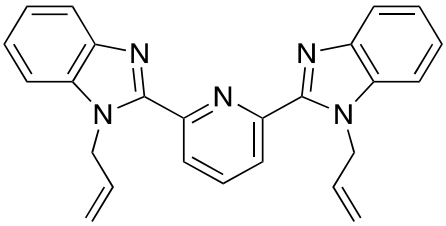

Allyl-BZIMPY was synthesized according to the experimental reported in the literature.[66] The synthesis was scaled up by a factor of 6.7X. **Yield**: 43.8%. **^{1}H NMR** ($CDCl_3$, 400 MHz): δ 4.92 (dd, 2H, ^{3}J=18 Hz, ^{2}J= 2 Hz), 5.12 (dd, 2H, ^{3}J=10 Hz, ^{4}J=2 Hz), 5.41 (m, 4H), 5.91 (ddt, 2H, ^{3}J=18 Hz, ^{3}J= 10 Hz, ^{4}J=5 Hz), 7.38 (m, 4H), 7.44 (m, 2H), 7.87 (m, 2H), 8.05 (t, 1H, ^{3}J= 8 Hz), 8.38 (d, 2H, ^{3}J=8 Hz)

2,6-bis(1-benzyl-1H-benzo[d]imidazol-2-yl)pyridine (Bn-BZIMPY)

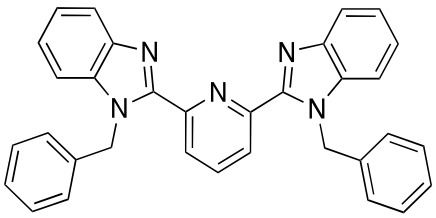

Benzyl-BZIMPY was synthesized according to procedure reported in the literature.[40] The reaction was scaled up by a factor of 51x. **Yield:** 65.1%.**^{1}H NMR** ($CDCl_3$, 400 MHz): δ 5.54 (s, 4H), 6.81 (d, 4H, J=8.0 Hz), 7.15-7.25 (m, 12 H), 7.88 (d, 2H, J=7.6 Hz), 8.01 (t, 1H, J=7.8 Hz), 8.38 (d, 2H, J=8.0 Hz)

[H_2-NAllyl-BZIMPY][OTf]$_2$

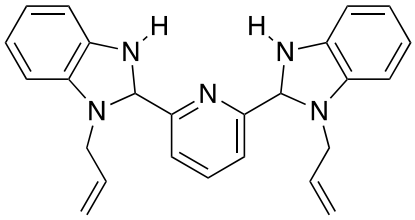

A solution of NAllyl BZIMPY (0.225 g, 0.58 mmol) was prepared in 5 mL of DCM. To the solution 0.1 mL of triflic acid (0.17 g, 1.1 mmol) was added and stirred for 1 hour to yield a white suspension. The suspension was washed with hexanes to yield a white solid.
Yield: 0.229 g, 100%
^{1}H NMR (CD_3CN, 400 Hz) : δ 5.22 (t, 2H), 5.26 (t, 2H), 5.35 (s, 1H), 5.39 (m, 4H), 6.15 (m, 2H), 7.74 (m, 4H), 7.89 (m, 2H), 8.07 (m, 2H), 8.39 (d, 2H, J=7.8 Hz), 8.52 (t, 1H). ^{13}C NMR (CD_3CN, 400 Hz) : δ 49.6, 113.4, 114.7, 118.6, 122.1, 127.4, 127.9, 128.8, 130.2, 132.8, 141.1, 142.9, 145.5. ^{19}F (CD_3CN, 400 Hz) : δ -79.3

Lewis Acids Synthetic Methods

General Methods: All manipulations were carried out under an atmosphere of N_2 in the Vacuum Atmosphere Corporation (VAC) glovebox or using standard Schlenk methods. All glassware was dried in an oven at 250 ^{o}C for several hours before usage. All solvents were obtained from Sigma Aldrich and stored over activated 3 Å molecular sieves for a minimum of 72 hours. All reagents were obtained from commercial suppliers and used as received. The ligands were synthesized under standard air conditions and kept in the glovebox. Samples were loaded and capped in the NMR tubes inside the glovebox and sealed with a cap and Parafilm prior to removal. NMR spectra were obtained on Bruker Avance 300 (300 MHz) spectrometer and JEOL Delta (400 MHz) spectrometer at 298 K. HRMS spectra were obtained on a Micromass Q-TOF I Electrospray Ionisation mass spectrometer. Infrared Spectra were conducted using the KBr powder and a standard steel press. The spectra were collected using the ABB Bomem MB Series spectrometer. XRD analysis was performed on Bruker KAPPA APEX II with the APEX II CCD detector. UV-Vis maximum absorption was collected on Shimadzu UV-2550 spectrophotometer. Elemental analysis was completed on the PerkinElmer 2400 combustion CNH analyser at the University of Windsor.

[Allyl-BZIMPY-PPh][OTf]$_2$ (1a)

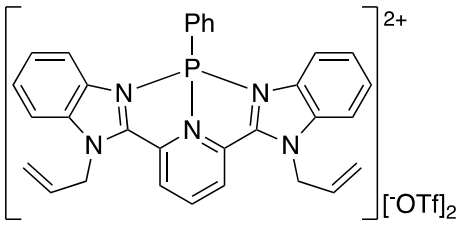

In a 20 mL vial, a solution of Allyl-BZIMPY (0.442g, 1.1 mmol) was prepared and stirred in 7 mL of dichloromethane (DCM) for one minute at room temperature. In a separate 20 mL vial, a solution of dichlorophenylphosphine ($PhPCl_2$, 0.202 g, 1.1 mmol) and trimethylsilyl trifluoromethanesulfonate (TMSOTf, 0.502 g, 2 mmol) were mixed in 2 mL of DCM and added to the vial containing Allyl-BZIMPY solution to obtain a bright yellow suspension. The suspension was stirred for one hour and then allowed to settle. The supernatant was removed and the yellow solid was washed with hexanes (3 x 5 mL). The yellow powder was then dried under vacuum to obtain the final product.

Yield: 0.878 g, 86%

^{1}H NMR (CD_3CN, 400 MHz): δ 5.27 (d, J=16.9 Hz, 2H), 5.43 (d, J=12.3, 2H), 5.54 (m, 4H), 6.26 (m, 2H), 7.42 (d, 2H), 7.76 (m, 4H), 7.95 (d, J=8.2, 2H), 8.18 (d, J=7.8, 2H), 9.07 (d, J=7.8, 2H) 9.24 (t, 1H).**^{13}C NMR** (CD_3CN, 400 MHz): δ 49.4, 114.7, 117.3, 119.8, 120.5, 123.6, 127.8, 128.2, 129.1, 130.6, 131.1, 132.8, 136.6, 138.3, 140.5, 150.3. **^{31}P NMR** (CD_3CN, 400 MHz): δ 10.7 **^{19}F NMR** (CD_3CN, 400 MHz): δ -79.3 **FT-IR** (KBr pellet, cm-^{1}): 3091 (w), 1629 (w), 1504 (m), 1482 (m), 1260 (s), 1224 (s), 1158 (s), 1030 (s), 814 (w), 755 (m), 699 (w), 636 (s). **UV-Vis (λ_{max})** : 323 nm. **Elemental Analysis**; Calcd for $C_{33}H_{26}N_5PF_6O_6S_2$: C, 49.70; H 3.29; N 8.78. Found: C, 49.40; H, 2.95, N, 8.75.

[Benzyl-BZIMPY-PPh][OTf]$_2$ (1b)

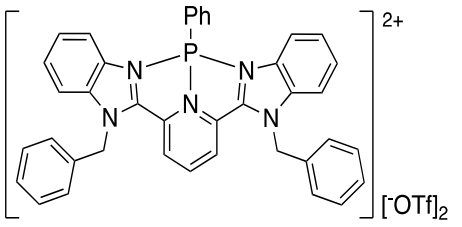

A 20 mL vial was charged with Benzyl-BZIMPY (0.554g, 1.1 mmol) in 7 mL of DCM. In a separate 20 mL vial, a mixture of $PhPCl_2$ (0.202g, 1.1 mmol) and TMSOTf (1g, 4 mmol) was prepared and stirred in DCM, then transferred dropwise into Benzyl-BZIMPY solution producing a bright yellow suspension. The suspension was stirred for one hour and allowed to settle. The supernatant was removed and the yellow solid was washed with hexanes (3 x 5 mL). The yellow powder was then dried under vacuum resulting in the desired product.

Yield: 0.831 g, 83%

^{1}H NMR (CD_3CN, 400 MHz): 5.45 (m, 4H), 6.15 (q, J=6.9 Hz, 4H), 7.39 (m, 12H), 7.77 (m, 6H), 8.22 (t, 1H), 8.92 (d, J=7.8, 2H), 9.02 (m, 2H).**^{13}C NMR** (CD_3CN, 400 MHz): δ 50.6, 114.8, 117.5, 119.8, 127.4, 127.9, 128.3, , 129.1, 129.8, 130.3, 130.8, 131.1, 131.2, 132.8, 135.5, 138.6, 138.6, 140.5, 141.6, 150.3. **^{31}P NMR** (CD_3CN, 400 MHz) δ 10.9. **^{19}F NMR** (CD_3CN, 400 MHz): δ -79.3 **FT-IR(KBr pellet, cm-^{1}):** 3020 (w), 1631 (w), 1508 (m), 1482 (m), 1453 (w), 1260 (s), 1224 (m), 1029 (s), 752 (w), 697 (w), 637 (s). **UV-Vis (λ_{max}):** 321 nm. **Elemental Analysis;** Calcd for $C_{41}H_{30}N_5PF_6O_6S_2$: C, 54.89; H 3.37; N 7.81. Found: C, 54.98; H, 3.20, N, 7.78.

[Allyl-BZIMPY-PNMe$_2$][OTf$^-$]$_2$ (2a)

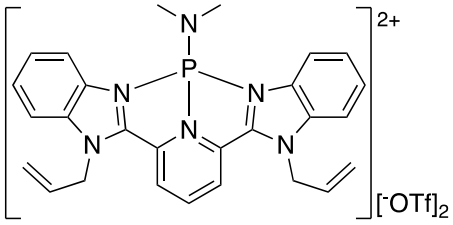

A 100 mL Schlenk flask was charged with Allyl-BZIMPY (0.250g, 1.1mmol) in 5 mL of DCM. A separate 50 mL Schlenk flask was charged with a mixture of TMSOTf (0.28 g, 2 mmol) and dimethylphosphoramidous dichloride (Me_2NPCl_2, 0.11 g, 1.1 mmol) in 2 mL of DCM, which was then cannula transferred into the flask containing Allyl-BZIMPY solution to obtain a bright orange suspension. The suspension was stirred for one hour and then allowed to settle. The supernatant was removed by filtration and the remaining yellow powder was washed with hexanes (3 x 5 mL). The powder was dried under vacuum to yield the desired product.

Yield: 0.729 g, 94%

^{1}H NMR (CD_3CN, 400 MHz): δ 2.81 (d, *J* = 13.1 Hz, 6H), 5.24 (d, *J* = 17.0 Hz, 2H), 5.52 – 5.35 (m, 6H), 6.34 – 6.17 (m, 2H), 7.83 – 7.71 (m, 4H), 7.92 (d, *J* = 7.8 Hz, 2H), 8.13 (d, *J* = 7.5 Hz, 2H), 8.70 (d, *J* = 8.2 Hz, 2H), 8.97 (s, 1H). **^{13}C NMR** (CD_3CN 400 MHz): δ 149.49, 142.27, 137.42, 135.52, 130.15, 128.89, 127.97, 127.64, 127.60, 118.70, 117.39, 113.55, 73.23, 48.84. **^{31}P NMR** (CD_3CN, 400 MHz): δ 95.29. **^{19}F NMR** (CD_3CN, 400 MHz): δ -79.28. **FR-IR** (KBr pellet, cm^{-1}): 3061(w), 1622 (s), 1605 (m), 1528 (s), 1434 (s), 1258 (m), 1157 (m), 1029 (s), 998 (s), 734 (s), 701 (m), 637 (s). **UV-Vis (λ_{max}):** 319 nm**. Elemental Analysis;** Calcd for $C_{29}H_{27}N_6PF_6O_6S_2$: C, 45.57; H 3.56; N 10.99. Found: C, 41.73; H, 3.67, N, 9.95.

[Benzyl-BZIMPY-PNMe$_2$][OTf$^-$]$_2$ (2b)

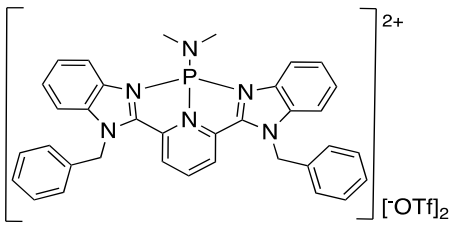

A 100 mL Schlenk flask was charged with Benzyl-BZIMPY (0.250g, 1.1mmol) in 5 mL of DCM. A separate 50 mL Schlenk flask was charged with a mixture of TMSOTf (0.28 g, 2 mmol) and Me_2NPCl_2 (0.11 g, 1.1 mmol) in 2 mL of DCM, which was then cannula transferred into the flask containing Benzyl-BZIMPY solution to obtain a bright orange suspension. The suspension was stirred for one hour and then allowed to settle. The supernatant was removed by filtration and the remaining yellow powder was washed with hexanes (3 x 5 mL). The powder was dried under vacuum to yield the desired product.

Yield: 0.405 g, 93%

^{1}H NMR (CD_3CN, 400 MHz): δ 2.49 (d, *J* = 13.0 Hz, 6H), 5.74 (d, *J* = 9.2 Hz, 4H), 7.00 – 6.92 (m, 4H), 7.04 (t, *J* = 6.3 Hz, 6H), 7.46 – 7.35 (m, 4H), 7.52 (dd, *J* = 4.8, 3.3 Hz, 2H), 7.84 (dd, *J* = 5.5, 3.7 Hz, 2H), 8.24 (d, *J* = 8.2 Hz, 2H), 8.42 (t, 1H). **^{13}C NMR** (CD_3CN, 400 MHz) δ 149.2, 142.3, 142.2, 142.1, 137.6, 135.5, 133.2, 129.3, 128.9, 128.7, 127.9, 127.3, 127.3, 126.5, 122.5, 113.6, 49.9, 39.6**. ^{31}P NMR** (CD_3CN, 400 MHz) δ 95.30. **^{19}F NMR** (CD_3CN, 400 MHz) δ -79.37. **FT-IR** (KBr

pellet, cm-[1]): 3062 (w), 1622 (w), 1606 (w), 1560 (m), 1527 (s), 1467 (w), 1454 (w), 1259 (b), 1157 (b), 1029 (s), 999 (s), 734 (m), 637 (s). **UV-Vis (λ_{max}): 320 nm. Elemental Analysis:** Calcd for $C_{37}H_{31}N_6PF_6O_6S_2$: C, 51.43; H, 3.62; N, 9.73. Found: C, 50.88; H, 3.62, N, 9.55.

[Allyl-BZIMPY-PPh][BArF$_{24}$]$_2$ (1c)

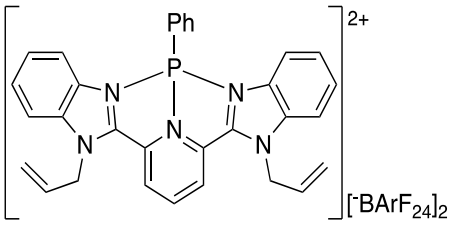

A 100 mL round bottom flask was charged with Allyl-BZIMPY (0.144g, 1.1mmol) in 5 mL of DCM. A separate 50 mL Schlenk flask was charged with a mixture of Sodium Tetrakis[3,5-bis(trifluoromethyl)phenyl] borate ($NaBArF_{24}$, 0.653g, 2 mmol) and $PhPCl_2$ (0.07 g, 1.1 mmol) in 10 mL of DCM, which was then added dropwise into the flask containing Allyl-BZIMPY solution to obtain a bright yellow suspension. The suspension was stirred for one hour and then allowed to settle. The solution was removed by filtration and the solvent was reduced to 1 mL in volume. The solution was added dropwise into a 50 mL round bottom flask containing stirring hexanes resulting in the formation of a fine yellow powder. The supernatant was removed by filtration and the desired product was further dried under vacuum.
Yield: 0.793 g (89 %)
^{1}H NMR (CD_2Cl_2, 400 MHz): δ 5.10 (d, *J* = 17.2 Hz, 2H). 5.30 (d, *J* = 4.3 Hz, 2H), 5.56 – 5.34 (m, 6H), 6.39 – 5.96 (m, 4H), 7.45 – 7.27 (m, 4H), 7.89 – 7.72 (m, 4H), 8.05 (d, *J* = 8.1 Hz, 2H), 8.78 (d, *J* = 7.7 Hz, 2H), δ 9.11 (t, 1H) **^{13}C NMR** (CD_2Cl_2, 400 MHz): δ 39.6, 48.9, 113.6, 118.8, 127.6, 127.9, 128.9, 129.1, 129.8, 130.1, 130.8, 131.1, 131.2, 132.8, 135.5, 137.4, 138.6, 141.9, 142.3, 149.5 **^{31}P NMR (**CD_2Cl_2, 400 MHz**):** δ 14.9 **^{19}F NMR (CD_2Cl_2, 400 MHz)**: δ -62.7, **^{11}B (CD_2Cl_2, 400 MHz):** δ -7.45. **FT-IR** (KBr pellet, cm-[1]): 3075 (w), 1631 (m), 1611 (m), 1507 (s), 1483 (s), 1356 (m), 1287 (m), 1090 (s), 887 (s), 839 (s), 745 (s), 712(s), 682 (s)**. UV-Vis** (λ_{max}): **327 nm. Elemental Analysis**; Calcd for $C_{95}H_{50}N_5PB_2F_{48}$: C, 51.26; H, 2.26; N, 3.14. Found: C, 51.49; H, 2.41, N, 3.18.

[Benzyl-BZIMPY-PPh][BArF$_{24}$]$_2$ (1d)

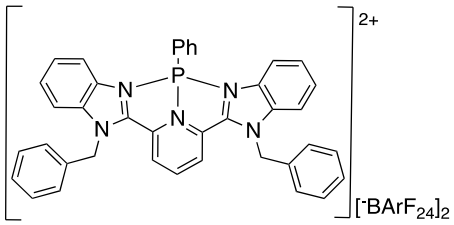

A 100 mL round bottom flask was charged with Benzyl-BZIMPY (0.181g, 1.1mmol) in 5 mL of DCM. A separate 50 mL Schlenk flask was charged with a mixture of $NaBArF_{24}$, (1.307g, 2 mmol) and $PhPCl_2$ (0.07 g, 1.1 mmol) in 10 mL of DCM, which was then added dropwise into the flask containing Benzyl-BZIMPY solution to obtain a bright yellow suspension. The suspension was stirred for one hour and then allowed to settle. The solution was removed by filtration and the solvent was reduced to 1 mL in volume. The solution was added dropwise into a 50 mL round bottom flask

containing stirring hexanes resulting in the formation of a fine yellow powder. The supernatant was removed by filtration and the desired product was further dried under vacuum.
Yield: 0.754 g (87%**)**
^{1}H NMR (CD_2Cl_2, 400 MHz): δ δ 5.10 (d, J = 16.8 Hz, 4H), 5.30 (d, J = 4.6 Hz, 4H), 5.49-5.42 (m, 12H), 6.15 (td, J = 11.1, 5.1 Hz, 2H), 7.49-7.36 (m, 2H), 7.82-7.67 (m, 2H), 8.05 (d, J = 9.2 Hz, 2H), 8.78 (d, J = 7.6 Hz, 2H), 9.11 (t, 1H). **^{13}C NMR (**CD_2Cl_2**, 400 MHz)** : δ 39.6, 48.9, 113.6, 118.8, 127.6, 127.9, 128.9, 129.1, 129.8, 130.1, 130.8, 131.1, 131.2, 132.8, 135.5, 137.4, 138.6, 141.9, 142.3, 149.5 **^{31}P NMR** (CD_2Cl_2, 400 MHz) δ 15.3 **^{19}F NMR (CD_2Cl_2, 400 MHz)**: δ -62.7, **^{11}B (CD_2Cl_2, 400 MHz):** δ -7.62. **FT-IR** (KBr pellet, cm-^{1}): 2963 (w), 1611 (m), 1506 (s), 1483 (s), 1355 (m), 1278 (m), 1095 (w), 1085 (w), 887 (m), 839 (s), 745 (s), 713 (s), 682 (s), 670 (s). **UV-Vis** (λ_{max}): 322 nm. **Elemental Analysis**; Calcd for $C_{103}H_{54}N_5PB_2F_{48}$: C, 53.19; H, 2.34; N, 3.01. Found: C, 52.91; H, 2.33, N, 2.87.

[Allyl-BZIMPY-PNMe$_2$][BArF$_{24}$]$_2$ (2c)

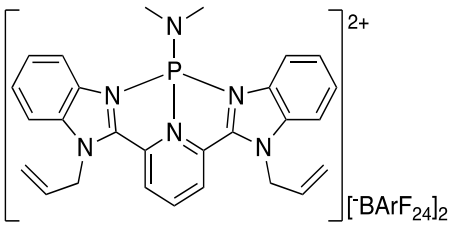

A 100 mL round bottom flask was charged with Allyl-BZIMPY (0.200g, 1.1mmol) in 5 mL of DCM. A separate 50 mL Schlenk flask was charged with a mixture of $NaBArF_{24}$, (0.905 g, 2 mmol) and Me_2NPCl_2 (0.05 g, 1.1 mmol) in 10 mL of DCM, which was then added dropwise into the flask containing Allyl-BZIMPY solution to obtain a bright yellow suspension. The suspension was stirred for one hour and then allowed to settle. The solution was removed by filtration and the solvent was reduced to 1 mL in volume. The solution was added dropwise into a 50 mL round bottom flask containing stirring hexanes resulting in the formation of a fine yellow powder. The supernatant was removed by filtration and the desired product was further dried under vacuum.
Yield: 0.980 g (87%)
^{1}H NMR (CD_2Cl_2, 400 MHz): δ 2.84 (d, *J* = 14.2 Hz, 6H), 5.11 (d, *J* = 17.3 Hz, 2H), 5.52 – 6.10 (m, 6H), 6.30 – 6.10 (m, 4H), 7.66- 7.50 (m, 4H), 8.04 (d, *J* = 8.3 Hz, 2H), 8.55 (d, *J* = 8.1 Hz, 2H), 8.89 (t, *J* = 8.1 Hz, 1H). **^{13}C NMR** (CD_2Cl_2, 400 MHz): δ 161.7, 149.50, 141.92, 139.3, 137.53, 135.31, 134.79, 131.32, 130.14, 129.31, 129.03, 129.00, 128.97, 128.94, 128.72, 128.69, 128.65, 128.38, 127.84, 125.94, 123.23, 120.83, 120.52, 117.66, 117.55, 117.51, 117.47, 113.27, 54.01, 53.94, 53.74, 53.47, 53.20, 52.93, 49.29, 39.91, 39.83. **^{31}P NMR** (CD_2Cl_2, 400 MHz): δ 89.2. **^{19}F NMR** (CD_2Cl_2, 400 MHz): δ -62.7. **^{11}B NMR** (CD_2Cl_2, 400 MHz) δ -7.68. **FT-IR** (KBr pellet, cm-^{1}): 2963 (w), 1611 (w), 1529 (w), 1475 (w), 1353 (s), 1278 (s), 1111 (m), 1089 (m), 988 (w), 941 (w), 886 (s), 838 (s), 810 (w), 745 (s), 712 (s), 662 (s). **UV-Vis** (λ_{max}): **311 nm. Elemental Analysis;** Calcd for $C_{99}H_{55}B_2F_{48}N_6P$: C, 49.8; H, 2.34; N, 3.19. Found: C, 49.3; H, 2.18; N: 3.69

[Benzyl-BZIMPY-PNMe$_2$][BArF$_{24}$]$_2$ (2d)

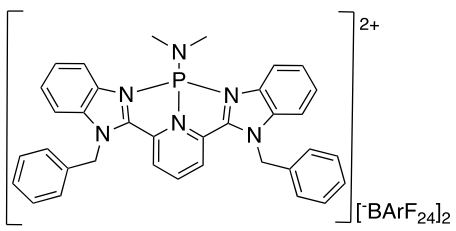

A 100 mL round bottom flask was charged with Benzyl-BZIMPY (0.250g, 1.1mmol) in 5 mL of DCM. A separate 50 mL Schlenk flask was charged with a mixture of $NaBArF_{24}$, (1.443g, 2 mmol) and Me_2NPCl_2 (0.05 g, 1.1 mmol) in 10 mL of DCM, which was then added dropwise into the flask containing Benzyl-BZIMPY solution to obtain a bright yellow suspension. The suspension was stirred for one hour and then allowed to settle. The solution was removed by filtration and the solvent was reduced to 1 mL in volume. The solution was added dropwise into a 50 mL round bottom flask containing stirring hexanes resulting in the formation of a fine yellow powder. The supernatant was removed by filtration and the desired product was further dried under vacuum.
Yield: 1.01 g (99%)
^{1}H NMR (CD_2Cl_2, 400 MHz): δ 2.85 (d, *J* = 14.2 Hz, 6H), 5.29 (d, *J* = 17.0 Hz, 2H), 5.96 (m, 6H), 7.10 (m, 2H), 7.43 – 7.32 (m, 4H), 7.67 (m, 4H), 7.86 (d, *J* = 7.8 Hz, 2H), 8.09 (d, *J* = 8.6 Hz, 2H), 8.35 (d, *J* = 8.1 Hz, 2H), 8.64 (t, *J* = 8.1 Hz, 1H). **^{13}C NMR** (CD_2Cl_2, 400 MHz): δ 162.47, 161.98, 161.48, 160.98, 149.41, 141.84, 139.55, 139.47, 138.10, 135.26, 134.80, 131.52, 130.79, 130.48, 130.32, 130.25, 130.01, 129.32, 129.03, 129.00, 128.98, 128.95, 128.72, 128.69, 128.65, 128.35, 125.94, 125.83, 125.77, 125.57, 125.42, 123.23, 120.52, 117.74, 117.55, 117.51, 117.47, 113.40, 54.01, 53.94, 53.74, 53.67, 53.47, 53.40, 53.20, 52.92, 50.68, 39.91. ^{31}P NMR (CD_2Cl_2, 400 MHz): δ 88.7. **^{19}F NMR** (CD_2Cl_2, 400 MHz) δ -62.7. **^{11}B NMR** (CD_2Cl_2, 400 MHz) δ -7.66. **FT-IR** (KBr pellet, cm^{-1}): 2963 (w), 1611 (m), 1528 (m), 1356 (s), 1278 (m), 1090 (m), 1084 (s), 989 (w), 886 (m), 838 (m), 807 (w), 745 (s), 712 (s), 681 (s), 669 (s). **UV-Vis** (λ_{max}): 325 nm. **Elemental Analysis; Calcd for** $C_{99}H_{55}B_2F_{48}N_6P$: C, 51.86; H, 2.42; N, 3.67. Found: C, 51.63; H, 2.81; N: 3.61

Gutmann-Beckett Method

A solution of triethylphosphine oxide (Et_3PO, 1 eqv.) was prepared in 1 mL of solvent and added to a solution of dicationic Lewis acid in 2 mL of solvent. The mixture was stirred for 15 minutes and the ^{31}P NMR spectrum was obtained. The details of the reaction are displayed in Table below

Table 8: Experimental details of the Gutmann-Beckett test.

Compound amount (g) (0.075 mmol, 1 eqv.)	Et_3PO amount (g) (0.075 mmol, 1 eqv.)	^{31}P NMR chemical shift (ppm)	Gutmann-Beckett AN	Solvent
1a – 0.059	0.01	81.1 (br)	68	CH_3CN
1b – 0.067	0.01	103.4 (br)	116	CH_3CN
1c – 0.057	0.01	106.2 (br), 178.5 (s)	116	CH_2Cl_2
1d – 0.064	0.01	106.2 (s)	116	CH_2Cl_2
2a – 0.166	0.01	102.9 (br), 135.2 (s)	120	CH_3CN
2b – 0.173	0.01	103.2 (br), 135.5 (s)	120	CH_3CN
2c – 0.163	0.01	106.2 (br), 136.7 (s)	120	CH_2Cl_2
2d – 0.171	0.01	102.9 (br), 135 (s)	112	CH_2Cl_2

Reactivity of 2d with other Gutmann-Beckett reagents

A solution of a Gutmann-Beckett reagent was dissolved in 1 mL of dichloromethane (CH_2Cl_2) and added dropwise to a solution of [Benzyl-BZIMPY-$PNMe_2$][$BArF_{24}$]$_2$ (2d) dissolved in 1 mL of CH_2Cl_2. The mixture was stirred and 31P NMR was obtained immediately. The details are outlined in Table 9 below.

Table 9: Experimental details of reactivity between 2d and other Gutmann-Beckett reagents.

Gutmann-Beckett reagent	Amount of GB	Amount of 2d	Ratio (GB:2d)	^{31}P NMR chemical shift (ppm)
Trioctylphosphine oxide (Oct_3PO)	0.01 g, 0.026 mmol	0.059 g, 0.026 mmol	1:1	97.7, 134.8
Trioctylphosphine oxide (Oct_3PO)	0.01 g, 0.026 mmol	0.029 g, 0.013 mmol	2:1	99.6, 134.8, 136.2
Triphenylphosphine Oxide (Ph_3PO)	0.01 g, 0.036 mmol	0.082 g, 0.036 mmol	1:1	135.6

Stoichiometric and Catalytic Reactions

Reactivity of Lewis acids with triphenylphosphine (PPh_3)

A solution of PPh_3 (0.01g, 0.038 mmol, 1 eqv.) was prepared in 1 mL of solvent and added to a solution of dicationic Lewis acid dissolved in 2 mL of solvent. The mixture was stirred and the ^{31}P NMR was obtained and monitored over 24h. The reaction details are listed in Table 10 below. The spectral details are displayed in the appendix.

Table 10: Experimental details of reactivity between dicationic Lewis acids (1a-d and 2a-d) and triphenylphosphine.

Compound	Compound amount	PPh_3 amount	Ratio LA:PPh_3	Solvent
1a	0.030 g, 0.038 mmol	0.01g, 0.038 mmol	1:1	CH_3CN
1b	0.034 g, 0.038 mmol	0.01g, 0.038 mmol	1:1	CH_3CN
1c	0.088 g, 0.038 mmol	0.01g, 0.038 mmol	1:1	CH_2Cl_2
1d	0.089 g, 0.038 mmol	0.01g, 0.038 mmol	1:1	CH_2Cl_2
2a	0.029 g, 0.038 mmol	0.01g, 0.038 mmol	1:1	CH_3CN
2b	0.033g, 0.038 mmol	0.01g, 0.038 mmol	1:1	CH_3CN
2c	0.088 g, 0.038 mmol	0.01g, 0.038 mmol	1:1	CH_2Cl_2
2d	0.089 g, 0.038 mmol	0.01g, 0.038 mmol	1:1	CH_2Cl_2
2d	0.175 g, 0.076 mmol	0.01g, 0.038 mmol	1:0.5	CH_2Cl_2
2d	0.089 g, 0.038 mmol	0.02g, 0.076 mmol	1:2	CH_2Cl_2
2d	0.089 g, 0.038 mmol	0.03 g, 0.114 mmol	1:3	CH_2Cl_2

Reactivity of Lewis acids with H_2O and D_2O

A 5mL vial was charged with 0.01 g of dicationic Lewis acid and placed in a fumehood. H_2O or D_2O was added to the vial with the Lewis acid just enough to cover the solid and allowed to stir. A colour change from bright yellow and red to white was observed. ^{1}H and ^{31}P NMR were obtained. ^{1}H NMR spectra exhibited one peak at 4.80 ppm for H_2O.

Catalytic reactivity of Lewis acids

Dimerization of 1,1-Diphenylethylene

In a 20 mL vial, a solution of the phosphenium catalyst (10% mol) was prepared in 0.6 mL CD_3CN for compounds 1a, 1b, 2a and 2d and CD_2Cl_2 for compounds 1c, 1d and 2c, 2d. 1,1-diphenylethylene (0.3 mmol) was added at ambient temperature and the reaction mixture was transferred to a NMR tube. The sample was sealed, aggregated and allowed to react at ambient temperature for 24 hours. The conversion to the desired product (1-methyl-1,3,3-triphenyl-2,3-dihydro-1H-indene) was not observed for any of the catalysts. Supporting spectra are listed in the appendix.

Hydrodefluorination of 1-fluoropentane

In a 20 mL vial, a solution of the phosphenium catalyst (10% mol) was prepared in 0.25 mL of CD_3CN for compounds 1a, 1b, 2a and 2d and CD_2Cl_2 for compounds 1c, 1d and 2c, 2d. Triethyl silane (Et_3SiH, 0.3 mmol) was added at ambient temperature, the reaction was briefly stirred, and then 1-fluoropentane was added (0.3 mmol). The reaction mixture was transferred to a J-Young NMR tube and left at ambient temperature for 24 h, while being monitored by ^{19}F NMR spectroscopy after 1h, 5h and 24 h. The reaction was heated to 70^{o}C and allowed to react for 24 h to achieve higher conversion. The results of the reaction are shown in Scheme 11 and supporting spectra can be found in the appendix.

Hydrosilylation of α-methylstyrene

In a 20 mL vial, a solution of the phosphenium catalyst (10% mol) was prepared in 0.25 mL of CD_3CN for compounds 1a, 1b, 2a and 2d and CD_2Cl_2 for compounds 1c, 1d and 2c, 2d. Triethyl silane (Et_3SiH, 0.3 mmol) was added at ambient temperature, the reaction mixture was briefly stirred, and then α-methylstyrene (0.4 mmol) was added. The mixture was transferred to a NMR tube and monitored by ^1H NMR over 1h, 5h and 24h. The results of the catalytic conversion are displayed in Scheme 12 and supporting spectra can be found in the appendix.

Dehydrocoupling of Phenol with Et_3SiH

In a 20 mL vial, a solution of the phosphenium catalyst (10 %mol) was prepared in 0.25 mL of CD_3CN for compounds 1a, 1b, 2a and 2d and CD_2Cl_2 for compounds 1c, 1d and 2c, 2d. Triethyl silane (Et3SiH, 0.3 mmol) was added at ambient temperature, the reaction mixture was briefly stirred, and then added to a vial containing phenol (0.3 mmol). The mixture was transferred to a NMR tube and monitored by ^1H NMR over 1h, 5h and 24h. The results of the catalytic conversion are displayed in Scheme 13 and supporting spectra can be found in the appendix.

Hydroarylation of Diphenylamine with 1,1-diphenylethylene

In a 20 mL vial, a solution of the phosphenium catalyst (10 %mol) was prepared in 0.25 mL of CD_3CN for compounds 1a, 1b, 2a and 2d and CD_2Cl_2 for compounds 1c, 1d and 2c, 2d. Diphenylamine (Ph_2NH, 0.3 mmol) was added at ambient temperature, the reaction mixture was briefly stirred, and then added to a vial containing and 1,1-diphenylethylene ($Ph_2C_2H_2$, 0.3 mmol). The mixture was transferred to a NMR tube and monitored by ^1H NMR over 1h, 5h and 24h. The results of the catalytic conversion are displayed in Scheme 7 and supporting spectra can be found in the appendix.

Hydroarylation of Pyrrole with 1,1-diphenylethylene

In a 20 mL vial, a solution of the phosphenium catalyst (10 %mol) was prepared in 0.25 mL of CD_3CN for compounds 1a, 1b, 2a and 2d and CD_2Cl_2 for compounds 1c, 1d and 2c, 2d. 1,1-diphenylethylene ($Ph_2C_2H_2$, 1.41 mmol) was added at ambient temperature, the reaction mixture was briefly stirred, and then added to a vial containing pyrrole (0.7 mmol). The mixture was transferred to a NMR tube and monitored by ^1H NMR over 1h, 5h and 24h. The results of the catalytic conversion are displayed in Scheme 8 and supporting spectra can be found in the appendix.

Hydrothiolation of 1,1-diphenylethylene with Thiophenol

In a 20 mL vial, a solution of the phosphenium catalyst (10 %mol) was prepared in 0.25 mL of CD_3CN for compounds 1a, 1b, 2a and 2d and CD_2Cl_2 for compounds 1c, 1d and 2c, 2d. 1,1-diphenylethylene ($Ph_2C_2H_2$, 0.5 mmol) was added at ambient temperature, the reaction mixture was briefly stirred, and then added to a vial containing thiophenol (PhSH, 0.6 mmol). The mixture was transferred to a NMR tube and monitored by ^1H NMR over 1h, 5h and 24h. The results of the catalytic conversion are displayed in Scheme 9 and supporting spectra can be found in the appendix.

Computational Methods

Electronic structure calculations, including geometry optimizations and frequency calculations, were performed with the *Gaussian 16* package[44] using M06-2X[45] functional and the def2-TZVP[46] basis set with the inclusion of Grimme's GD3 empirical dispersion[47] method. The absence of any imaginary frequencies with an absolute magnitude greater than 10 cm^{-1} confirmed that each optimized structure was indeed located at a minimum on its potential energy hypersurface. Natural population analyses were performed on optimized structures using *NBO 6.0*[50] at the M06-2X/def2-TZVP level of theory. Fluoride ion affinities (FIAs) were calculated as previously proposed, using the experimental FIA of carbonyl difluoride.[67]

References.

(1) Power, P. P. Main-Group Elements as Transition Metals. *Nature* **2010**, *463* (7278), 171–177. https://doi.org/10.1038/nature08634.

(2) R. Jaffe, J. Price, G. Ceder, R. Eggert, T. Graedel, K. Gschneidner, M. Hitzman, F. Houle, A. Hurd, R. Kelley, A. King, D. Milliron, B. S. and F. S. Energy Critical Elements: Securing Materials for Emerging Technologies. *Min. Eng.* **2011**, *63* (8), 33–34.

(3) Ortega, C. Element Recovery and Sustainability. *Green Process. Synth.* **2014**, *3* (4), 303–303. https://doi.org/10.1515/gps-2014-0041.

(4) Hunt, A. J.; Matharu, A. S.; King, A. H.; Clark, J. H. The Importance of Elemental Sustainability and Critical Element Recovery. *Green Chem.* **2015**, *17* (4), 1949–1950. https://doi.org/10.1039/c5gc90019k.

(5) King, R. B. *Inorganic Chemistry of Main Group Elements*; 1995.

(6) Chivers, T. *Main Group and Noble Gas Chemistry*; Elsevier Inc., 2013. https://doi.org/10.1016/b978-0-12-409547-2.05369-5.

(7) Zhuang, Z. P.; Dai, X.; Dong, W. Da; Jiang, L. Q.; Wang, L.; Li, C. F.; Yang, J. X.; Wu, L.; Hu, Z. Y.; Liu, J.; et al. Tris(Trimethylsilyl) Borate as Electrolyte Additive Alleviating Cathode Electrolyte Interphase for Enhanced Lithium-Selenium Battery. *Electrochim. Acta* **2021**, *393*. https://doi.org/10.1016/j.electacta.2021.139042.

(8) Reiter, D.; Holzner, R.; Porzelt, A.; Frisch, P.; Inoue, S. Silylated Silicon–Carbonyl Complexes as Mimics of Ubiquitous Transition-Metal Carbonyls. *Nat. Chem.* **2020**, *12* (12), 1131–1135. https://doi.org/10.1038/s41557-020-00555-4.

(9) Zhao, Lili; Pan, Sudip; Zhou, Mingfei; Frenking, G. Comment on "Observation of Alkaline Earth Complexes M(CO)8 (M = Ca, Sr, or Ba) That Mimic Transition Metals." *Science (80-.).* **2019**, *365* (6453), 1–5. https://doi.org/10.1126/science.aay2355.

(10) Légaré, M. A.; Bélanger-Chabot, G.; Rang, M.; Dewhurst, R. D.; Krummenacher, I.; Bertermann, R.; Braunschweig, H. One-Pot, Room-Temperature Conversion of Dinitrogen to Ammonium Chloride at a Main-Group Element. *Nat. Chem.* **2020**, *12* (11), 1076–1080. https://doi.org/10.1038/s41557-020-0520-6.

(11) Naber J.E., de Jong K.P, Stork W.H.J, Kuipers H.P.C.E., P. M. F. M. Chapter 2 Catalytic

Processes in Industry. In *Studies in Surface Science and Catalysis*; 1994; pp 2197–2219. https://doi.org/doi.org/10.1016/S0167-2991(08)63783-0.

(12) Leitao, E. M.; Jurca, T.; Manners, I. Catalysis in Service of Main Group Chemistry Offers a Versatile Approach to P-Block Molecules and Materials. *Nat. Chem.* **2013**, *5* (10), 817–829. https://doi.org/10.1038/nchem.1749.

(13) Bouhadir, G.; Bourissou, D. Unusual Geometries in Main Group Chemistry. *Chem. Soc. Rev.* **2004**, *33* (4), 210–217. https://doi.org/10.1039/b306615k.

(14) Weskamp, T.; Kohl, F. J.; Hieringer, W.; Gleich, D.; Herrmann, W. A. Highly Active Ruthenium Catalysts for Olefin Metathesis: The Synergy of N-Heterocyclic Carbenes and Coordinatively Labile Ligands. *Angew. Chemie - Int. Ed.* **1999**, *38* (16), 2416–2419. https://doi.org/10.1002/

(15) Pagliaro, M.; Pandarus, V.; Ciriminna, R.; Béland, F.; DemmaCarà, P. Heterogeneous versus Homogeneous Palladium Catalysts for Cross-Coupling Reactions. *ChemCatChem* **2012**, *4* (4), 432–445. https://doi.org/10.1002/cctc.201100422.

(16) Corma, A.; García, H. Lewis Acids as Catalysts in Oxidation Reactions: From Homogeneous to Heterogeneous Systems. *Chem. Rev.* **2002**, *102* (10), 3837–3892. https://doi.org/10.1021/cr010333u.

(17) Salim, S. S.; Bell, A. T. Effects of Lewis Acid Catalysts on the Hydrogenation and Cracking of Three-Ring Aromatic and Hydroaromatic Structures Related to Coal. *Fuel* **1984**, *63* (4), 469–476. https://doi.org/10.1016/0016-2361(84)90281-3.

(18) Yang, Y.; Zhang, Y.; Wang, J. Lewis Acid Catalyzed Direct Cyanation of Indoles and Pyrroles with N-Cyano-N-Phenyl-p-Toluenesulfonamide (NCTS). *Org. Lett.* **2011**, *13* (20), 5608–5611. https://doi.org/10.1021/ol202335p.

(19) Deshpande, N.; Parulkar, A.; Joshi, R.; Diep, B.; Kulkarni, A.; Brunelli, N. A. Epoxide Ring Opening with Alcohols Using Heterogeneous Lewis Acid Catalysts: Regioselectivity and Mechanism. *J. Catal.* **2019**, *370*, 46–54. https://doi.org/10.1016/j.jcat.2018.11.038.

(20) Beatty, R. *Phosphorus*; Marshall Cavendish Corporation: New York, 2001.

(21) Emsley, J. *The 13th Element: The Sordid Tale of Murder, Fire, and Phosphorus*; 2002. https://doi.org/047144149X.

(22) Fernández-García, C.; Coggins, A. J.; Powner, M. W. A Chemist's Perspective on the Role of Phosphorus at the Origins of Life. *Life* **2017**, *7* (3). https://doi.org/10.3390/life7030031.

(23) Balázs, G.; Seitz, A.; Scheer, M. Activation of White Phosphorus (P4) by Main Group Elements and Compounds. *Compr. Inorg. Chem. II (Second Ed. From Elem. to Appl.* **2013**, *1*, 1105–1132. https://doi.org/10.1016/B978-0-08-097774-4.00143-1.

(24) McWilliams, A. R.; Dorn, H.; Manners, I. New Inorganic Polymers Containing Phosphorus. **2002**, *220*, 141–167. https://doi.org/10.1007/3-540-45731-3_6.

(25) Wittig, G.; Haag, W. Über Triphenyl-phosphinmethylene Als Olefinbildende Reagenzien (II. Mitteil.1)). *Chem. Ber.* **1955**, *88* (11), 1654–1666. https://doi.org/10.1002/cber.19550881110.

(26) Cowley, A. H.; Kemp, R. A. Synthesis and Reaction Chemistry of Stable Two-Coordinate Phosphorus Cations (Phosphenium Ions). *Chem. Rev.* **1985**, *85* (5), 367–382. https://doi.org/10.1021/cr00069a002.

(27) Gudat, D.; Haghverdi, A.; Hupfer, H.; Nieger, M. Stability and Electrophilicity of Phosphorus Analogues of Arduengo Carbenes—An Experimental and Computational Study. *Chem. - A Eur. J.* **2000**, *6* (18), 3414–3425. https://doi.org/10.1002/1521-3765(20000915)6:18<3414::aid-chem3414>3.0.co;2-p.

(28) Burford, N.; Ragogna, P. J. New Synthetic Opportunities Using Lewis Acidic Phosphines. *J. Chem. Soc. Dalt. Trans.* **2002**, No. 23, 4307–4315. https://doi.org/10.1039/b208715d.

(29) Slattery, J. M.; Hussein, S. How Lewis Acidic Is Your Cation? Putting Phosphenium Ions on the Fluoride Ion Affinity Scale. *Dalt. Trans.* **2012**, *41* (6), 1808–1815. https://doi.org/10.1039/c1dt11636c.

(30) Dunn, N. L.; Ha, M.; Radosevich, A. T. Main Group Redox Catalysis: Reversible P III/P V Redox Cycling at a Phosphorus Platform. *J. Am. Chem. Soc.* **2012**, *134* (28), 11330–11333. https://doi.org/10.1021/ja302963p.

(31) Chitnis, S. S.; Krischer, F.; Stephan, D. W. Catalytic Hydrodefluorination of C−F Bonds by an Air-Stable PIII Lewis Acid. *Chem. - A Eur. J.* **2018**, *24* (25), 6543–6546. https://doi.org/10.1002/chem.201801305.

(32) Gilhula, J. C.; Radosevich, A. T. Tetragonal Phosphorus(v) Cations as Tunable and Robust Catalytic Lewis Acids. *Chem. Sci.* **2019**, *10* (30), 7177–7182. https://doi.org/10.1039/c9sc02463h.

(33) Strauß, B.; Gutmann, V.; Linert, W. Investigations on the Spin-Crossover Complex [Fe(Bzimpy)2](ClO4)2 and Its Mn2+, Co2+, Ni2+ and Zn2+ Analogues. *Monatshefte für Chemie Chem. Mon.* **1993**, *124* (4), 391–399. https://doi.org/10.1007/BF00814135.

(34) Wang Jianqi, Zhu Ying, Wang Shuangxi, Gao Yici, S. Q. SYNTHESIS AND CRYSTAL STRUCTURE OF THE COMPLEX [Lu (Bzimpy-H)(NO3)2(CH3OH2) Bzimpy 2CH3OH. **1994**, *13* (9), 1405–1409.

(35) Zhang, Y.; Zhou, Q. F.; Huo, G. F.; Yin, G. Q.; Zhao, X. L.; Jiang, B.; Tan, H.; Li, X.; Yang, H. B. Hierarchical Self-Assembly of an Alkynylplatinum(Ll) Bzimpy-Functionalized Metallacage via Pt···Pt and π-π Interactions. *Inorg. Chem.* **2018**, *57* (7), 3516–3520. https://doi.org/10.1021/acs.inorgchem.7b02777.

(36) Günnaz, S. Evaluation of Cu(II) Bzimpy Complexes by 1H-NMR and Catalytic Activities. *J. Coord. Chem.* **2020**, *73* (20–22), 3014–3027. https://doi.org/10.1080/00958972.2020.1840561.

(37) Swidan, A.; St Onge, P. B. J.; Binder, J. F.; Suter, R.; Burford, N.; MacDonald, C. L. B. 2,6-Bis(Benzimidazol-2-Yl)Pyridine Complexes of Group 14 Elements. *Dalt. Trans.* **2019**, *48* (22), 7835–7843. https://doi.org/10.1039/c9dt00995g.

(38) Kocherga, M.; Castaneda, J.; Walter, M. G.; Zhang, Y.; Saleh, N. A.; Wang, L.; Jones, D. S.; Merkert, J.; Donovan-Merkert, B.; Li, Y.; et al. Si(Bzimpy)2-a Hexacoordinate Silicon Pincer Complex for Electron Transport and Electroluminescence. *Chem. Commun.* **2018**, *54* (100), 14073–14076. https://doi.org/10.1039/c8cc07681b.

(39) Swidan, A.; Binder, J. F.; Onge, B. J. S.; Suter, R.; Burford, N.; Macdonald, C. L. B. 2,6-Bis(Benzimidazol-2-Yl)Pyridines as More Electron-Rich and Sterically Accessible Alternatives to 2,6-Bis(Imino)Pyridine for Group 13 Coordination Chemistry. *Dalt. Trans.* **2019**, *48* (4), 1284–1291. https://doi.org/10.1039/c8dt04276d.

(40) Inkaya, E.; Günnaz, S.; Özdemir, N.; Dayan, O.; Dinçer, M.; Çetinkaya, B. Synthesis, Spectroscopic Characterization, X-Ray Structure and DFT Studies on 2,6-Bis(1-Benzyl-1H-

Benzo[d]Imidazol-2-Yl)Pyridine. *Spectrochim. Acta - Part A Mol. Biomol. Spectrosc.* **2013**, *103*, 255–263. https://doi.org/10.1016/j.saa.2012.11.039.

(41) CORBRIDGE, D. E. C. *Phosphorus Chemistry, Biochemistry and Technology*, 6th editio.; Taylor & Francis Group, LLC, 2013; Vol. 273. https://doi.org/10.1038/273324a0.

(42) Sinclair, H.; Suter, R.; Burford, N.; McDonald, R.; Ferguson, M. J. Pyridine, Thiophosphine, and Selenophosphine Complexes of the Phenylphosphine Dication. *Can. J. Chem.* **2018**, *96* (7), 689–693. https://doi.org/10.1139/cjc-2017-0596.

(43) Chang, Y. C.; Hu, C. Y.; Liang, Y. H.; Hong, F. E. Computational and 31P NMR Studies of Moisture-Metastable Cyclic Diaminophosphine Oxide Preligands. *Polyhedron* **2016**, *105*, 123–136. https://doi.org/10.1016/j.poly.2015.12.017.

(44) M. J. Frisch, G. W. Trucks, H. B. Schlegel, G. E. Scuseria, M. A. Robb, J. R. Cheeseman, G. Scalmani, V. Barone, G. A. Petersson, H. Nakatsuji, X. Li, M. Caricato, A. V. Marenich, J. Bloino, B. G. Janesko, R. Gomperts, B. Mennucci, H. P. Hratchian, J. V., and D. J. F. Gaussian 16, Revision A.03. Gaussian, Inc: Wallingford CT 2016.

(45) Zhao, Y.; Truhlar, D. G. The M06 Suite of Density Functionals for Main Group Thermochemistry, Thermochemical Kinetics, Noncovalent Interactions, Excited States, and Transition Elements: Two New Functionals and Systematic Testing of Four M06-Class Functionals and 12 Other Function. *Theor. Chem. Acc.* **2008**, *120* (1–3), 215–241. https://doi.org/10.1007/s00214-007-0310-x.

(46) Weigend, F. Accurate Coulomb-Fitting Basis Sets for H to Rn. *Phys. Chem. Chem. Phys.* **2006**, *8* (9), 1057–1065. https://doi.org/10.1039/b515623h.

(47) Grimme, S.; Antony, J.; Ehrlich, S.; Krieg, H. A Consistent and Accurate Ab Initio Parametrization of Density Functional Dispersion Correction (DFT-D) for the 94 Elements H-Pu. *J. Chem. Phys.* **2010**, *132* (15). https://doi.org/10.1063/1.3382344.

(48) Marre, Marie-Rose; Sanchez, Michel; Wolf, Robert; Jaud, Joël; Galy, J. Les Liaisons Phosphore-Azote via l'etude Cristalline et Moleculaire d'un Iminodiazaphospholane. **1983**, No. 4.

(49) Brunel, J. M.; Legrand, O.; Escadrille, A. V; Niemen, N. First Iminodiazaphospholidines with a Stereogenic Phosphorus Center . Application to Asymmetric ´ Nierie Chimiques d '

Aix Marseille Iminophosphoranes Have Been Extensively Used for the High Yield Syntheses of a Large Variety of Imines . 1-5 Although Tri-. **1999**, No. 18, 5807–5808.

(50) E. D. Glendening, J. K. Badenhoop, A. E. Reed, J. E. Carpenter, J. A. Bohmann, C. M. Morales, C. R. L. and F. W. No Title. Theoretical Chemistry Institute, University of Wisconsin, Madison, WI 2013.

(51) Mehlmann, P.; Witteler, T.; Wilm, L. F. B.; Dielmann, F. Isolation, Characterization and Reactivity of Three-Coordinate Phosphorus Dications Isoelectronic to Alanes and Silylium Cations. *Nat. Chem.* **2019**, *11* (12), 1139–1143. https://doi.org/10.1038/s41557-019-0348-0.

(52) Waked, A. E.; Chitnis, S. S.; Stephan, D. W. P(v) Dications: Carbon-Based Lewis Acid Initiators for Hydrodefluorination. *Chem. Commun.* **2019**, *55* (61), 8971–8974. https://doi.org/10.1039/c9cc04010b.

(53) Lafortune, J. H. W.; Szkop, K. M.; Farinha, F. E.; Johnstone, T. C.; Postle, S.; Stephan, D. W. Probing Steric Influences on Electrophilic Phosphonium Cations: A Comparison of [(3,5-(CF3)2C6H3)3PF]+ and [(C6F5)3PF]+. *Dalt. Trans.* **2018**, *47* (33), 11411–11419. https://doi.org/10.1039/c8dt02594k.

(54) Busca, G. *Heterogeneous Catalytic Materials: Solid State Chemistry, Surface Chemistry and Catalytic Behaviour.*; Elsevier B.V.: Amsterdam, 2014.

(55) MacDonald, Charles L.B., Lafortune James H.W., Varga Ksenia., Swidan Ala'aeddeen., Ovens Jeffrey S., Qu Zheng-Wang., Grimme Stefan. Interesting and Unanticipated Reactivity of Group 15 Dications Supported by BZIMPY Ligands. In *IUPAC CCCE 2021 - 48th World Chemistry Congress & 104th Canadian Chemistry Conference and Exhibition*; Calgary, AB, 2022.

(56) Ellis, B. D.; MacDonald, C. L. B. Redetermination of a Cyclic Triphosphenium Hexachlorostannate Salt at 173 K. *Acta Crystallogr. Sect. E Struct. Reports Online* **2006**, *62* (6), 1235–1236. https://doi.org/10.1107/S1600536806016345.

(57) Tang G., Zhou G.J., Ni F., Hu L.M., Z. Y. F. 31P NMR and ESI-MS Studies on Some Intermediates of the Peptide Coupling Reagents Triphenyl-Chlorophosphoranes. *Chinese Chem. Lett.* **2005**, *16* (3), 385–388.

(58) Pérez, M.; Mahdi, T.; Hounjet, L. J.; Stephan, D. W. Electrophilic Phosphonium Cations Catalyze Hydroarylation and Hydrothiolation of Olefins. *Chem. Commun.* **2015**, *51* (56), 11301–11304. https://doi.org/10.1039/c5cc03572d.

(59) Bayne, J. M.; Holthausen, M. H.; Stephan, D. W. Pyridinium-Phosphonium Dications: Highly Electrophilic Phosphorus-Based Lewis Acid Catalysts. *Dalt. Trans.* **2016**, *45* (14), 5949–5957. https://doi.org/10.1039/c5dt03796d.

(60) Mallov, I.; Stephan, D. W. Ferrocenyl-Derived Electrophilic Phosphonium Cations (EPCs) as Lewis Acid Catalysts. *Dalt. Trans.* **2016**, *45* (13), 5568–5574. https://doi.org/10.1039/c6dt00105j.

(61) Arduengo, A. J.; Stewart, C. A.; Davidson, F.; Dixon, D. A.; Becker, J. Y.; Culley, B. S. A.; Mizenl, M. B. The Synthesis, Structure, and Chemistry of 10-Pn-3 Systems: Tricoordinate Hypervalent Pnicogen Compounds. **1987**, *109* (3).

(62) McCarthy, S. M.; Lin, Y. C.; Devarajan, D.; Chang, J. W.; Yennawar, H. P.; Rioux, R. M.; Ess, D. H.; Radosevich, A. T. Intermolecular N-H Oxidative Addition of Ammonia, Alkylamines, and Arylamines to a Planar Σ3-Phosphorus Compound via an Entropy-Controlled Electrophilic Mechanism. *J. Am. Chem. Soc.* **2014**, *136* (12), 4640–4650. https://doi.org/10.1021/ja412469e.

(63) Zhao, W.; McCarthy, S. M.; Lai, T. Y.; Yennawar, H. P.; Radosevich, A. T. Reversible Intermolecular E-H Oxidative Addition to a Geometrically Deformed and Structurally Dynamic Phosphorous Triamide. *J. Am. Chem. Soc.* **2014**, *136* (50), 17634–17644. https://doi.org/10.1021/ja510558d.

(64) Cui, J.; Li, Y.; Ganguly, R.; Inthirarajah, A.; Hirao, H.; Kinjo, R. Metal-Free σ-Bond Metathesis in Ammonia Activation by a Diazadiphosphapentalene. *J. Am. Chem. Soc.* **2014**, *136* (48), 16764–16767. https://doi.org/10.1021/ja509963m.

(65) Addison, A. W.; Burke, P. J. Synthesis of Some Imidazole- and Pyrazole- Derived Chelating Agents. *J. Heterocycl. Chem.* **1981**, *18* (4), 803–805. https://doi.org/10.1002/jhet.5570180436.

(66) Swidan, A.; Binder, J. F.; Onge, B. J. S.; Suter, R.; Burford, N.; Macdonald, C. L. B. 2,6-Bis(Benzimidazol-2-Yl)Pyridines as More Electron-Rich and Sterically Accessible

Alternatives to 2,6-Bis(Imino)Pyridine for Group 13 Coordination Chemistry. *Dalt. Trans.* **2019**, *48* (4), 1284–1291. https://doi.org/10.1039/c8dt04276d.

(67) Christe, K. O.; Dixon, D. A.; McLemore, D.; Wilson, W. W.; Sheehy, J. A.; Boatz, J. A. On a Quantitative Scale for Lewis Acidity and Recent Progress in Polynitrogen Chemistry. *J. Fluor. Chem.* **2000**, *101* (2), 151–153. https://doi.org/10.1016/S0022-1139(99)00151-7.

Appendix.

Characterizational Spectra

1a - [Allyl-BZIMPY-PPh][OTf]$_2$

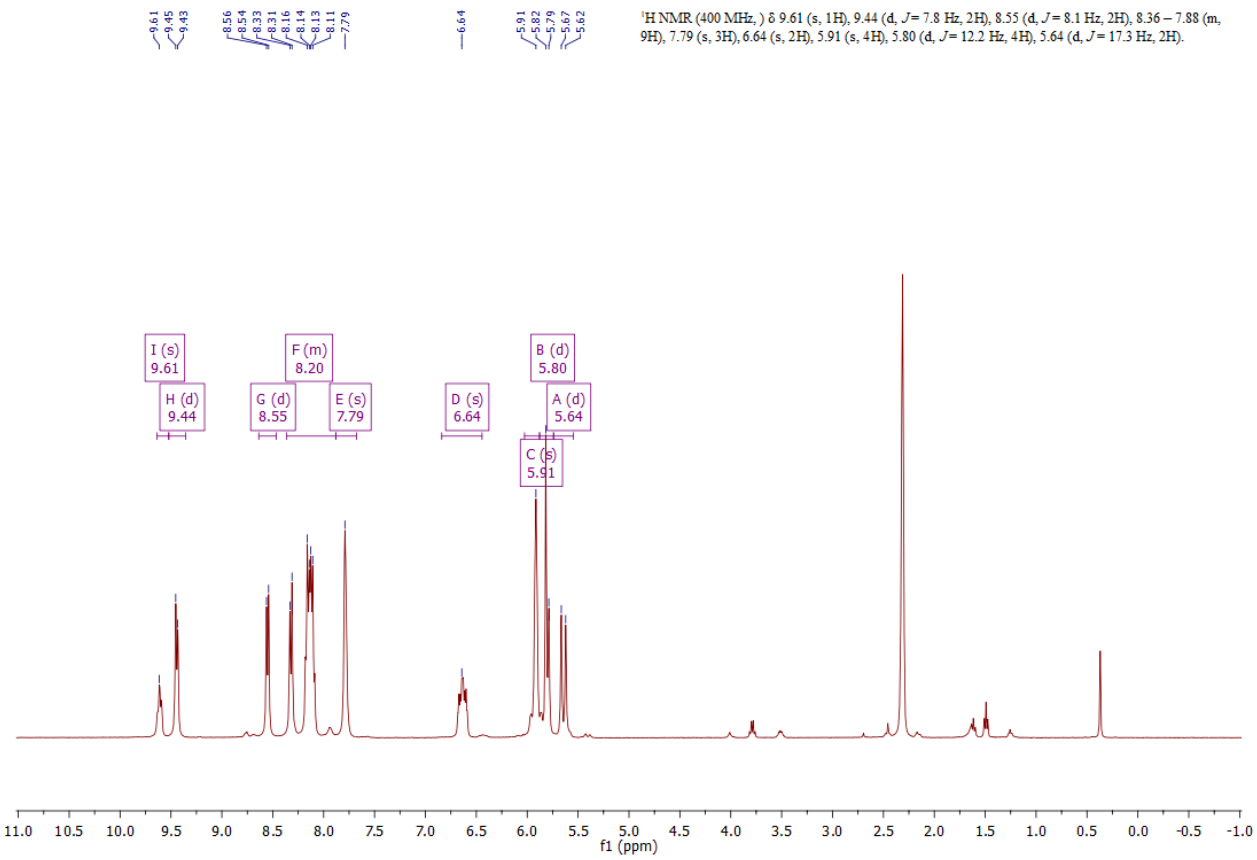

Figure 27: ^{1}H NMR of 1a in CD_3CN

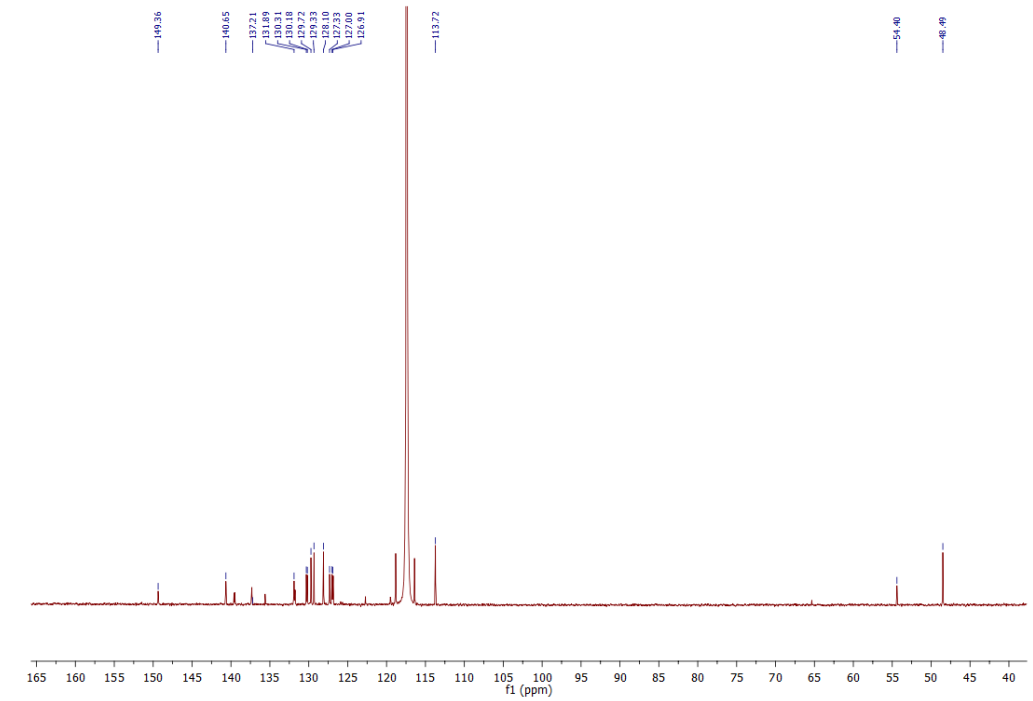

Figure 28: ^{13}C NMR of 1a done in CD_3CN

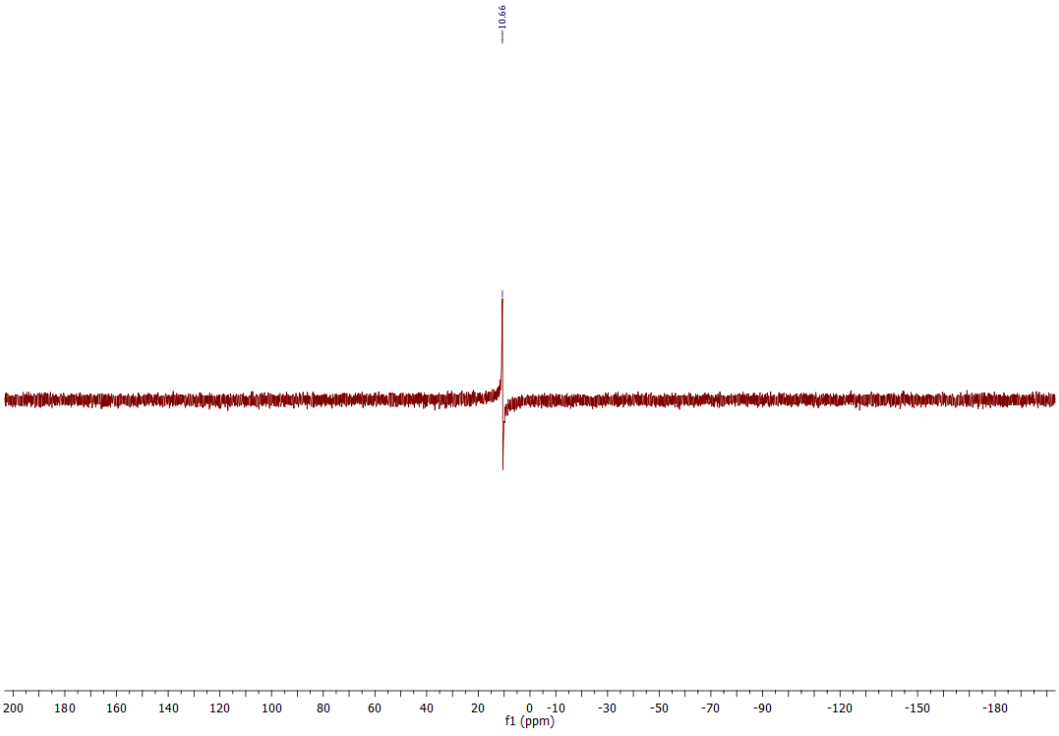

Figure 29: ^{31}P NMR of 1a done in CD_3CN

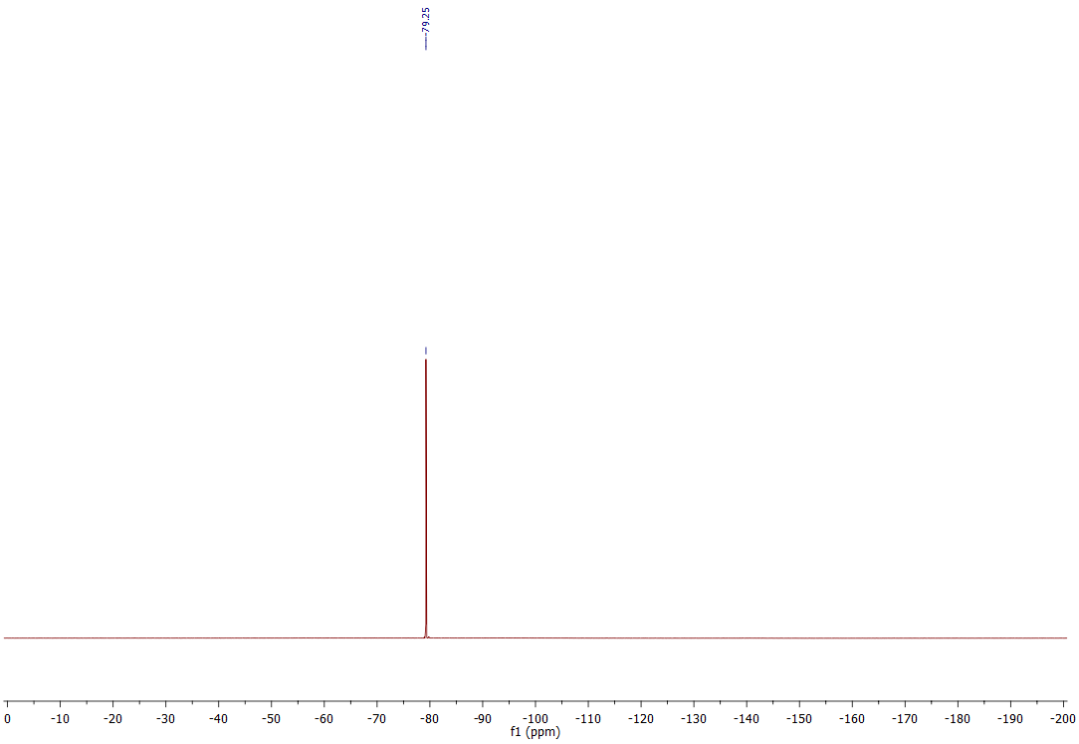

Figure 30: ^{19}F NMR of 1a done in CD_3CN

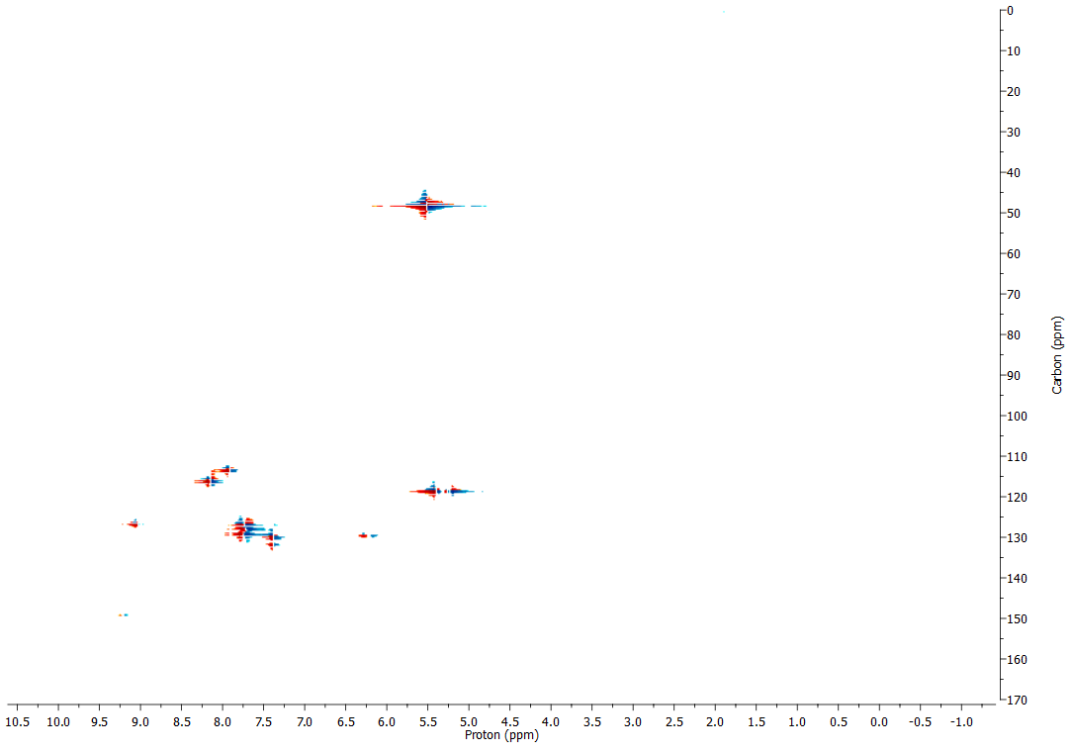

Figure 31: HSQC of 1a in CD_3CN

1b - [Benzyl-BZIMPY-PPh][OTf]$_2$

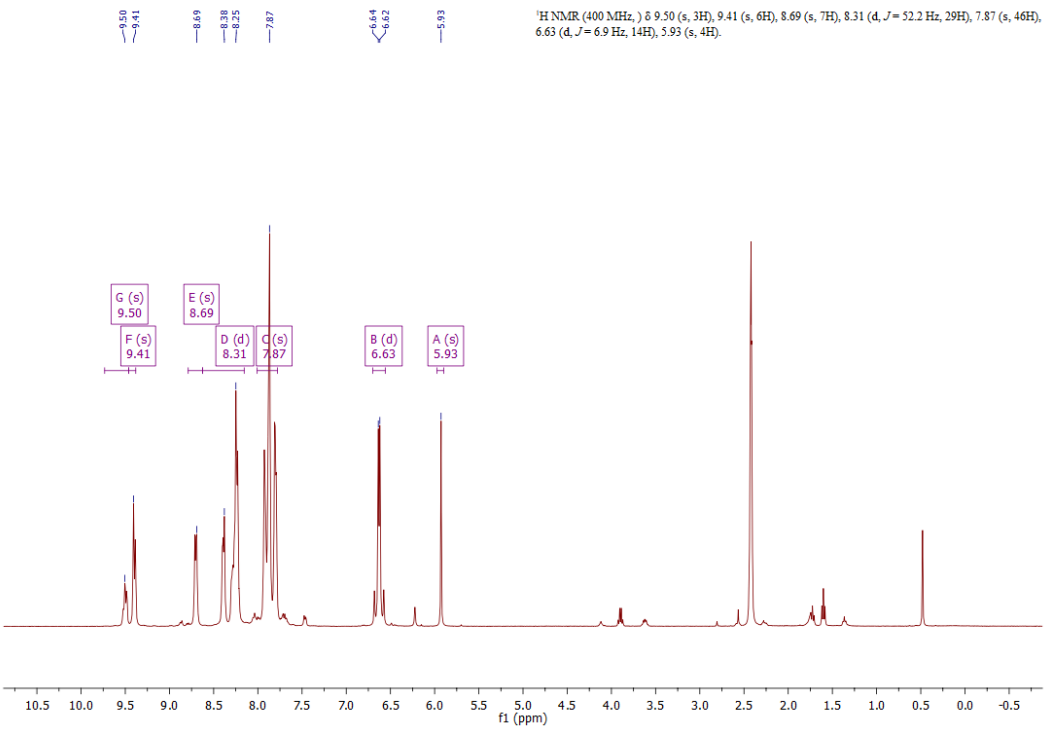

Figure 32: ^{1}H NMR of 1b done in CD_3CN

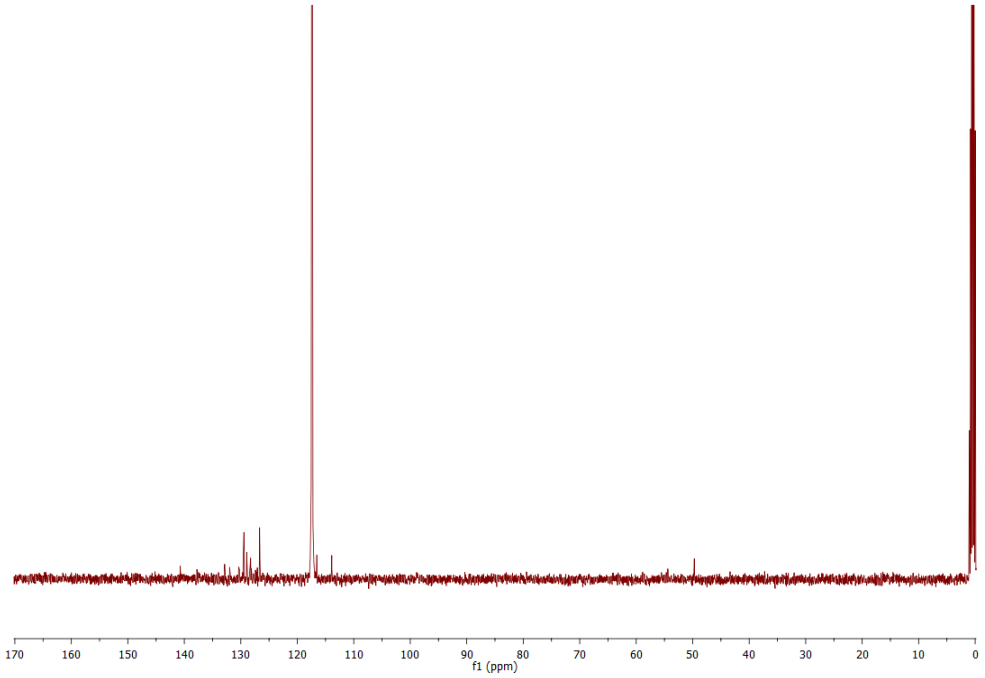

Figure 33: ^{13}C NMR of 1b done in CD_3CN

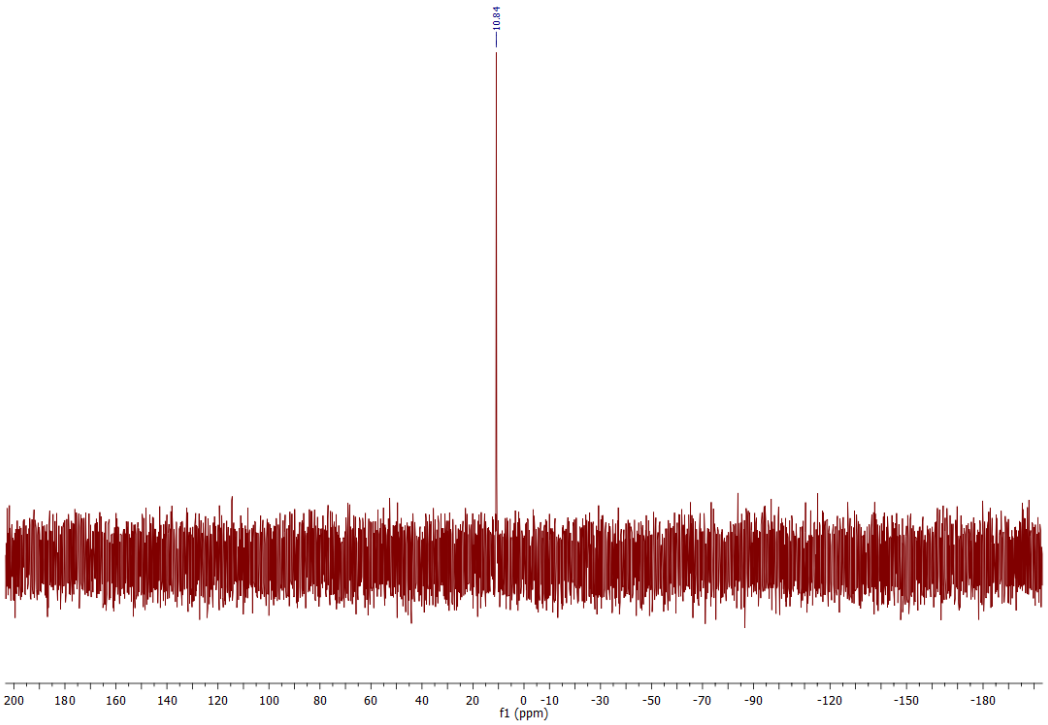

Figure 34: ^{31}P NMR of 1b done in CD_3CN

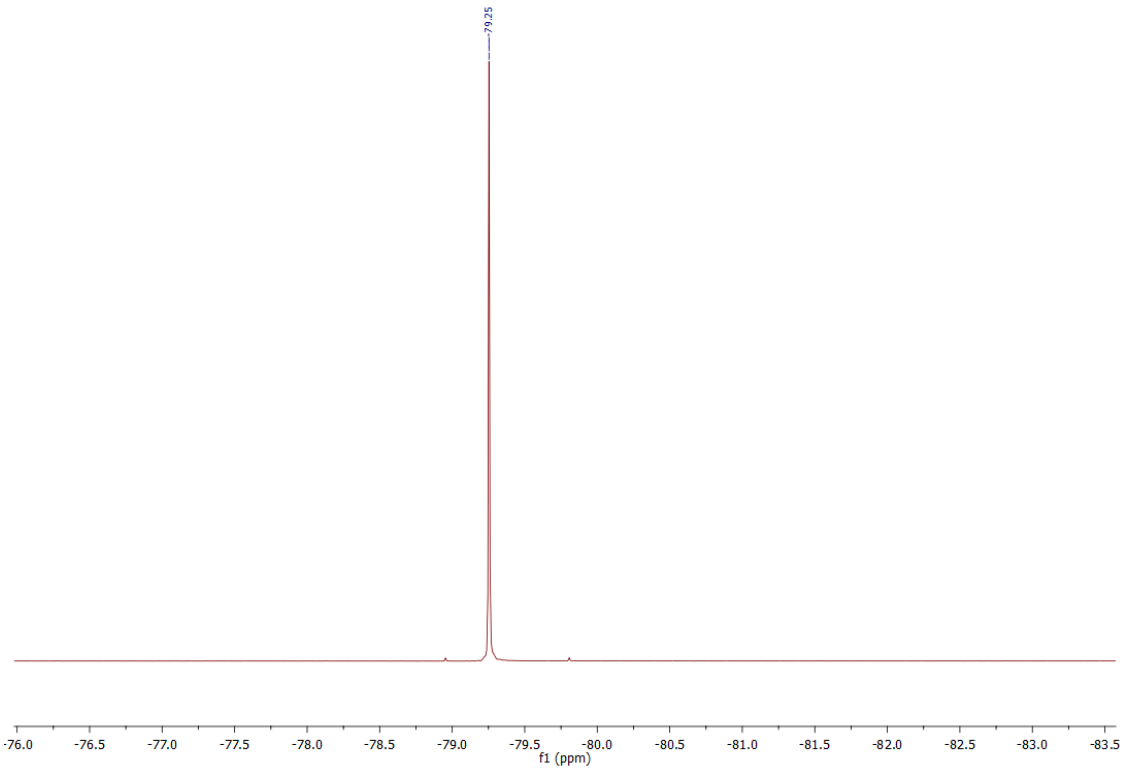

Figure 35:^{19}F NMR of 1b done in CD_3CN

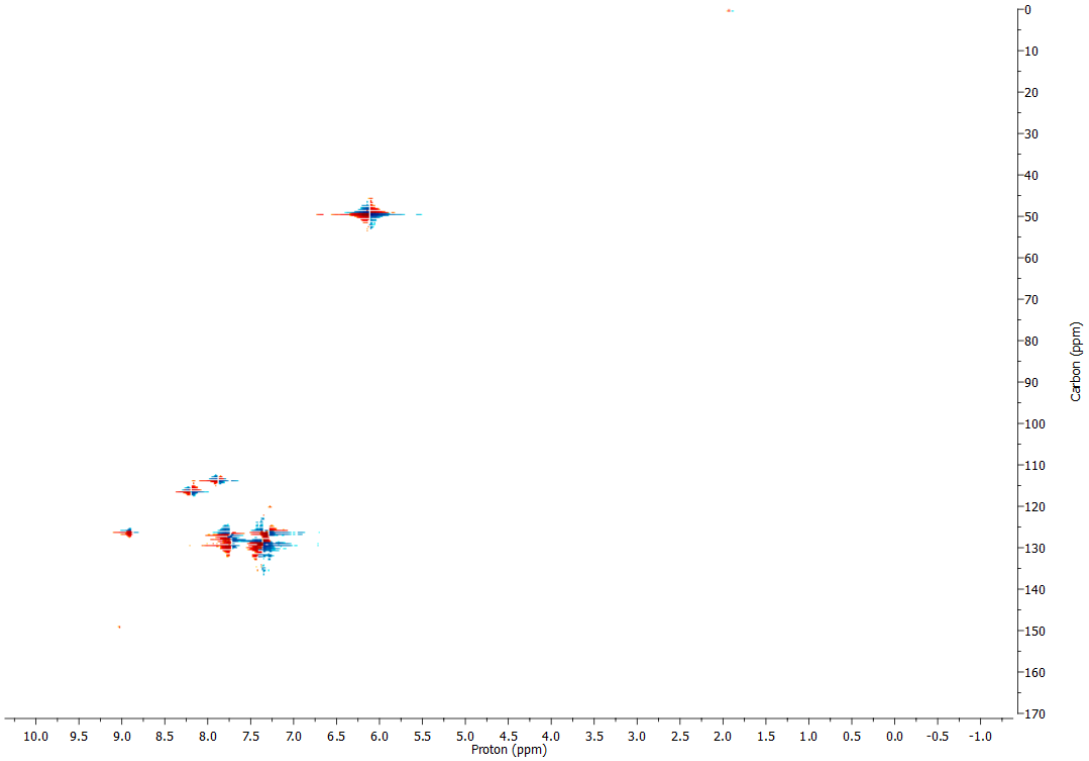

Figure 36: HSQC spectrum of 1b done in CD_3CN

1c - [Allyl-BZIMPY-PPh][$BArF_{24}$]$_2$

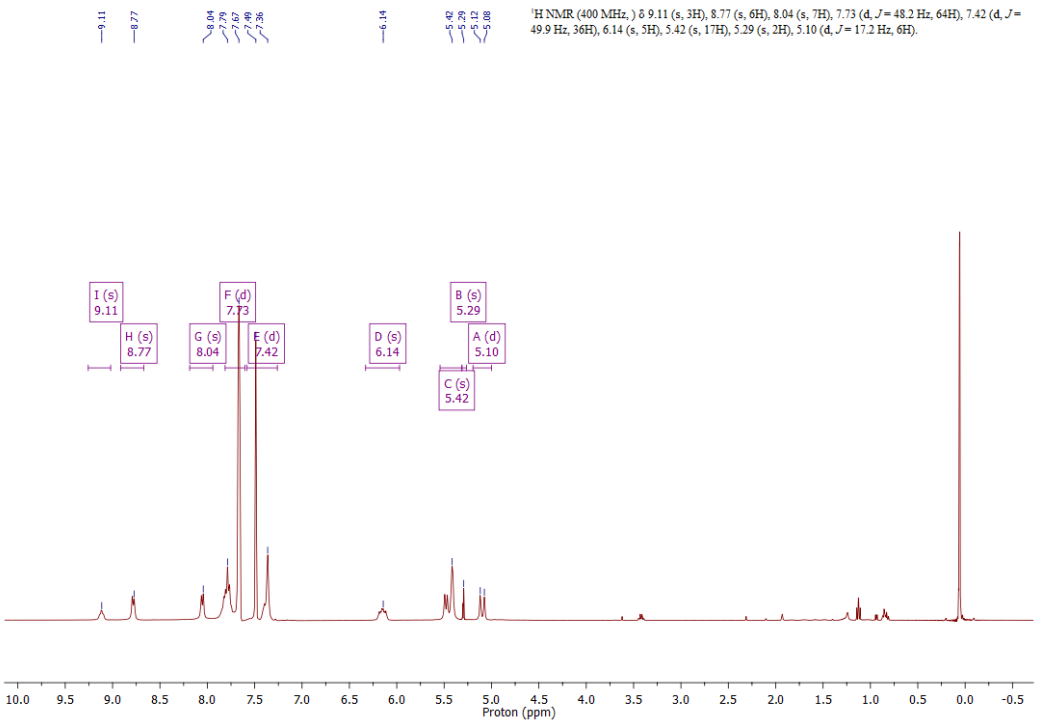

Figure 37: ^{1}H NMR of 1c in CD_2Cl_2

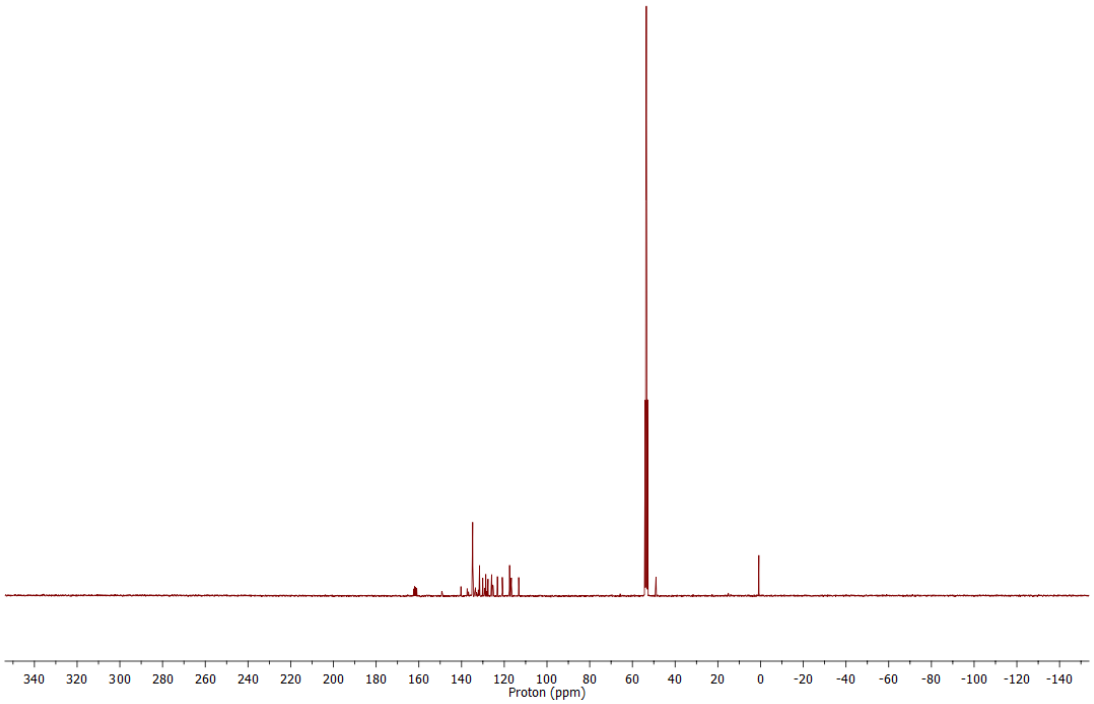

Figure 38: ^{13}C NMR of 1c done in CD_2Cl_2

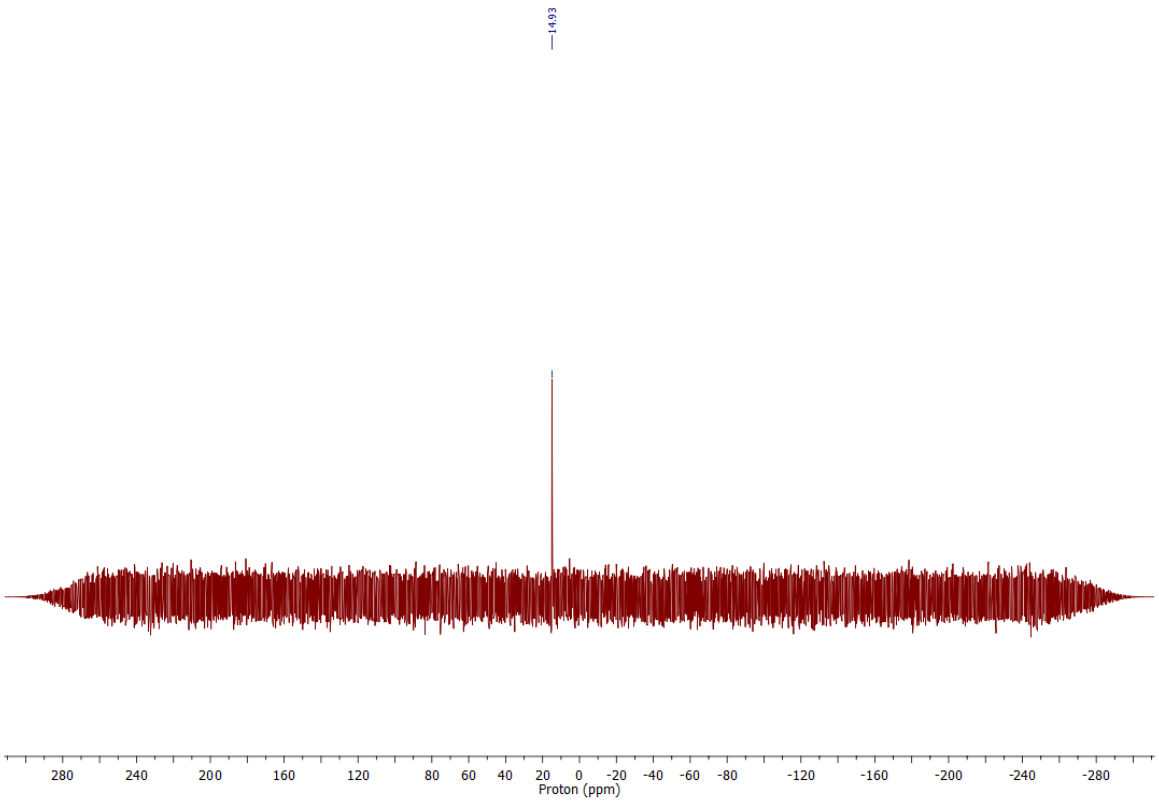

Figure 39: ^{31}P NMR of 1c done in CD_2Cl_2

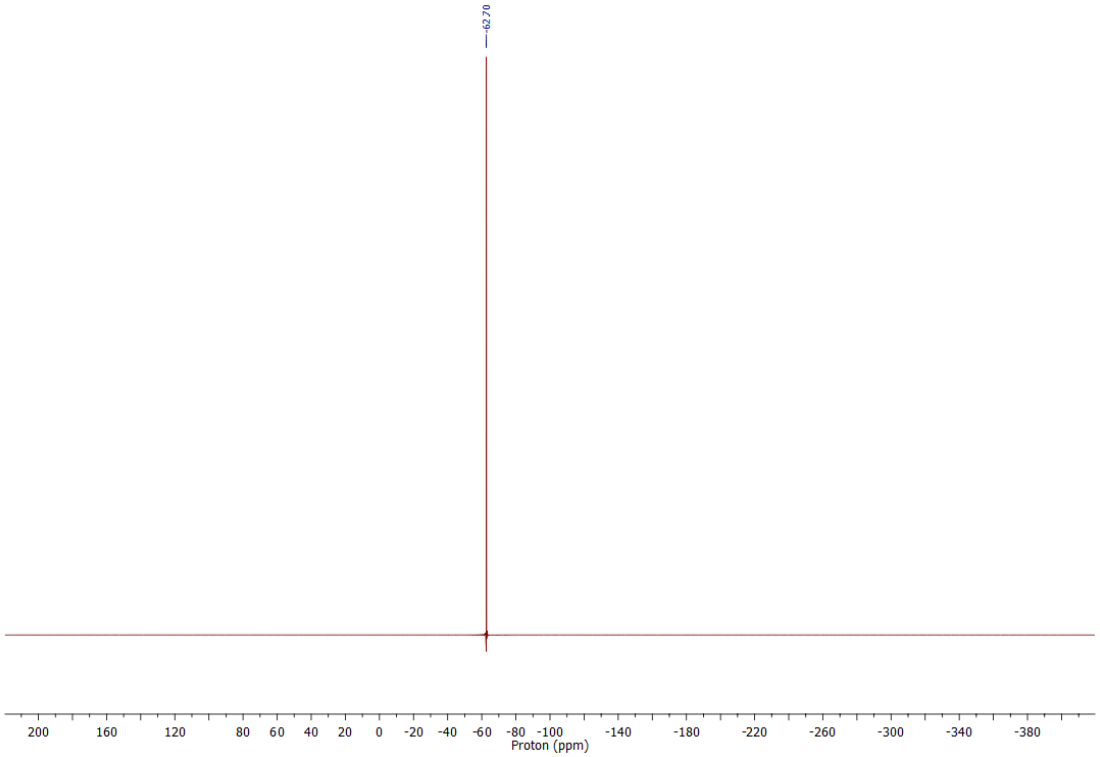

Figure 40: ^{19}F NMR of 1c done in CD_2Cl_2

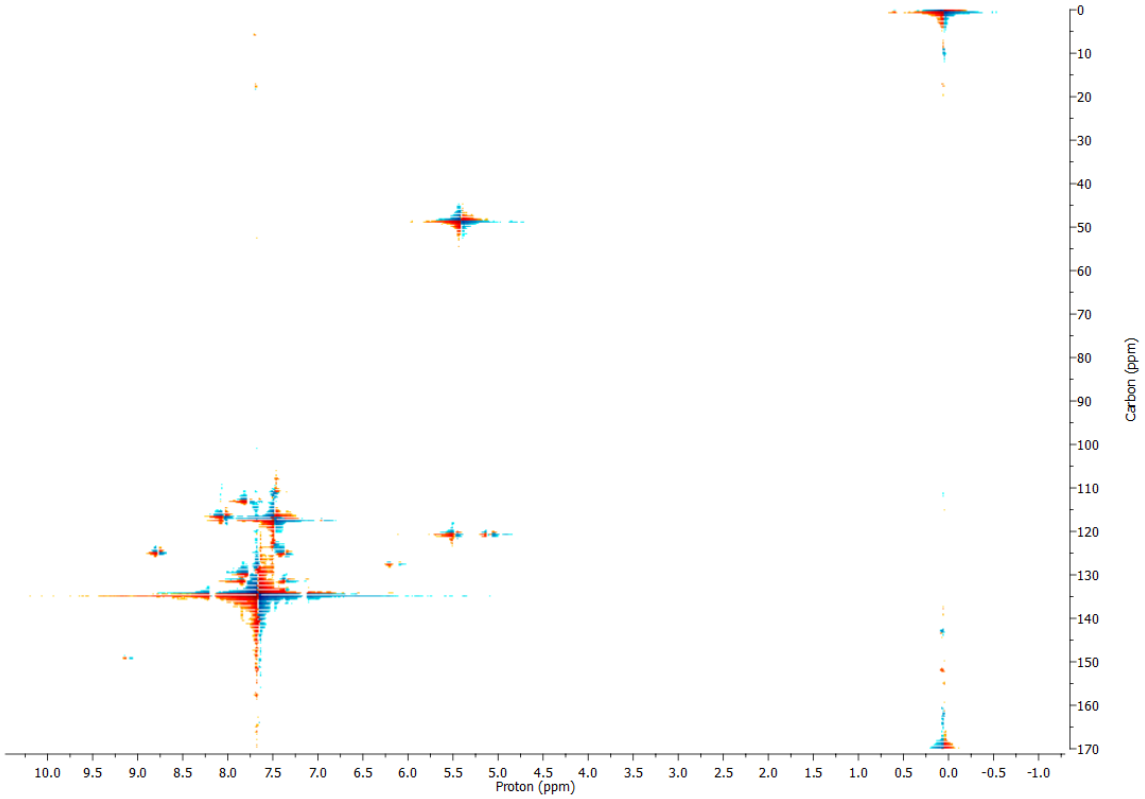

Figure 41: HSQC spectrum of 1c done in CD_2Cl_2

1d - [Benzyl-BZIMPY-PPh][$BArF_{24}$]$_2$

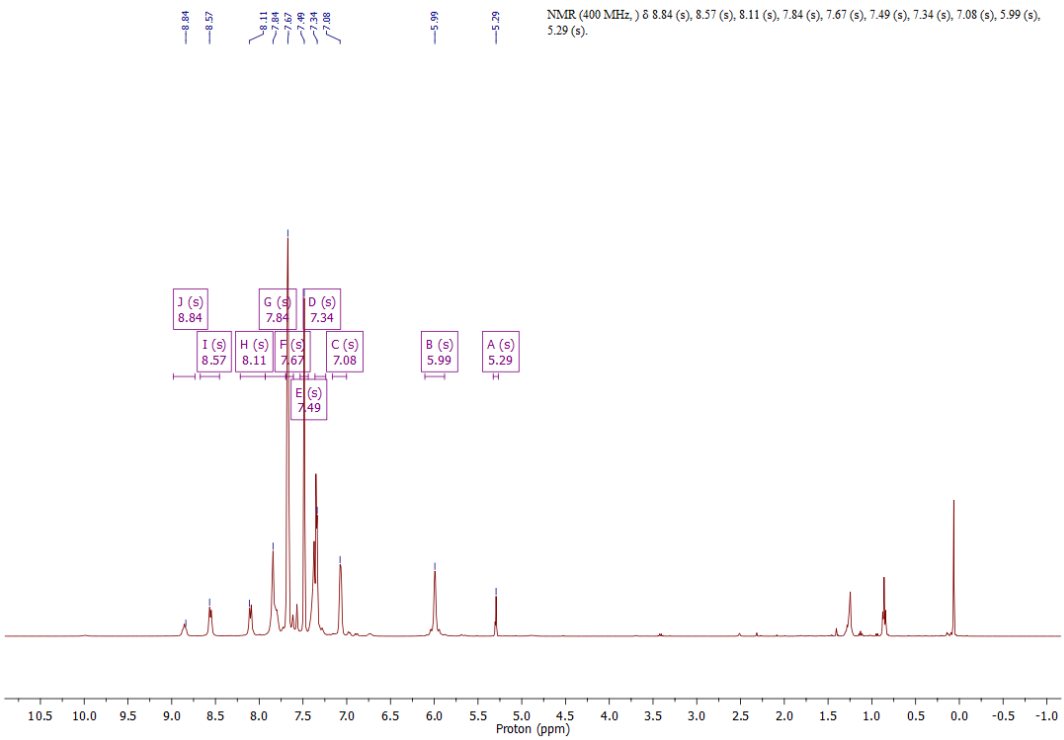

Figure 42: ^{1}H NMR of 1d done in CD_2Cl_2

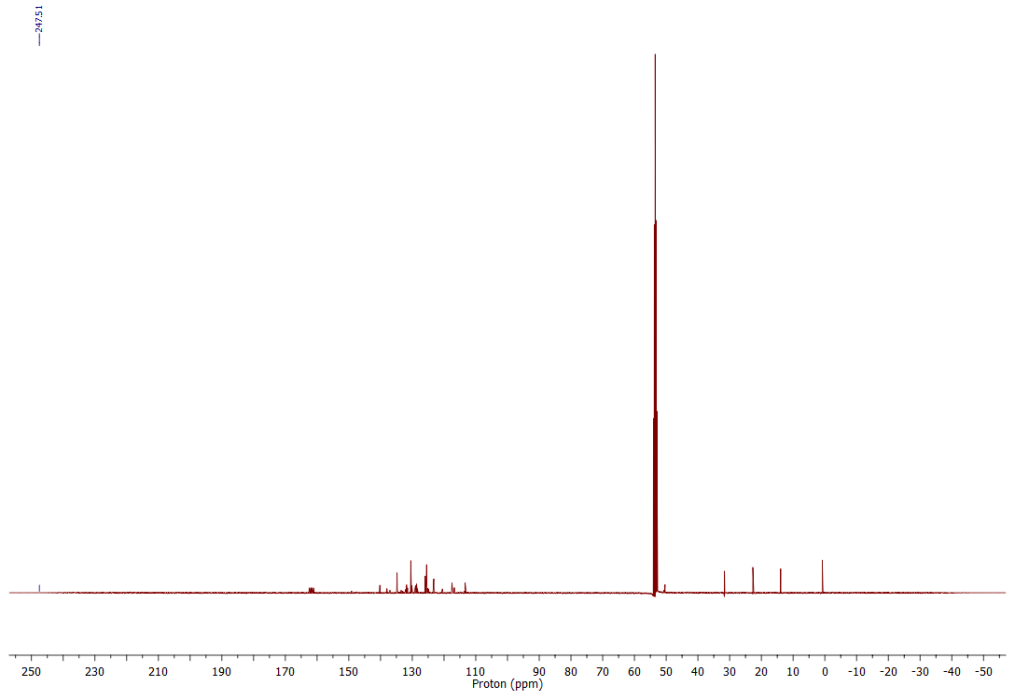

Figure 43: ^{13}C NMR of 1d done in CD_2Cl_2

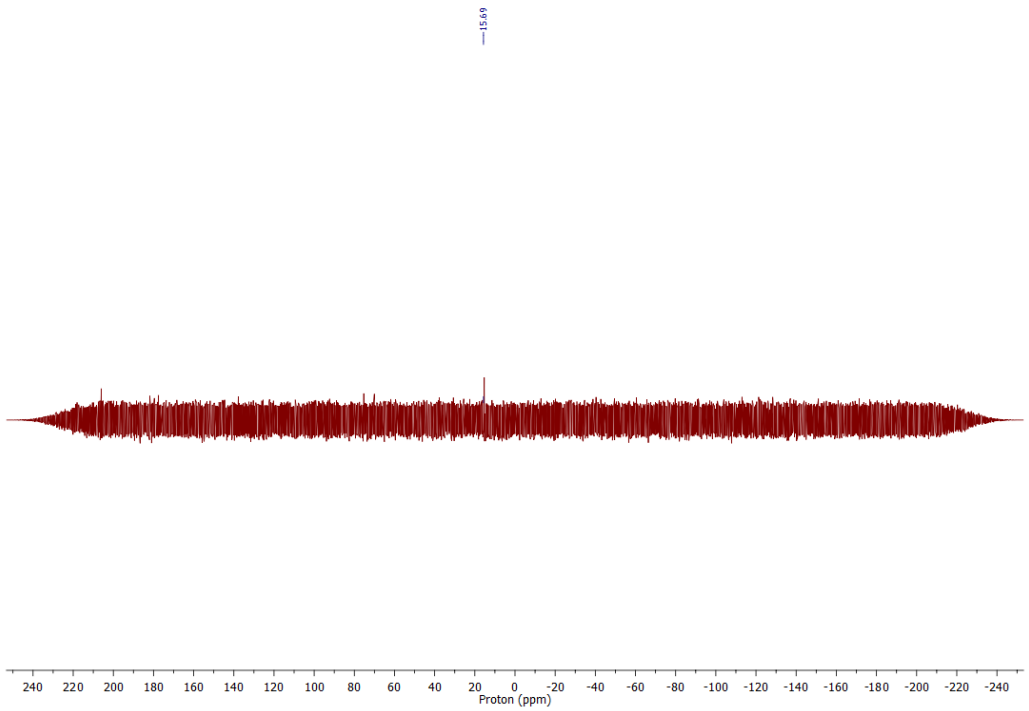

Figure 44: ^{31}P NMR of 1d done in CD_2Cl_2

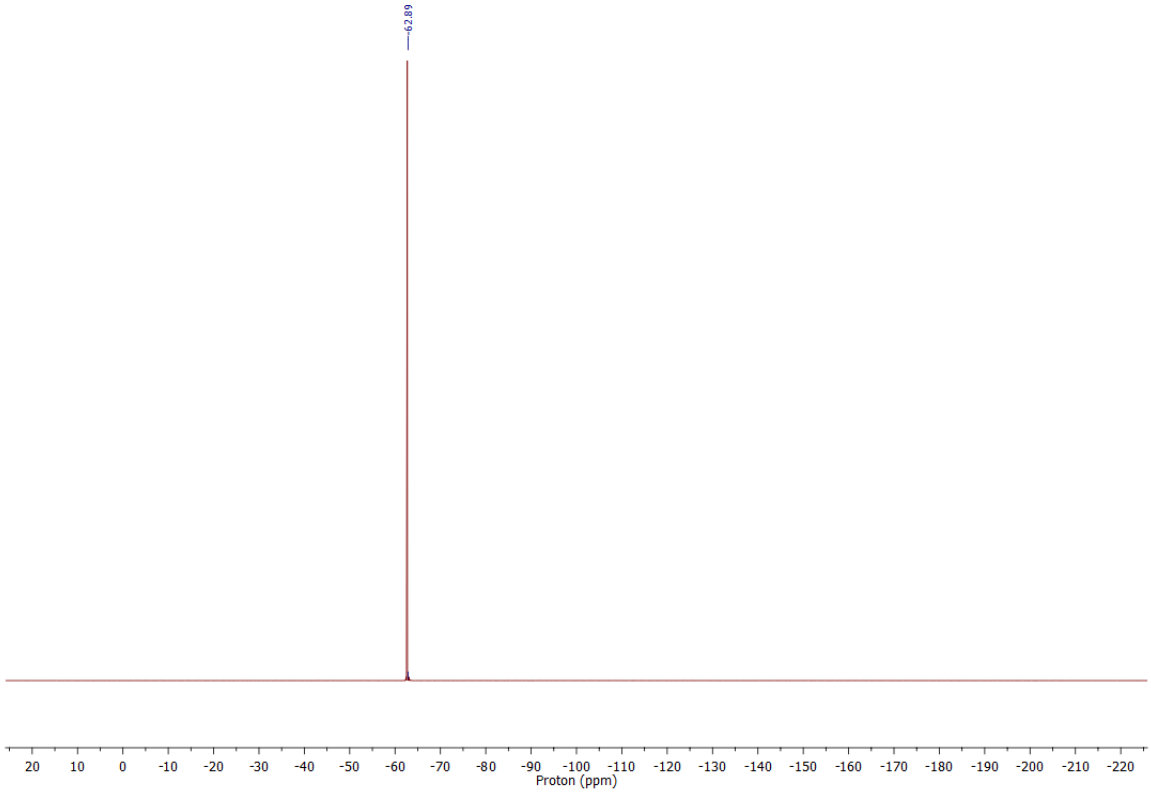

Figure 45: ^{19}F NMR of 1d one in CD_2Cl_2

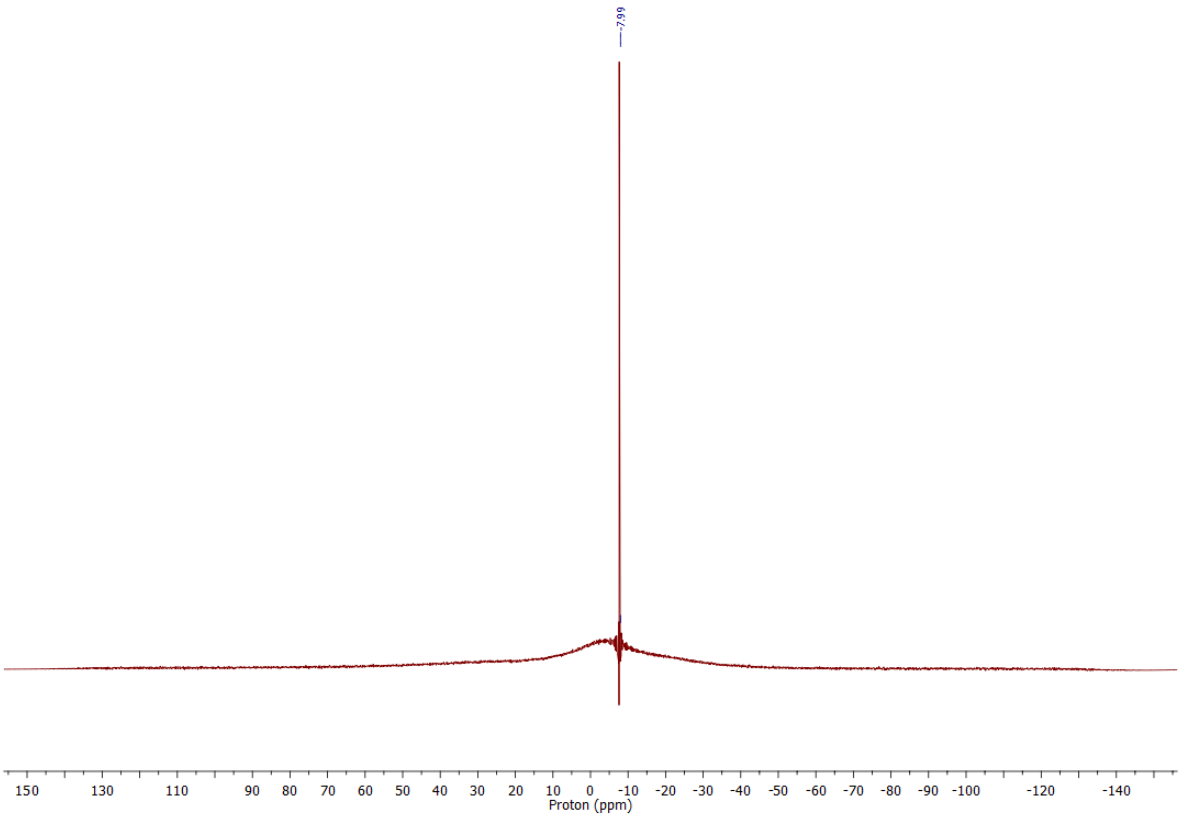

Figure 46: ^{11}B NMR of 1d one in CD_2Cl_2

2a – [Allyl-BZIMPY-PNMe$_2$][OTf]$_2$

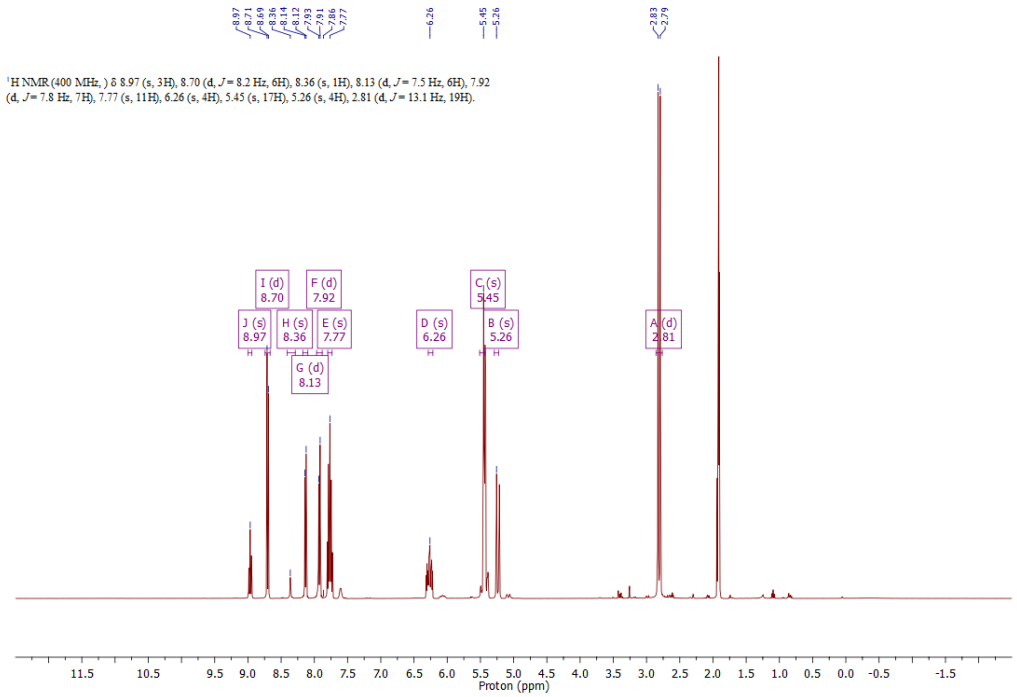

Figure 47: ^{1}H NMR of 2a done in CD_3CN

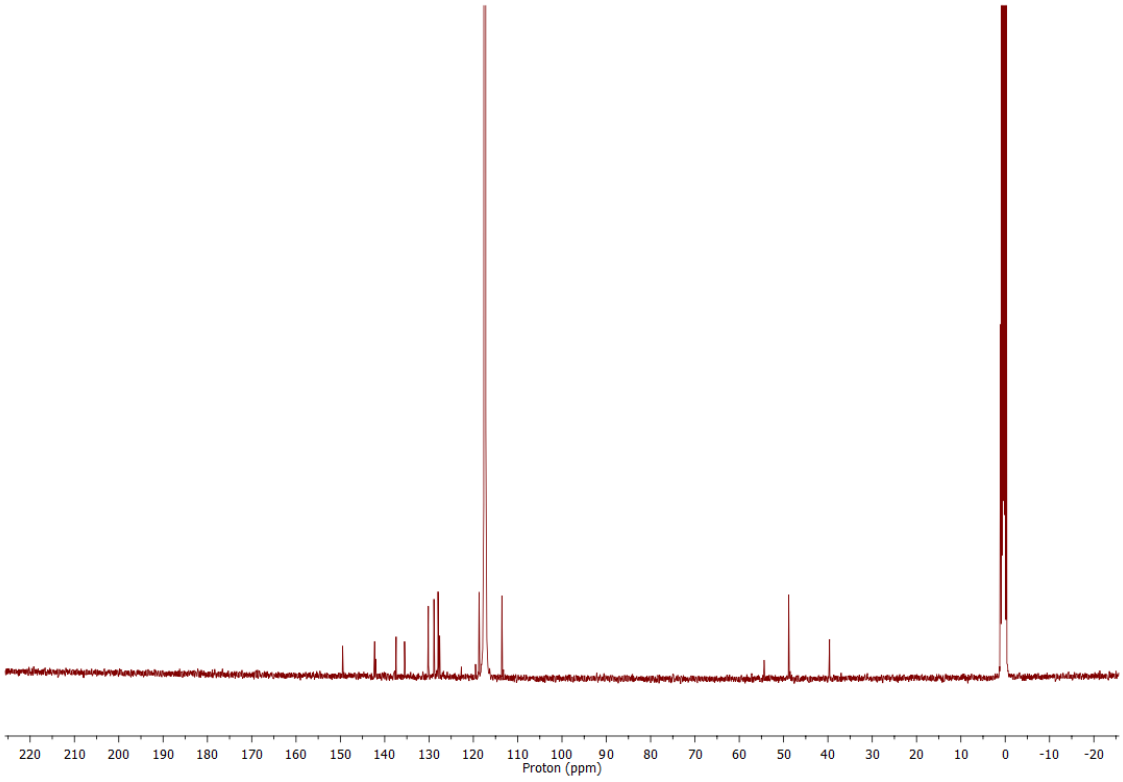

Figure 48: ^{13}C NMR of 2a done in CD_3CN

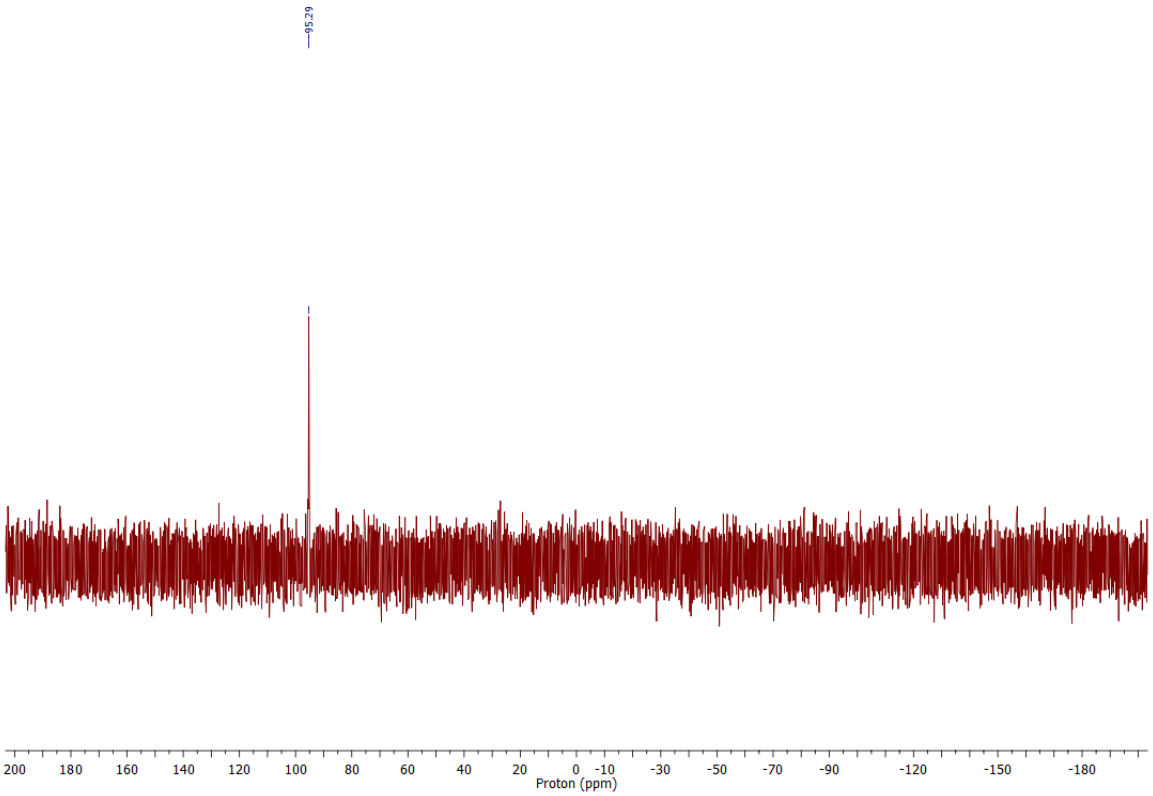

Figure 49: ^{31}P NMR of 2a done in CD_3CN

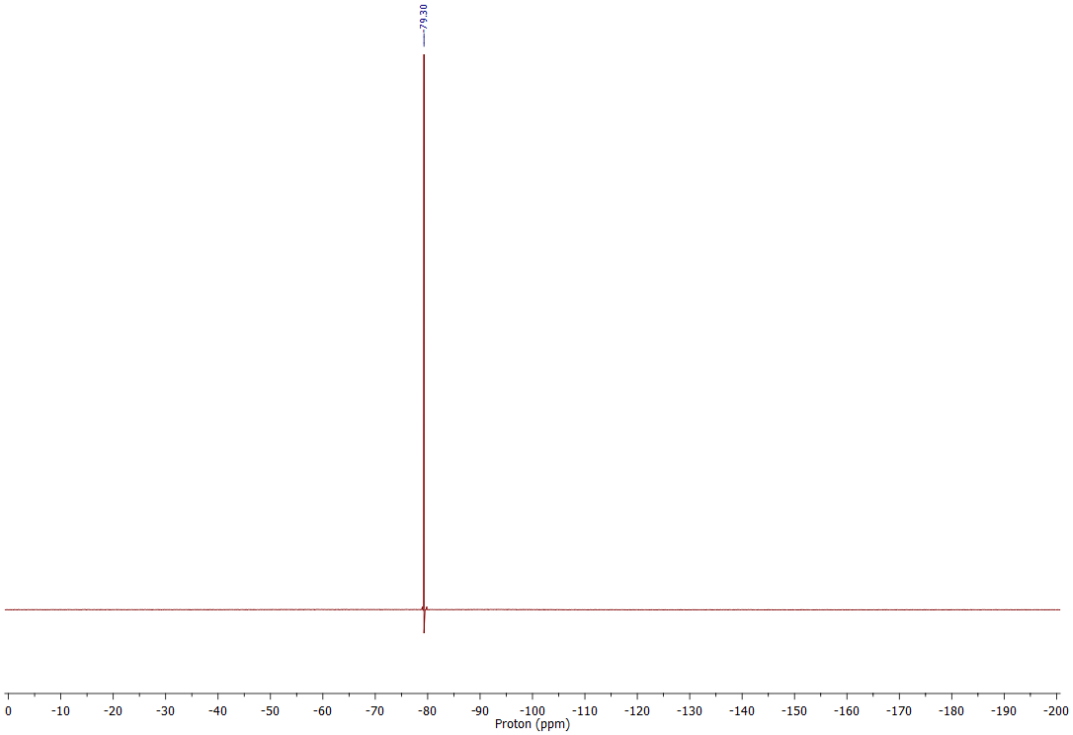

Figure 50: ^{19}F NMR of 2a done in CD_3CN

2b – [Benzyl-BZIMPY-PNMe$_2$][OTf]$_2$

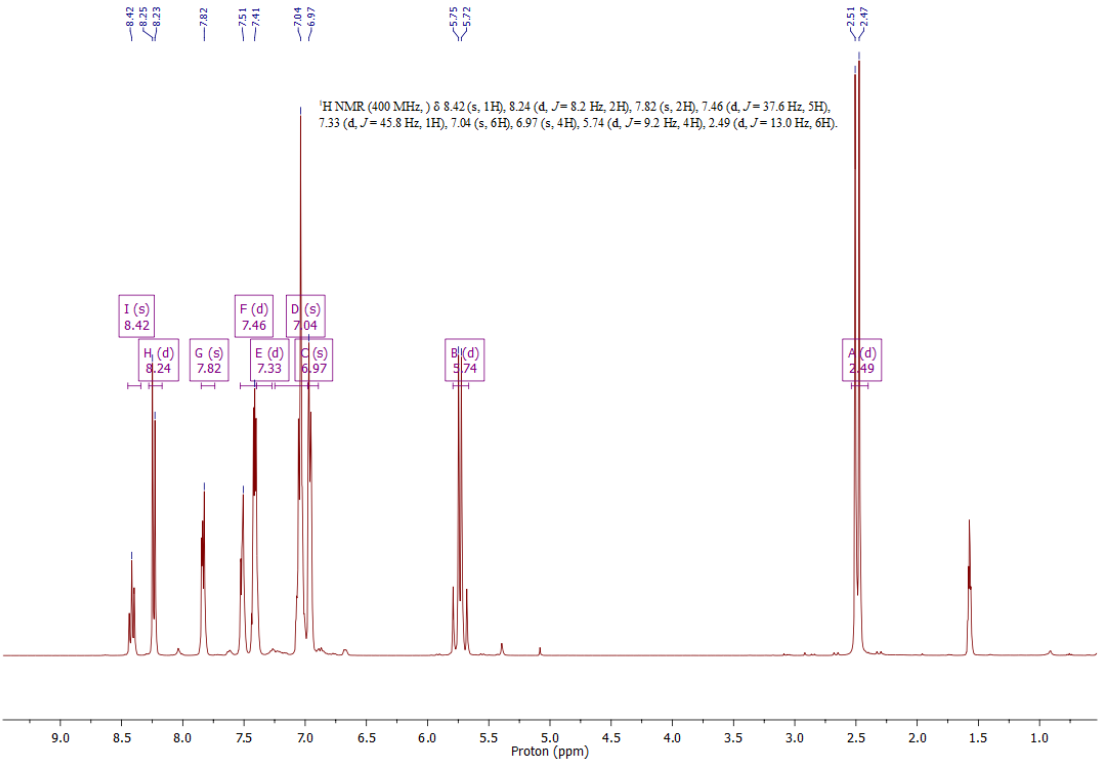

Figure 51: ^{1}H NMR of 2b done in CD_3CN

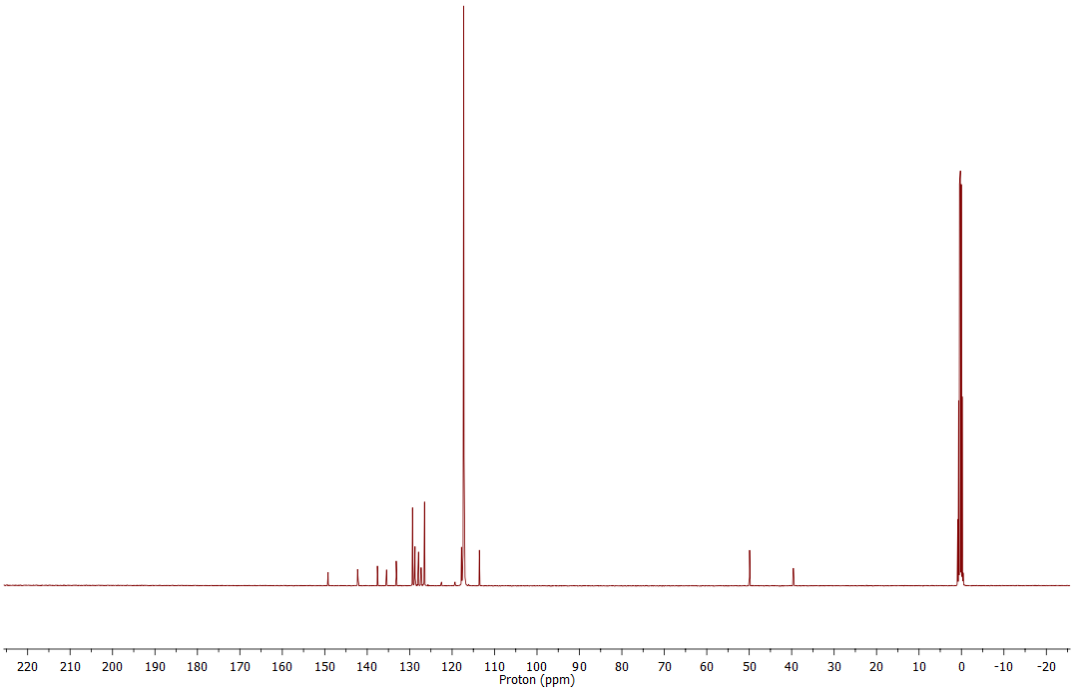

Figure 52: ^{13}C NMR of 2b done in CD_3CN

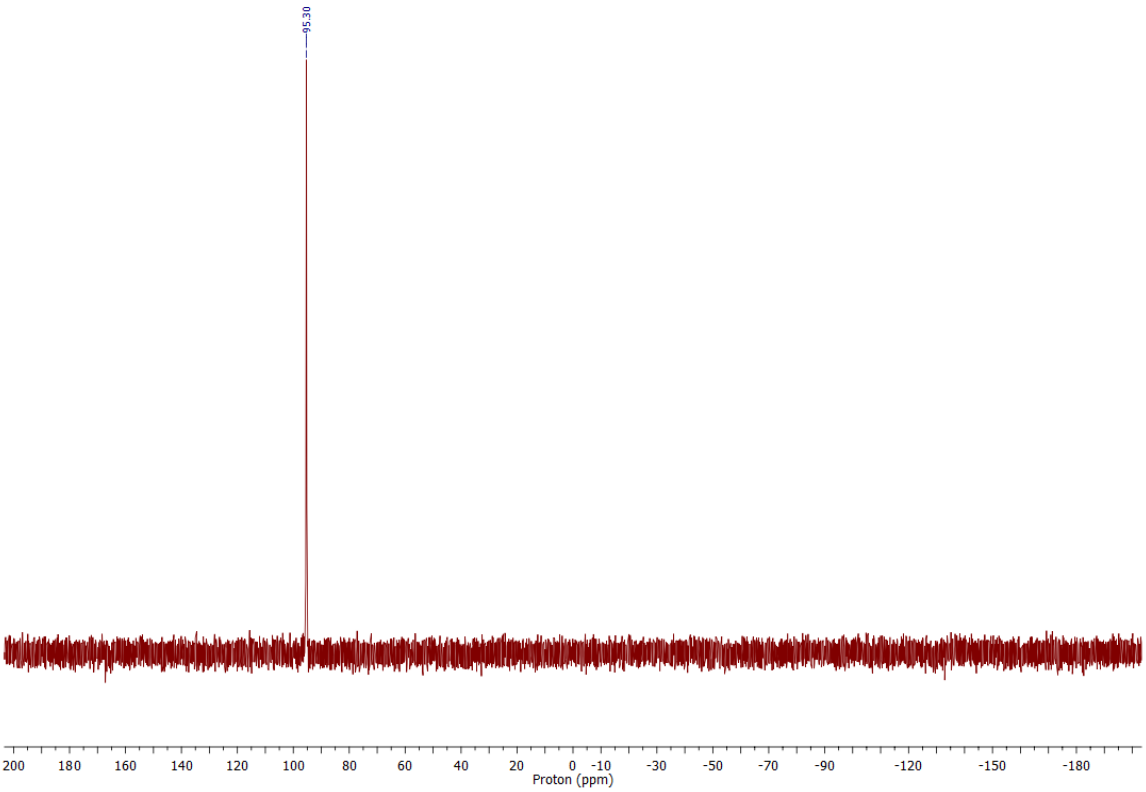

Figure 53: ^{31}P NMR of 2b done in CD_3CN

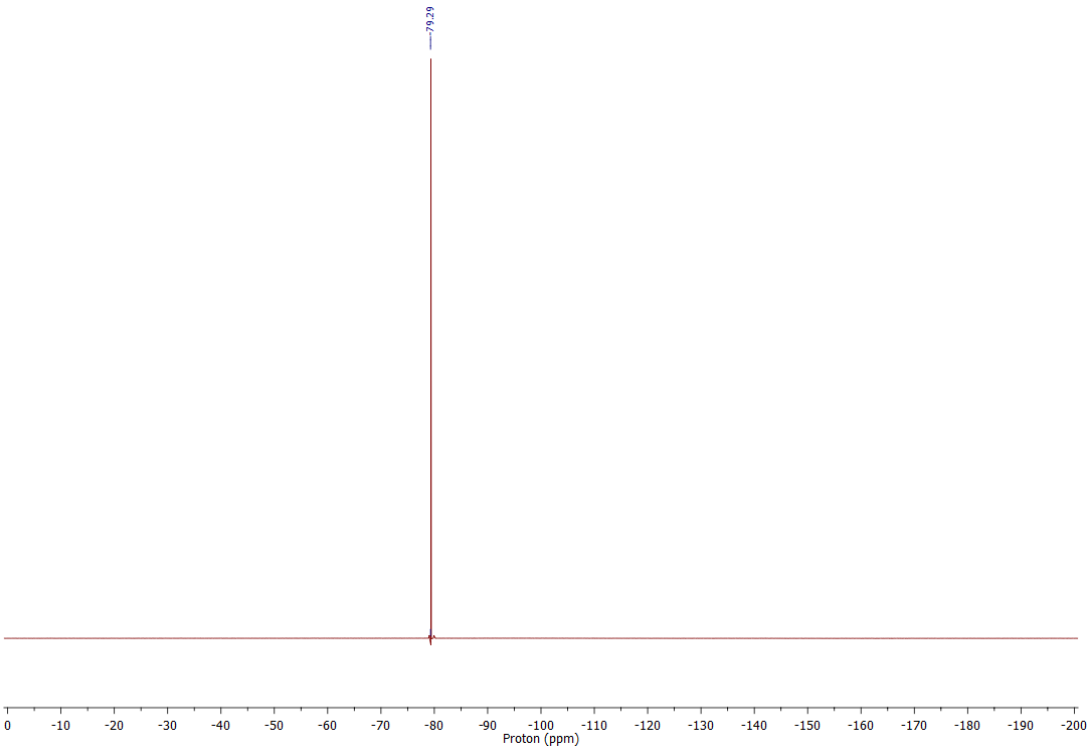

Figure 54: ^{19}F NMR of 2b done in CD_3CN

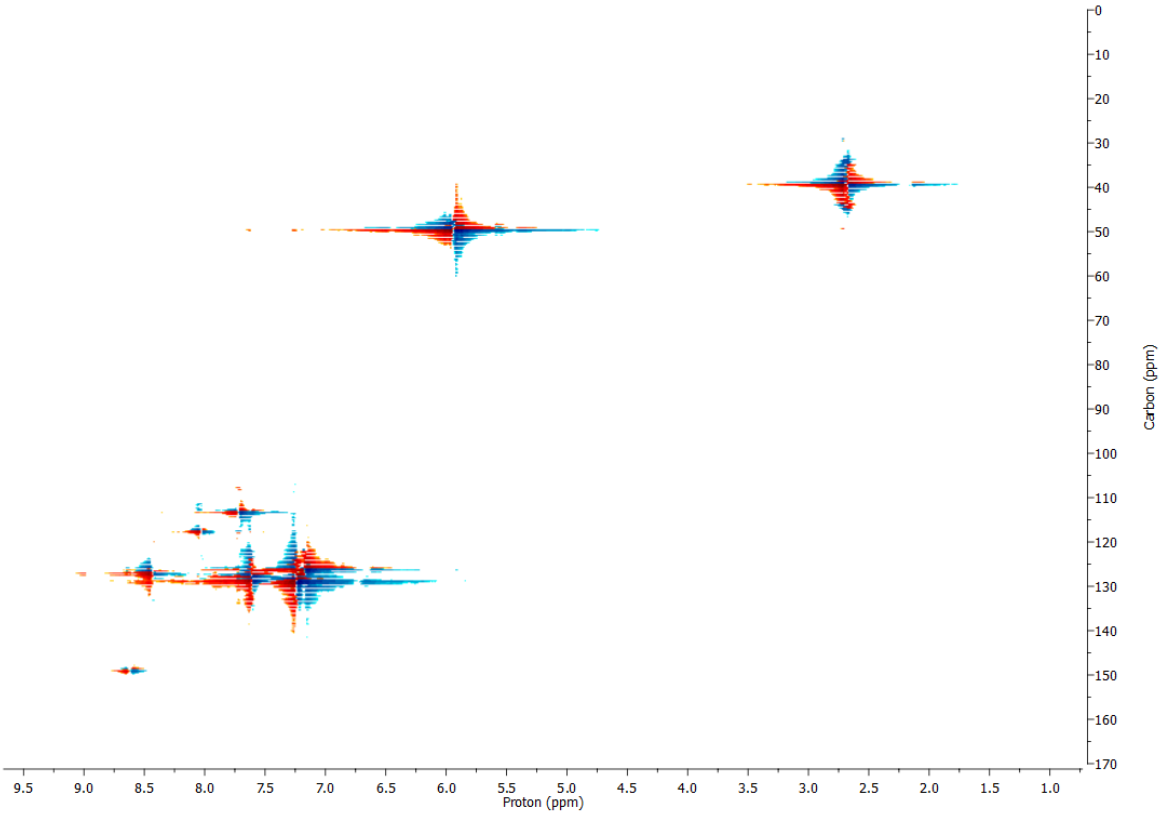

Figure 55: HSQC spectrum of 2b done in CD_3CN

2c – [Allyl-BZIMPY-PNMe$_2$][BArF$_{24}$]$_2$

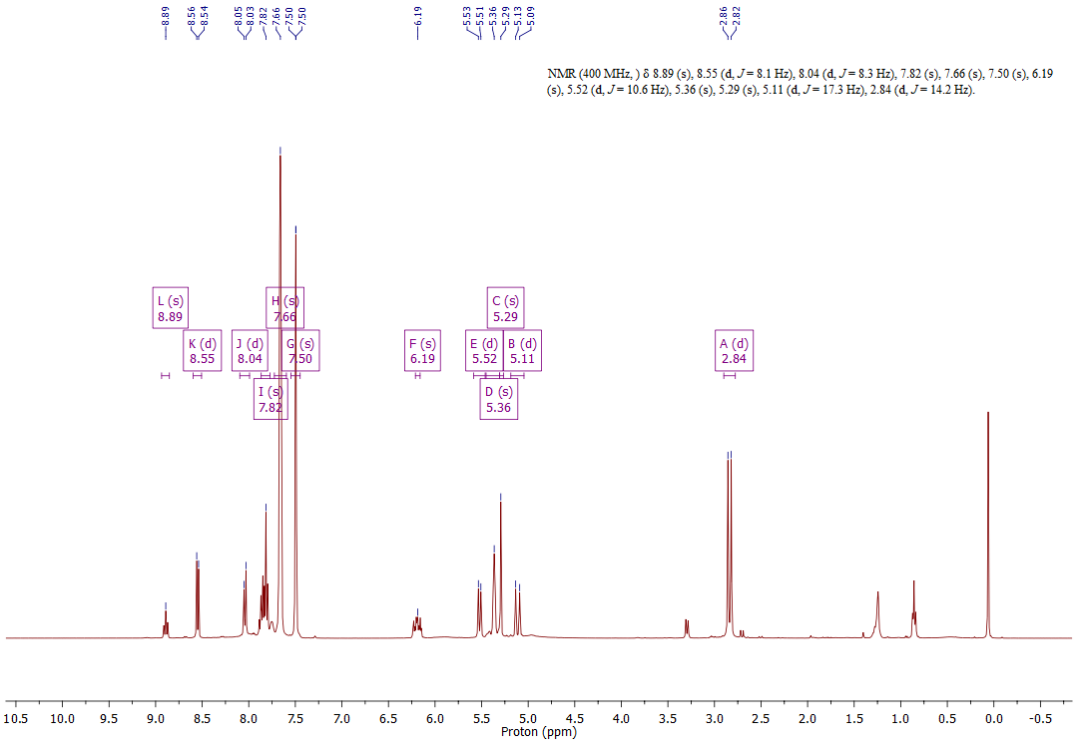

Figure 56: ^{1}H NMR of 2c done in CD_2Cl_2

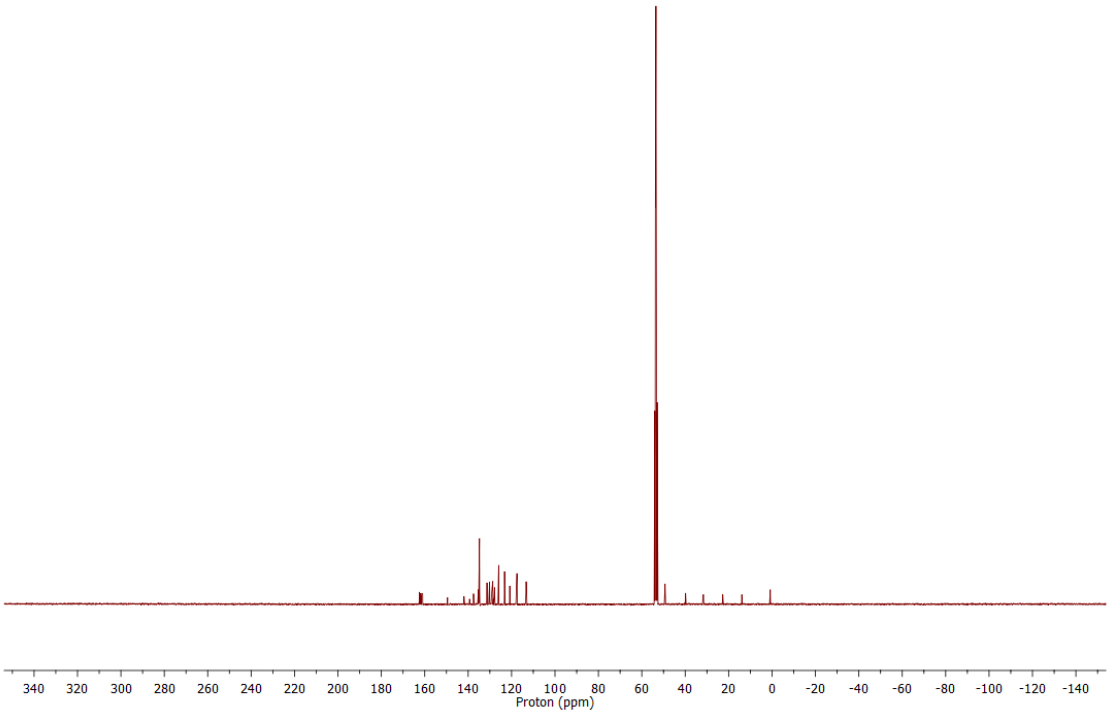

Figure 57: ^{13}C NMR of 2c done in CD_2Cl_2

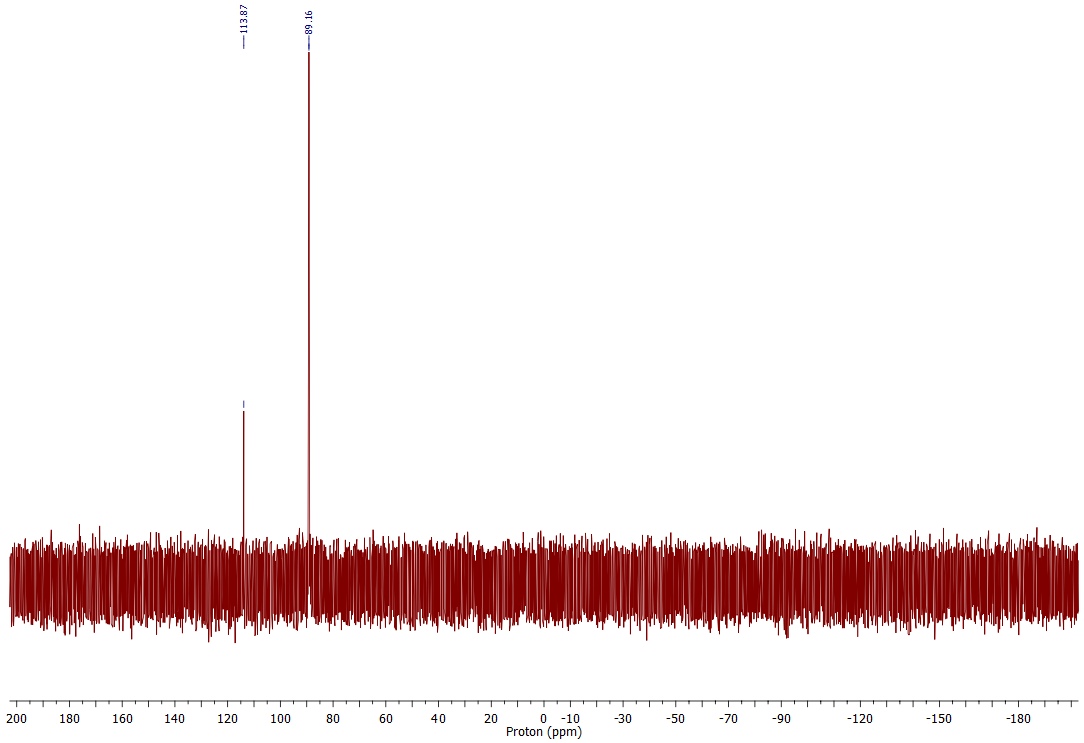

Figure 58: ^{31}P NMR of 2c done in CD_2Cl_2

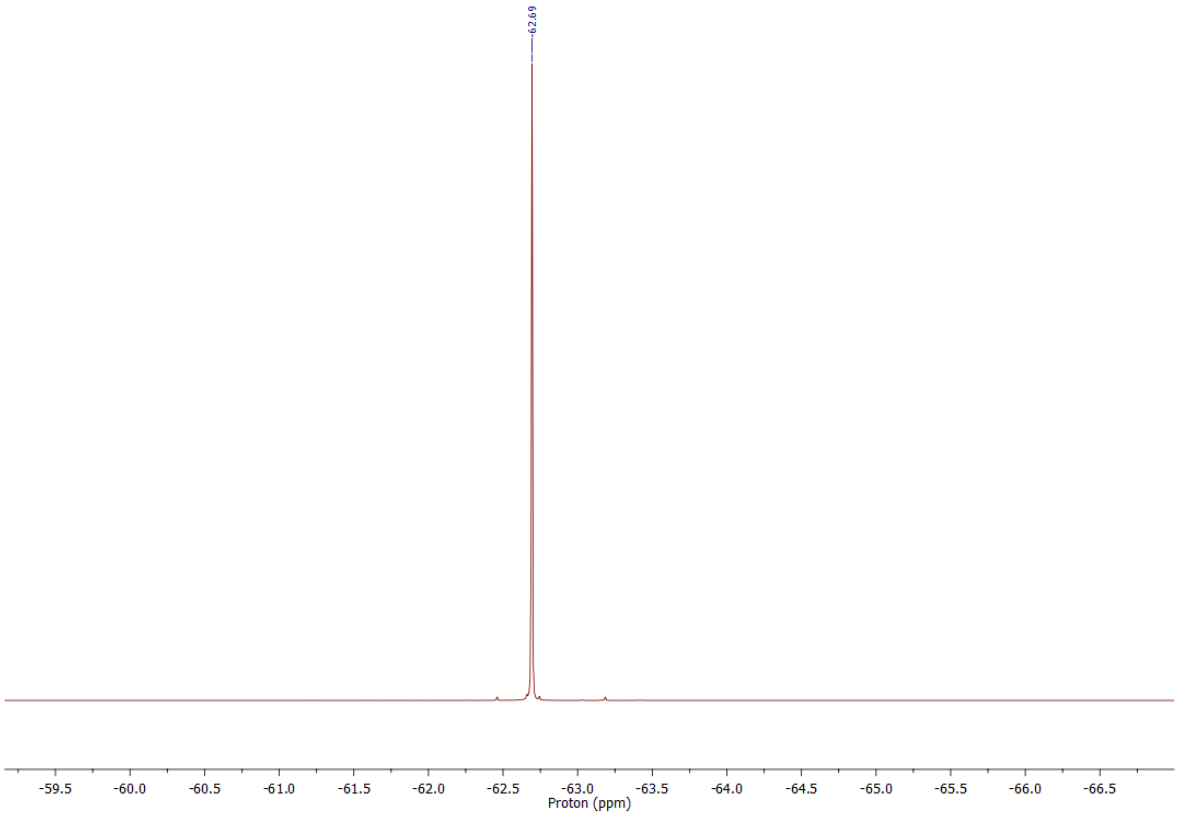

Figure 59: ^{19}F NMR of 2c done in CD_2Cl_2

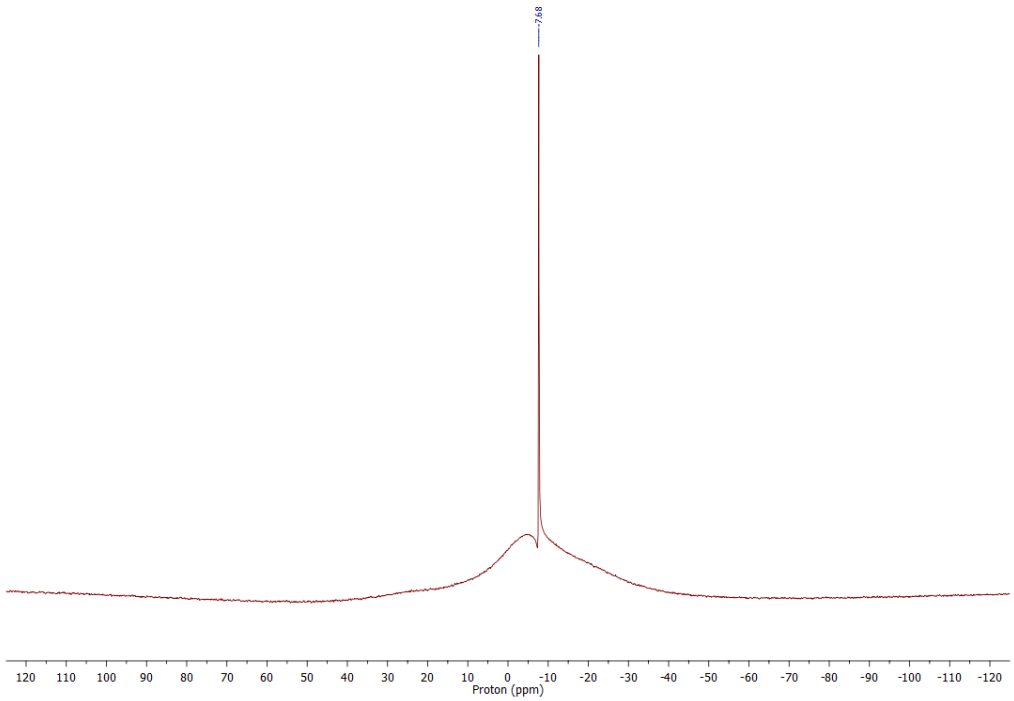

Figure 60: ^{11}B NMR of 2c done in CD_2Cl_2

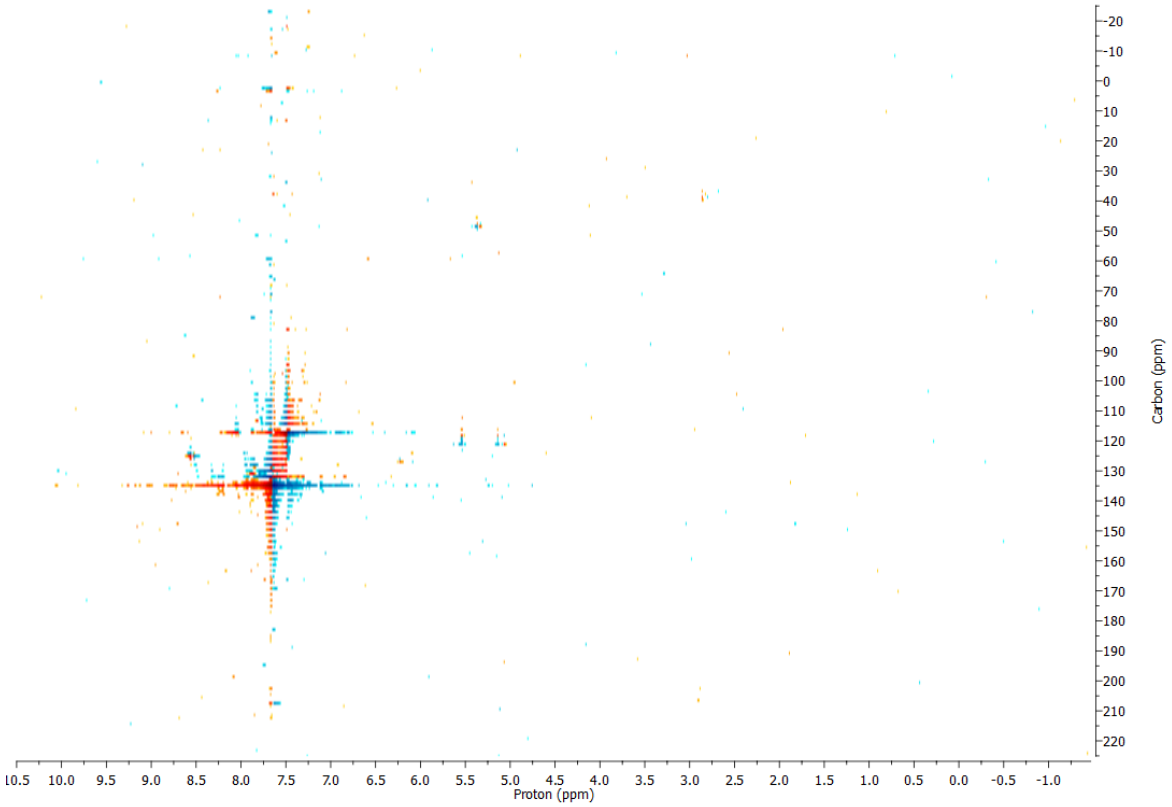

Figure 61: HSQC spectrum of 2c done in CD_2Cl_2

2d – [Benzyl-BZIMPY-PNMe$_2$][BArF$_{24}$]$_2$

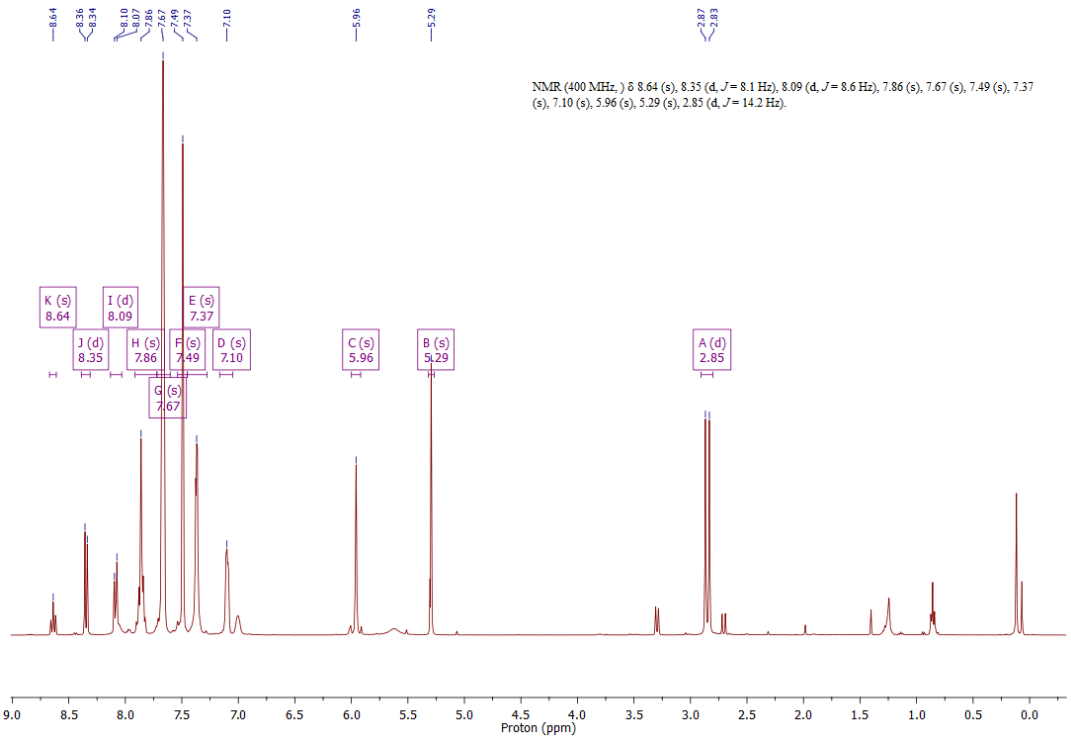

Figure 62: ^{1}H NMR of 2d done in CD_2Cl_2

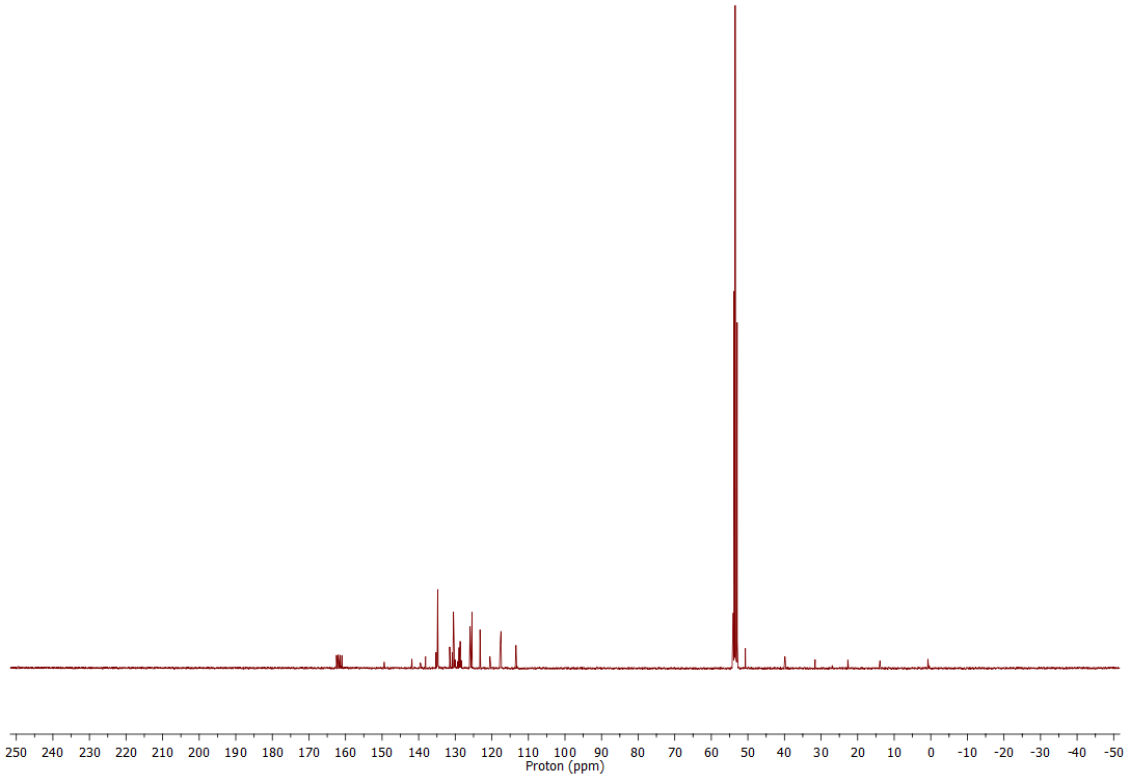

Figure 63: ^{13}C NMR of 2d done in CD_2Cl_2

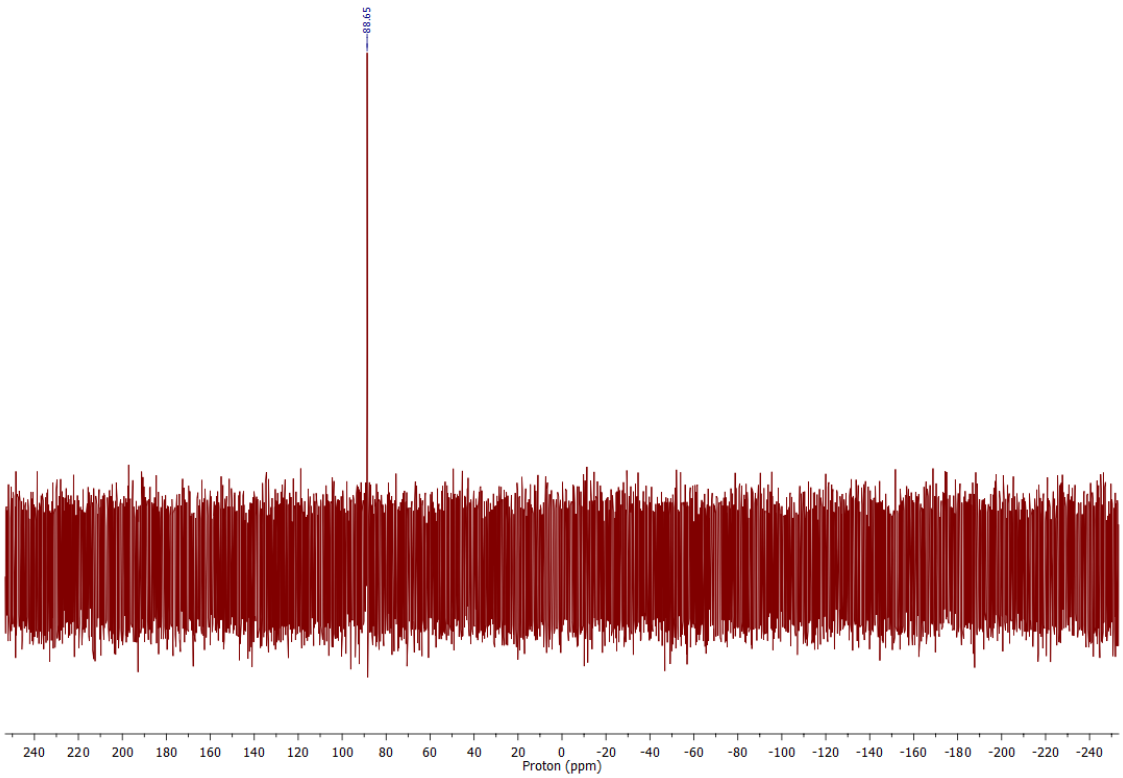

Figure 64: ^{31}P NMR pf 2d done in CD_2Cl_2

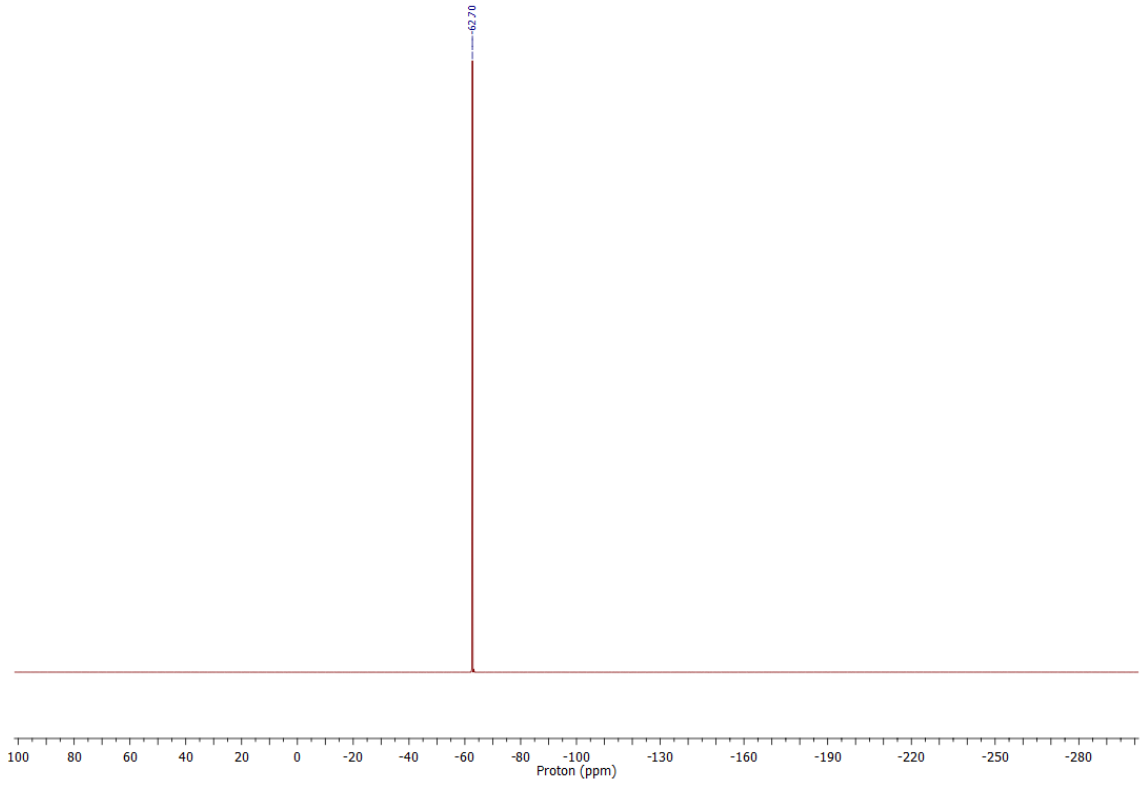

Figure 65: ^{19}F NMR of 2d done in CD_2Cl_2

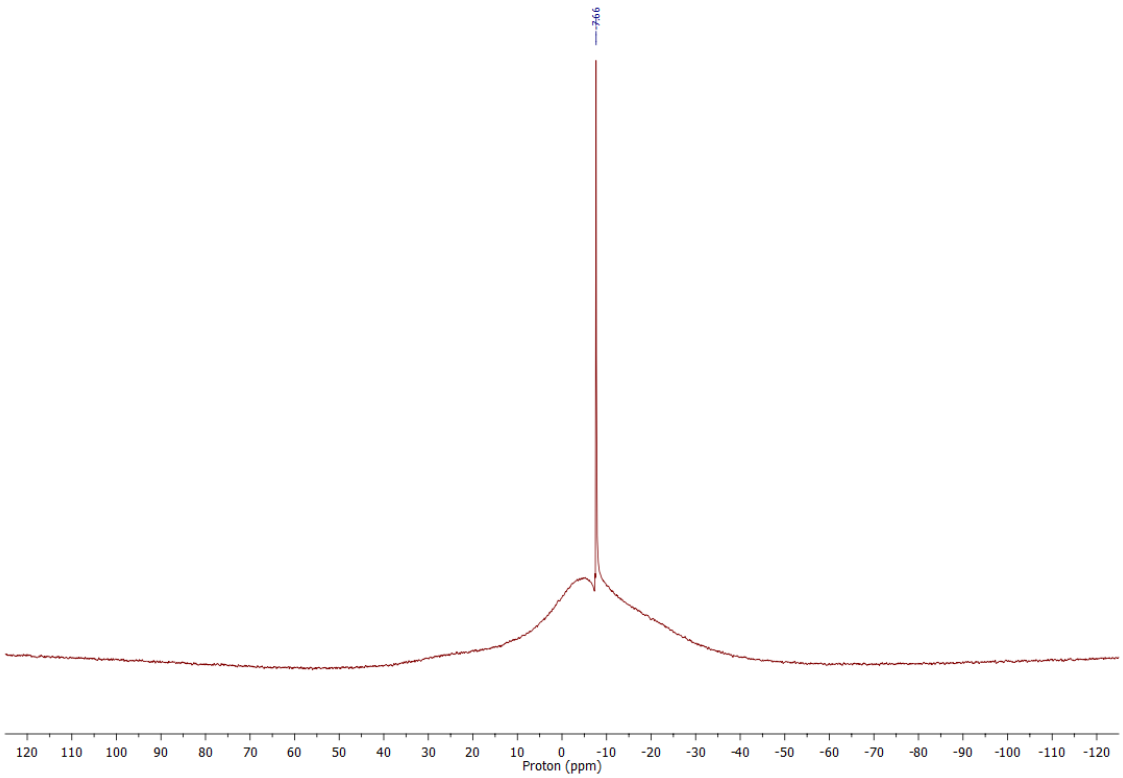

Figure 66: ^{11}B NMR of 2d done in CD_2Cl_2

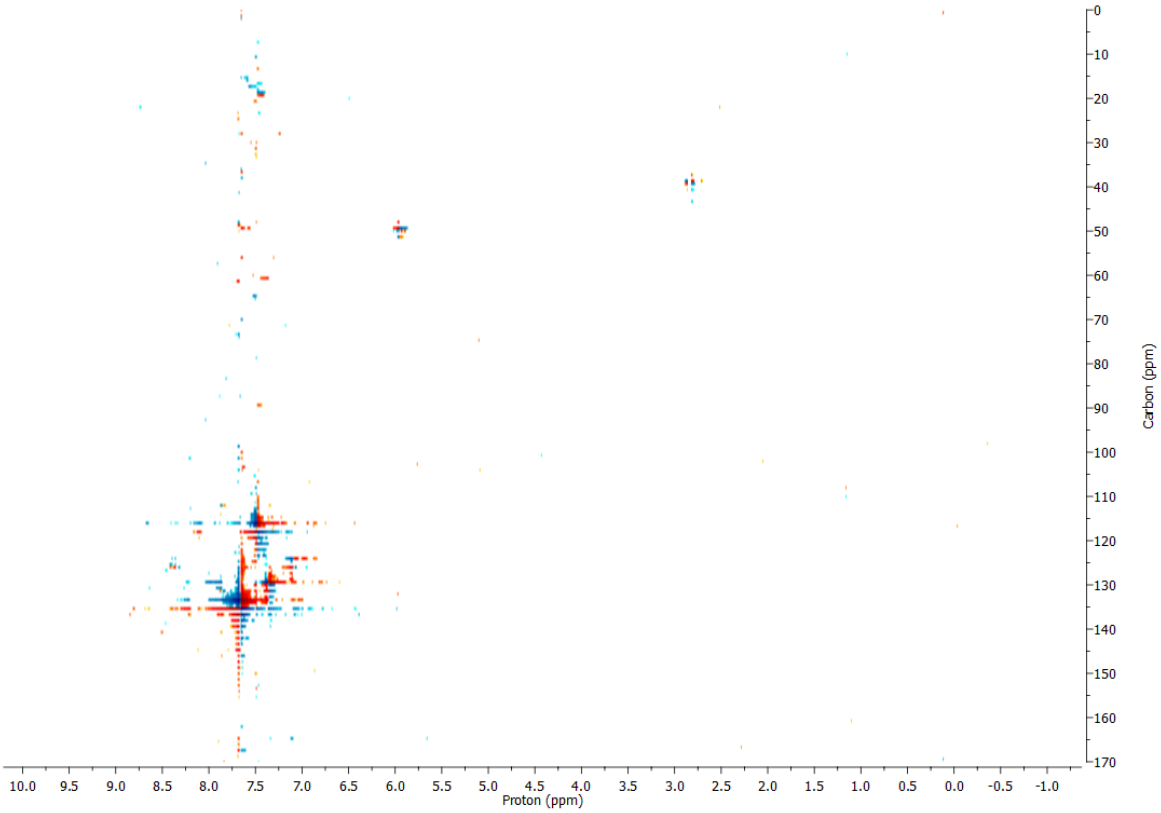

Figure 67: HSQC spectrum of 2d done in CD_2Cl_2

Reactivity and Other spectra

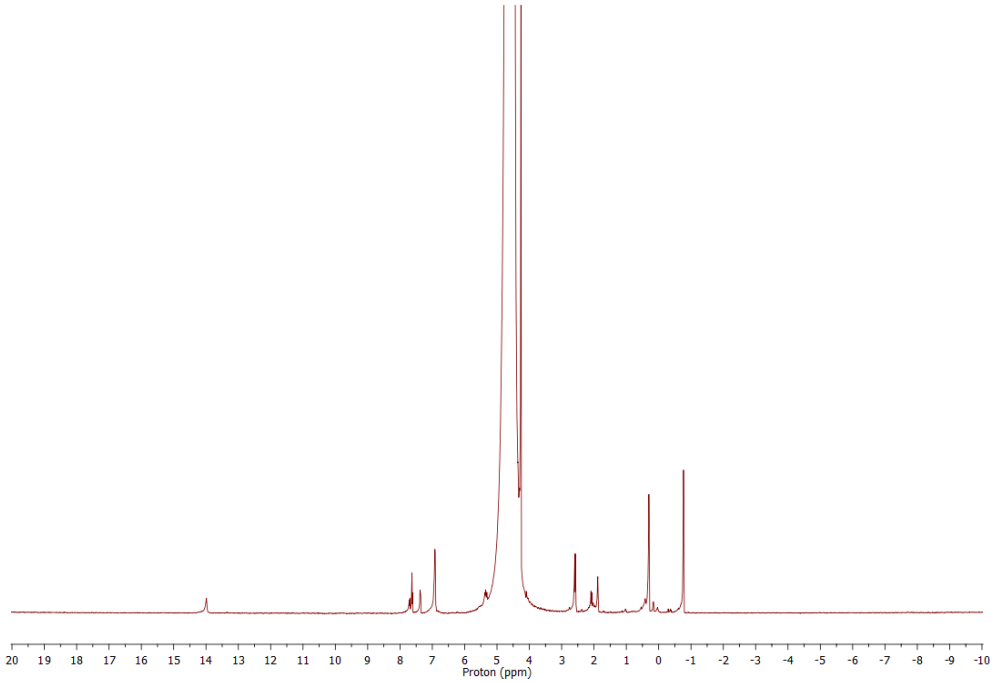

Figure 68: ^{1}H NMR of the reaction between Allyl-BZIMPY ligand and triflic acid (HOTf)

H_2O and D_2O Studies

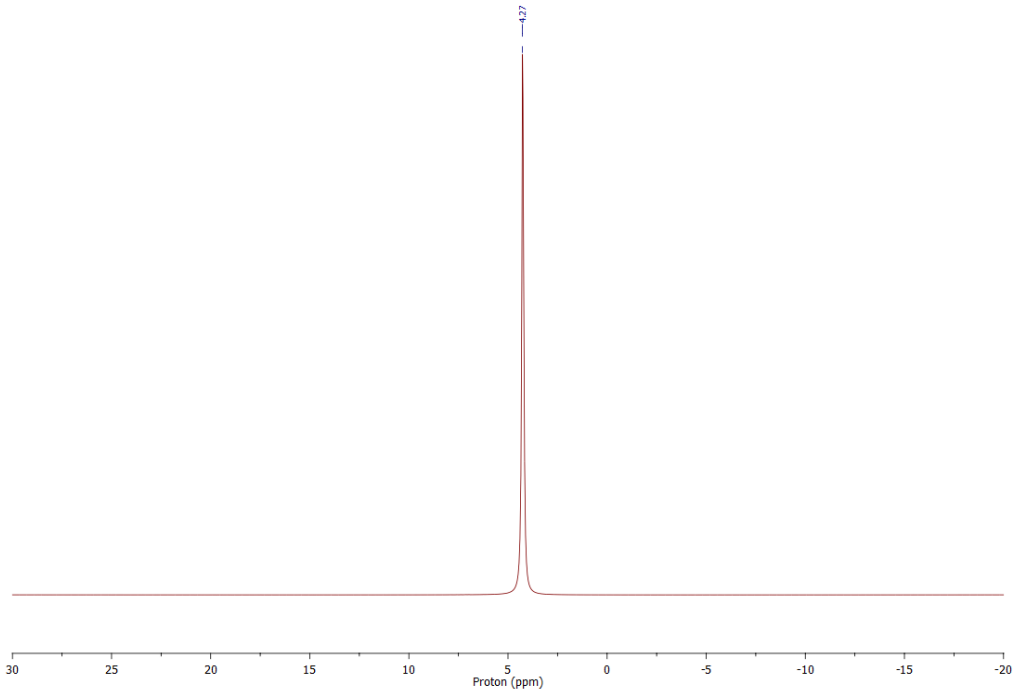

Figure 69: ^{1}H NMR of the reaction between 1a and D_2O.The spectra look the same for all the other Lewis acids.

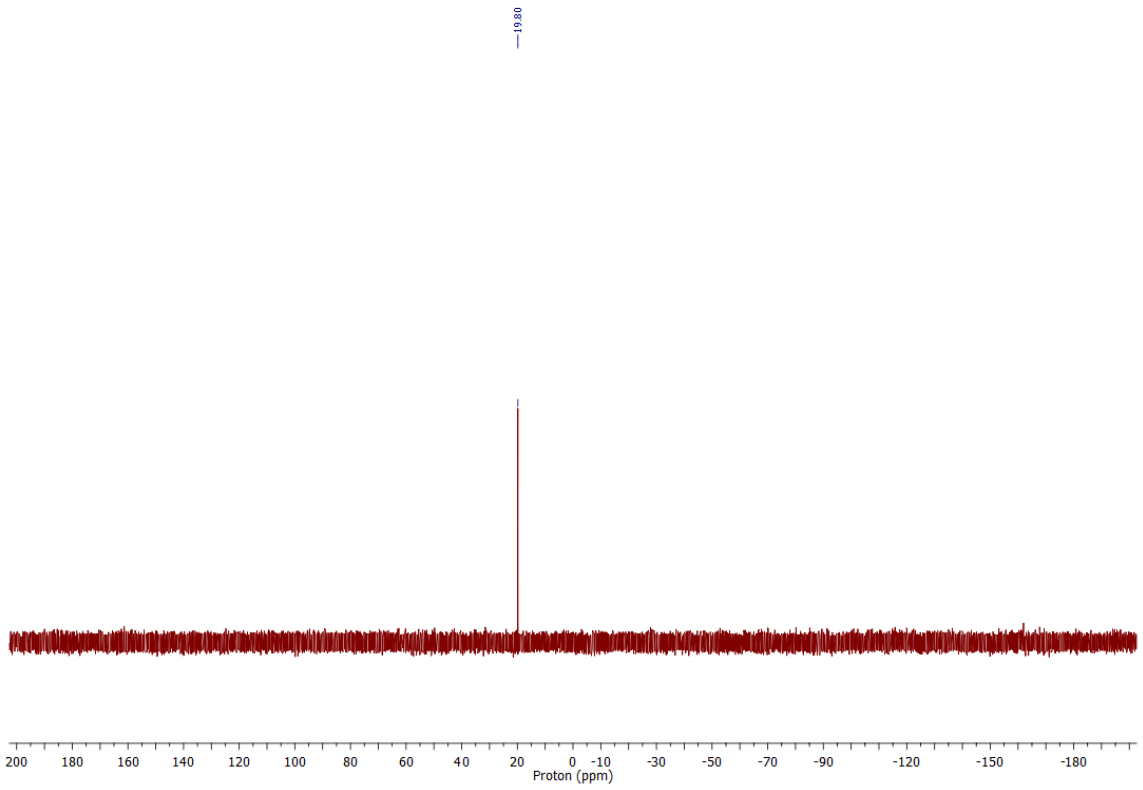

Figure 70: ^{31}P NMR of the reaction of 1a with D_2O

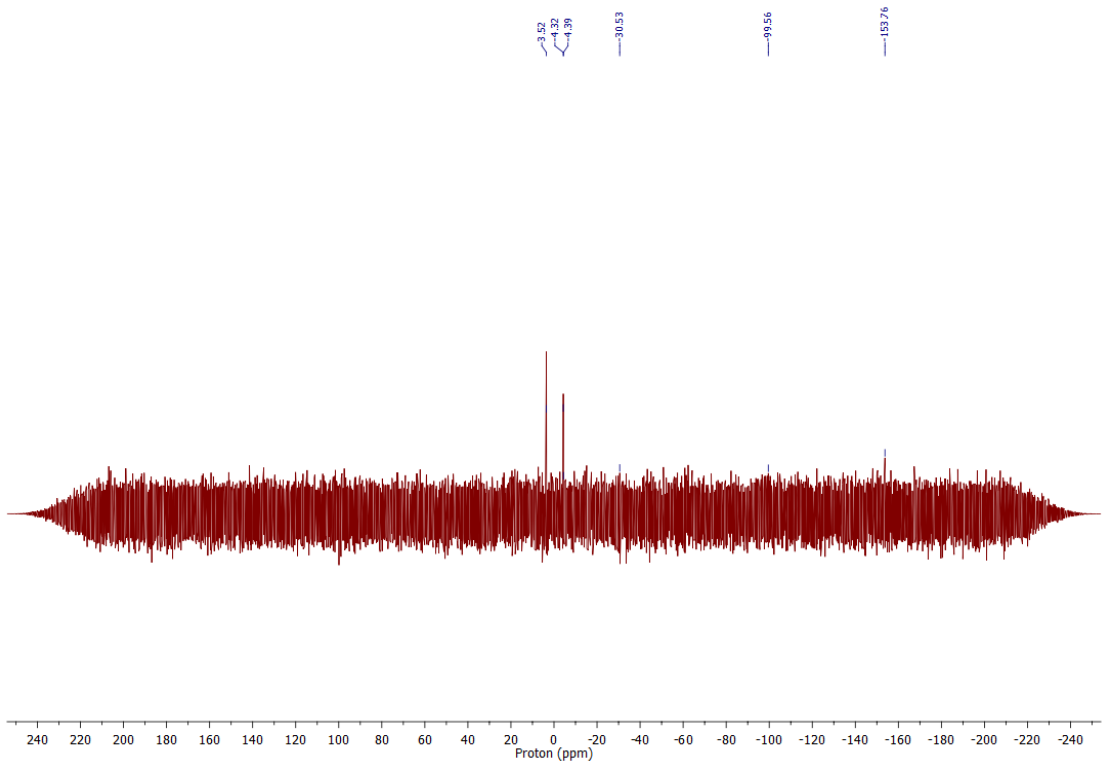

Figure 71: ^{31}P NMR of the reaction between 2a and D_2O

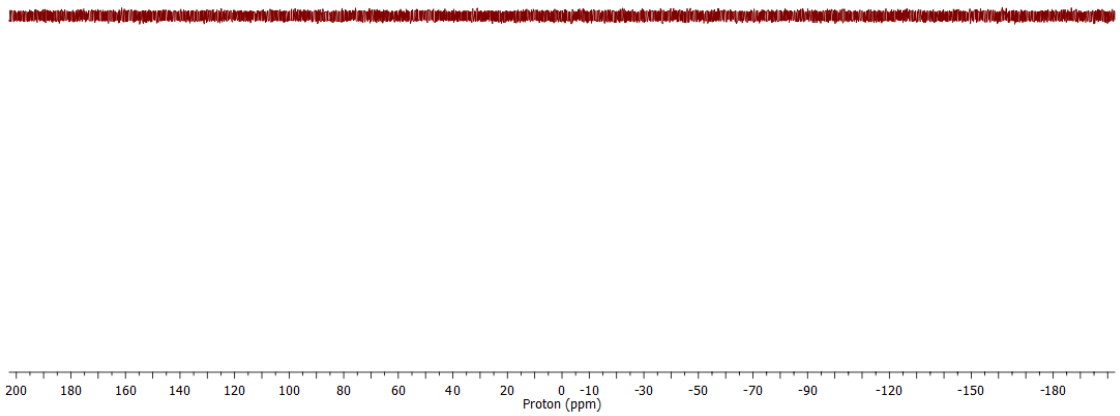

Figure 72: ^{31}P NMR of the reaction between 1c and D_2O

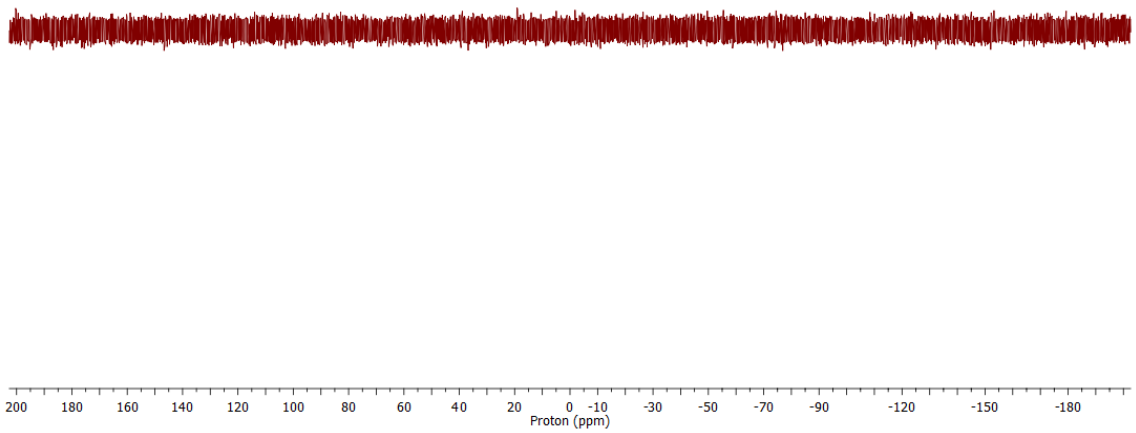

Figure 73: ^{31}P NMR of the reaction between 1d and D_2O

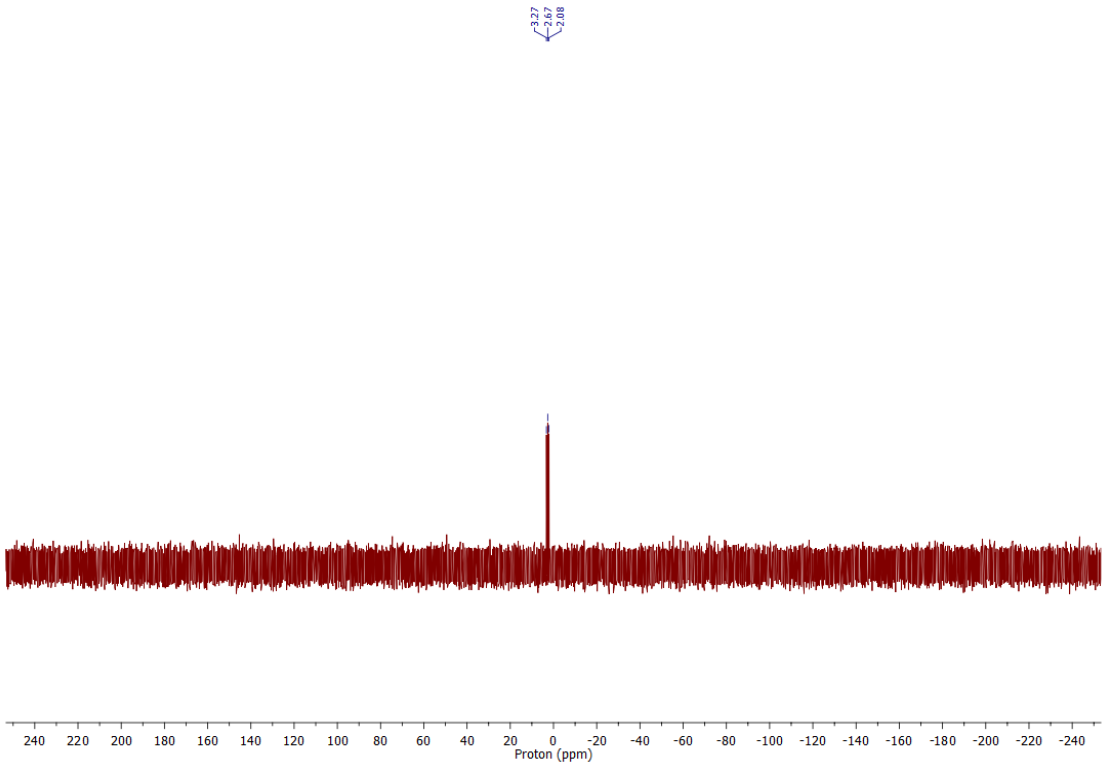

Figure 74: ^{31}P NMR of the reaction between 2c and H_2O

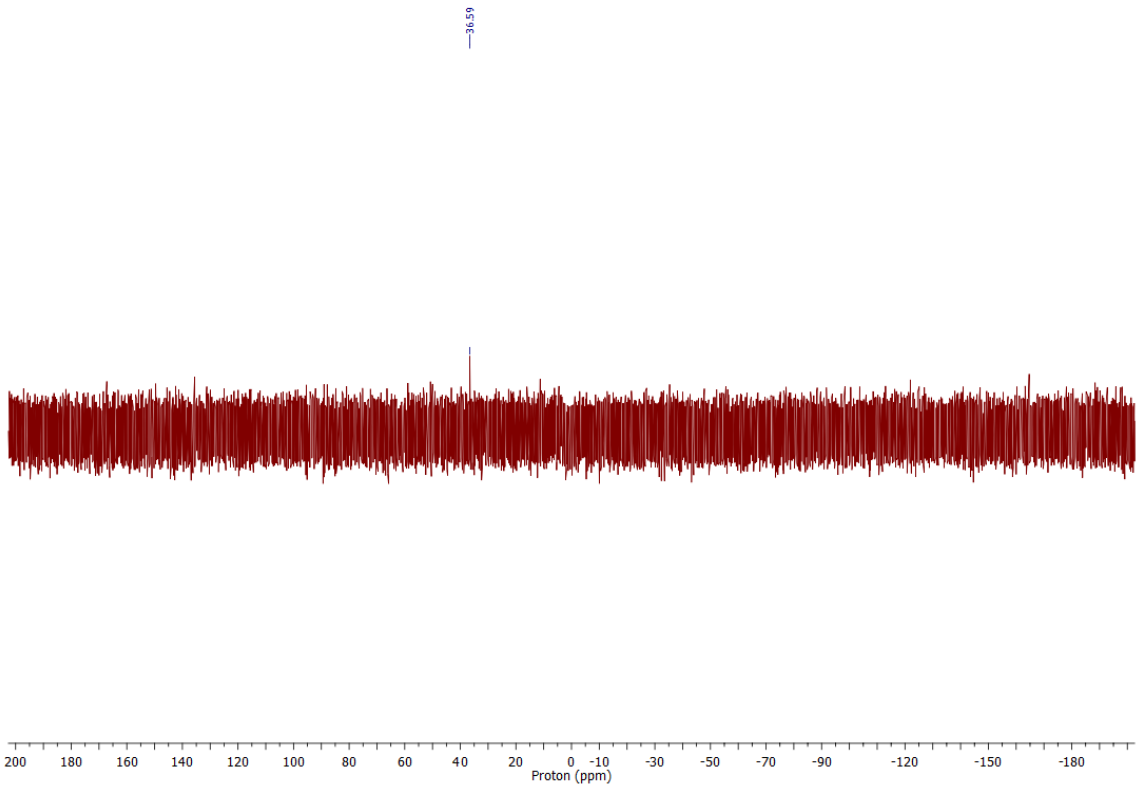

Figure 75: ^{31}P NMR of the reaction between 2d and H_2O

Determination of Lewis acidity – Gutmann Beckett results

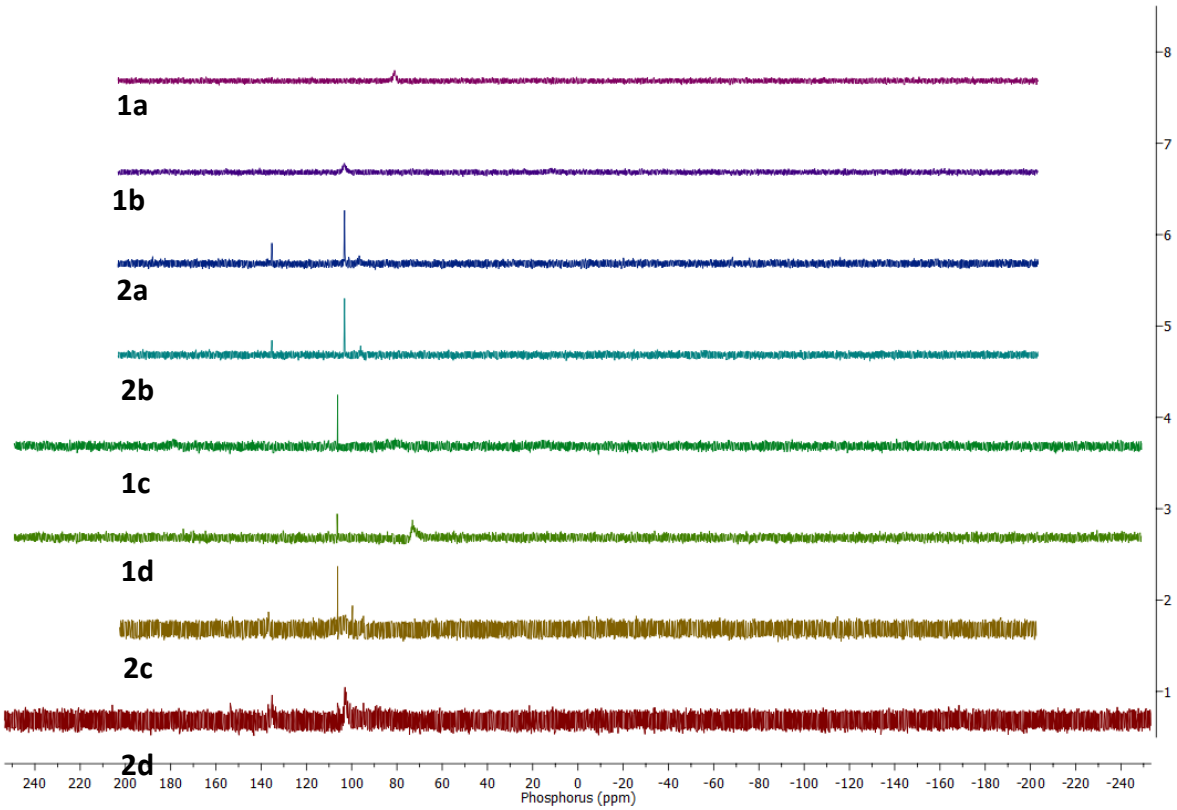

Figure 76: ^{31}P NMR of the chemical shifts in the reaction of dicationic Lewis acids in a 1:1 mole ratio with triethylphosphine oxide (Et_3PO) to determine Lewis acidity.

Catalytic Reactivity Spectra

Hydroarylation of Diphenylamine with 1,1-diphenylethylene Spectra

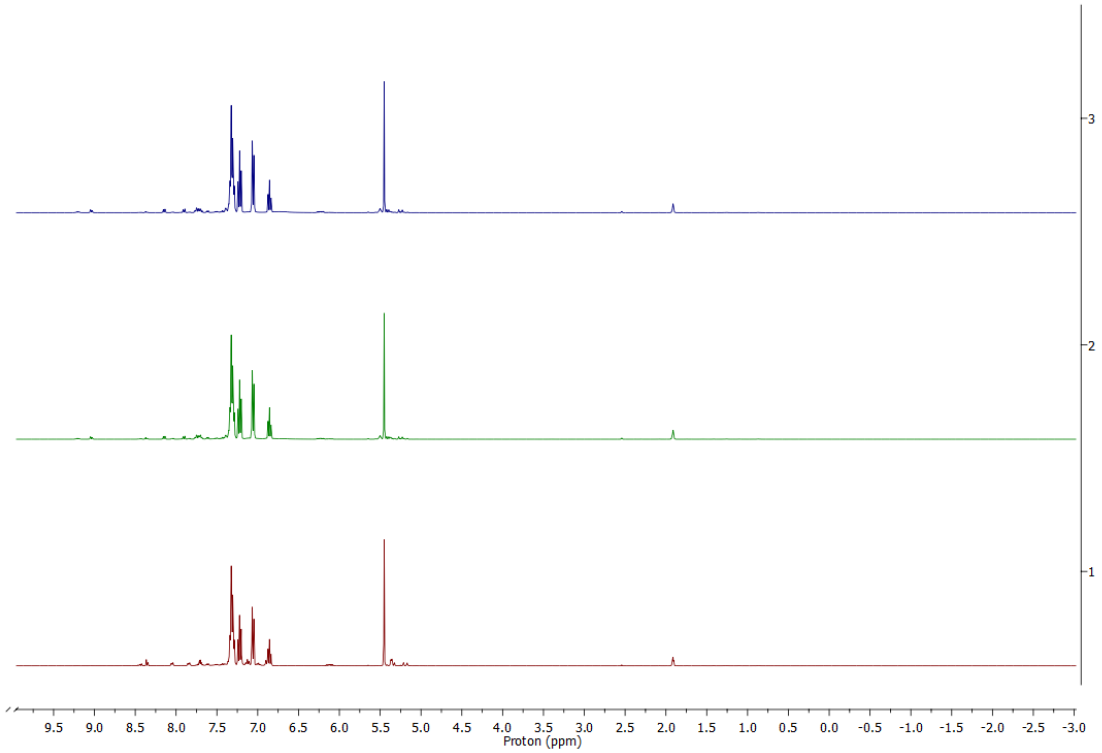

Figure 77: Hydroarylation of diphenylamine with 1,1-diphenylethylene using 10% mol 1a catalyst after 1h, 5h and 24h.

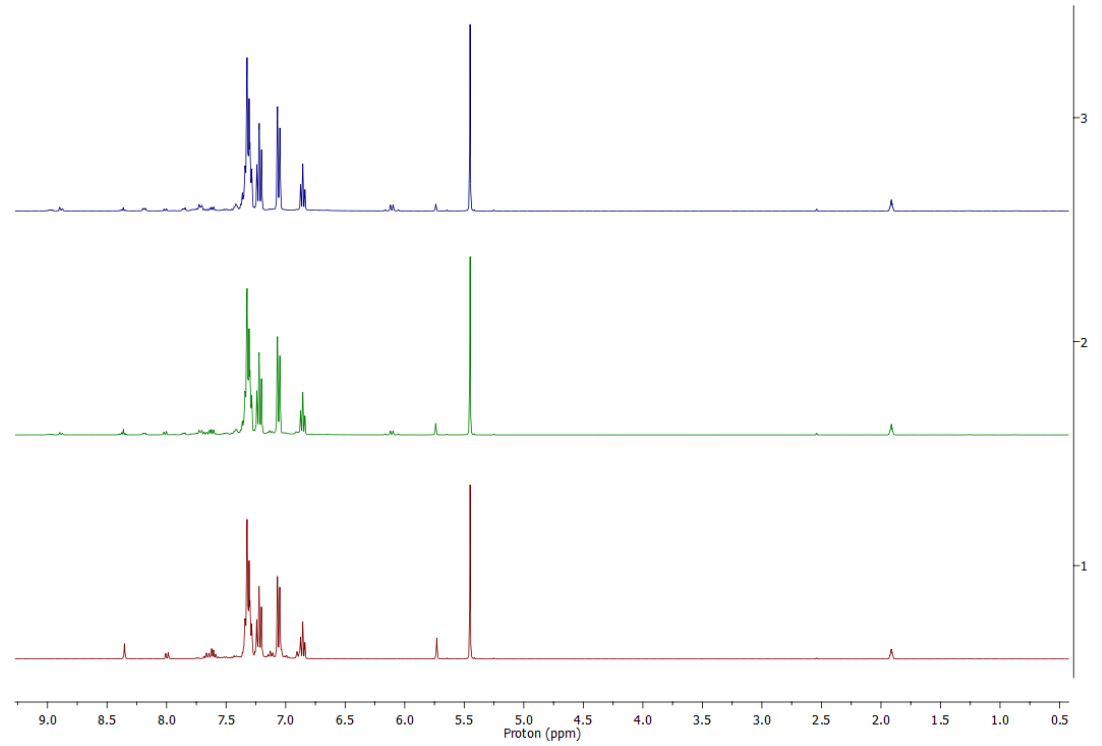

Figure 78: Hydroarylation of diphenylamine with 1,1-diphenylethylene using 10% mol 1b catalyst after 1h, 5h and 24h

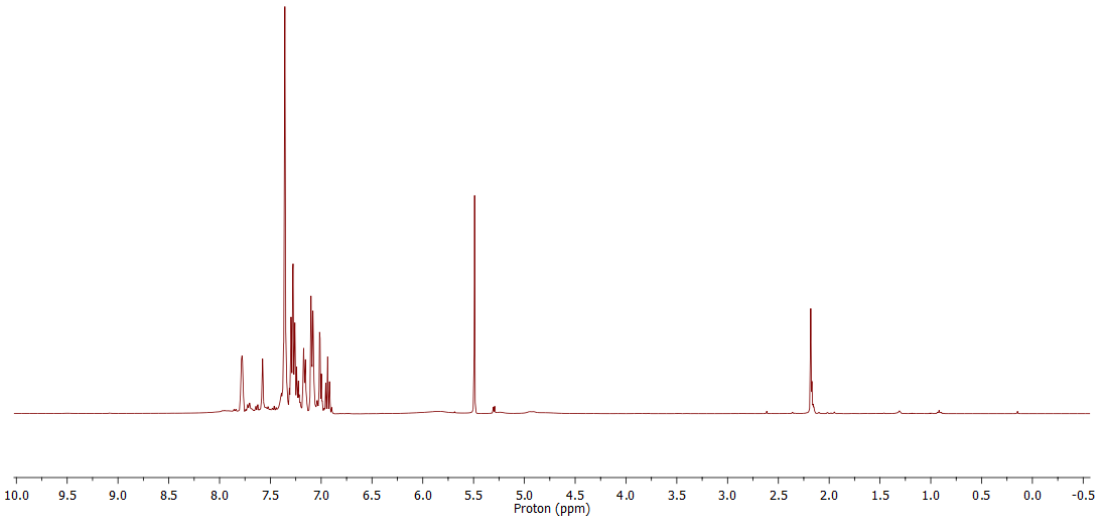

Figure 79: Hydroarylation of diphenylamine with 1,1-diphenylethylene using 10% mol 1c catalyst after 24h

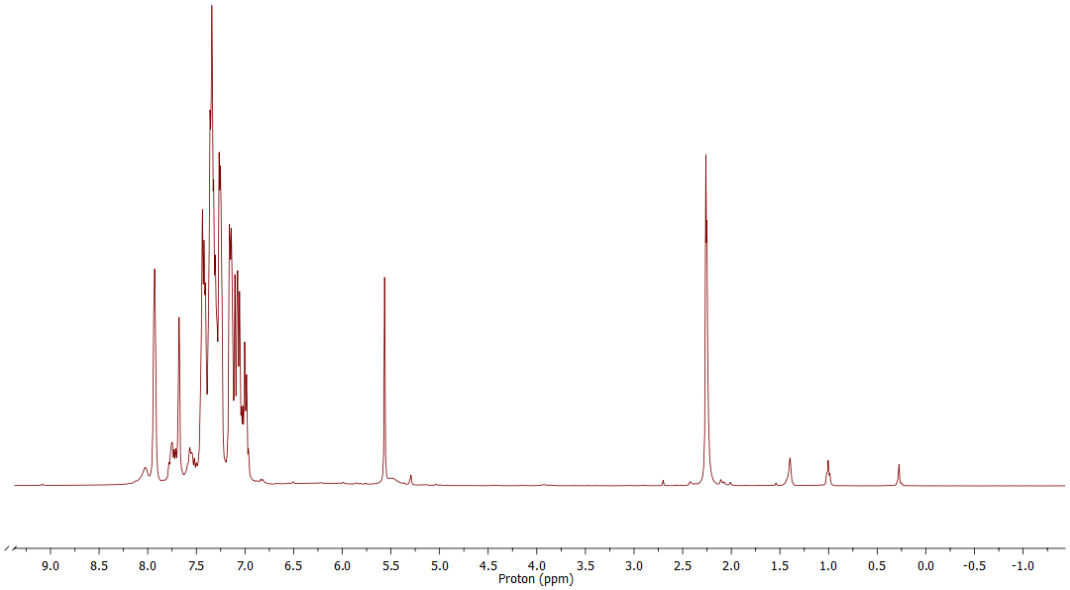

Figure 80: Hydroarylation of diphenylamine with 1,1-diphenylethylene using 10% mol 1d catalyst after 24h

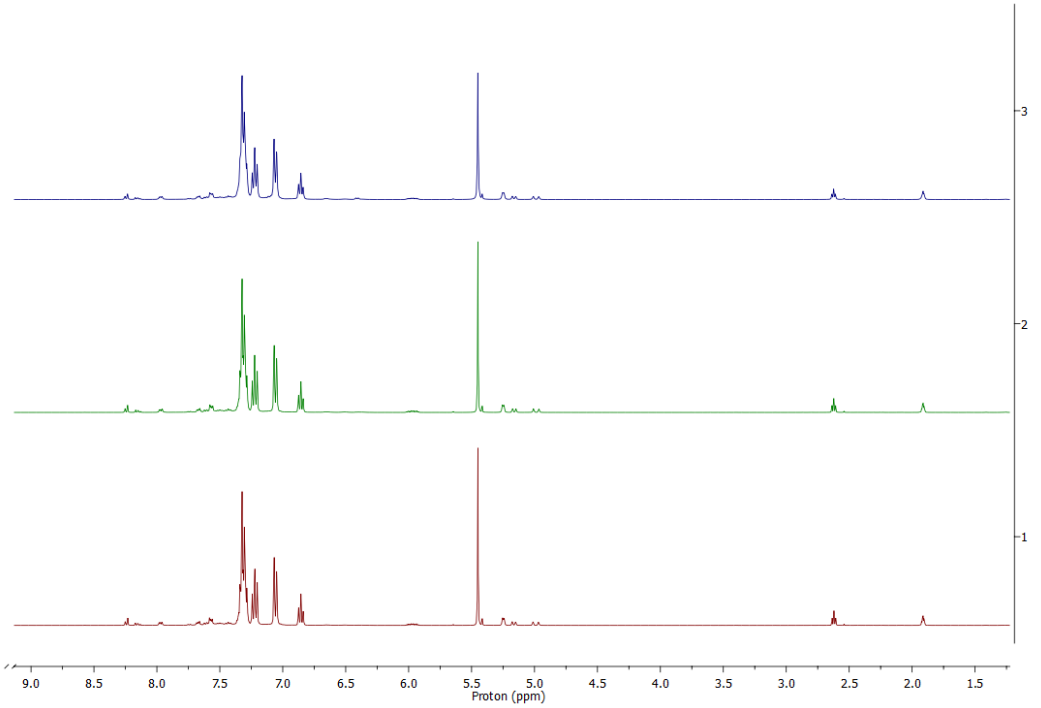

Figure 81: Hydroarylation of diphenylamine with 1,1-diphenylethylene using 10% mol 2a catalyst after 1h, 5h and 24h

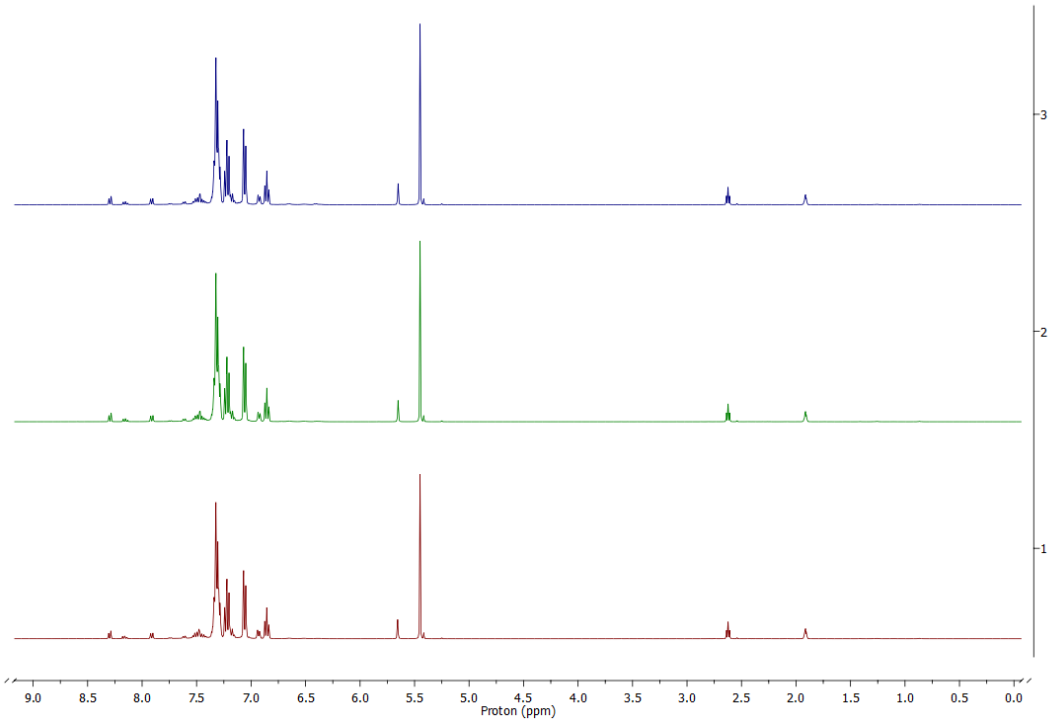

Figure 82: Hydroarylation of diphenylamine with 1,1-diphenylethylene using 10% mol 2b catalyst after 1h, 5h and 24h.

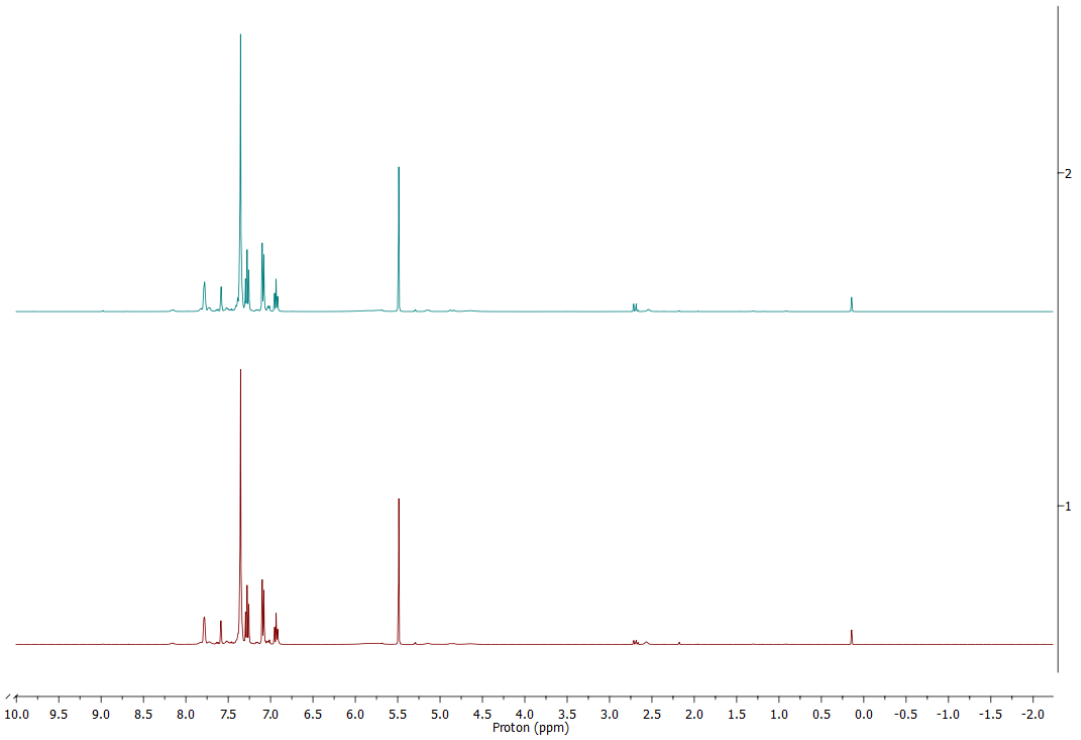

Figure 83: Hydroarylation of diphenylamine with 1,1-diphenylethylene using 10% mol 2c catalyst after 1h and 24h.

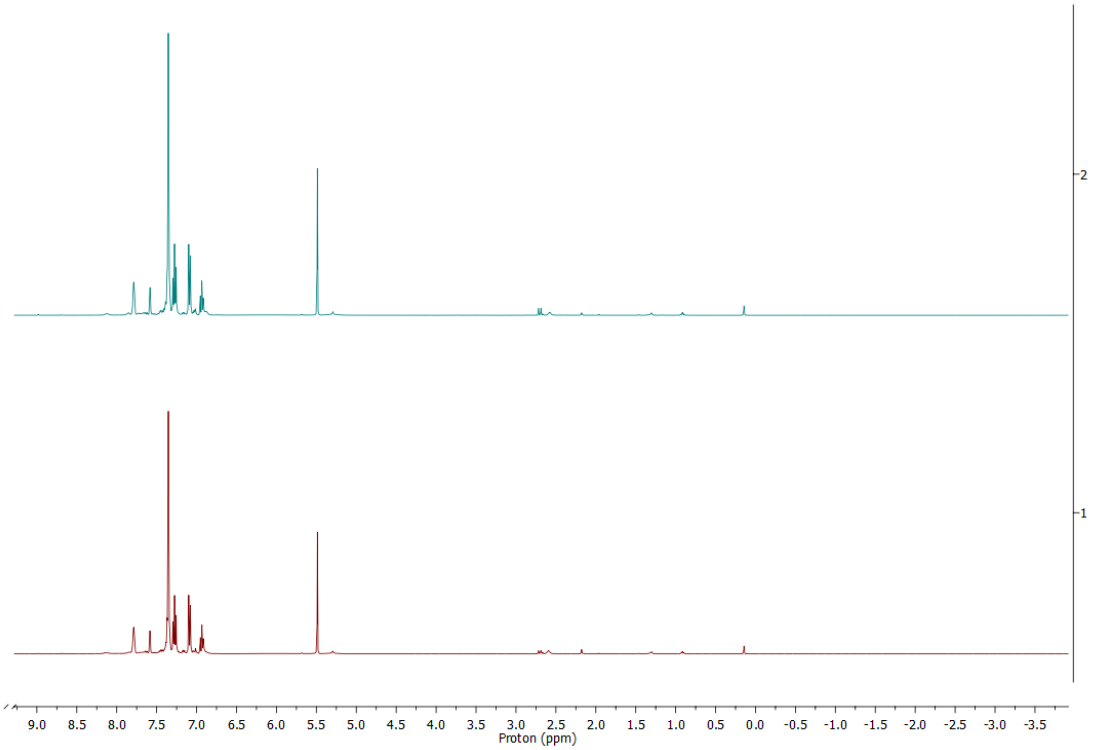

Figure 84: Hydroarylation of diphenylamine with 1,1-diphenylethylene using 10% mol 2d catalyst after 1h and 24h.

Hydroarylation of Pyrrole with 1,1-diphenylethylene Spectra

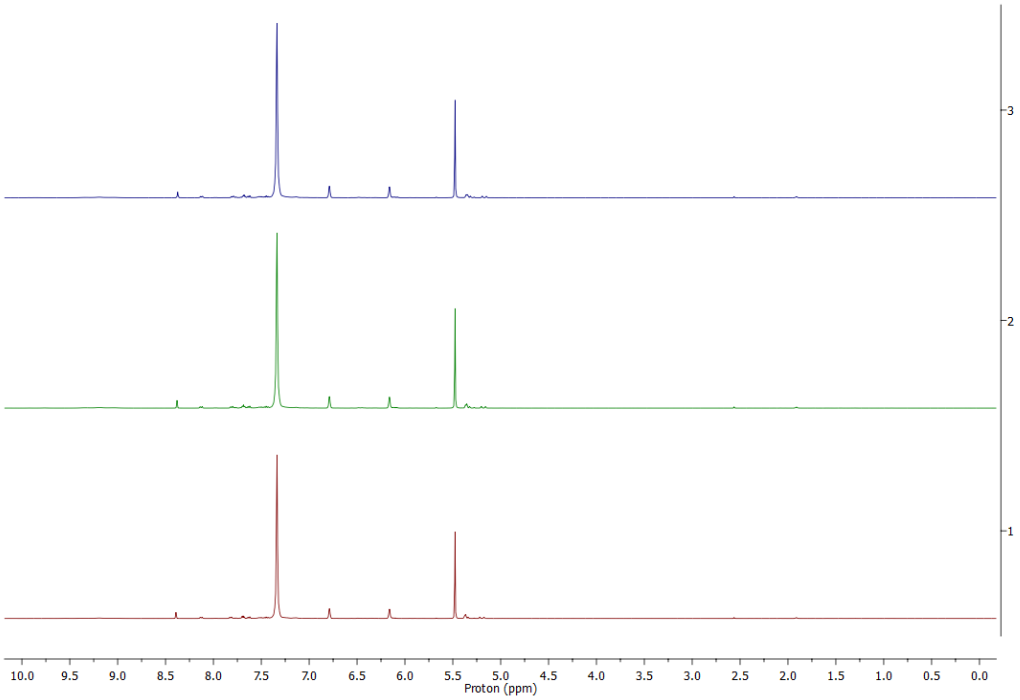

Figure 85: Hydroarylation of Pyrrole with 1,1-diphenylethylene using 10% mol 1a catalyst after 1h, 5h and 24h.

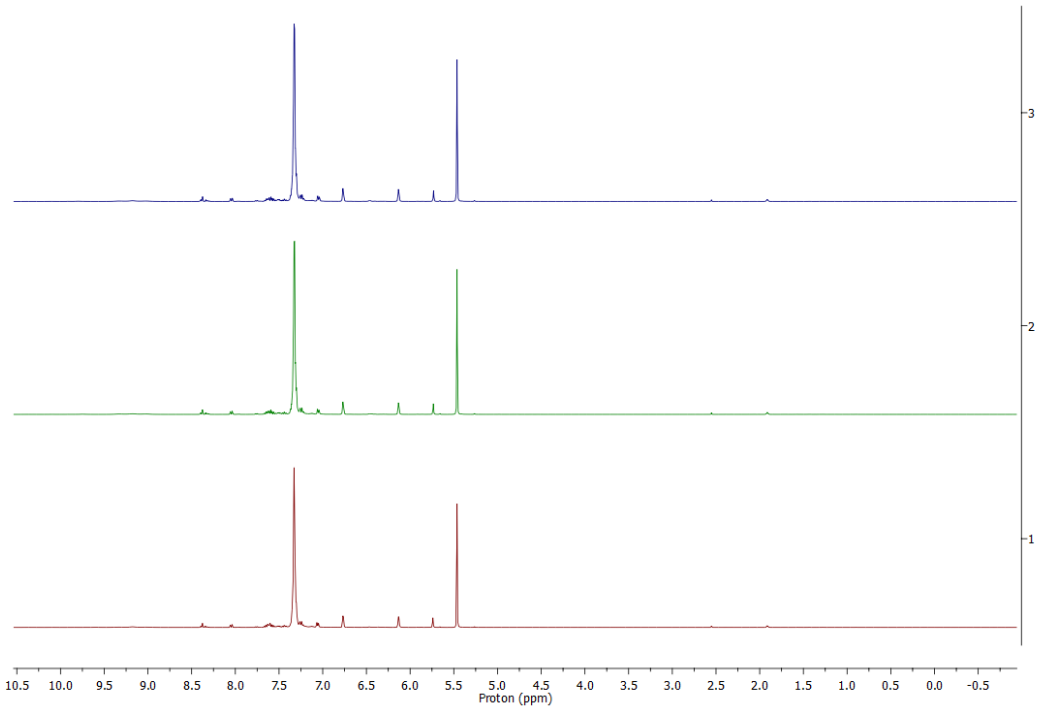

Figure 86: Hydroarylation of Pyrrole with 1,1-diphenylethylene using 10% mol 1b catalyst after 1h, 5h and 24h.

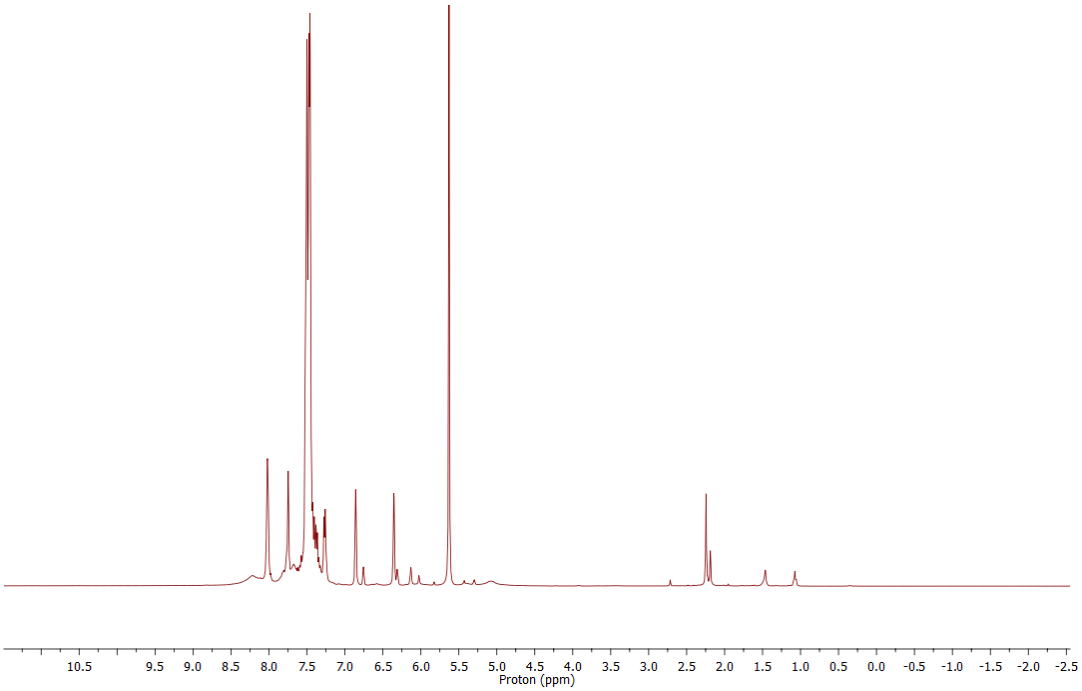

Figure 87: Hydroarylation of Pyrrole with 1,1-diphenylethylene using 10% mol 1c catalyst after 24h.

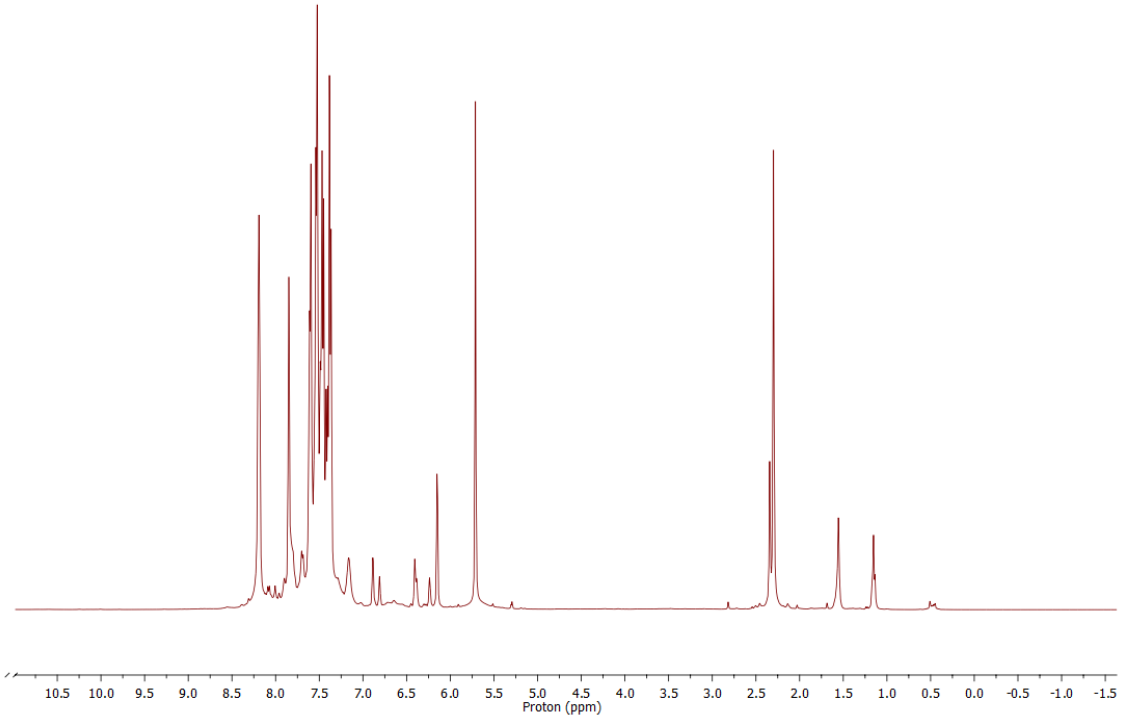

Figure 88: Hydroarylation of Pyrrole with 1,1-diphenylethylene using 10% mol 1d catalyst after 24h.

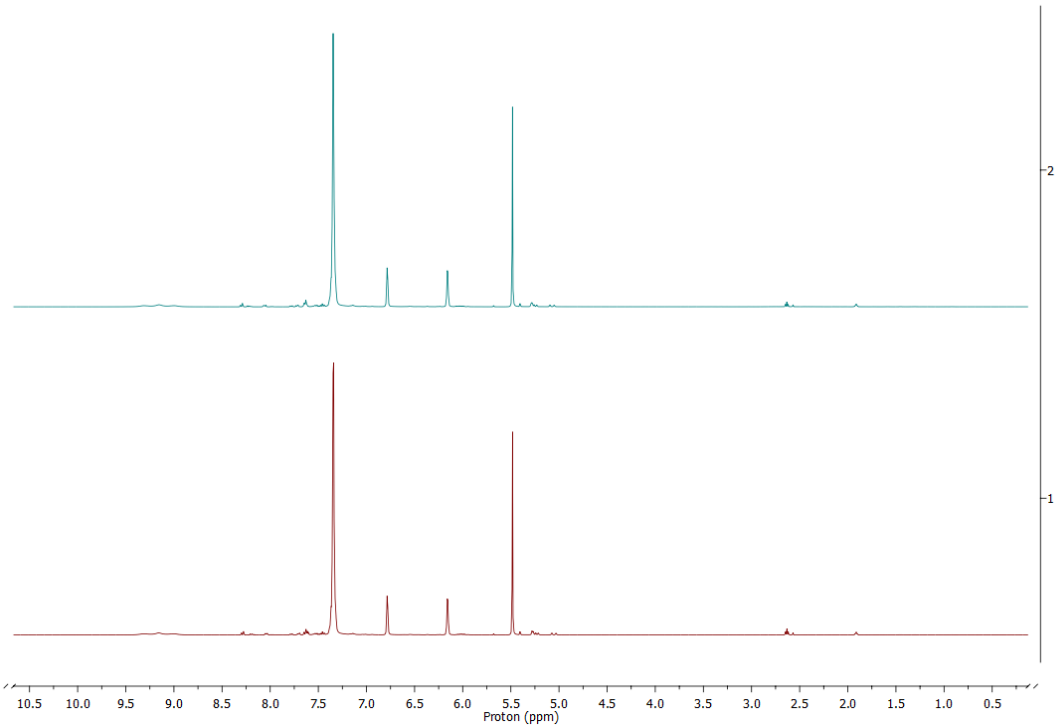

Figure 89: Hydroarylation of Pyrrole with 1,1-diphenylethylene using 10% mol 2a catalyst after 1h and 24h.

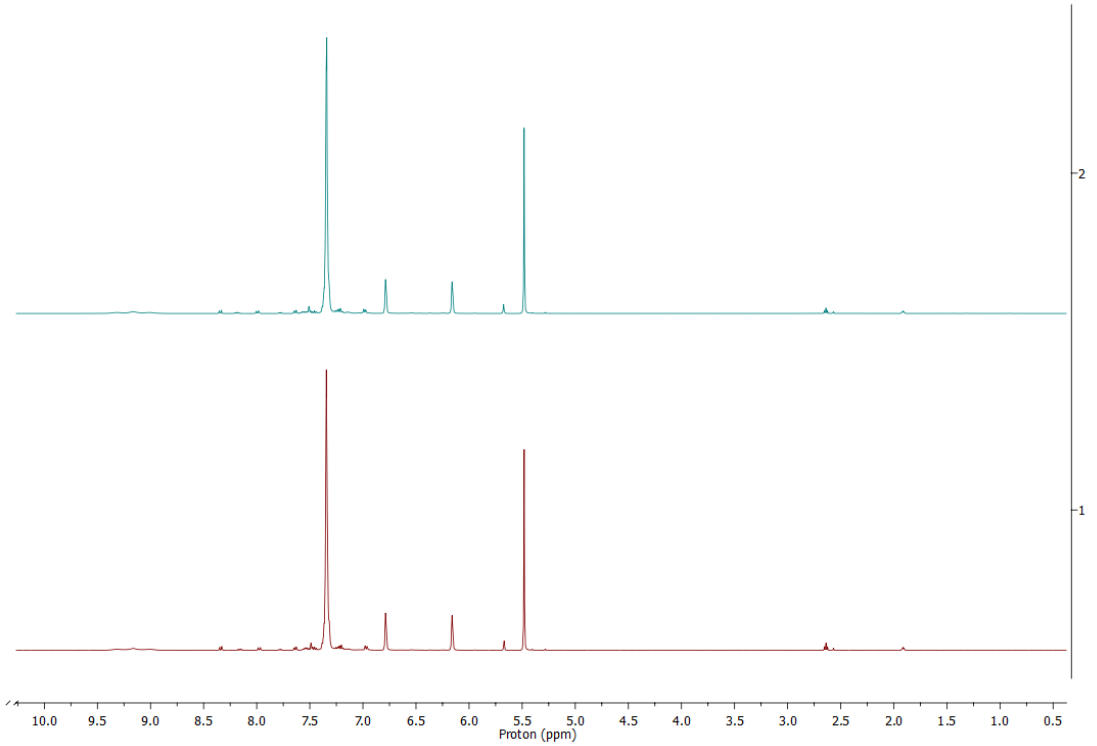

Figure 90: Hydroarylation of Pyrrole with 1,1-diphenylethylene using 10% mol 2a catalyst after 1h and 24h.

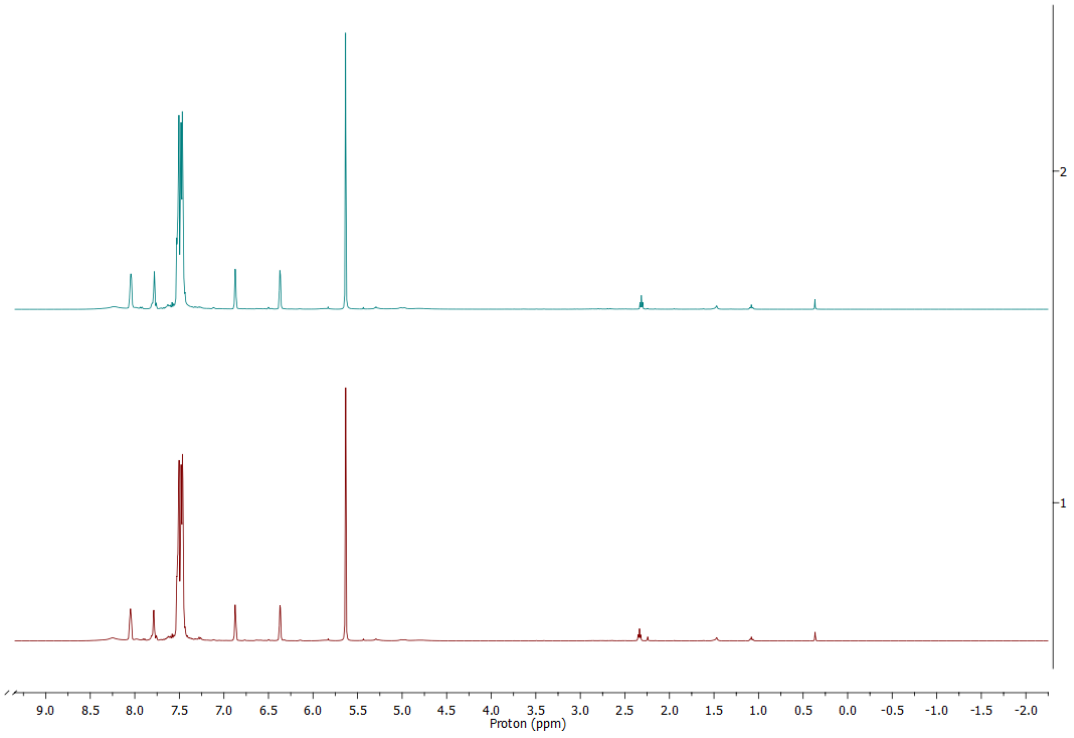

Figure 91: Hydroarylation of Pyrrole with 1,1-diphenylethylene using 10% mol 2c catalyst after 1h and 24h.

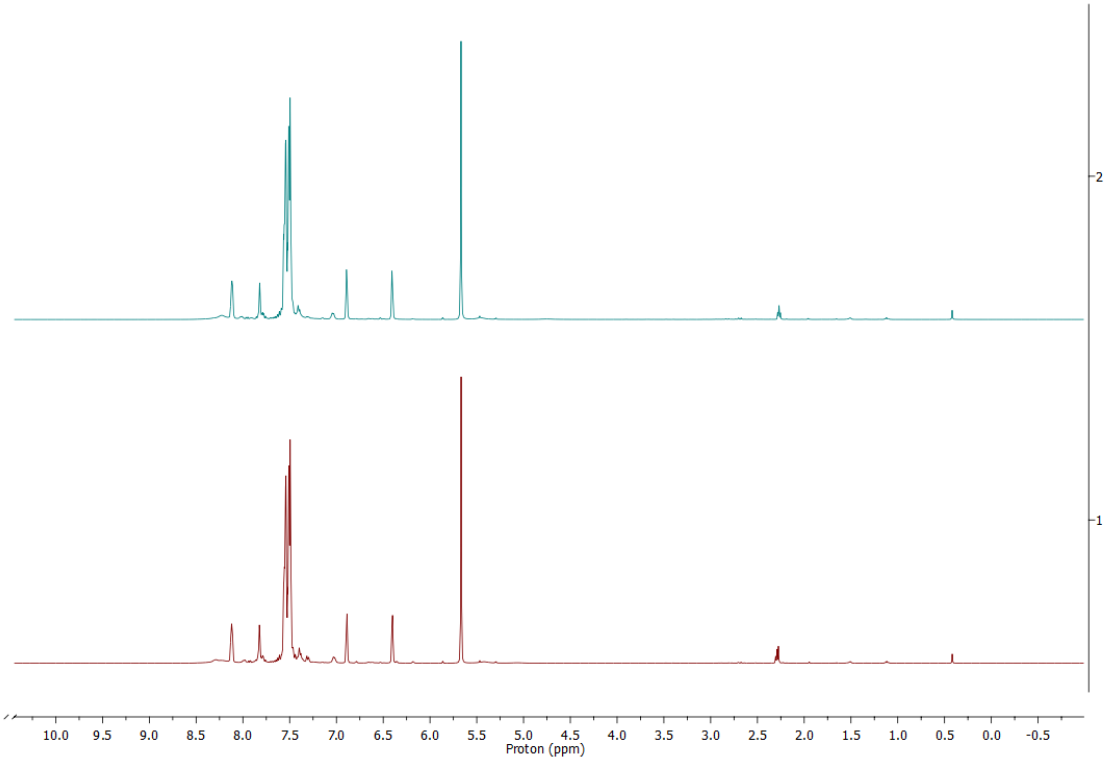

Figure 92: Hydroarylation of Pyrrole with 1,1-diphenylethylene using 10% mol 2d catalyst after 1h and 24h.

Hydrothiolation of 1,1-diphenylethylene with Thiophenol Spectra

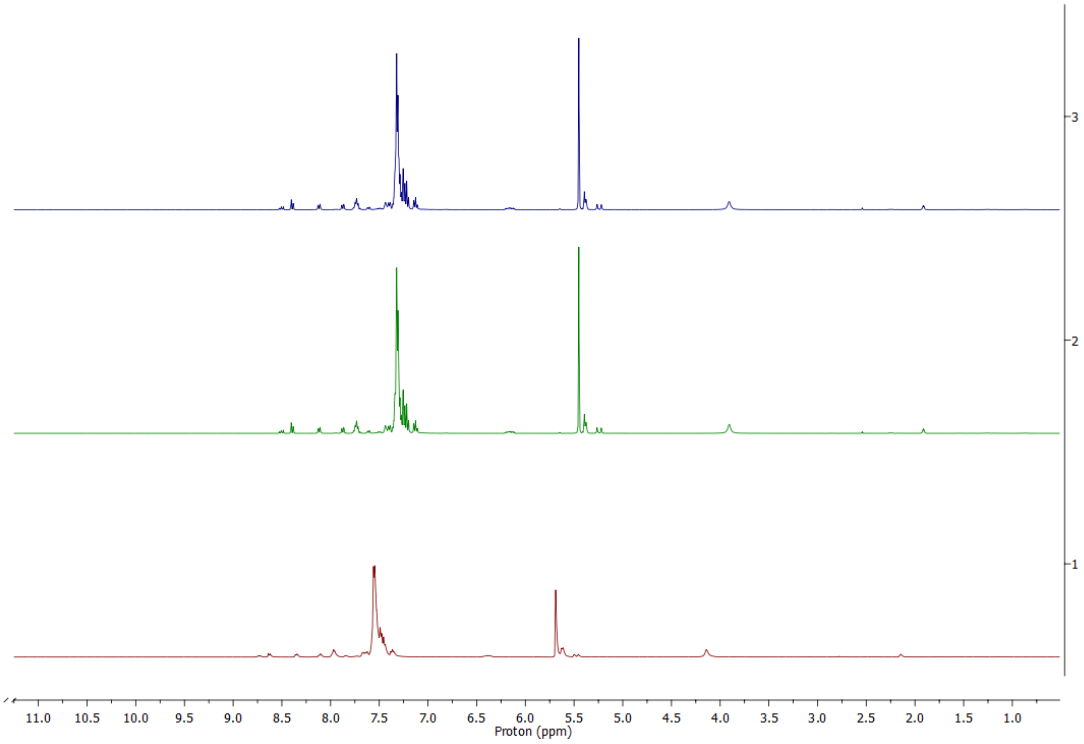

Figure 93: Hydrothiolation of 1,1-diphenylethylene with Thiophenol using 10% mol of 1a catalyst after 1h, 5h and 24h

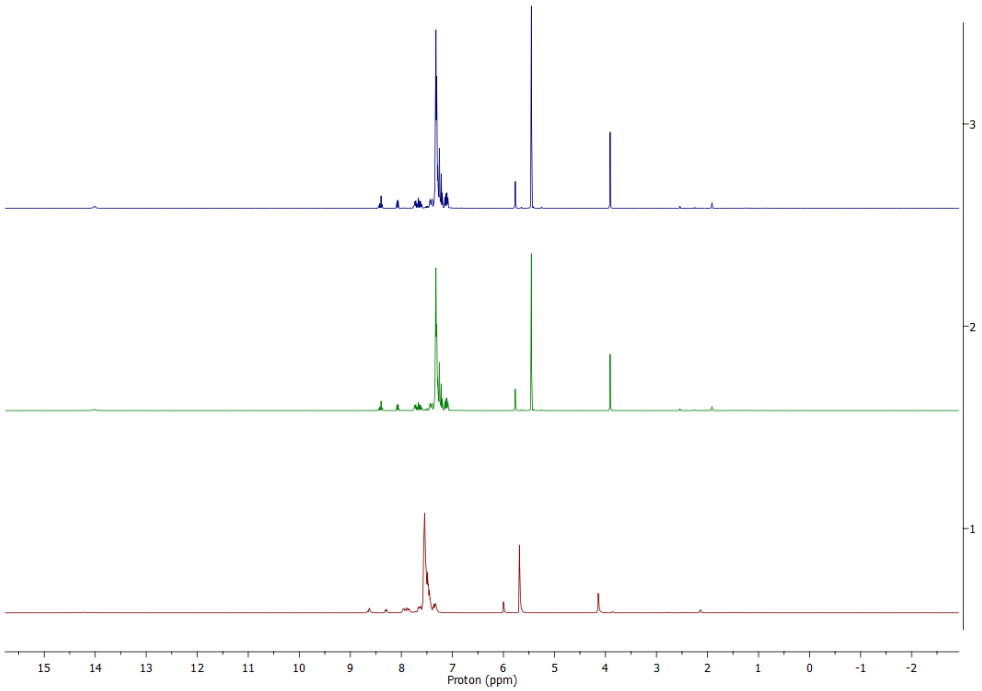

Figure 94: Hydrothiolation of 1,1-diphenylethylene with Thiophenol using 10% mol of 1b catalyst after 1h, 5h and 24h

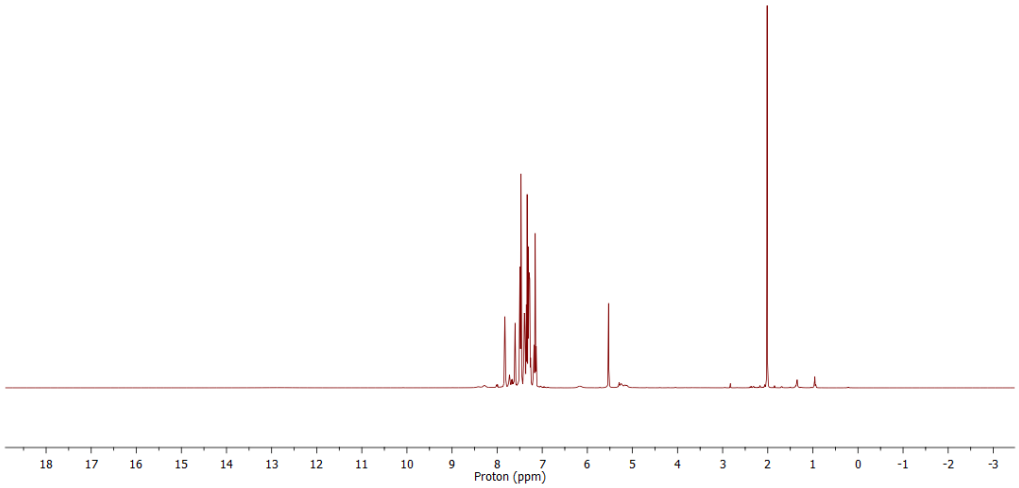

Figure 95: Hydrothiolation of 1,1-diphenylethylene with Thiophenol using 10% mol of 1c catalyst after 24h

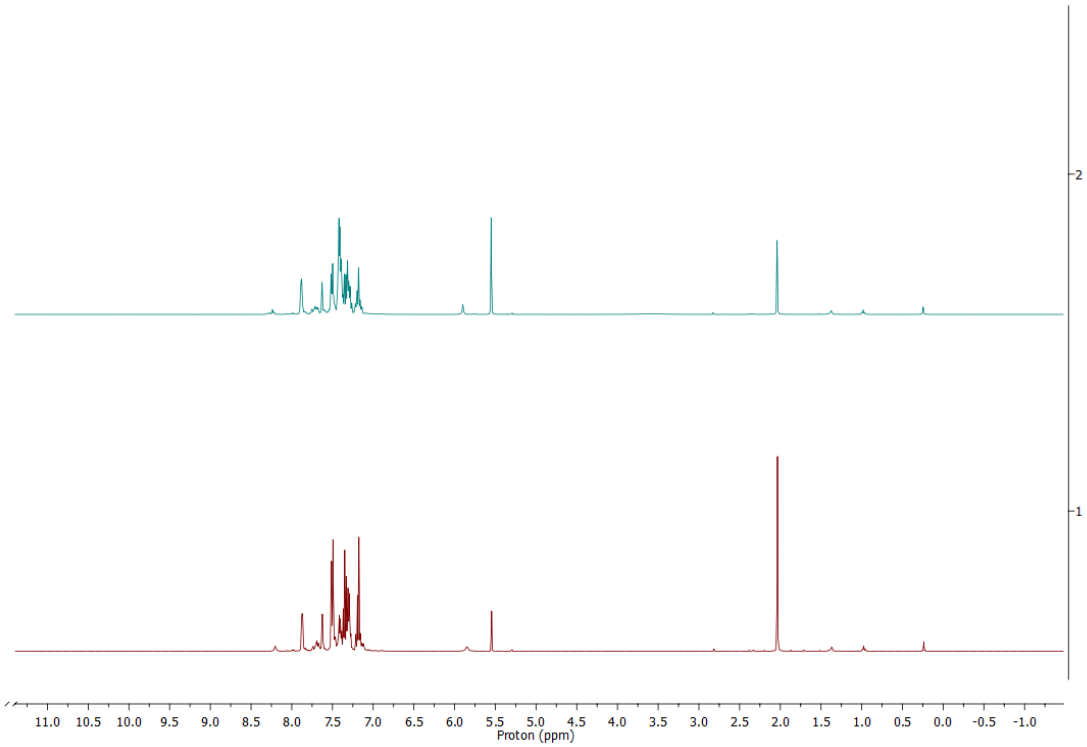

Figure 96: Hydrothiolation of 1,1-diphenylethylene with Thiophenol using 10% mol of 1c catalyst after 1h and 24h

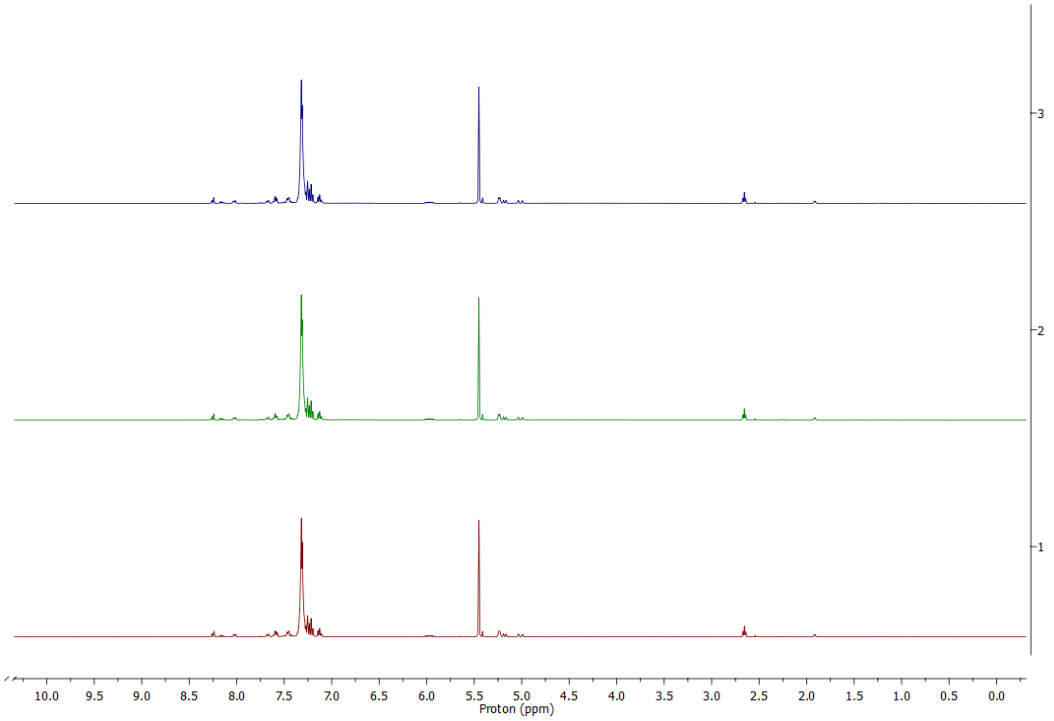

Figure 97: Hydrothiolation of 1,1-diphenylethylene with Thiophenol using 10% mol of 2a catalyst after 1h, 5h and 24h

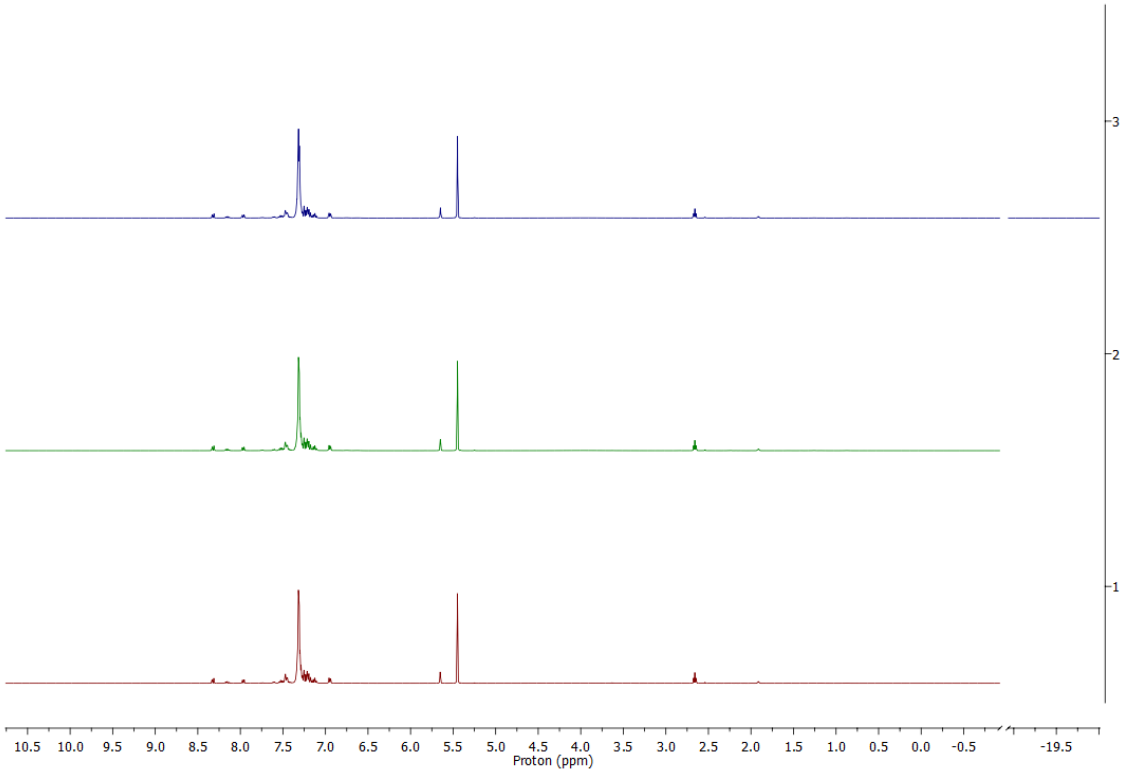

Figure 98: Hydrothiolation of 1,1-diphenylethylene with Thiophenol using 10% mol of 2b catalyst after 1h, 5h and 24h

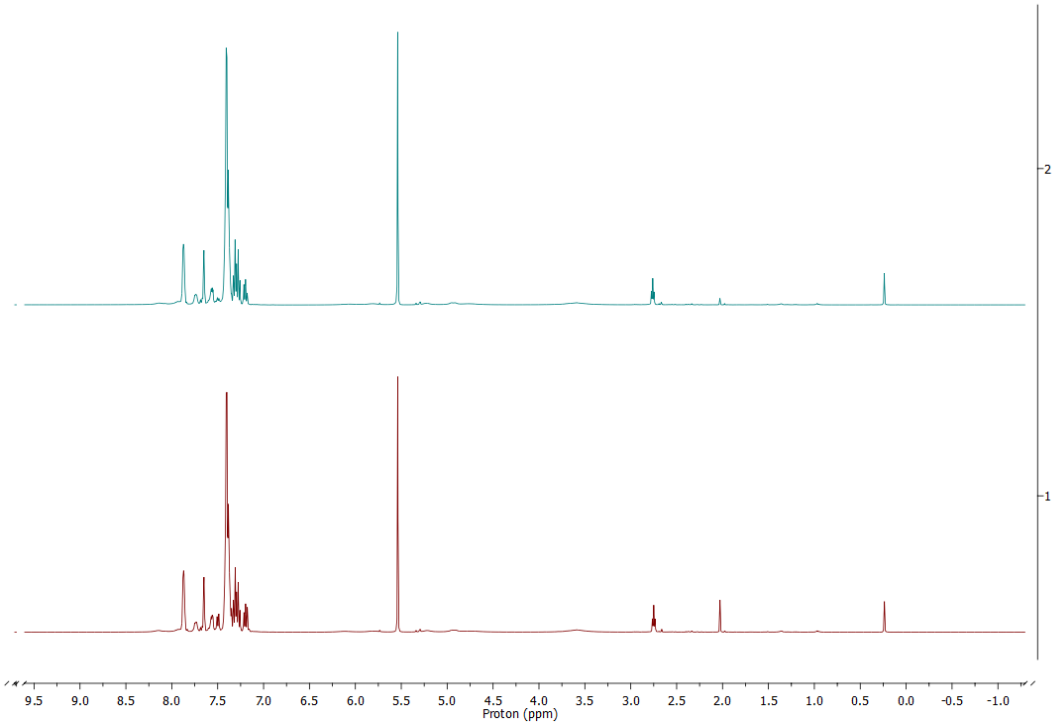

Figure 99: Hydrothiolation of 1,1-diphenylethylene with Thiophenol using 10% mol of 2c catalyst after 1h and 24h

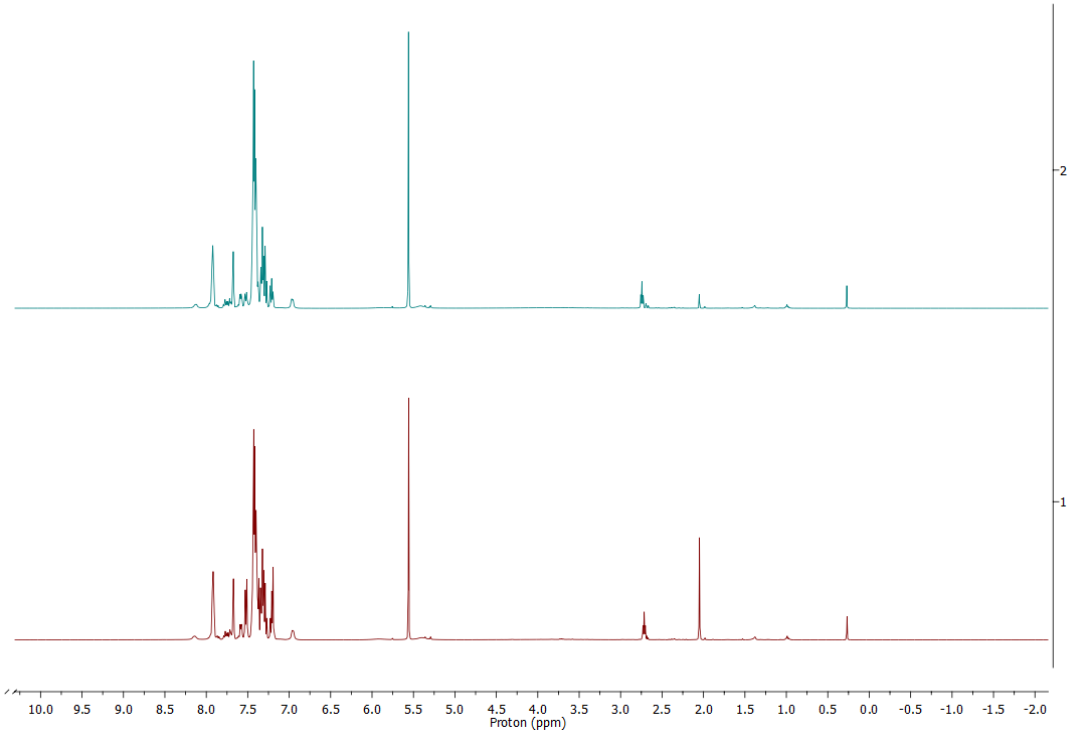

Figure 100: Hydrothiolation of 1,1-diphenylethylene with Thiophenol using 10% mol of 2d catalyst after 1h and 24h

Dimerization of 1,1-Diphenylethylene Spectra

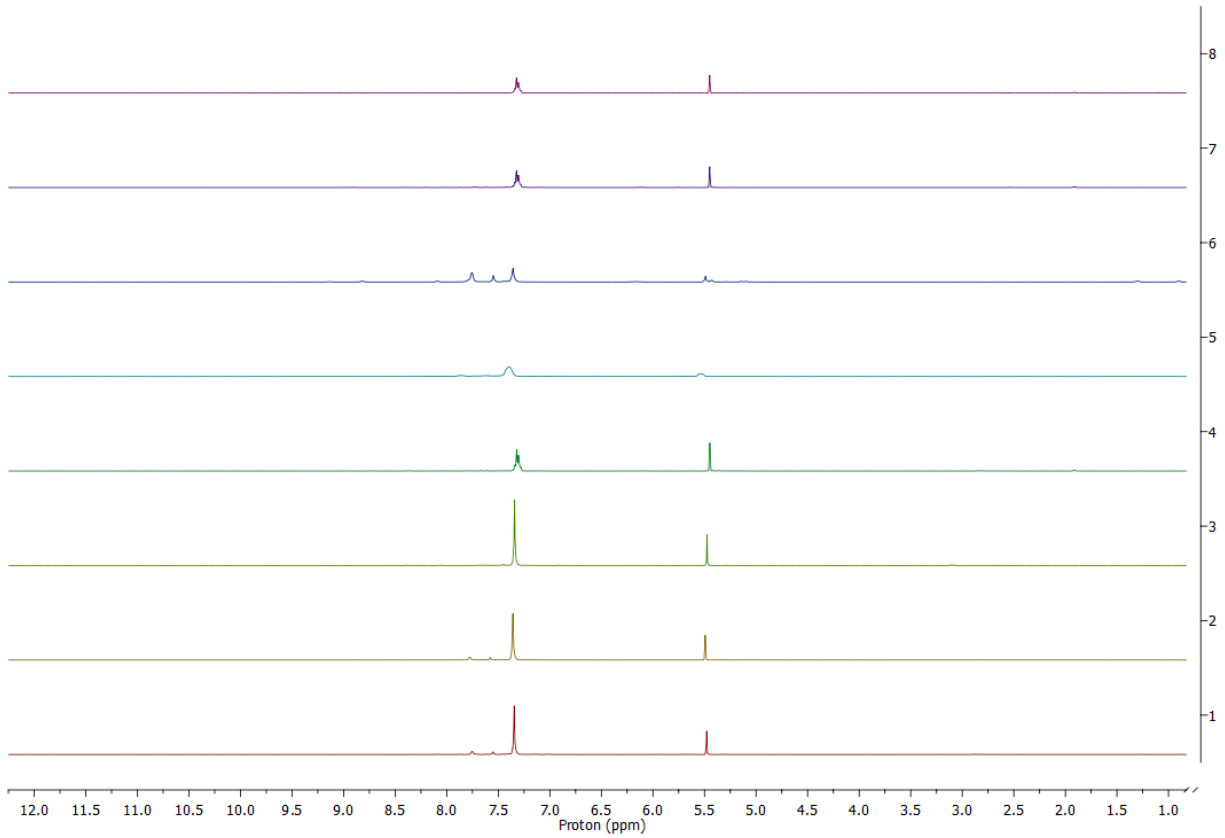

Figure 101: Combined ^{1}H NMR spectra of dimerization of 1,1-diphenylethylene using 10%mol catalysts 1a-d and 2a-d from top to bottom after 24h

Hydrodefluorination of 1-fluoropentane

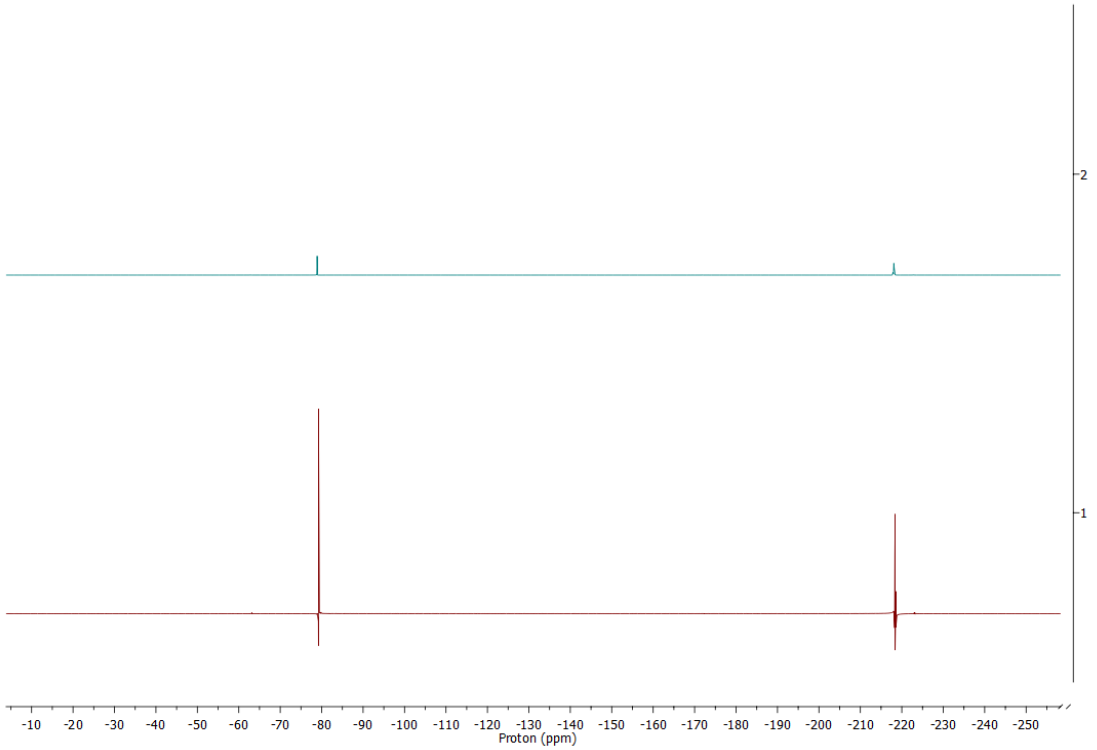

Figure 102: ^{19}F NMR spectra of Hydrodefluorination of 1-fluoropentane using 10% mol of 1a catalyst after 1h and 24h

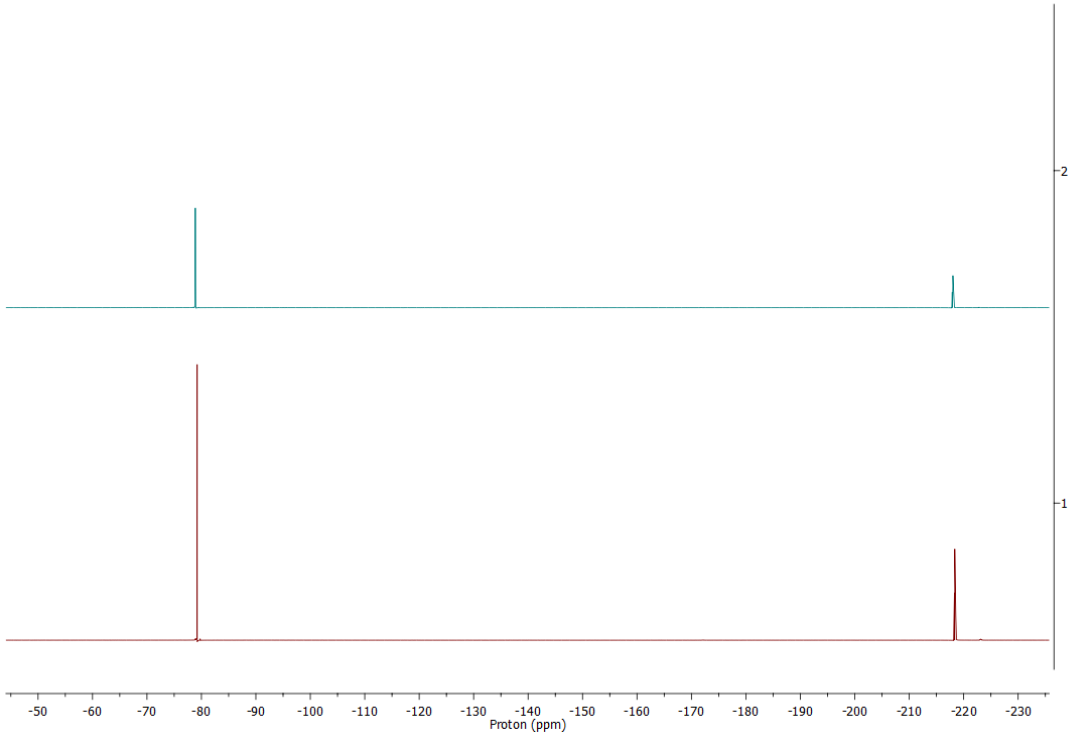

Figure 103: ^{19}F NMR spectra of Hydrodefluorination of 1-fluoropentane using 10% mol of 1b catalyst after 1h and 24h

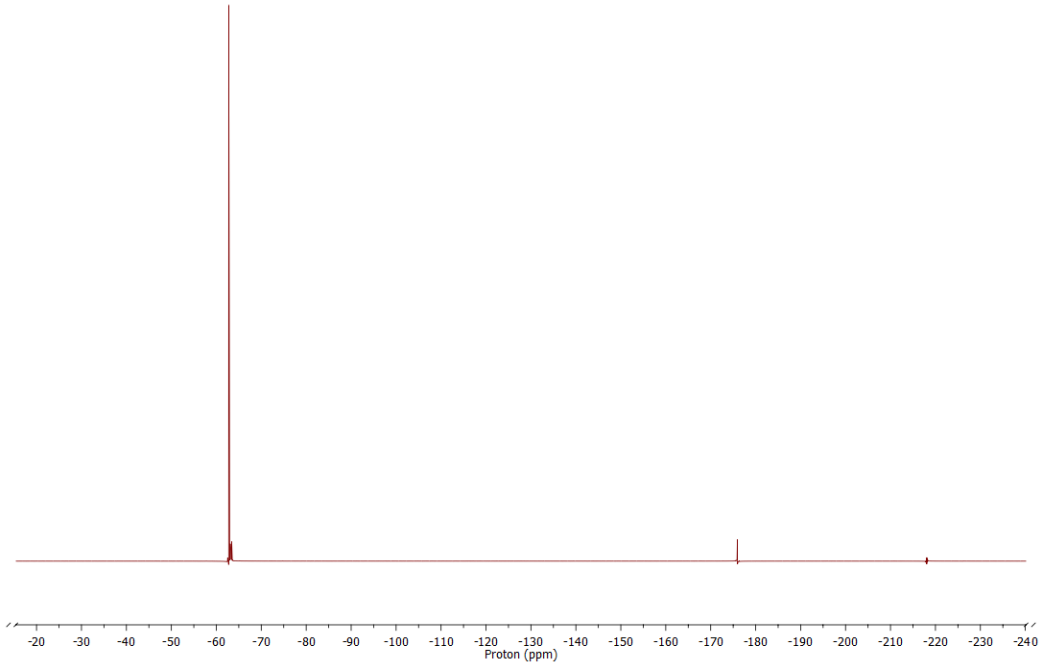

Figure 104: ^{19}F NMR spectra of Hydrodefluorination of 1-fluoropentane using 10% mol of 1c catalyst after 24h at 70°C

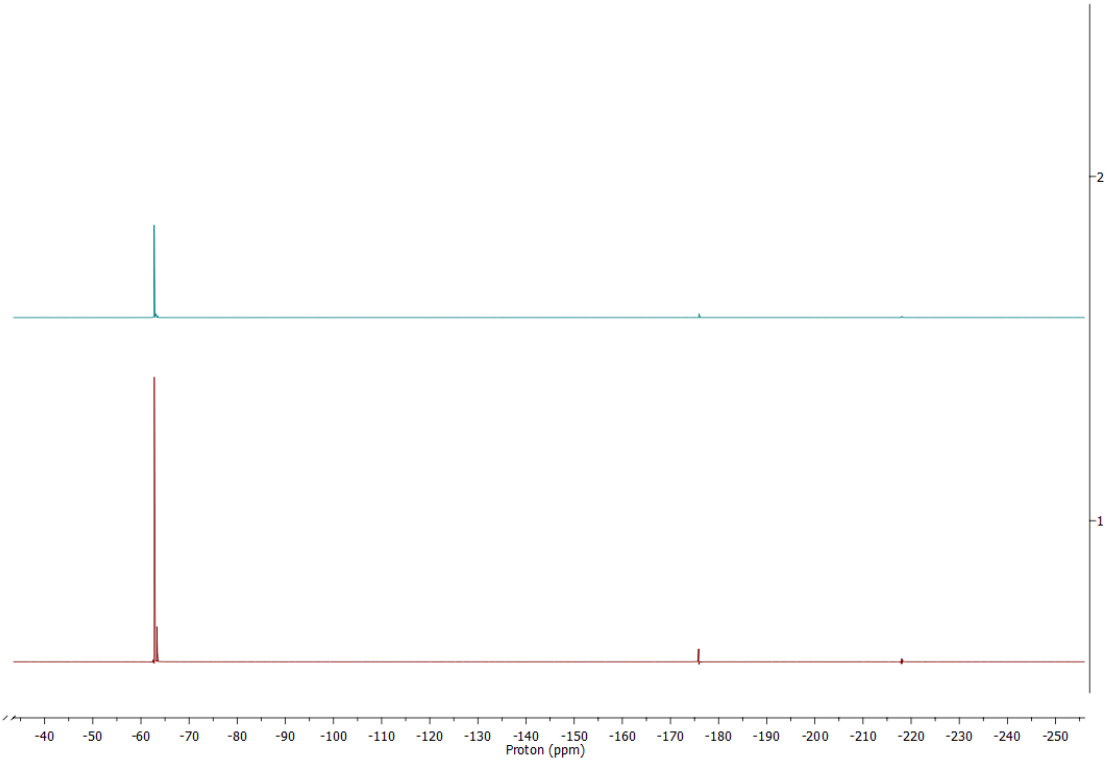

Figure 105: ^{19}F NMR spectra of Hydrodefluorination of 1-fluoropentane using 10% mol of 1d catalyst after 24h at room temperature and after 24h at 70°C

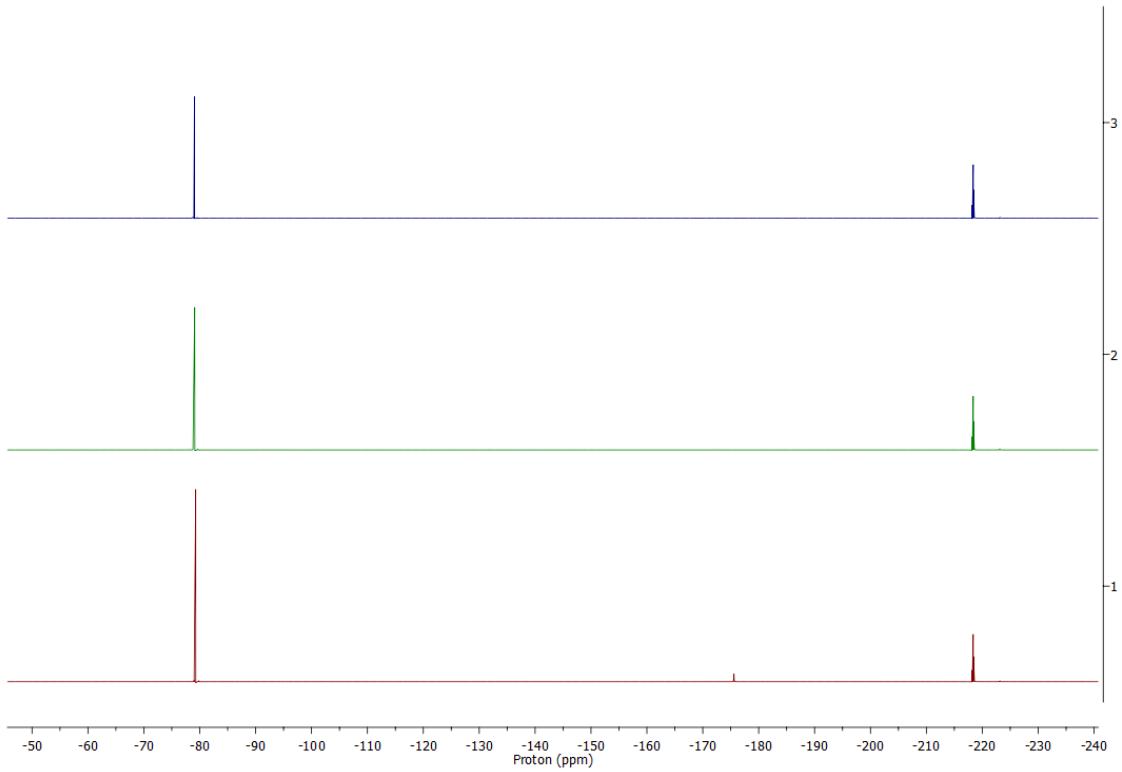

Figure 106: ^{19}F NMR spectra of Hydrodefluorination of 1-fluoropentane using 10% mol of 2a catalyst after 1h, 5h and 24h

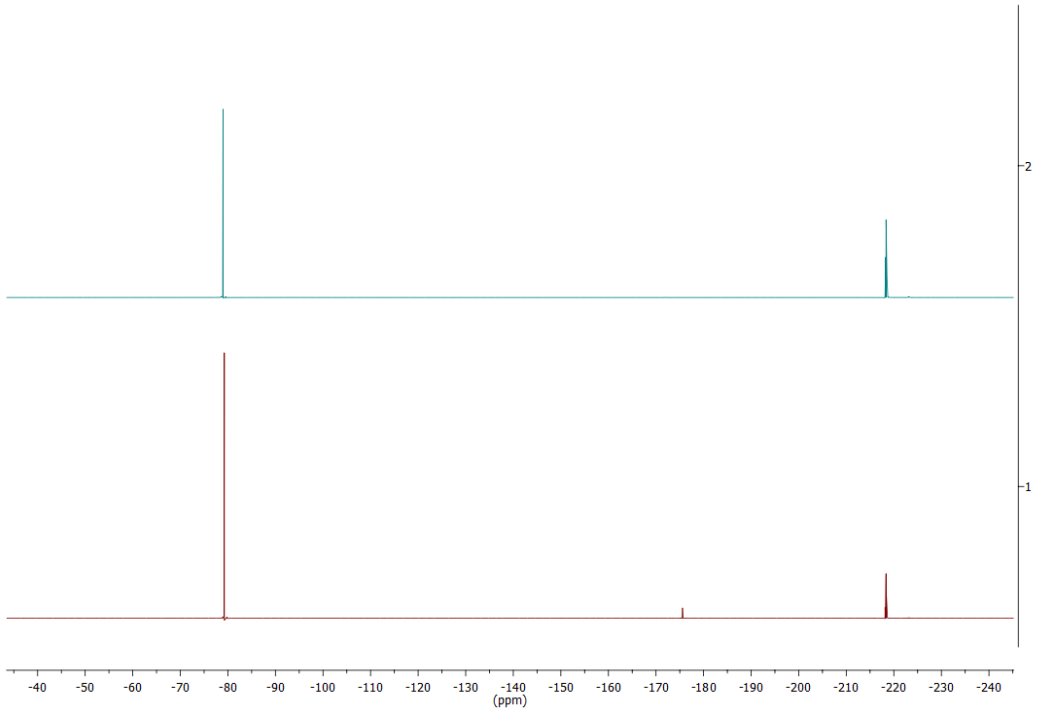

Figure 107: ^{19}F NMR spectra of Hydrodefluorination of 1-fluoropentane using 10% mol of 2b catalyst after 1h and 24h

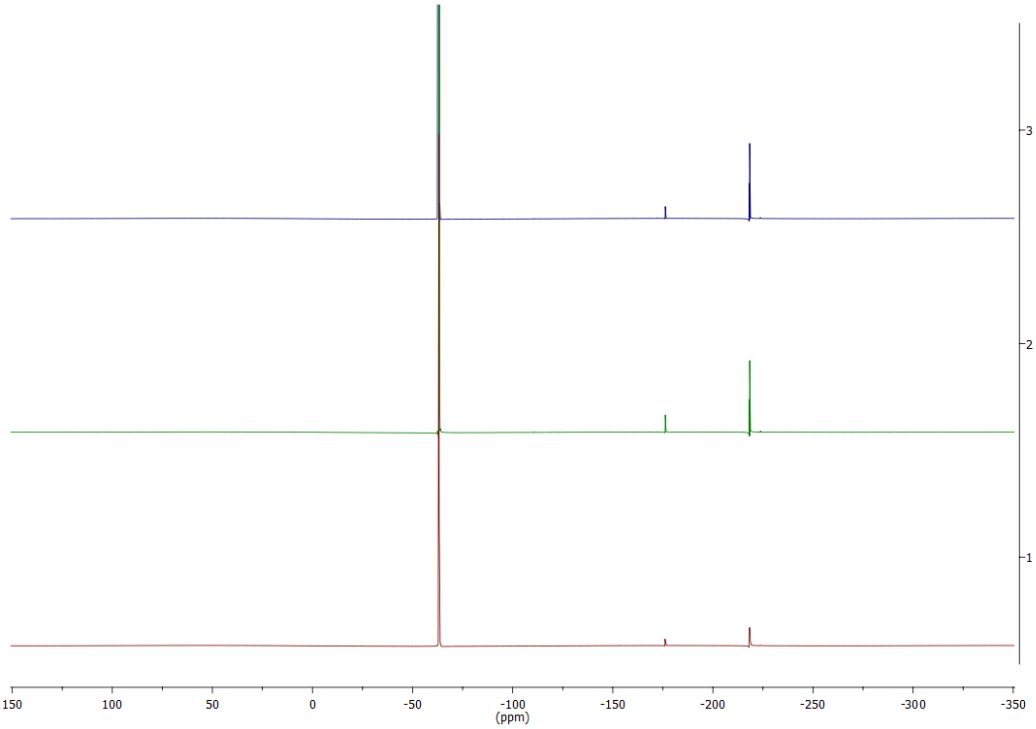

Figure 108: ^{19}F NMR spectra of Hydrodefluorination of 1-fluoropentane using 10% mol of 2c catalyst after 1h, 5h and 24h

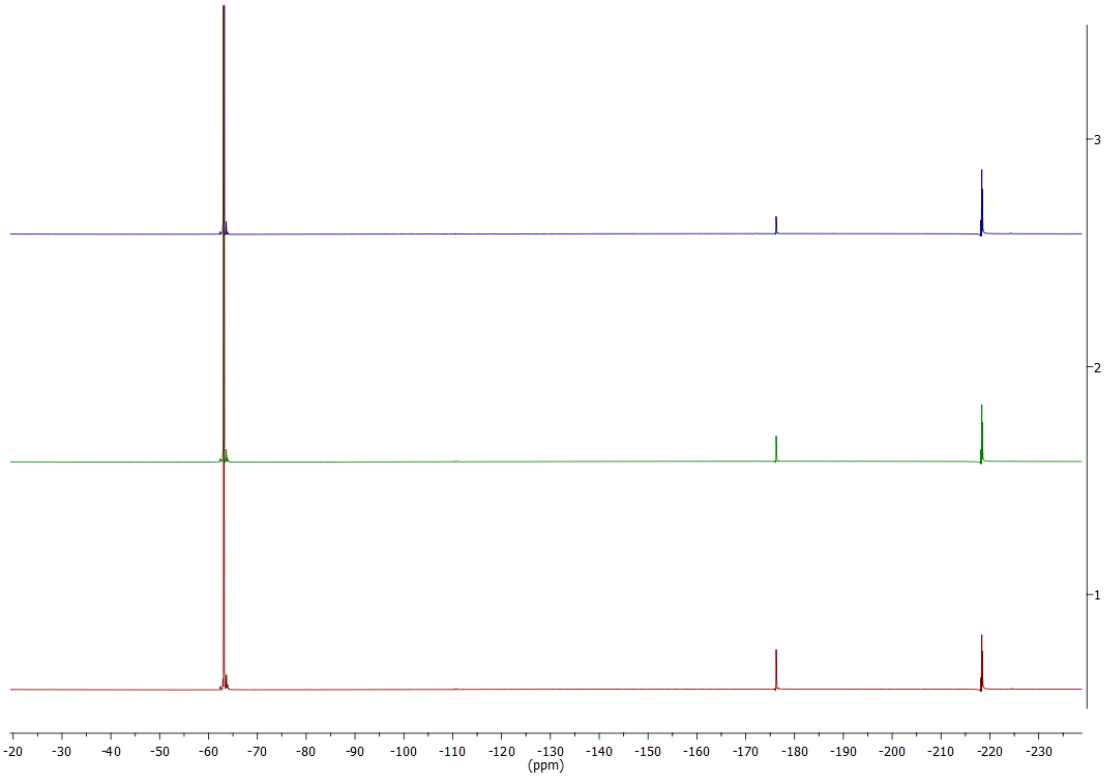

Figure 109: ^{19}F NMR spectra of Hydrodefluorination of 1-fluoropentane using 10% mol of 2d catalyst after 1h, 5h and 24h

Hydrosilylation of α-methylstyrene Spectra

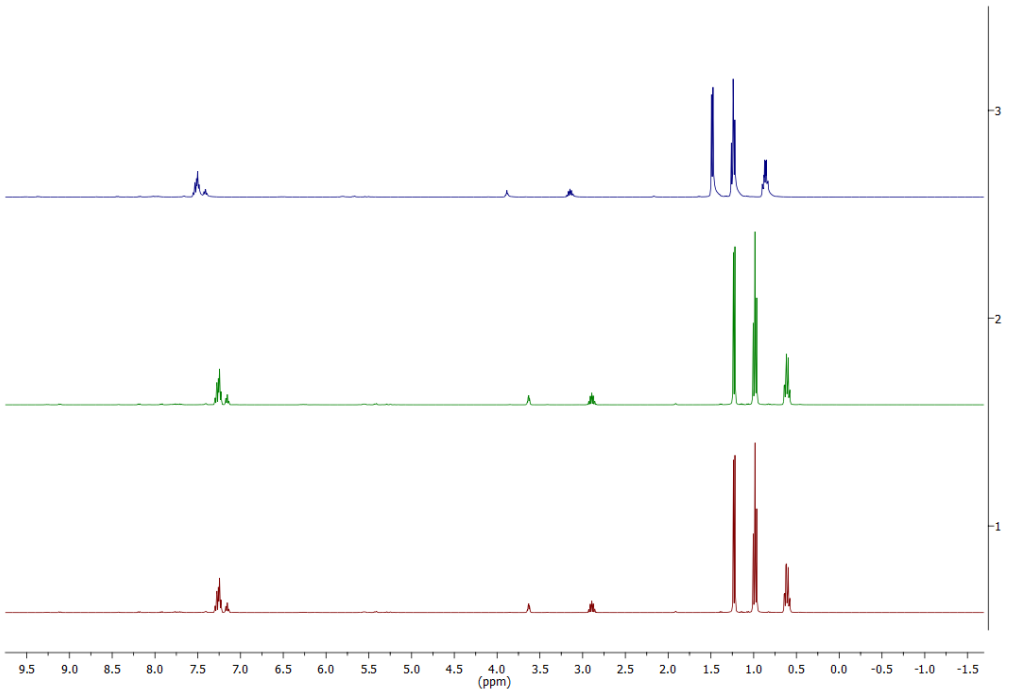

Figure 110: ^{1}H spectra of hydrosilylation of α -methylstyrene using 10% mol of 1a catalyst after 1h, 5h and 24h

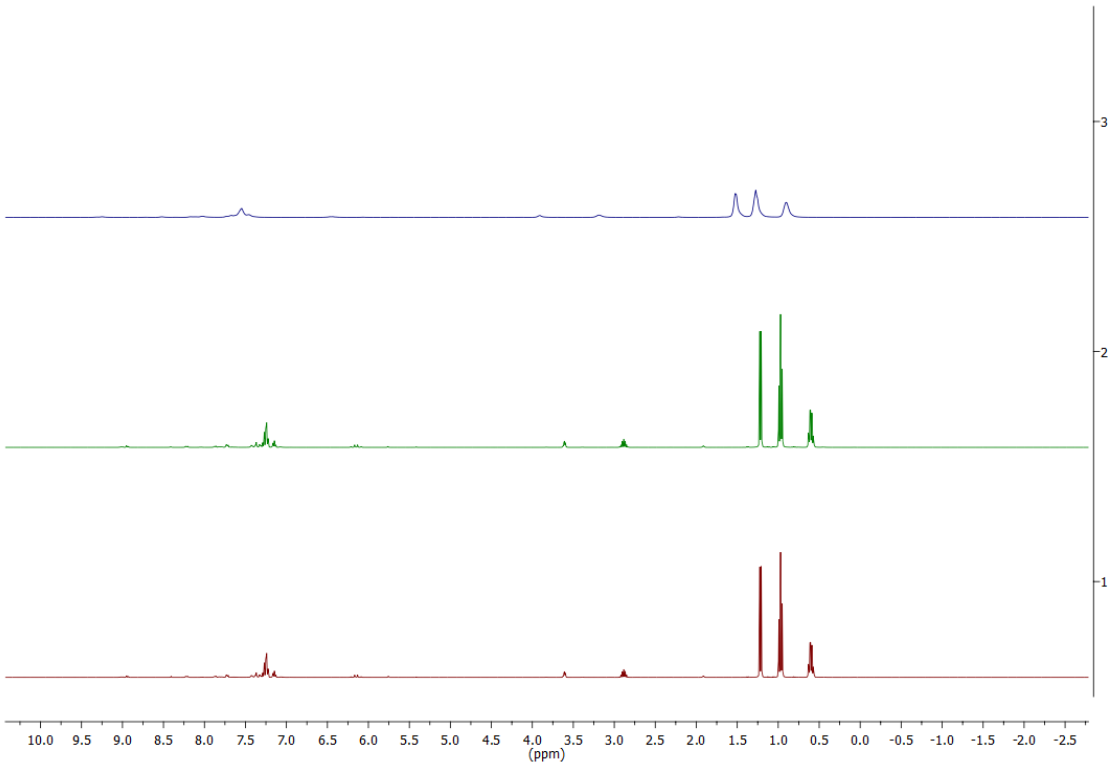

Figure 111: ^{1}H spectra of hydrosilylation of α -methylstyrene using 10% mol of 1b catalyst after 1h, 5h and 24h

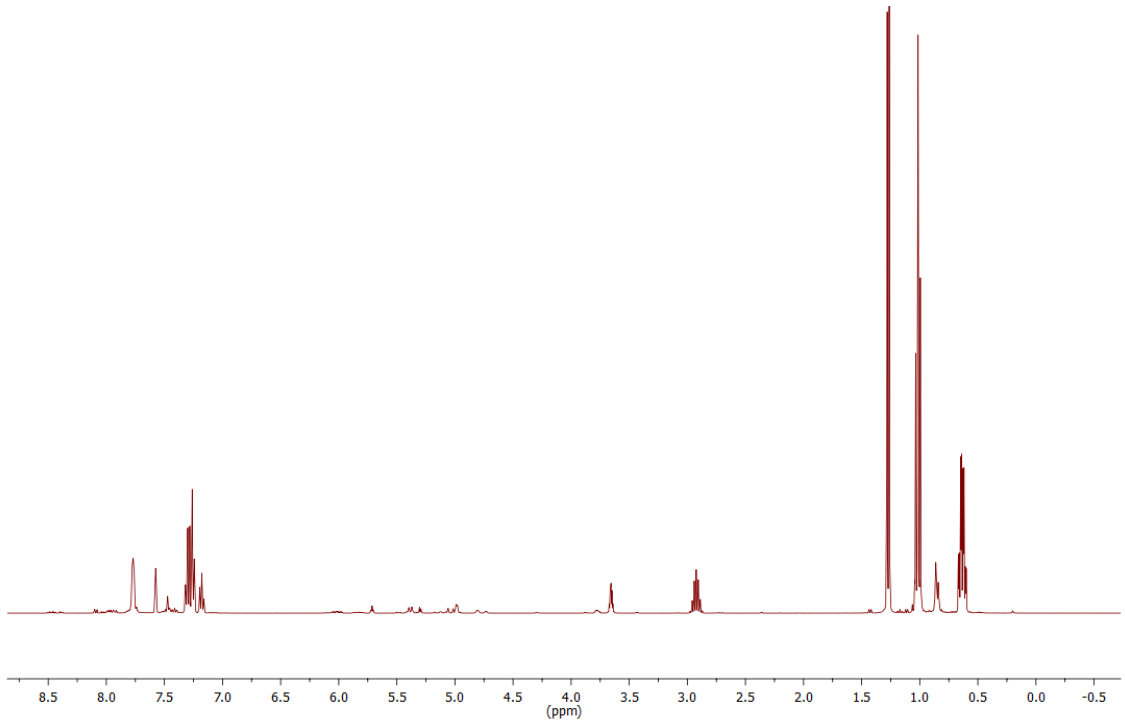

Figure 112: ^{1}H spectra of hydrosilylation of α -methylstyrene using 10% mol of 1c catalyst after 24h

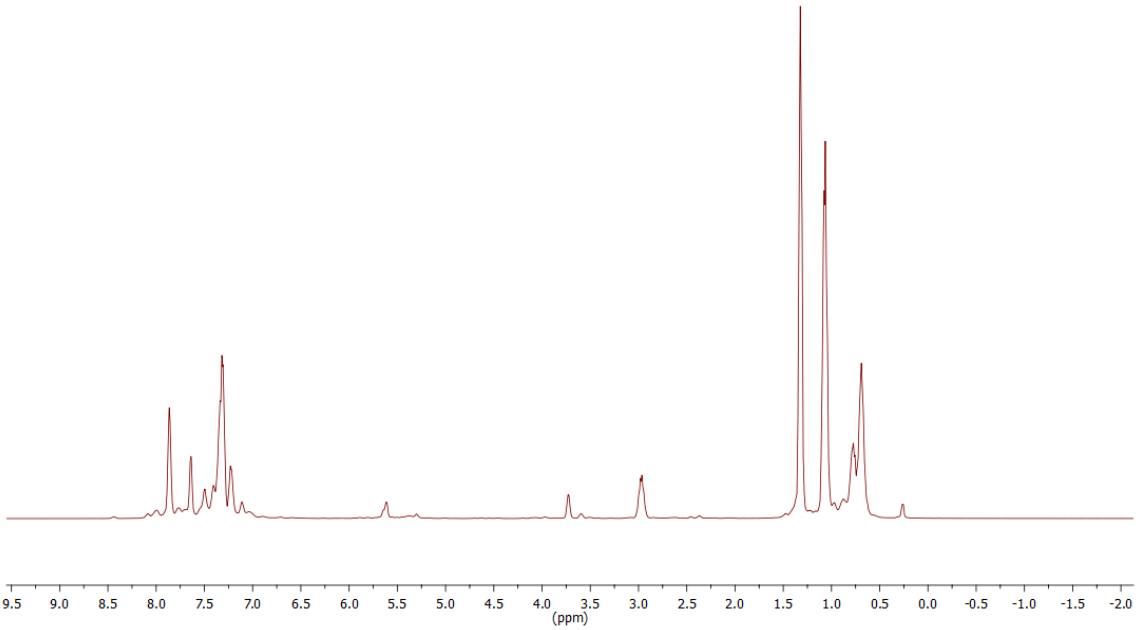

Figure 113: ^{1}H spectra of hydrosilylation of α -methylstyrene using 10% mol of 1d catalyst after 24h

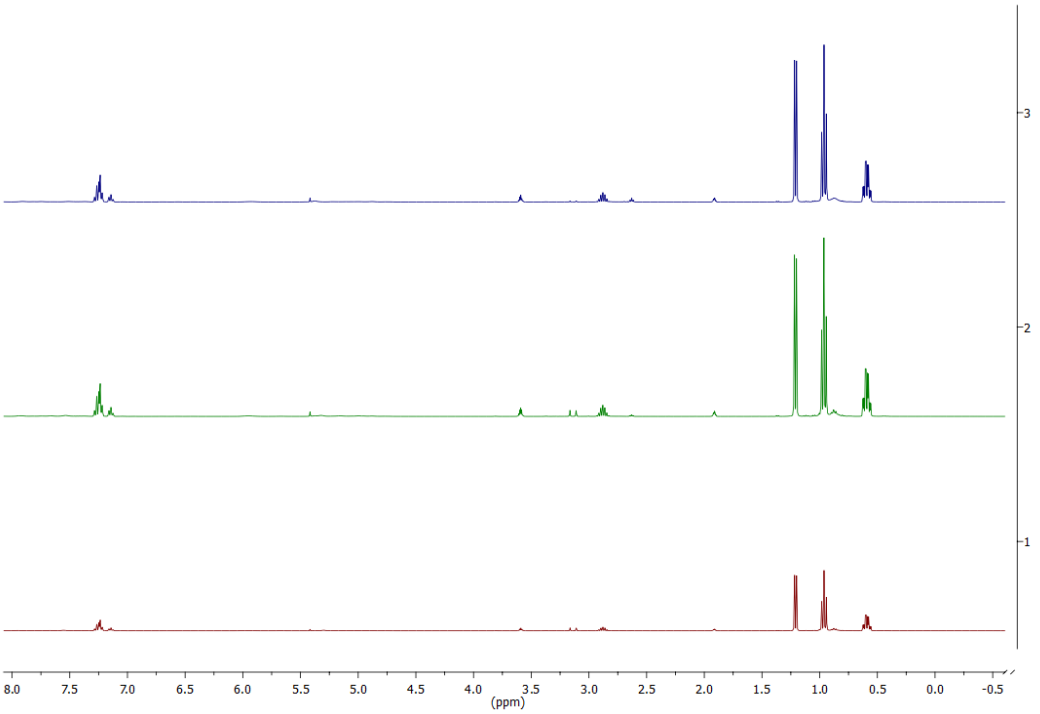

Figure 114: ^{1}H spectra of hydrosilylation of α -methylstyrene using 10% mol of 2a catalyst after 1h, 5h and 24h

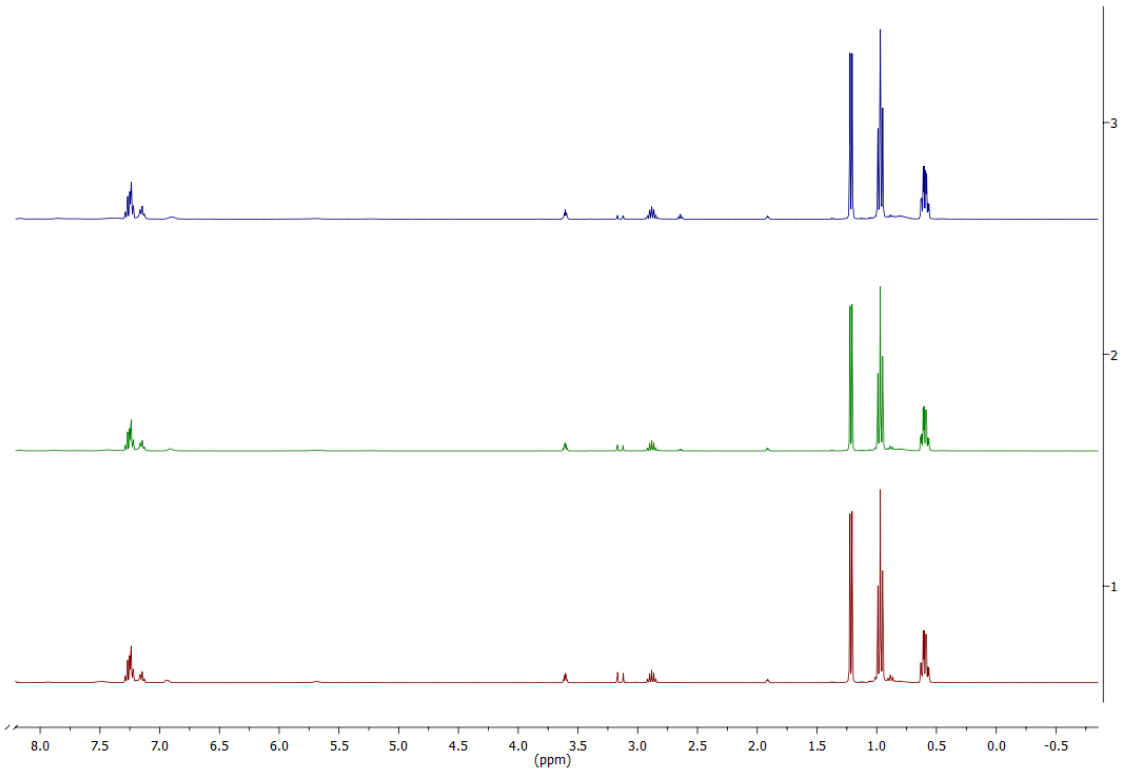

Figure 115: ^{1}H spectra of hydrosilylation of α -methylstyrene using 10% mol of 2b catalyst after 1h, 5h and 24h

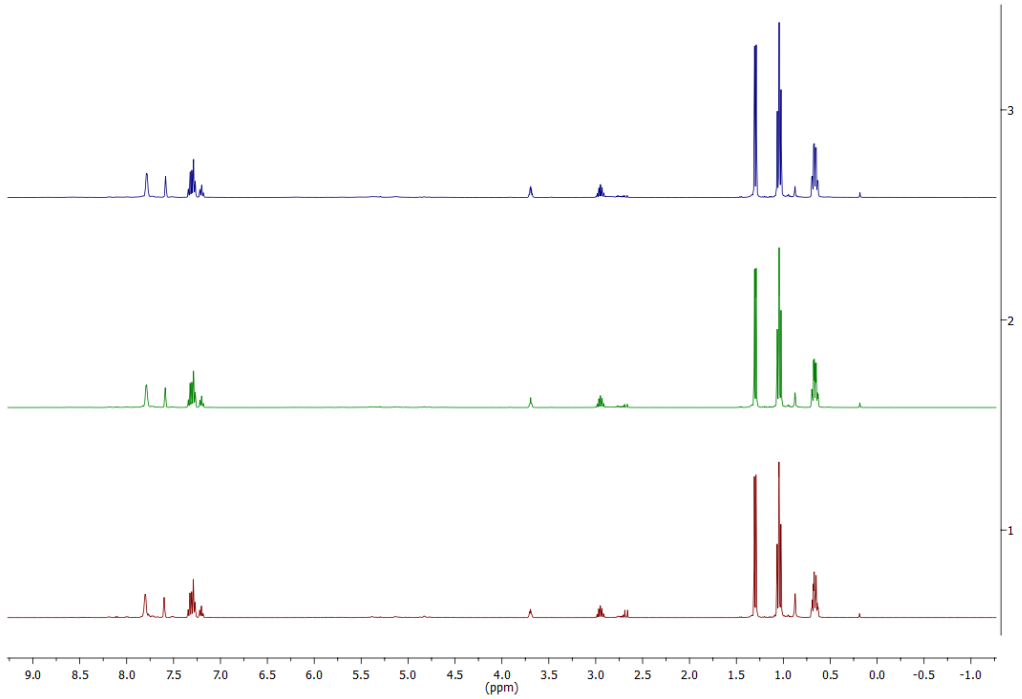

Figure 116: ^{1}H spectra of hydrosilylation of α -methylstyrene using 10% mol of 2c catalyst after 1h, 5h and 24h

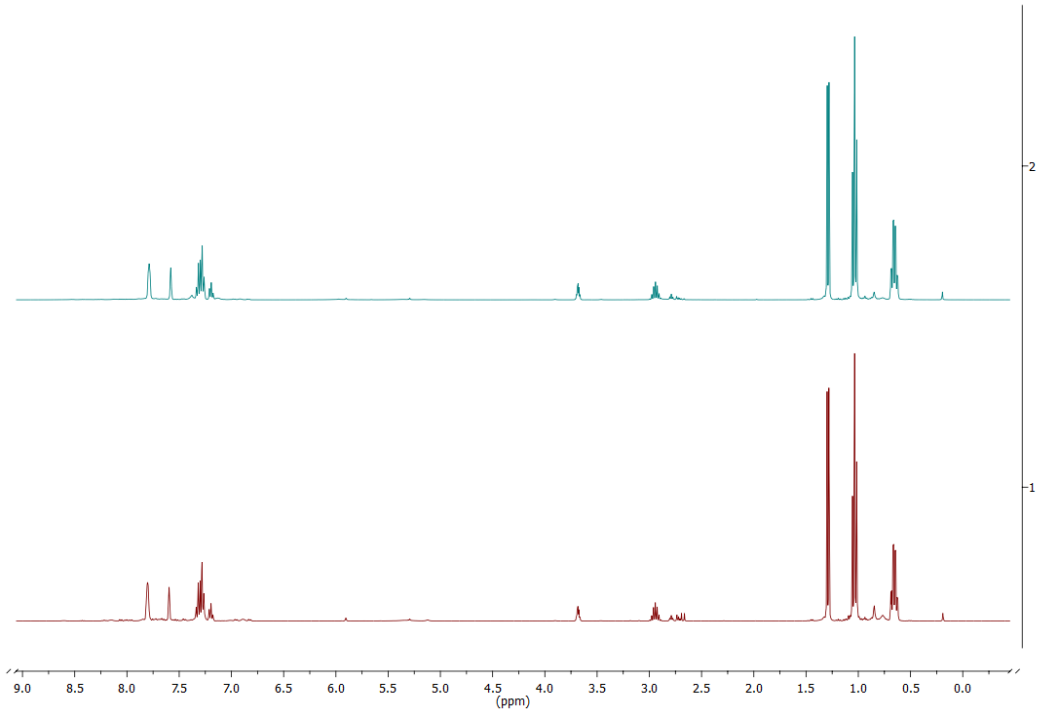

Figure 117: ^{1}H spectra of hydrosilylation of α -methylstyrene using 10% mol of 2d catalyst after 1h and 24h

Dehydrocoupling of Phenol with Et_3SiH Spectra

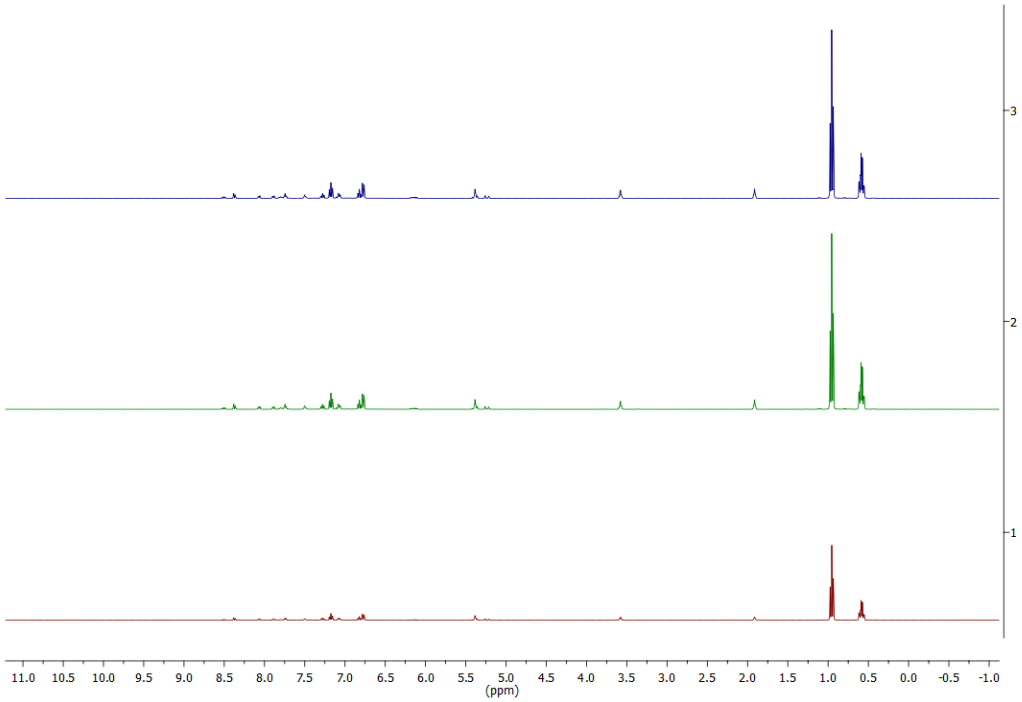

Figure 118: ^1H spectra of dehydrocoupling of phenol with Et_3SiH using 10%mol of 1a catalyst after 1h, 5h and 24h

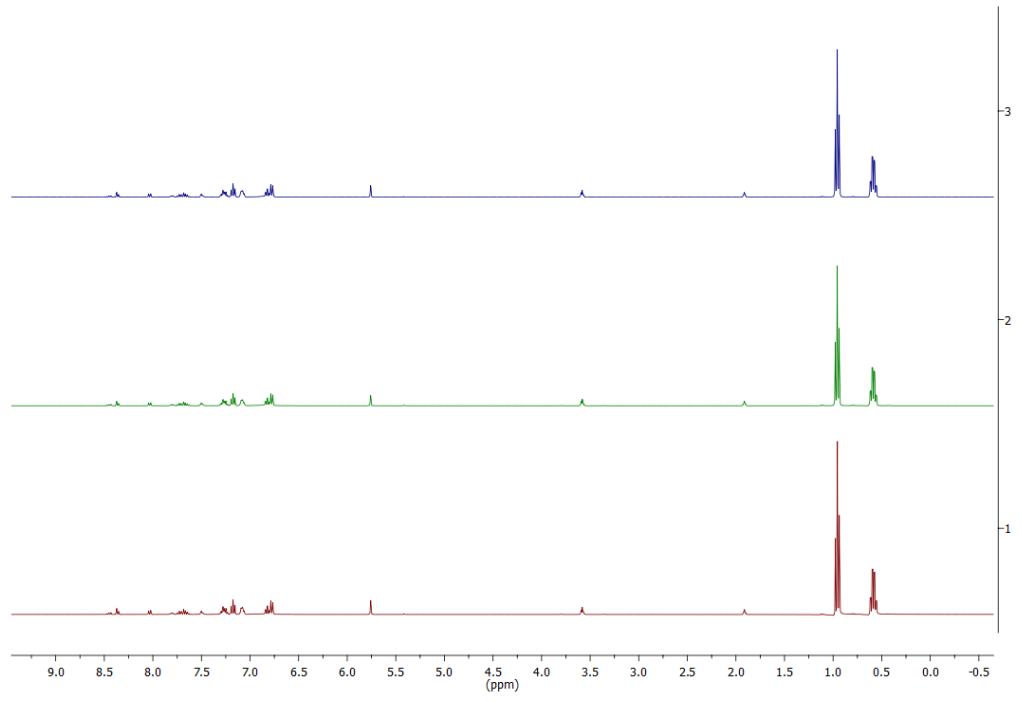

Figure 119: ^1H spectra of dehydrocoupling of phenol with Et_3SiH using 10%mol of 1b catalyst after 1h, 5h and 24h

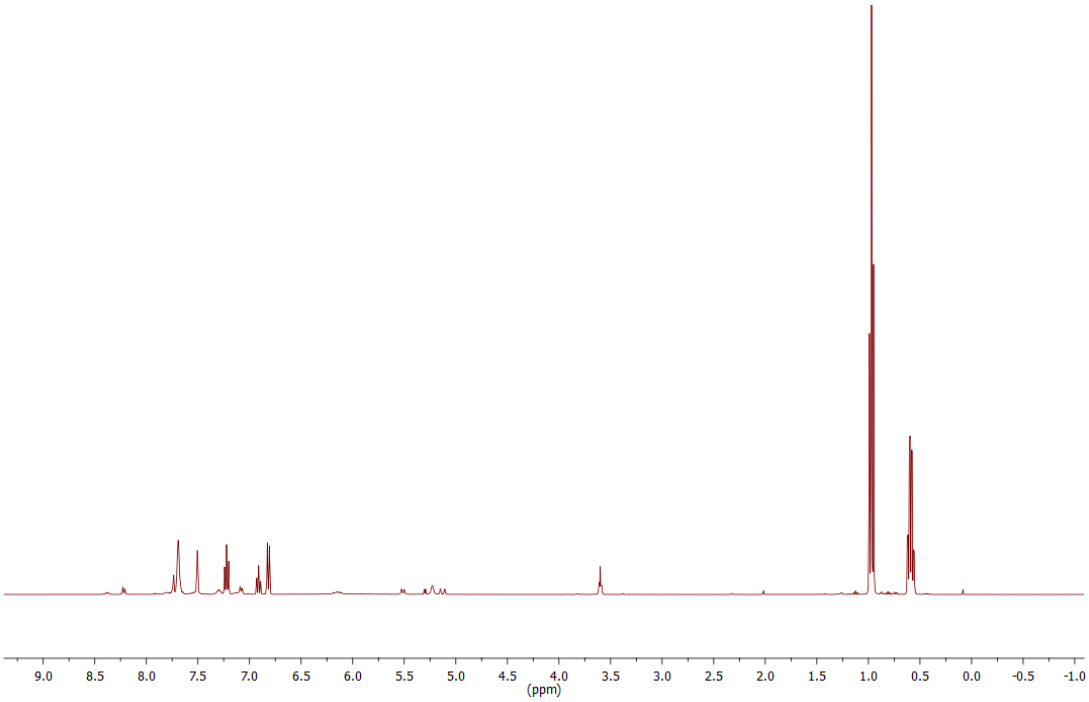

Figure 120: ^{1}H spectra of dehydrocoupling of phenol with Et_3SiH using 10%mol of 1c catalyst after and 24h

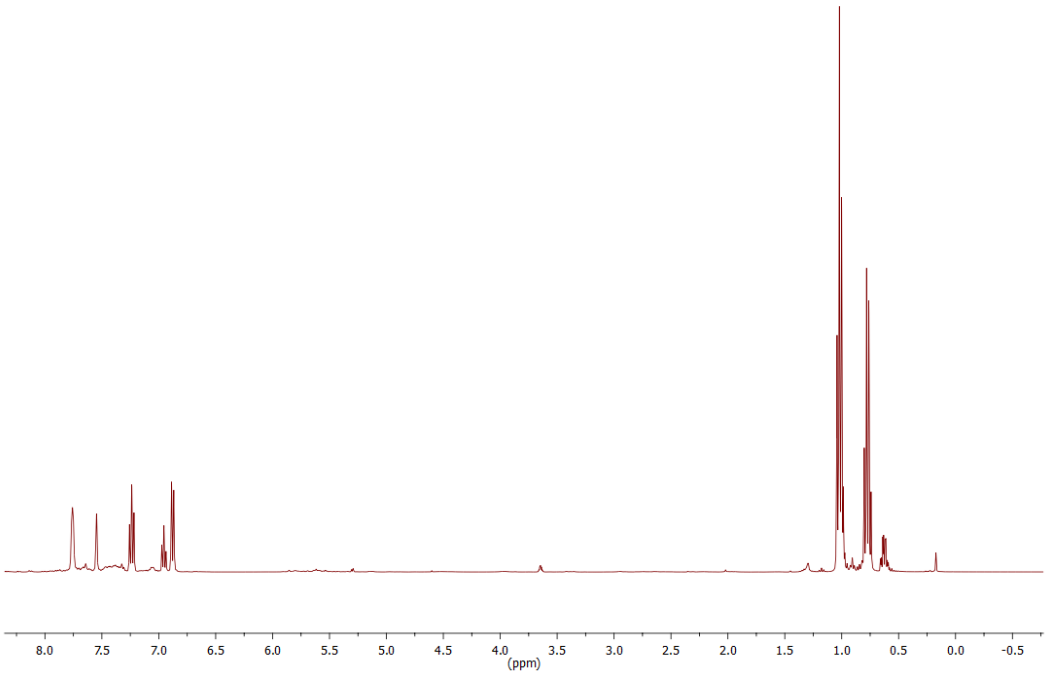

Figure 121: ^{1}H spectra of dehydrocoupling of phenol with Et_3SiH using 10%mol of 1d catalyst after 24h

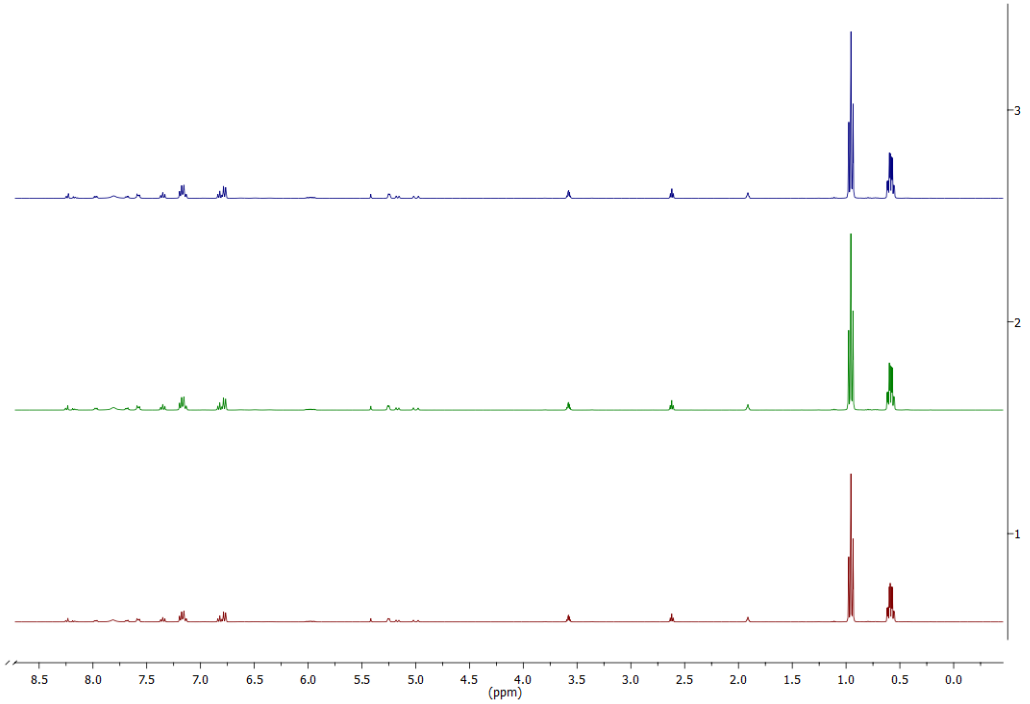

Figure 122: ^{1}H spectra of dehydrocoupling of phenol with Et_3SiH using 10%mol of 2a catalyst after 1h, 5h and 24h

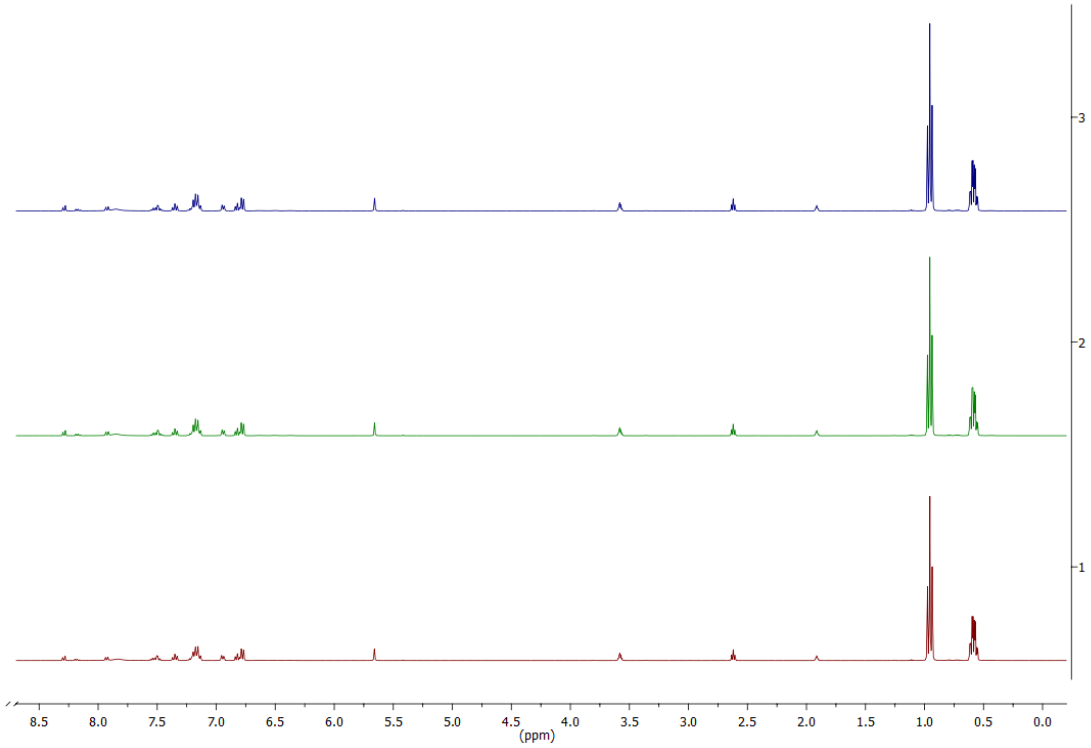

Figure 123: ^{1}H spectra of dehydrocoupling of phenol with Et_3SiH using 10%mol of 2b catalyst after 1h, 5h and 24h

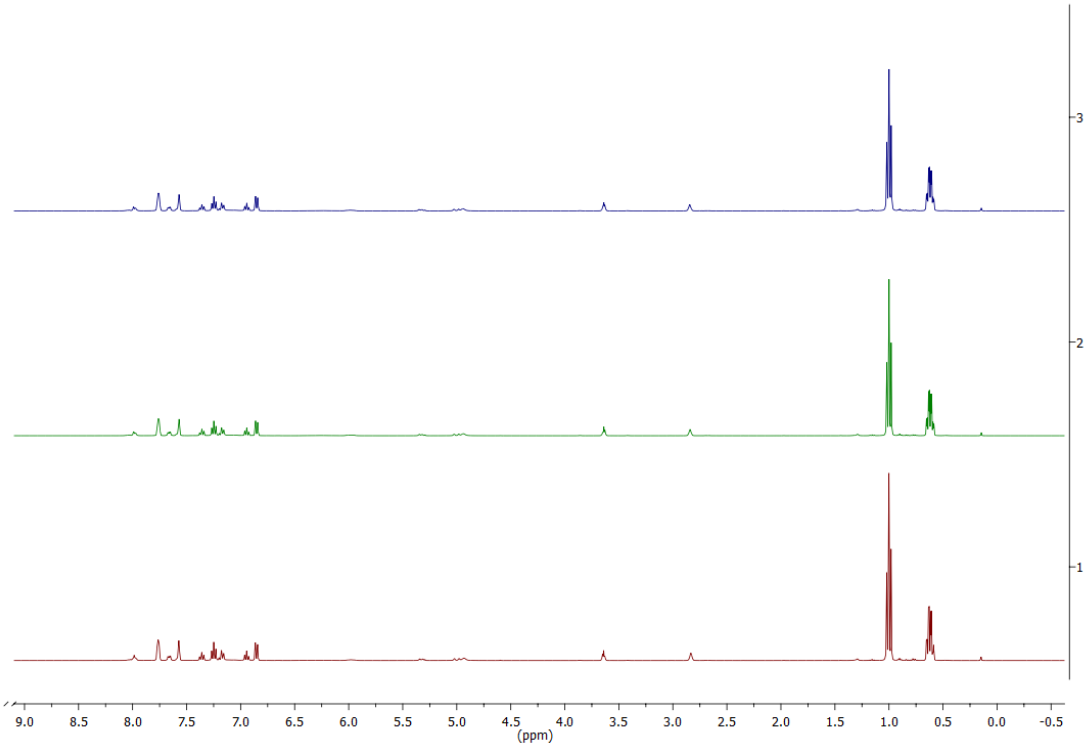

Figure 124: ^{1}H spectra of dehydrocoupling of phenol with Et_3SiH using 10%mol of 2c catalyst after 1h, 5h and 24h

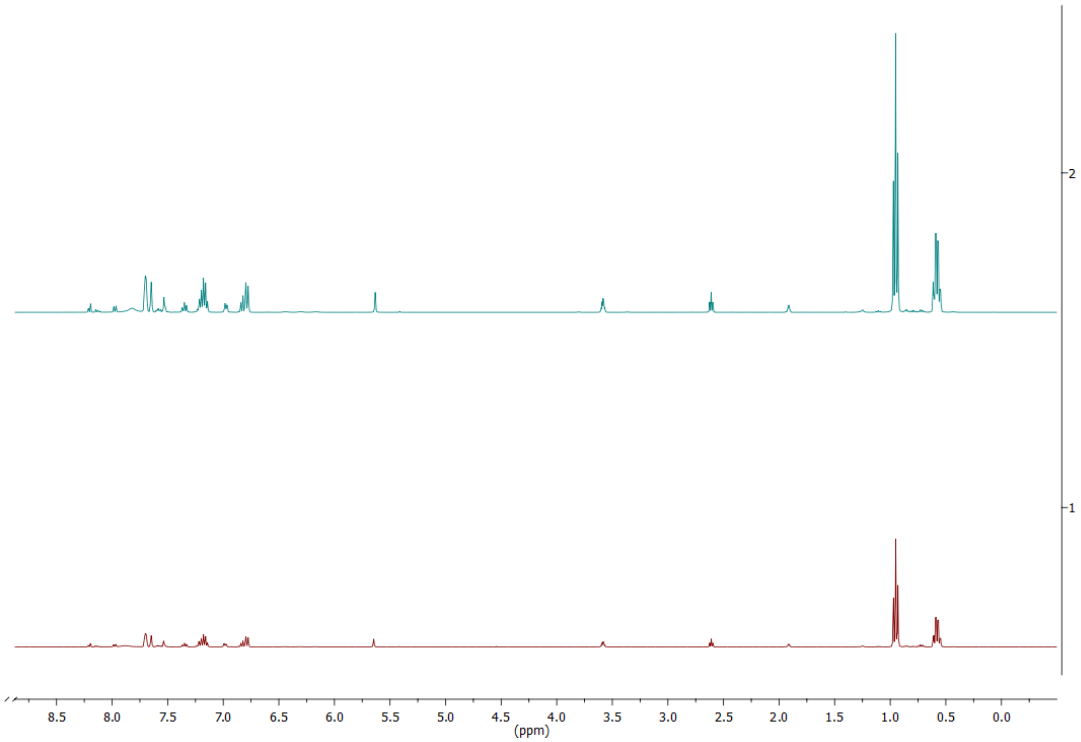

Figure 125: ^{1}H spectra of dehydrocoupling of phenol with Et_3SiH using 10%mol of 2d catalyst after 1h and 24h

Hydrodeoxygenation of Benzophenone Spectra

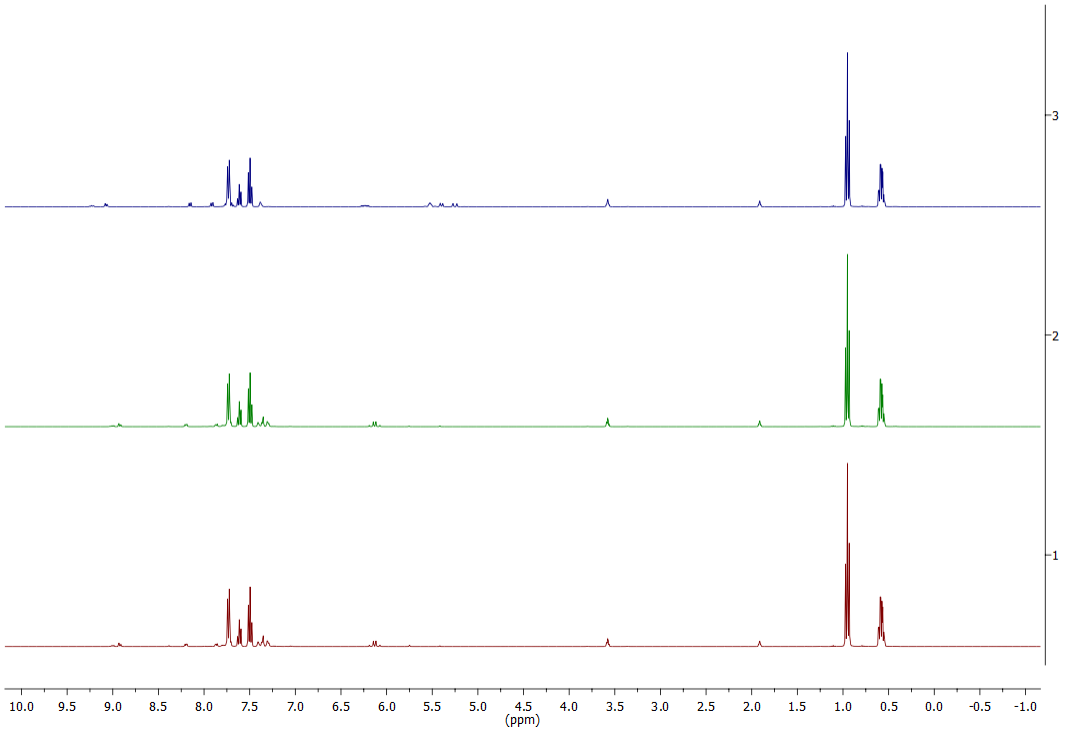

Figure 126: ^{1}H spectra of hydrodeoxygenation of benzophenone using 10% mol of 1a catalyst after 1h, 5h and 24h

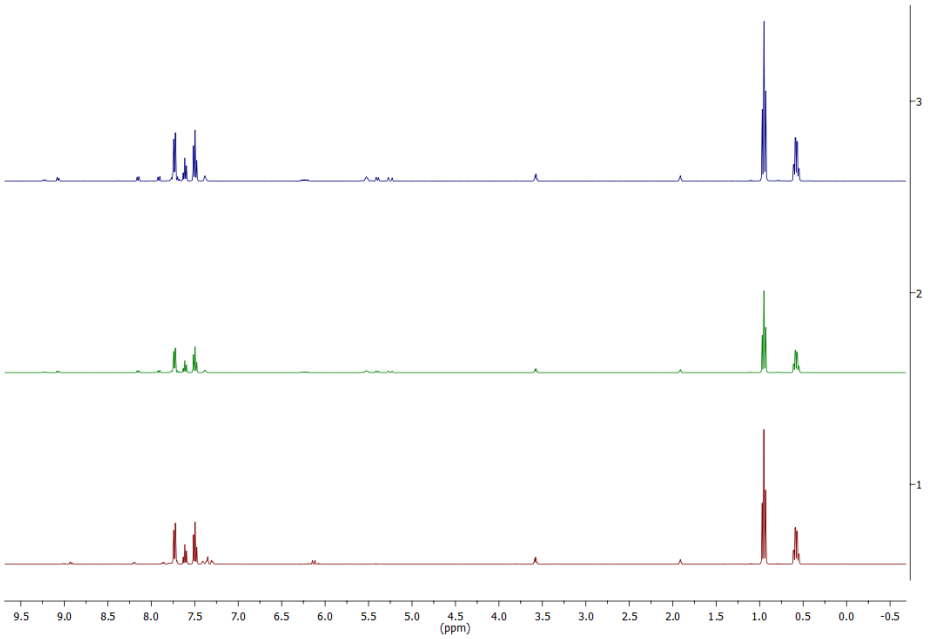

Figure 127: [1]H spectra of hydrodeoxygenation of benzophenone using 10% mol of 1b catalyst after 1h, 5h and 24h

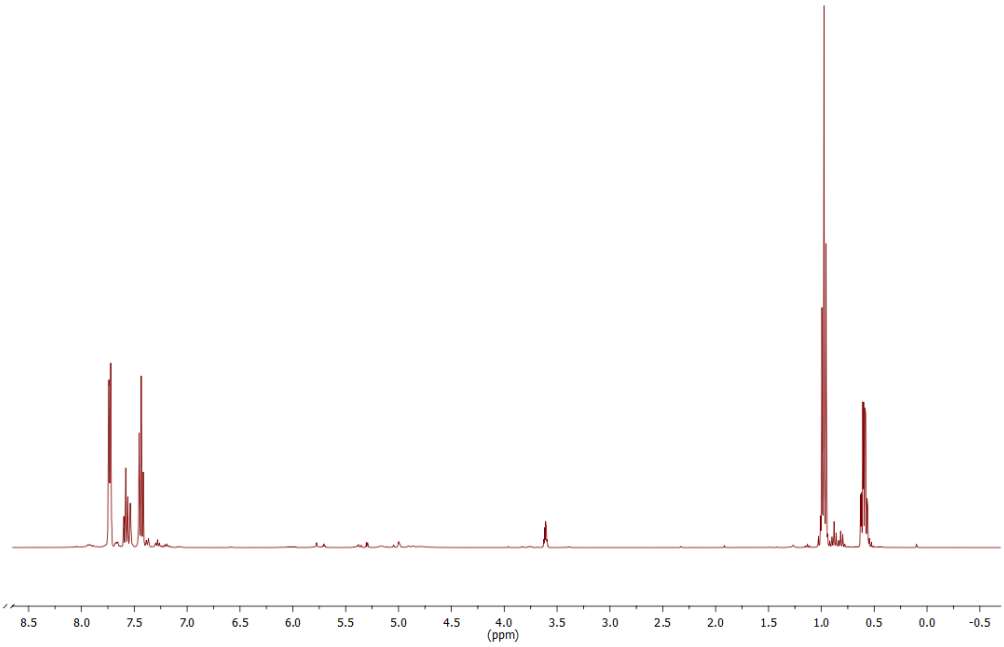

Figure 128: [1]H spectra of hydrodeoxygenation of benzophenone using 10% mol of 1c catalyst after 24h

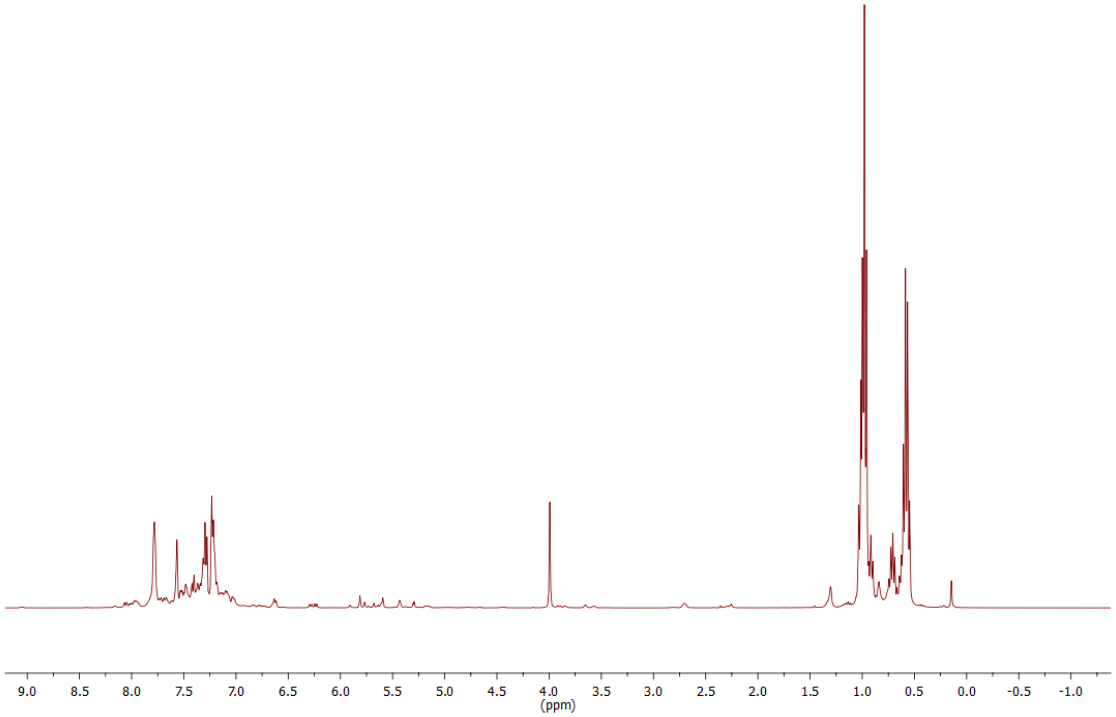

Figure 129: ^{1}H spectra of hydrodeoxygenation of benzophenone using 10% mol of 1d catalyst after 24h

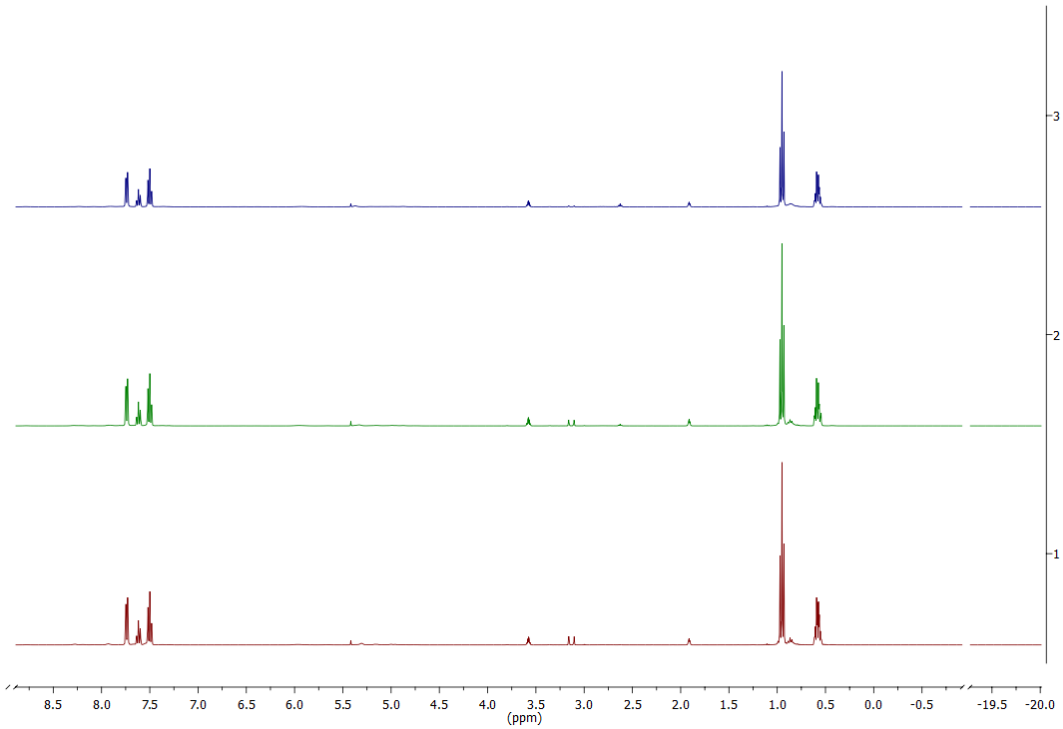

Figure 130: ^{1}H spectra of hydrodeoxygenation of benzophenone using 10% mol of 2a catalyst after 1h, 5h and 24h

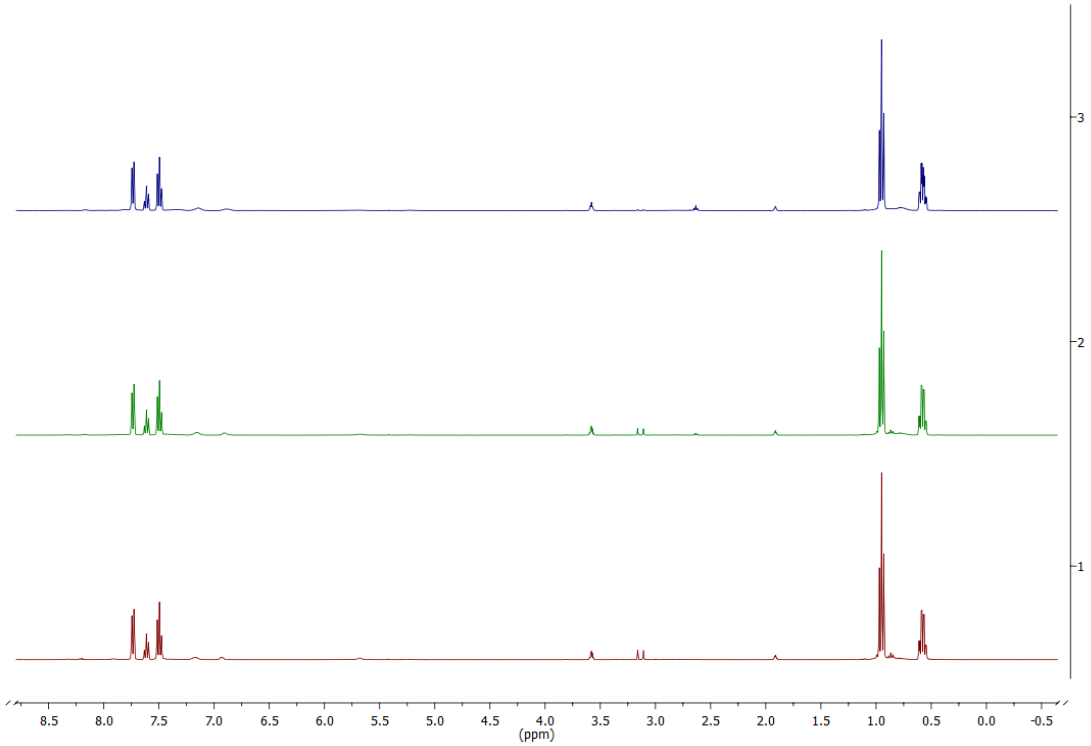

Figure 131: ^{1}H spectra of hydrodeoxygenation of benzophenone using 10% mol of 2b catalyst after 1h, 5h and 24h

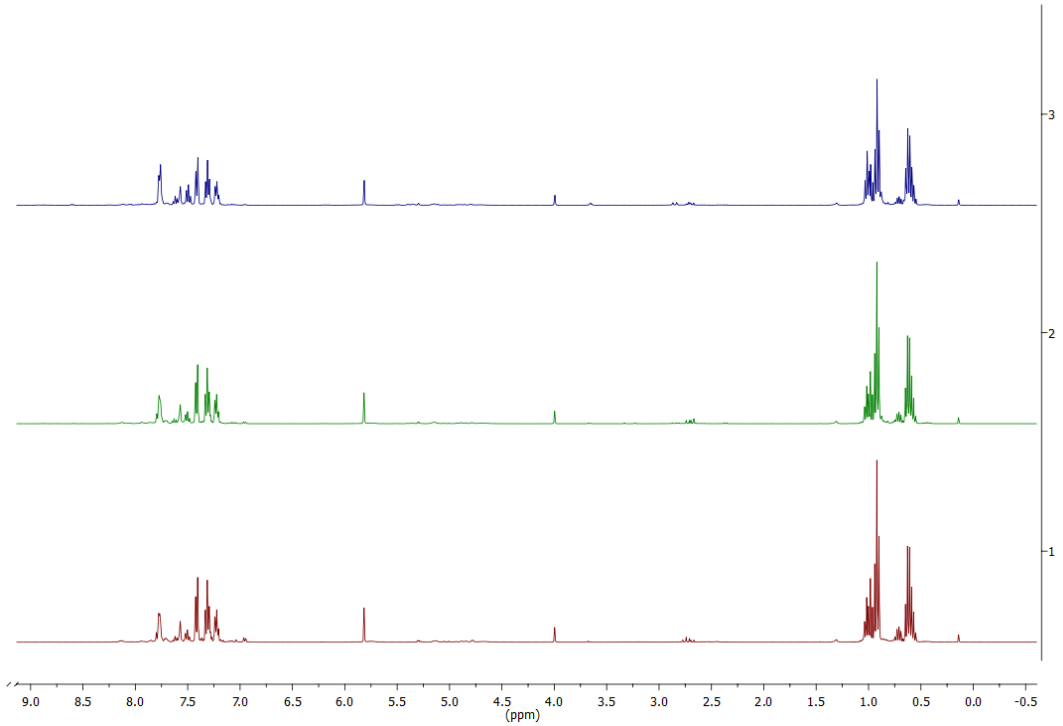

Figure 132: ^{1}H spectra of hydrodeoxygenation of benzophenone using 10% mol of 2c catalyst after 1h, 5h and 24h

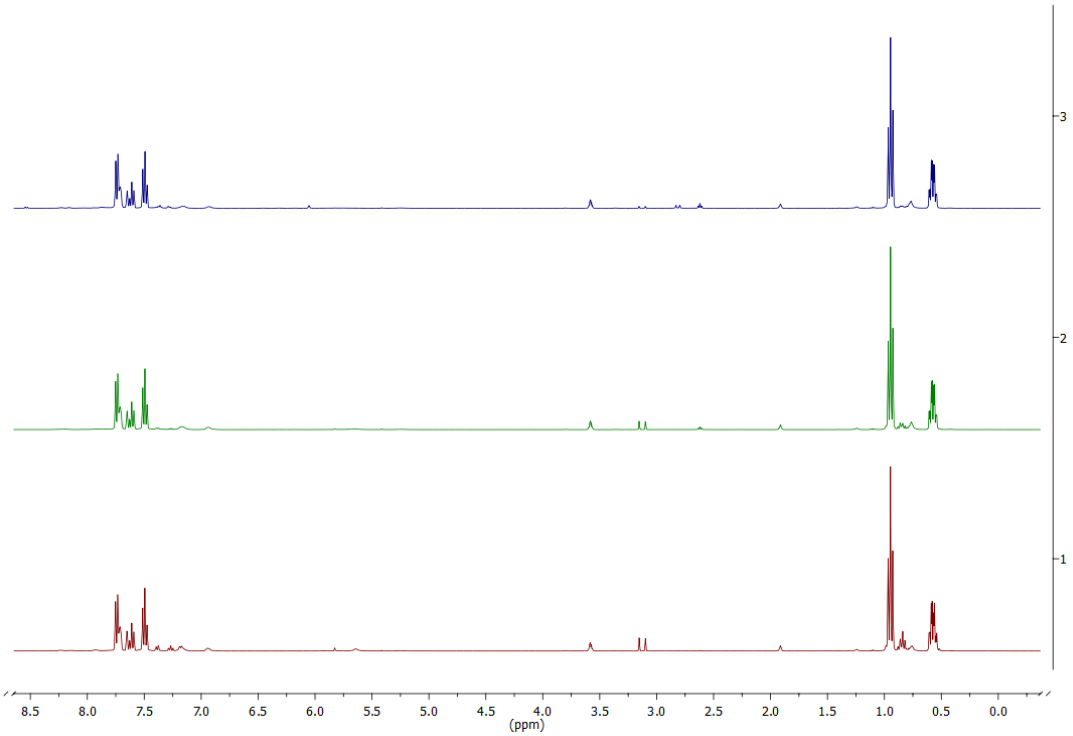

Figure 133: ^{1}H spectra of hydrodeoxygenation of benzophenone using 10% mol of 2d catalyst after 1h, 5h and 24h

Other spectra:

Infrared Spectra

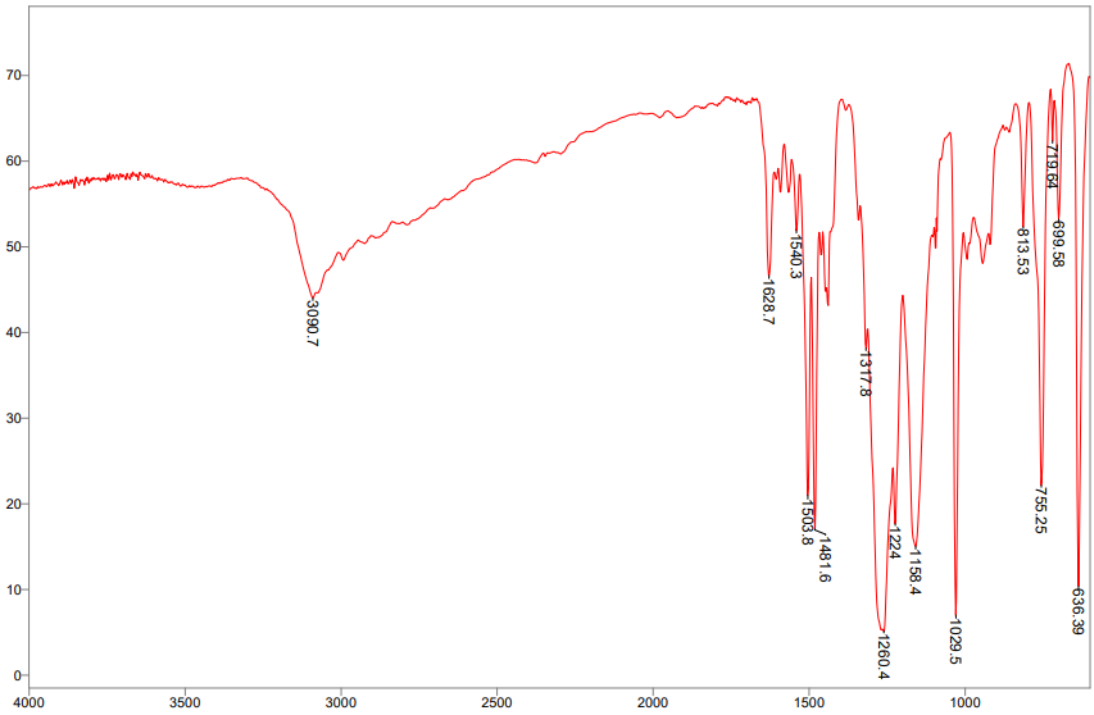

Figure 134: Infrared spectrum collected using KBr pellet for 1a

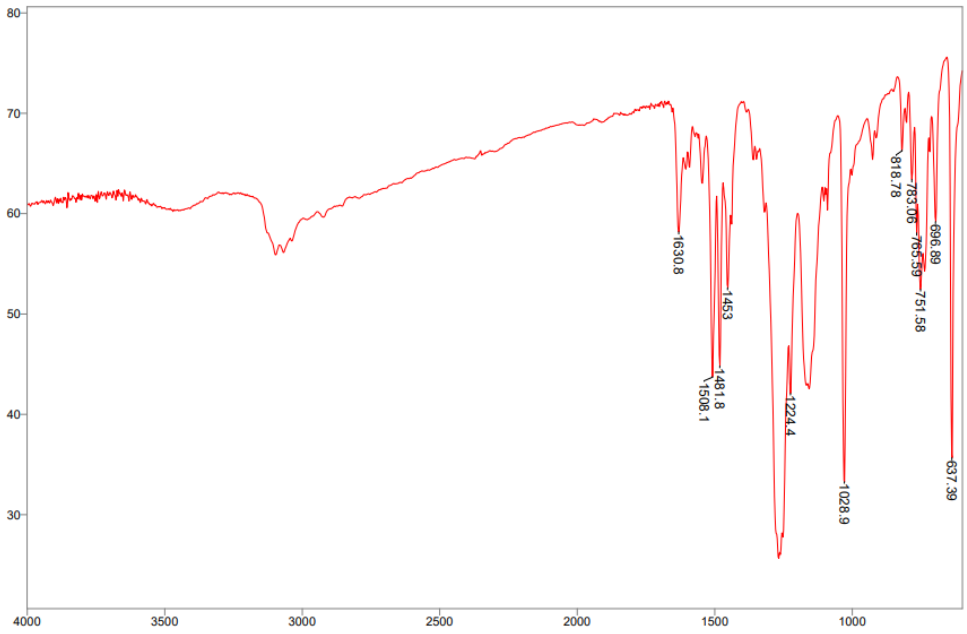

Figure 135: Infrared spectrum collected using KBr pellet for 1b

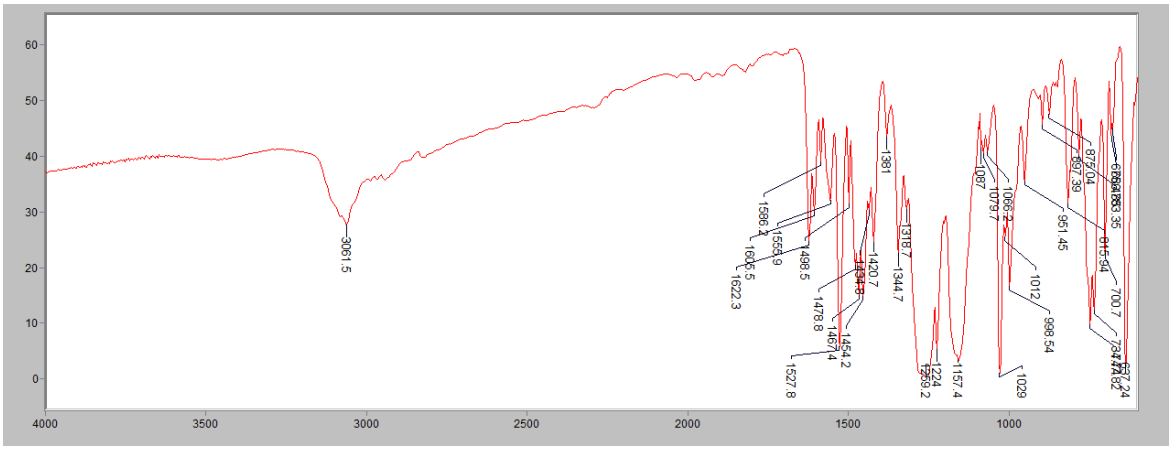

Figure 136: Infrared spectrum collected using KBr pellet for 2b

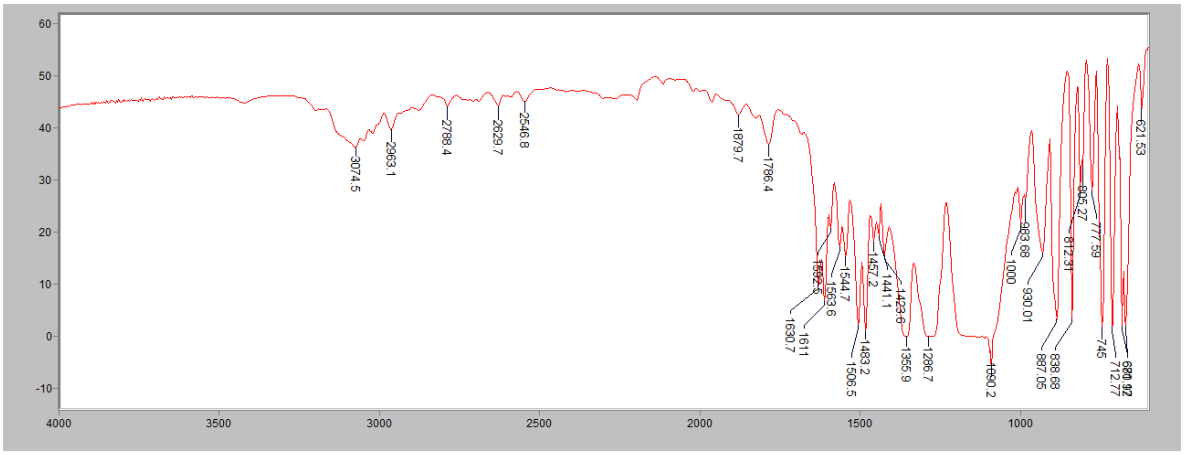

Figure 137: Infrared spectrum collected using KBr pellet for 1c

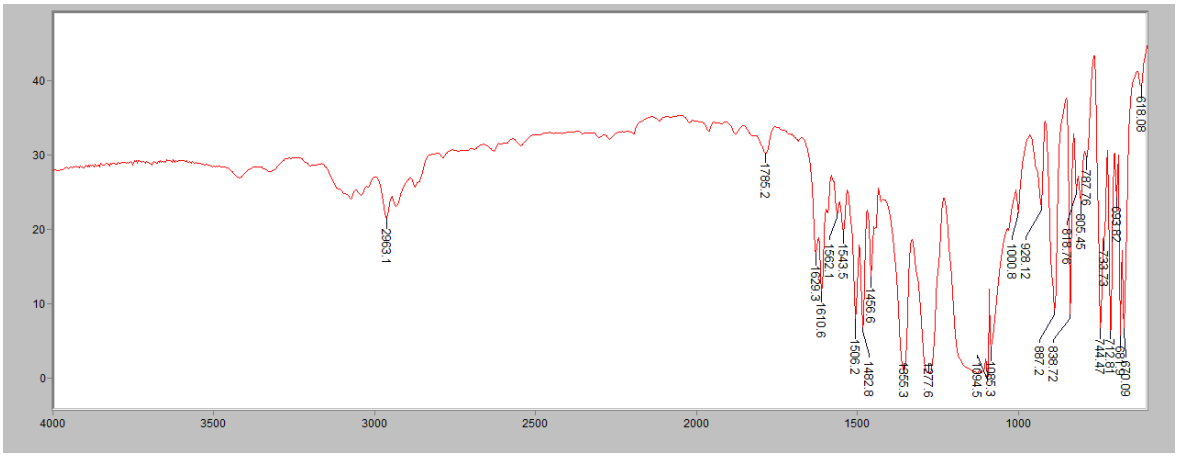

Figure 138: Infrared spectrum collected using KBr pellet for 1d

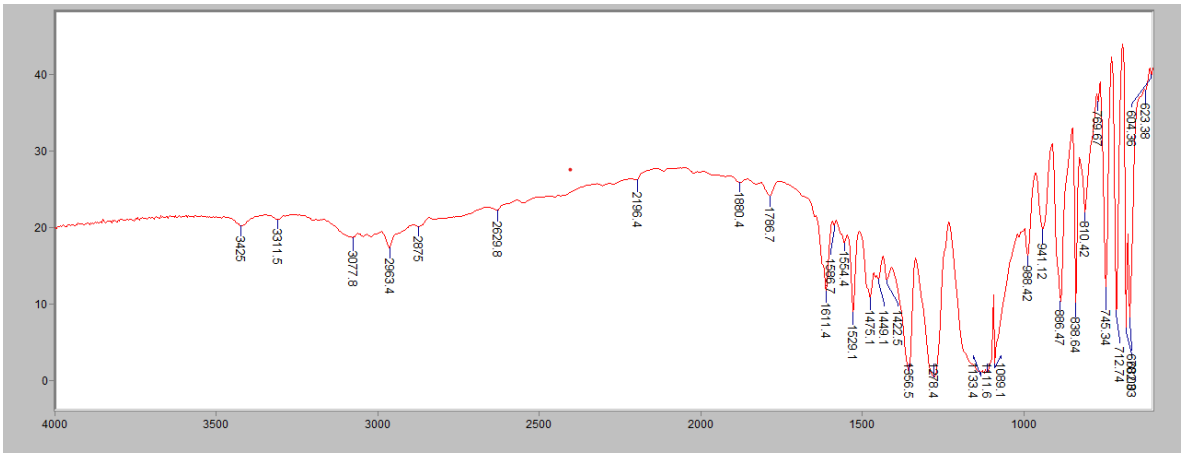

Figure 139: Infrared spectrum collected using KBr pellet for 2c

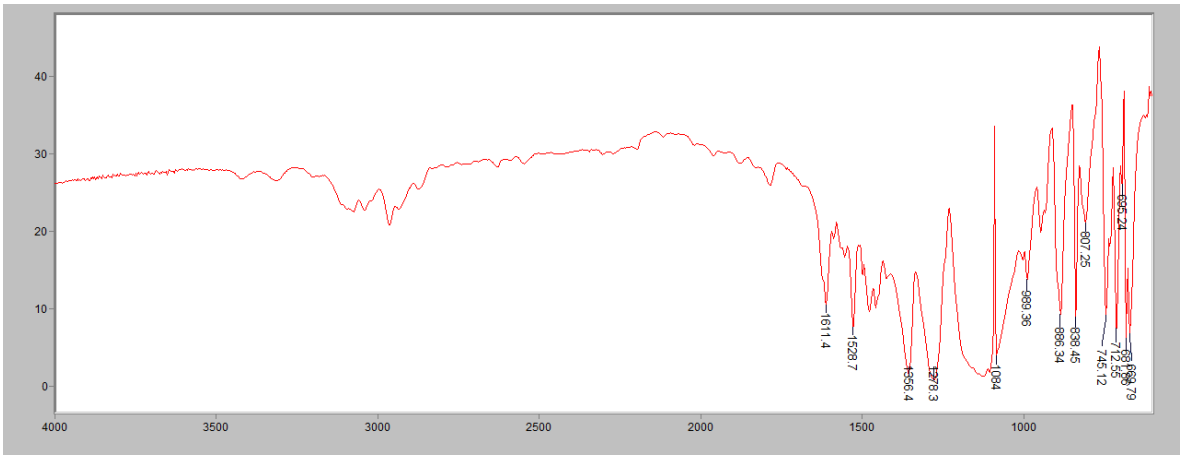

Figure 140: Infrared spectrum collected using KBr pellet for 2d